

An-Najah National University
Faculty of Graduates Studies

**Effect of Using Fiber Reinforced Polymers on the
Ductility of Retrofitted Reinforced Concrete Joint**

By

Yazan Bassam Abu-Tahnat

Supervisor

Dr. Mahmoud Dwaikat

Co- Supervisor

Dr. Mohammad Samaaneh

**This Thesis is Submitted in Partial Fulfillment of the Requirements for
the Degree of Master of Construction Engineering, Faculty of Graduate
Studies, An-Najah National University, Nablus, Palestine.**

2018

**Effect of Using Fiber Reinforced Polymers on the
Ductility of Retrofitted Reinforced Concrete Joint**

By

Yazan Bassam Abu-Tahnat

This Thesis was defended successfully on 24/1/2018 and approved by:

Defense Committee Member

Signature

- **Dr. Mahmoud Dwaikat /Supervisor**
- **Dr. Mohammad Samaaneh / Co- Supervisor**
- **Dr. Belal Almasri /External Examiner**
- **Dr. Mounther Dwaikat/ Internal Examiner**

Dedication

Praise be to Allah, Lord of the worlds

To the Prophet Mohammad

Blessings and Peace be upon him

To my father

To my mother

To my brothers

To my sister

To my precious ones

To all friends and colleagues

To my teachers

To everyone working in this field

To all of them

I literally dedicate this work

Acknowledgment

First of all, praise is to Allah for helping me in making this research possible. I would like to extend thanks to many people who helped me during my research work. Countless words are to be said in acknowledging the efforts of my enthusiastic supervisors – Dr. Mahmoud Dwaikat and Dr. Mohammed Samaaneh. Their tremendous academic support and continuous encouragement cannot be shortened in few words.

Special thanks to Prof. Dr. Mohammed Abu Jafar from the Physics Department for giving me an access to the Workstation at the computational physics laboratory to perform simulations of my studied scenarios.

Many thanks to the defense committee for their efforts in reviewing my thesis.

Special gratitude is to the Computer Engineering Department for providing me with the Department's computers to use during my research.

Special mention goes to Dr. Abdul Razzaq Touqan for encouraging me and helping me in building up my engineering sense.

Profound gratitude is to Dr. Monther Dwaikat from the Building Engineering Department for his grand academic support during my research.

Special mention goes to my parents, brothers, sister, friends and colleagues.

V
الإقرار

أنا الموقع أدناه مقدم الرسالة التي تحمل عنوان:

Effect of Using Fiber Reinforced Polymers on the Ductility of Retrofitted Reinforced Concrete Joint

أقر بأن ما اشتملت عليه هذه الرسالة إنما هي نتاج جهدي الخاص، باستثناء ما تم الإشارة إليه حيثما ورد ، وأن هذه الرسالة ككل، أو أي جزء منها لم يقدم لنيل أي درجة أو لقب علمي أو بحثي لدى أي مؤسسة تعليمية أو بحثية أخرى.

Declaration

The work provided in this thesis, unless otherwise referenced, is the researcher's own work, and has not been submitted elsewhere for any other degree or qualification

Student's Name:

اسم الطالب: يزن بسام أبو طحنات

Signature:

التوقيع :

Date:

التاريخ : 24/1/2018

Table of Contents

Dedication	III
Acknowledgment	IV
Declaration	V
Table of Contents	VI
Table of Figures	IX
Table of Tables.....	XVII
Abstract	XIX
1 Introduction.....	1
1.1 Overview.....	1
1.2 Definition of ductility	1
1.3 Scope of research	2
1.4 Research objectives.....	3
2 Literature review	5
2.1 Overview.....	5
2.2 Types of joints.....	5
2.3 Methods of strengthening RC joints	7
2.4 Numerical investigation of strengthening structures using CFRP....	27
2.5 Summary	27
3 Modeling	29
3.1 Overview.....	29
3.2 Material modeling	29
3.2.1 Concrete	29
3.2.2 Steel.....	37
3.2.3 Carbon Fiber-Reinforced Polymer (CFRP).....	38
3.3 Modeling of interfaces	40
3.4 Parameters for cohesive contact.....	41
3.5 Analysis type, loading and boundary conditions	43

3.6 Meshing type.....	44
4 Model verification.....	46
4.1 Overview.....	46
4.2 Sensitivity study.....	46
4.3 Clyde et al.(2000) test.....	47
4.4 Mahmoud et al. (2014) tests.....	50
4.5 El-Amory (2004) tests.....	55
4.6 Parametric study.....	60
4.6.1 General.....	60
4.6.2 Parameter ranges.....	60
5 Results and discussion.....	64
5.1 Overview.....	64
5.2 General behavior.....	64
5.3 Failure criteria.....	65
5.4 Results and discussion.....	65
5.4.1 Effect of column stirrups.....	66
5.4.2 Effect of joint stirrups continuity (A_v/s) _J	66
5.4.3 Effect of relative inertia (G).....	69
5.4.4 Effect of beam stirrups (A_v/s) _B	72
5.4.5 Effect of using CFRP.....	75
5.5 Failure modes.....	79
5.5.1 Ductile failure.....	79
5.5.2 Brittle failure.....	85
5.6 Data fitting.....	92
5.6.1 Ductility equation for exterior R.C beam-column joint without CFRP.....	92
5.6.2 Ductility equation for exterior reinforced beam-column joint with CFRP.....	100

VIII

5.7	Limitations of proposed equations.....	107
6	Analytical verification	108
6.1	Overview	108
6.2	Yield and ultimate moments capacity for beam	108
6.2.1	Methodology of calculating yield force.....	109
6.2.2	Methodology of calculating ultimate force	112
6.3	Beam shear capacity	114
6.4	Joint Shear capacity	116
6.5	Yield moment capacity for column	117
6.6	Yield and ultimate deflections	120
6.6.1	Methodology for calculating flexural deflection	122
6.6.2	Methodology for calculating shear deflection	125
6.6.3	Methodology for calculating axial deflection.....	127
6.7	Analytical results.....	129
7	Conclusions and recommendations	138
7.1	Overview	138
7.2	Research findings	138
7.3	Proposed equations	139
7.4	Future work	141
	References	142
	Appendix	150
	المخلص	ب

List of Figures

Figure 1.1: A typical illustration of an exterior joint	3
Figure 2.1: Types of joints	6
Figure 2.2: Forces acting on exterior R.C joint (Siva and Thirugnanam 2012)	7
Figure 2.3: Dimensions of prototype frame and one-third frame. (Ghobarah et al. 1996)	8
Figure 2.4: Reinforcement details for J1,J2,J3 and J4. (Ghobarah et al. 1996)	9
Figure 2.5: The assembling of beam and column steel jackets for J3. (Ghobarah et al. 1996).....	9
Figure 2.6: Test set-up. (Ghobarah et al. 1996)	10
Figure 2.7: Shear-angle curves for J1,J2,J3 and J4. (Ghobarah et al. 1996)	10
Figure 2.8: Reinforcement details for all units. (Jing et al. 2004)	12
Figure 2.9: Test set-up. (Jing et al. 2004)	12
Figure 2.10: Load-deflection curve of specimens. (Jing et al. 2004)	13
Figure 2.11: Tensile strength of various types of FRP against steel yield strength. (ACI 440. 2008).....	14
Figure 2.12: Comparison of tensile properties of fiber, matrix, and composite. (Campbell 2010).	14
Figure 2.13: CFRP at negative moment in composite girder. (Sharif et al. 2015) Figure 2.14: CFRP at positive moment in composite girder. (Sharif et al. 2015)	16
Figure 2.15: Reinforcement details for joint T1 and T1R. (Ghobarah and Said 2001).....	17
Figure 2.16: Proposed joint habitation scheme using FRP. (Ghobarah and Said 2001).....	17

Figure 2.17: Test set-up. (Ghobarah and Said 2001).....	18
Figure 2.18: Load –deflection curve of specimens. (Ghobarah and Said 2001)	18
Figure 2.19: Reinforcement details for joint T1 and T1R. (El-Amoury 2004)	19
Figure 2.20: Proposed joint habitation scheme using FRP for specimens T- S1RR, T-S4R and T-S5.(El-Amoury 2004)	20
Figure 2.21: Test set-up.(El-Amoury 2004).....	20
Figure 2.22: Load –deflection curve of specimens. (El-Amoury 2004).....	21
Figure 2.23: Dimensions and reinforcement details for the exterior R.C beam-column joint (Clyde et al. 2000).....	22
Figure 2.24: Dimensions and reinforcement details for the base control specimen (Mahmoud et al. 2014).	23
Figure 2.25: Schematic representation for the considered three groups (Mahmoud et al. 2014)	23
Figure 2.26: Details of joints in three groups(Mahmoud et al. 2014)	24
Figure 2.27: Dimensions and reinforcement details of all specimens. (Al- Salloum et al. 2002).....	25
Figure 2.28: Test set-up. (Al-Salloum et al. 2002)	25
Figure 2.29: Schematic representation of FRP repaired specimen. (Al- Salloum et al. 2002).....	26
Figure 2.30: Load –displacement curves for specimen before and after repair. (Al-Salloum et al. 2002).....	26
Figure 3.1: Response of concrete to uniaxial loading in (a) compression and (b) tension. (ABAQUS User Manual, 2013).....	30
Figure 3.2: Yield surface in plane stress. (ABAQUS User Manual, 2013)	32
Figure 3.3: Dilatation angle and eccentricity (ABAQUS User Manual, 2013).	35

Figure 3.4: Deviatoric cross section of failure surface. (ABAQUS User Manual, 2013).....36

Figure 3.5: Uniaxial load cycle (tension-compression-tension) assuming default values for the stiffness recovery factors: to $\omega_t = 0$ and $\omega_c = 1$. (ABAQUS User Manual, 2013)37

Figure 3.6: Typical stress-strain curve of steel38

Figure 3.7: Schematic of unidirectional FRP lamina.....39

Figure 3.8: Bond-slip curves models41

Figure 3.9: Location of loads and boundary conditions44

Figure 3.10: Finite Element Mesh Type45

Figure 4.1: Effect of mesh size47

Figure 4.2: Curves needed for define CDP model in ABAQUS for test by Clyde et al. (2000)48

Figure 4.3: Stress –plastic strain diagram for steel which is used for test by Clyde et al. (2000).49

Figure 4.4: Comparison between experimental and F.E. results for test by Clyde et al. (2000).50

Figure 4.5: Definition of concrete parameters for CDP model in ABAQUS for joints J0, JI0 and JI1 tested by Mahmoud et al. (2014)....52

Figure 4.6: Stress vs plastic strain curves for steel 240 MPa and 400 MPa. (Sharif et al. 2015)53

Figure 4.7: Comparison between experimental and F.E. results for joints J0, JI0 and JI1 tested by Mahmoud et al. (2014)54

Figure 4.8: Comparison between tension damage from F.E. and experimental test for joints J0 and JI0 tested by Mahmoud et al. (2014)55

Figure 4.9: Definition of concrete parameters for CDP model in ABAQUS for joints T-S1, T-S4R and T-S5 tested by El-Amoury et al. (2004).....57

Figure 4.10: Stress –plastic strain diagram for steel which is used for modeling of joints T-S1, T-S4R and T-S5.	58
Figure 4.11: Comparison between experimental and F.E. results for joints T-S1, T-S4R and T-S5 tested by El-Amoury et al. (2004)	59
Figure 5.1: Typical load –deflection curve for joints	65
Figure 5.2: Effect of column stirrups on the ductility.....	66
Figure 5.3: Effect of joints stirrups continuity on strength and ductility of joints with G equals 0.512 without CFRP.....	67
Figure 5.4: Effect of joints stirrups continuity on strength and ductility of joints with G equals 1 without CFRP.....	68
Figure 5.5: Effect of joints stirrups continuity on strength and ductility of joints with G equals 4.63 without CFRP.....	68
Figure 5.6: Effect of joints stirrups continuity on strength and ductility of joints with G equals 0.512 strengthened with CFRP	68
Figure 5.7: Effect of joints stirrups continuity on strength and ductility of joints with G equals 1 strengthened with CFRP	69
Figure 5.8: Effect of joints stirrups continuity on strength and ductility of joints with G equals 4.63 strengthened with CFRP	69
Figure 5.9: Effect of relative inertia on strength and ductility of joints with maximum $(A_v/s)_J$ without CFRP.....	70
Figure 5.10: Effect of relative inertia on strength and ductility of joints with minimum $(A_v/s)_J$ without CFRP.....	70
Figure 5.11: Effect of relative inertia on strength and ductility of joints with maximum $(A_v/s)_J$ strengthened with CFRP	71
Figure 5.12: Effect of relative inertia on strength and ductility of joints with minimum $(A_v/s)_J$ strengthened with CFRP.....	71
Figure 5.13: Effect of beams stirrups on strength and ductility of joints with maximum $(A_v/s)_J$ without CFRP.....	73

Figure 5.14: Effect of beams stirrups on strength and ductility of joints with minimum $(A_v/s)_J$ without CFRP	74
Figure 5.15: Effect of beams stirrups on strength and ductility of joints with maximum $(A_v/s)_J$ strengthened with CFRP	74
Figure 5.16: Effect of beams stirrups on strength and ductility of joints with minimum $(A_v/s)_J$ strengthened with CFRP	75
Figure 5.17: Effect of CFRP on strength and ductility of joints with maximum $(A_v/s)_J$	77
Figure 5.18: Effect of CFRP on strength and ductility of joints with minimum $(A_v/s)_J$	78
Figure 5.19: Cracks at failure before (G1-MaJ-MiB-0) and after (G1-MaJ-MiB-1) wrapping CFRP	79
Figure 5.20: Load –deflection curve for joint (G3-MaJ-MaB-0) with stages of behaviors	80
Figure 5.21: Cracking of beam for joint (G3-MaJ-MaB-0) (Normal stress in MPa)	81
Figure 5.22: Yielding of steel for joint (G3-MaJ-MaB-0) (Tensile stress in MPa)	81
Figure 5.23: F.E. resulting stress strain curve for points in the compression zone of beam for joint (G3-MaJ-MaB-0).....	82
Figure 5.24: Plastic Strain distribution at beam for joint (G3-MaJ-MaB-0)	82
Figure 5.25: Compression damage of Concrete for joint (G3-MaJ-MaB-0)	82
Figure 5.26: Load –deflection curve for joint (G1-MiJ-MaB-0) with stages of behaviors	83
Figure 5.27: Cracking of beam for joint (G1-MiJ-MaB-0) (Normal stress in MPa)	84

Figure 5.28: Yielding of steel for joint (G1-MiJ-MaB-0) (Tensile stress in MPa)	84
Figure 5.29: F.E. resulting Stress strain curve for points in the compression zone of beam for joint (G1-MiJ-MaB-0).....	85
Figure 5.30: Tension damage of concrete beam for joint (G1-MiJ-MaB-0)	85
Figure 5.31: Load –deflection curve for joint (G1-MaJ-MiB-0) with stages of behaviors	86
Figure 5.32: Cracking of beam for joint (G1-MaJ-MiB-0) (Normal stress in MPa)	87
Figure 5.33: Yielding of steel for joint (G1-MaJ-MiB-0) (Tensile stress in MPa)	87
Figure 5.34: Complete tension damage of concrete beam for joint (G1-MaJ-MiB-0)	87
Figure 5.35: Cracking of beam for joint (G1-MiJ-MiB-R) (Normal stress in MPa)	88
Figure 5.36: Yielding of steel for joint (G1-MiJ-MiB-R) (Tensile stress in MPa)	88
Figure 5.37: Complete tension damage of concrete beam for joint (G1-MiJ-MiB-R).....	89
Figure 5.38: Surface ductility fitting for joints without CFRP with brittle failure.....	94
Figure 5.39: Surface ductility fitting for joints without CFRP with ductile failure.....	94
Figure 5.40: Load deflection curves for independent models without CFRP	97
Figure 5.41: Relative errors as a function of relative stiffness (G) for models without CFRP	99

Figure 5.42: Relative errors as a function of transverse steel (A_v/s) for models without CFRP.....	99
Figure 5.43: Relation between ABAQUS ductility and ductility from equations (5.7) and (5.8) for models without CFRP	100
Figure 5.44: Surface ductility fitting for joints with CFRP	101
Figure 5.45: Load deflection curves for independent models with CFRP	104
Figure 5.46: Relative errors as a function of relative stiffness (G) for models with CFRP	106
Figure 5.47: Relative errors as a function of transverse steel (A_v/s) for models with CFRP.....	106
Figure 5.48: Relation between ABAQUS ductility and ductility from equation (5.9) for models with CFRP	107
Figure 6.1: Model of beam-column joint for analytical solution.....	109
Figure 6.2: Stress, strain and force distributions along cross section of beam at yield stage	109
Figure 6.3: stress strain curve of concrete 25MPa.....	112
Figure 6.4: Stress, strain and force distributions along cross section of column at ultimate stage.....	112
Figure 6.5: Stress, strain and force distributions along cross section of column at yield stage.....	118
Figure 6.6: Yield and ultimate moment diagrams for typical joint	122
Figure 6.7: Yield and ultimate curvature diagrams for typical joint	123
Figure 6.8: Virtual moment diagram for typical joint.....	123
Figure 6.9: shear diagrams at yield and ultimate stages for typical joint .	126
Figure 6.10: Virtual shear diagram for typical joint	126
Figure 6.11: Axial diagrams at yield and ultimate stages for typical joint	128
Figure 6.12: Virtual axial diagram for typical joint.....	128

Figure 6.13: Comparisons between ABAQUS results and analytical results
for yield and peak forces136

Figure 6.14: Comparisons between ABAQUS results and analytical results
for tip beam deflections at yield and peak forces.....137

List of Tables

Table 2.1: Properties of concrete and value of axial load at column for joints were tested by Clyde et al. (2000).....	22
Table 4.1: Properties of reinforcement bars which were used by Clyde et al. (2000).....	47
Table 4.2: Parameters of concrete used in test of Clyde et al.(2000) ($f_c = 46.2\text{MPa}$).....	48
Table 4.3: Properties of reinforcement bars used by Mahmoud et al. (2014)	50
Table 4.4: Properties of concrete for joints tested by Mahmoud et al. (2014)	51
Table 4.5: Properties of FRP sheet used by Mahmoud et al. (2014)	51
Table 4.6 Properties of epoxy used by Mahmoud et al. (2014).....	51
Table 4.7: Parameters of concrete for joints J0, JI0 and JI1 tested by Mahmoud et al. (2014)	52
Table 4.8: Properties for combined CFRP with matrix and stiffness of interaction for specimen JI1 tested by Mahmoud et al. (2014)	53
Table 4.9: Properties of reinforcement bars used by El-Amoury et al. (2004)	55
Table 4.10: Properties of concrete for joints tested by El-Amoury et al. (2004).....	55
Table 4.11: Properties of FRP sheets used by El-Amoury et al. (2004).....	56
Table 4.12: Properties of epoxy used by El-Amoury et al. (2004).....	56
Table 4.13: Parameters of concrete for joints T-S1, T-S4R and T-S5 tested by El-Amoury et al. (2004)	56

Table 4.14: Properties for combined FRP with matrix and stiffness of interaction for specimens T-S5 and T-S4R tested by El-Amoury et al. (2004).....	58
Table 4.15: Variable properties for all models	62
Table 4.16: Constant dimensions of beam-column models	63
Table 5.1: Maximum value of $(A_v/s)_B$ beyond which it has no effect on ductility	73
Table 5.2: Summary of F.E. results	90
Table 5.3: Comparing ABAQUS results and equation results for joints without CFRP	95
Table 5.4: Properties of random joints without CFRP.....	96
Table 5.5: Results of independent models without CFRP	98
Table 5.6: Comparing ABAQUS results and equation results for independent models without CFRP.....	98
Table 5.7: Comparing ABAQUS results and equation results for joint with CFRP	102
Table 5.8: Properties of random joints with CFRP.....	103
Table 5.9: Results of independent models with CFRP	104
Table 5.10: Comparing ABAQUS results and equation results for independent models with CFRP	105
Table 6.1: Comparisons between ABAQUS results and analytical results	130
Table 6.2: Yield and ultimate flexure, shear, axial deflections analytically.	133

Effect of Using Fiber Reinforced Polymers on the Ductility of**Retrofitted Reinforced Concrete Joint****By****Yazan Abu-Tahnat****Supervisor****Dr. Mahmoud Dwaikat****Co- Supervisor****Dr. Mohammad Samaaneh****Abstract**

Reinforced concrete (R.C) structures are common in Palestine. One considerable weakness in these structures is the connection between beams and columns. Several researchers showed that reinforced concrete joints suffer brittle failure due to combined effect of loading on the joints. Therefore, the ductility of the beam-column joints in reinforced concrete structures is an essential factor to prevent sudden failure of the joint. Different techniques were adapted by several researchers to increase the ductility and strength of beam-column joints including the use of high strength concrete, special stirrups and reinforcement configuration, steel plates and Fiber-Reinforced Polymer (FRP).

One way to improve the ductility of such joints is the use of sheet wraps of FRP. This research focuses on studying the effect of using FRP wraps on exterior RC beam-column joints. Finite Element (F.E.) analysis using commercial FE software (ABAQUS) is used to investigate the ductility behavior of RC joints strengthened by FRP. The model is validated using available published test data. This model is used to conduct a parametric study on the key factors that affect joints nonlinear behavior. Results are used

to develop simple conceptual equations to predict the ductility of exterior beam-column joints as a function of the applied FRP. Such equations can be used as an initial conceptual design step for checking the adequacy of RC beam-column joints in seismic design of RC buildings.

1 Introduction

1.1 Overview

A considerable weakness in R.C structures is the connection between beams and columns. Extensive studies were conducted to investigate the behavior of beam-column joints. Kaliluthin et al. (2014) and Uma and Prasad (1996) showed that R.C joints suffer brittle failure due to the combined effect of loading on the joints. Maintaining minimum ductility of beam-column joints in R.C structures is essential to prevent sudden failure of such joints which severely affects all the structure. Different techniques were adopted by several researchers to increase the ductility and strength of R.C beam-column joints. These include the use of high strength concrete, special stirrups and reinforcement configuration, steel plates, and the use of Fiber Reinforced Polymers (FRP). Most of the studies focused on using FRP for retrofitting and strengthening and some researchers investigated the improvement of joints ductility by FRP wraps. This study will focus on the ductility of exterior R.C beam-column joint strengthened by FRP.

1.2 Definition of ductility

Ductility describes the capacity of a material/section/member/structure to undergo large deformations without any significant reduction in strength. However, there are different levels of ductility such as, material ductility, section ductility, member ductility and structural ductility.

Material ductility, as determined from typical stress-strain curves, has the basic level of ductility which indicates the maximum ductility if all points of structure have the same behavior and stressed equally which is really difficult to happen. Sectional ductility is less than the material ductility because layers of materials in the section are not equally stressed. Member ductility is further less than sectional ductility because the member generally yields at certain locations only. Finally, the structural ductility is the lowest because any structure has many members, and not all members reach plastic capacity at the same time.

Generally, ductility of a structure is affected mostly by joint failures (Ghobarah and Said, 2002). Thus, ensuring sufficient ductility at the joints can increase overall structural ductility.

1.3 Scope of research

As mentioned earlier, a considerable weakness point in R.C structures is the connection between beams and columns. At the same time; ductility of R.C structure largely depends on the ductility of joints. Different techniques can be used to improve joint ductility. These techniques include using FRP sheets and wraps around the R.C joints. The main focus of this research is to investigate the effect of using FRP wraps on rotational ductility of R.C framed joints.

Three-dimensional (3-D) non-linear finite element (F.E.) model is built using commercial software ABAQUS. The model is verified using published experimental results. This model is used to conduct parametric study

investigating different main parameters that affect ductility of beam-column joint. Also, the ductility of R.C joint is verified using principles of simple mechanics.

Due to time limitations; the scope of this research is limited to exterior RC beam-column joints as shown in Figure .11. Also the analysis is limited to nonlinear static monotonic loading. Material and geometric nonlinearities are included in the model. The level of details for the joint is assumed to be consistent with typical frames used in Palestine. This study is limited to quantifying how much the ductility is improved when a certain arrangement of FRP is applied.

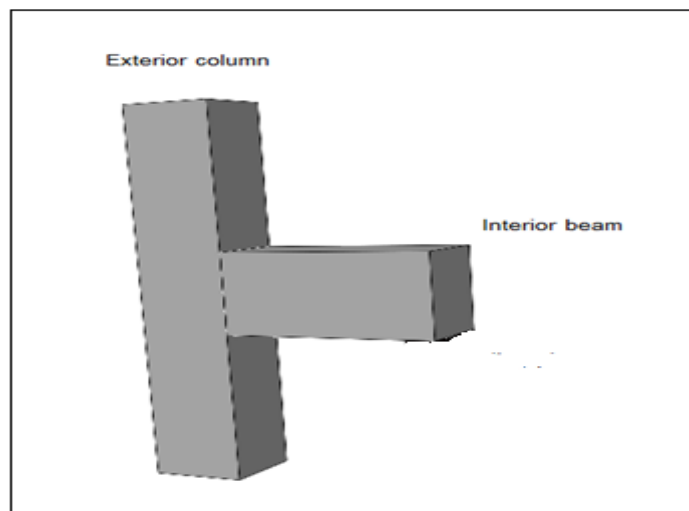


Figure 1.1: A typical illustration of an exterior joint

1.4 Research objectives

The main objective of this study is to quantify the effect of using certain wraps of FRP on R.C joint to undergo large plastic rotation before failure. To achieve this prime goal, the following tasks are performed:

- 1- Study literature on using FRP wraps for joint ductility and its effect on concrete confinement. This will be elaborated in Chapter 2.
- 2- Develop a 3-D non-linear F.E. model for R.C beam-column joint. The model includes both material and geometrical nonlinearities, and includes interfacial properties between FRP and concrete. The commercial (F.E.) software ABAQUS is used to create a generic parametric model of an exterior R.C beam-column joint with and without FRP wraps. Geometry, materials, and all the required input data are obtained from the literature and used to develop the model. FRP and adhesive properties are obtained from available published data too. The modeling process and related assumptions are explained in details in Chapter 3.
- 3- Verify the model by comparison with published experimental data. Sensitivity and parametric studies in order to identify the important and significant parameters that influence the ductility of the joint. This is presented in Chapter 4 of the thesis.
- 4- Correlate the results obtained from the F.E. models into a usable equation that predicts the joint ductility. This is shown in Chapter 5.
- 5- Verify the results by comparing numerical results with analytical results using basics of mechanics and plasticity. This is shown in details in Chapter 6.
- 6- Summarize the results and draw conclusions and recommendations for engineers on the use of FRP and future works as discussed in Chapter 7.

2 Literature review

2.1 Overview

Design of R.C beam-column joint has become a subject of interest for many researchers due to its unique importance in structures. RC beam–column joint is a critical point in the structures because it is generally subjected to combined effect of many types of loadings. The combined effect of many types of loadings makes the behavior of such joints very complex and difficult to predict, especially under dynamic and reversal loadings (Kaliluthin et al., 2014 and Uma and Prasad, 1996). Interaction of stresses due to combined loading can cause sudden failure in the joint. Therefore, such joints must be strengthened to prevent premature failure. The ability of the joint to deform plastically before failure is measured by its ductility. Generally, increasing the ductility of the joint, may lead to avoiding sudden failure.

2.2 Types of joints

In typical structures, different types of framed joints exist such as; corner-roof joint, corner joint, exterior-roof joint, exterior joint, and interior joint as shown in Figure 2.1.

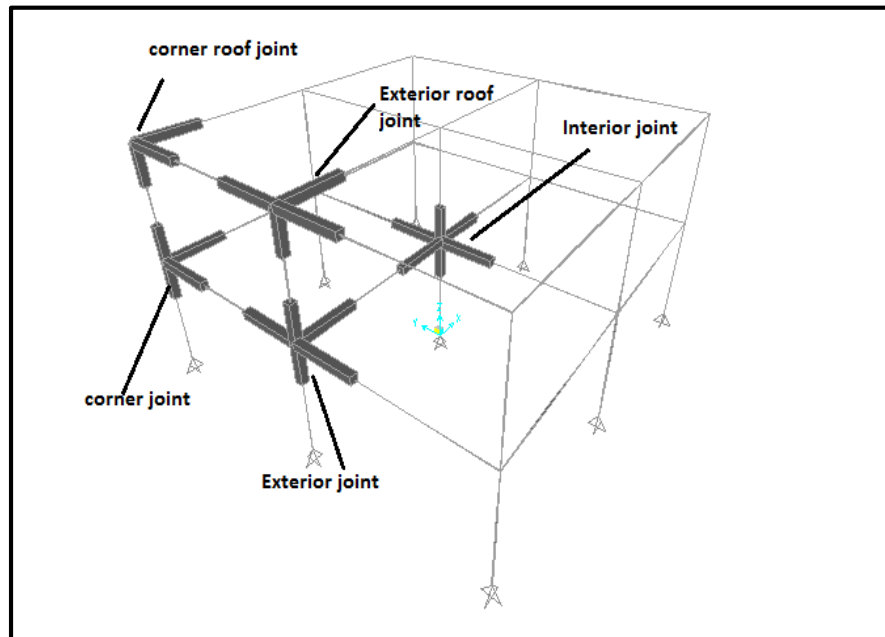


Figure 2.1: Types of joints

Each type of these joints undergoes different kind of behavior due to differences in combination of internal stresses acting on the joint. As shear and flexural stresses act simultaneously in a complex combination within the joint region, these stresses cause an internal diagonal tensile and compressive stresses. If the diagonal stress is large enough, it would lead to diagonal cracking (in tension) or crushing (in compression) of the concrete as shown in Figure 2.2 (Siva and Thirugnanam, 2012). Therefore, strengthening techniques and reinforcement detailing can vary depending on the expected behavior of each type of joints.

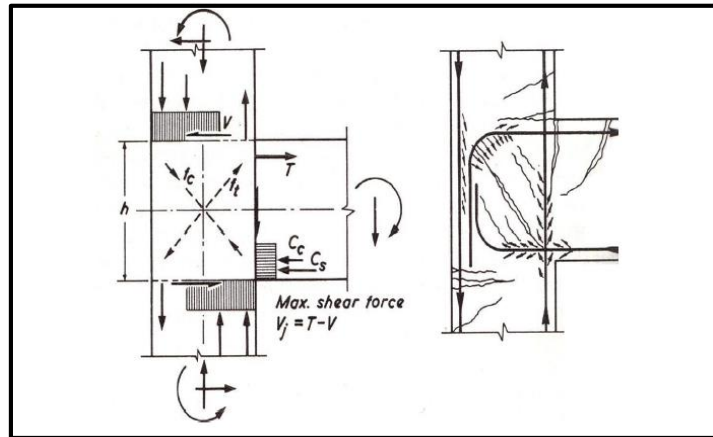


Figure 2.2: Forces acting on exterior R.C joint (Siva and Thirugnanam, 2012)

The ACI-ASCE 352 (1985) classifies the joints in two categories based on type of design loads and deformations:

- 1- Category 1: joints which are designed for strength only without considering the ductility. This type is designed for gravity and normal wind loads.
- 2- Category 2: joints which are designed for sustained strength under deformation reversals into the inelastic range. This type is designed to resist lateral loads such as earthquake, blast and cyclonic winds.

2.3 Methods of strengthening RC joints

Due to the importance of these joints, there are many strengthening techniques to improve the behavior of each type of joints, such as using steel jacking, improving the detailing of the joint and the use of FRP. An experimental exposition of these techniques will be displayed and discussed in the following sections.

For example, steel jacking is a common method used to strengthen the structural members. Ghobarah et al. (1996), experimentally tested four

specimens of beam-column joints with one-third scale as shown in Figure 2.3 under cyclic loading. Specimens J1, J3 and J4 have the same detailing of reinforcement, while the reinforcement for specimen J2 was detailed according to the Canadian seismic design code (CSA, 1994). The different reinforcement detailing of specimens is shown in Figure 2.4. Specimens J1 and J2 were built without steel jacketing, while specimen J3 was encased by a corrugated steel jacket on the beam and column, whereas J4 encased on column only. The assembly of beam and column steel jackets are shown in Figure 2.5. The specimens were placed in the testing machine, and then an axial load, representing the gravity load, was applied to the column and kept constant throughout the test. After that, cyclic displacements were applied to the free end of the beam as shown in Figure 2.6. The results of the experiments showed that the steel jacketing around beam and column caused remarkable increase of the ductility as shown in Figure 2.7.

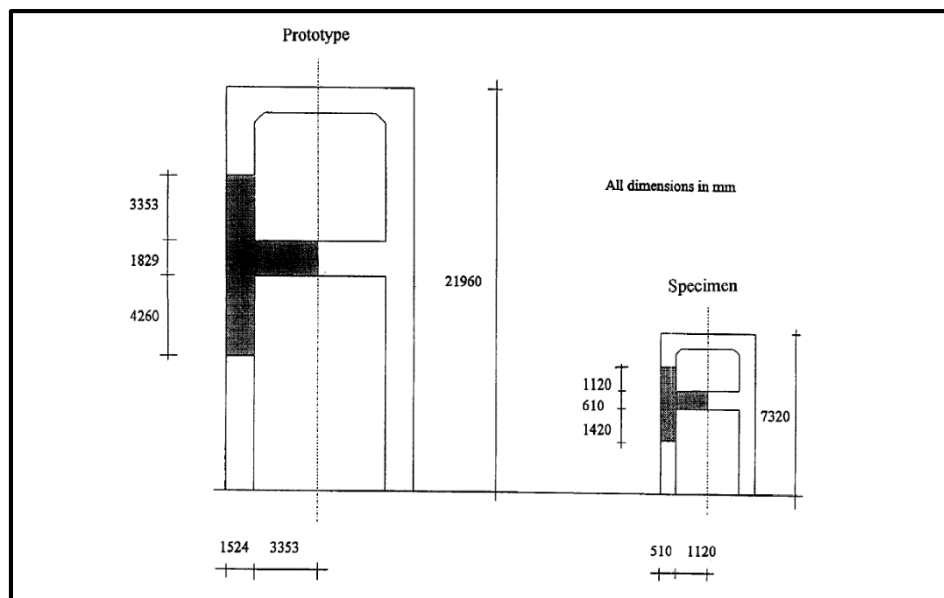


Figure 2.3: Dimensions of prototype frame and one-third frame (Ghobarah et al., 1996)

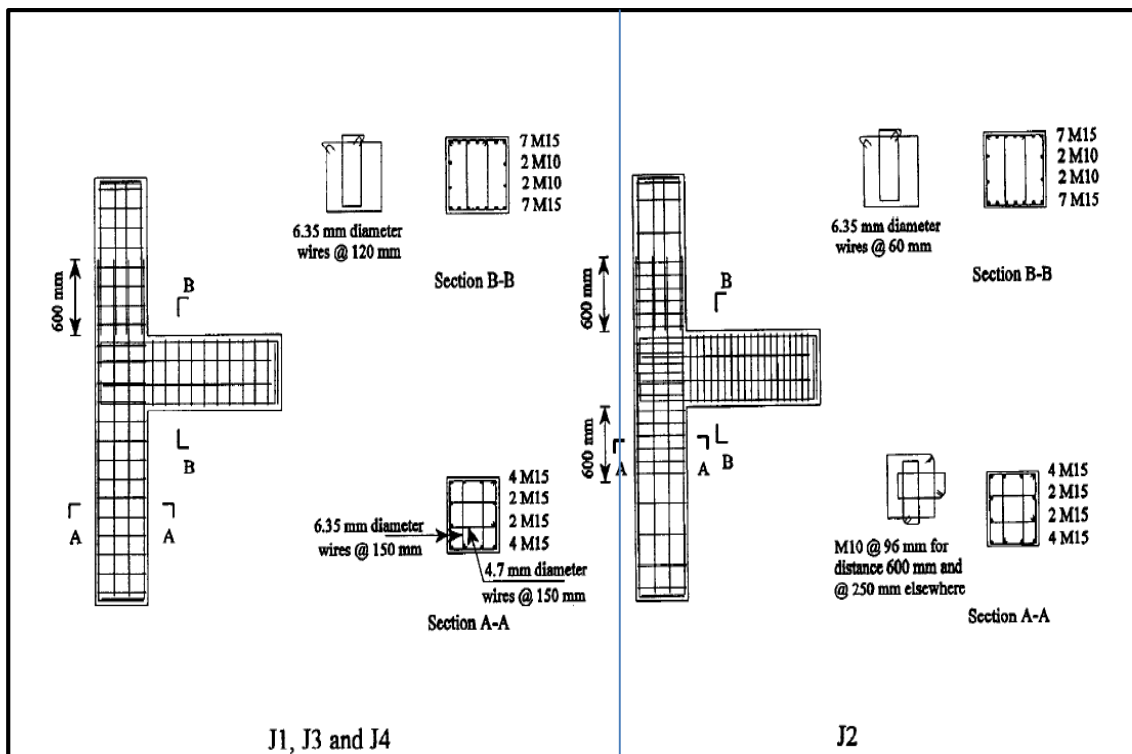


Figure 2.4: Reinforcement details for J1,J2,J3 and J4 (Ghobarah et al., 1996)

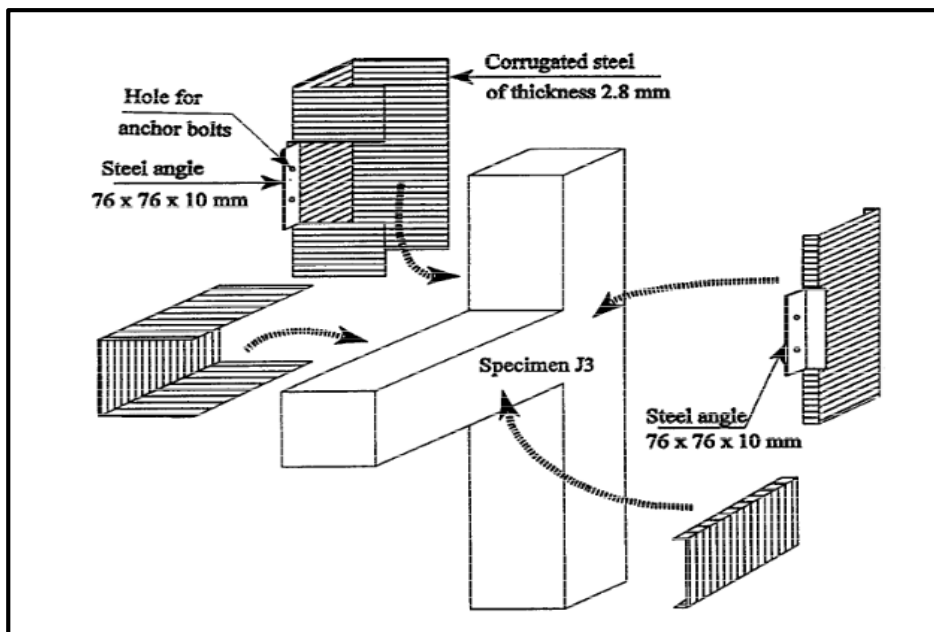


Figure 2.5: The assembling of beam and column steel jackets for J3 (Ghobarah et al., 1996)

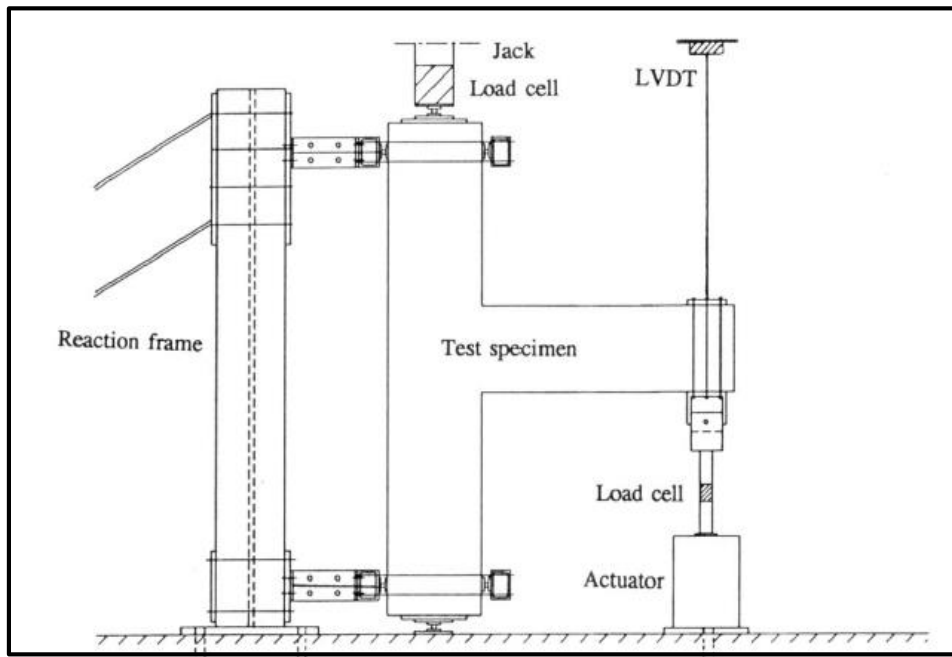


Figure 2.6: Test set-up (Ghobarah et al., 1996)

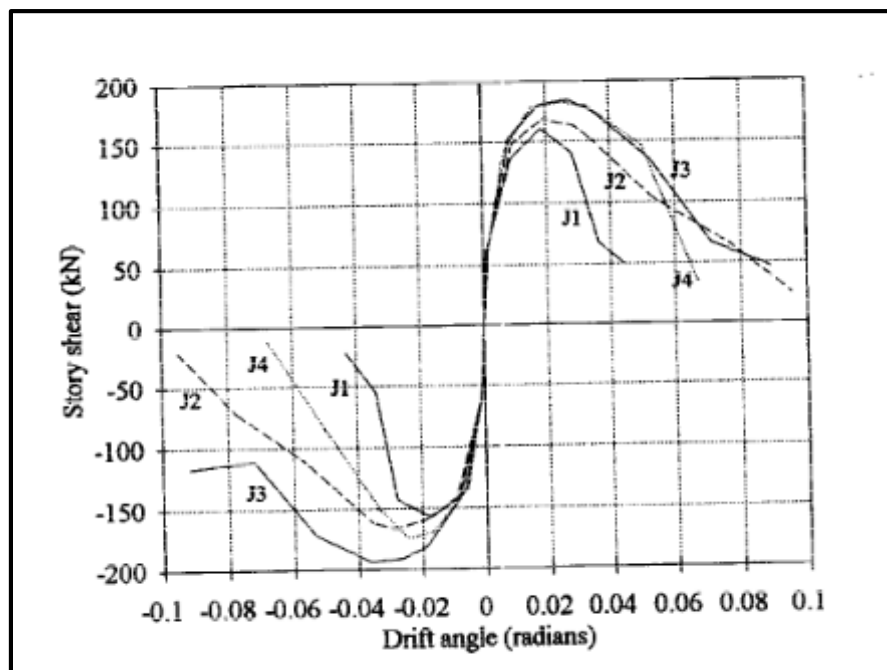
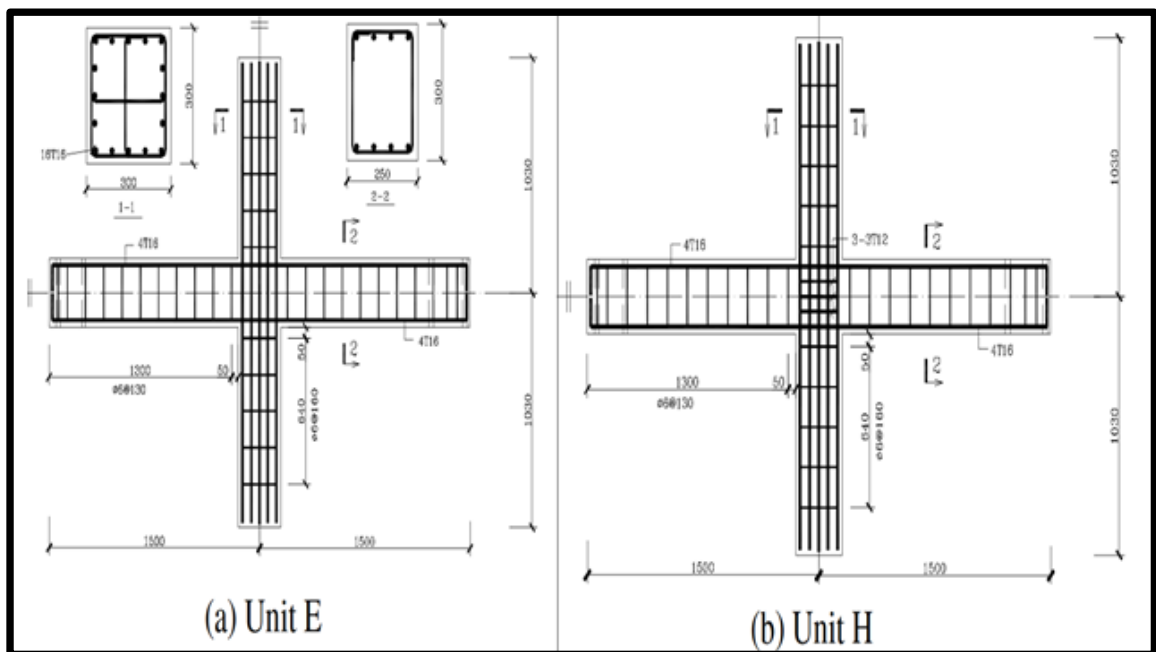


Figure 2.7: Shear-angle curves for J1,J2,J3 and J4 (Ghobarah et al., 1996)

Jing et al. (2004) conducted experimental investigation to capture the effect of different types of joint reinforcements detailing for low to moderate

seismic risk regions. All test units had the same dimensions of 250mmx300mm x3000mm and 300mmx300mmx2060mm for beam and column, respectively. The reinforcement details for each type of these specimens are shown in Figure 2.8. The specimens were placed in the testing machine and then a reversal quasi-static loading were applied to the free ends of the beams as shown in Figure 2.9. Load deflection curve for each specimen is shown in Figure 2.10. One of the main important results showed that the ductility for joint with column stirrups in joint is more than the ductility of joint without column stirrups in joint by 20%.



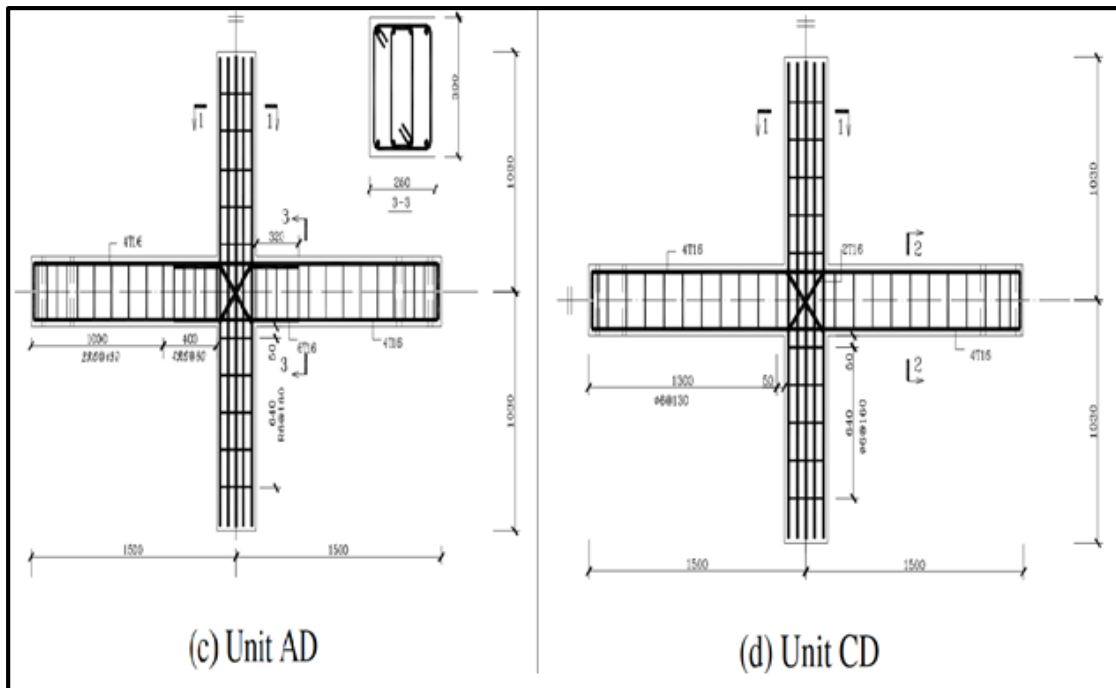


Figure 2.8: Reinforcement details for all units (Jing et al., 2004)

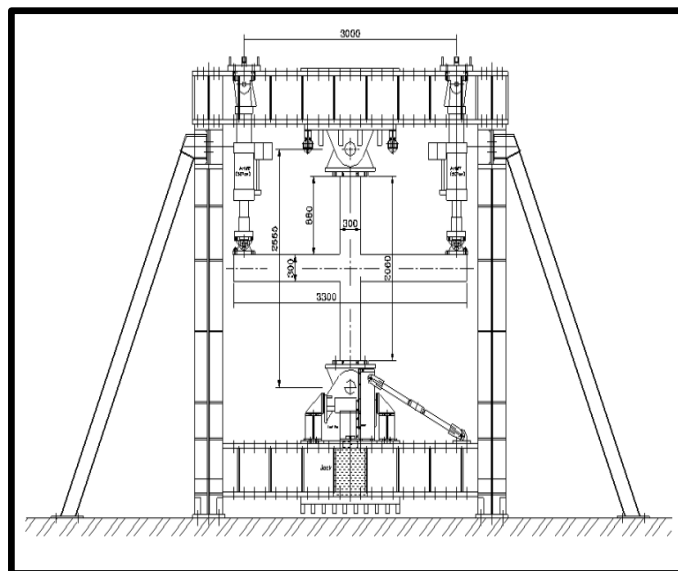


Figure 2.9: Test set-up (Jing et al., 2004)

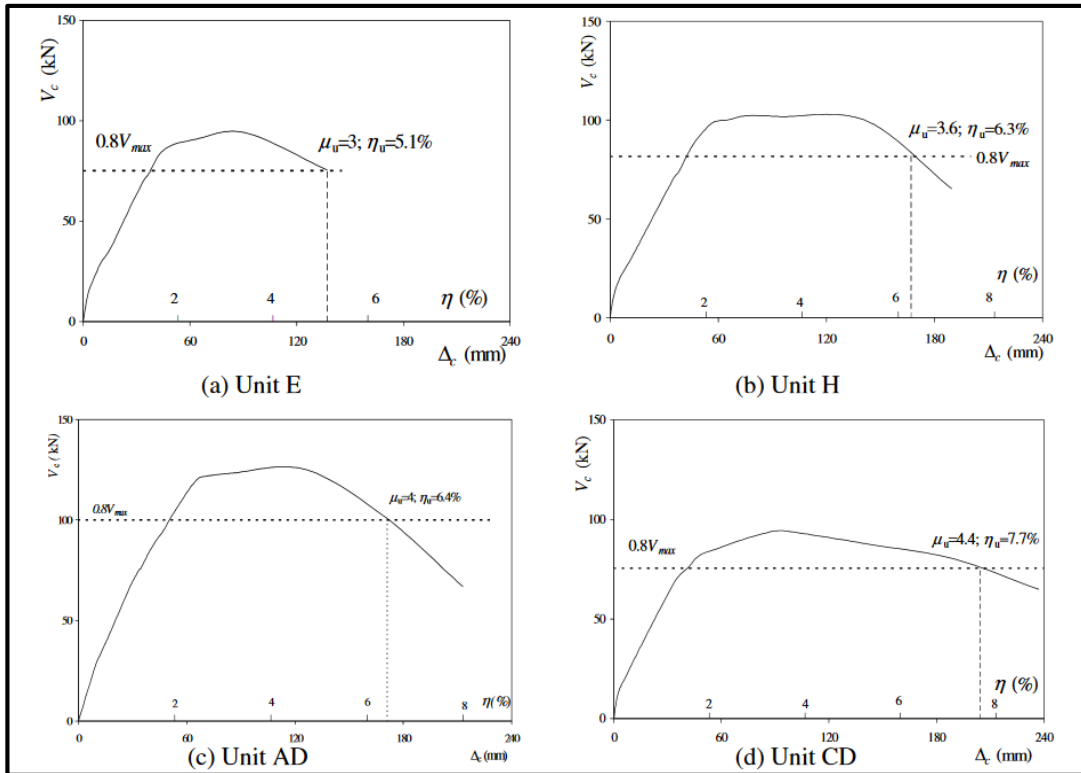


Figure 2.10: Load-deflection curve of specimens (Jing et al., 2004)

In the last decades, the use of Fiber Reinforced Polymer (FRP) composites presented an effective technique for strengthening concrete structures besides the use of steel jacketing.

FRP is a composite material made of a polymer matrix and is reinforced with fibers. The FRP sheets are typically bonded to the structures using proper epoxy (adhesive) material. The use of FRP is a matter of adding low-weight, high-tensile strength material to the structure. This material is used especially for strengthening and retrofitting parts of structures where principal tensile stresses exceed tensile strength of the element at that location. Generally four types of FRP are used to strengthen structures: Sprayed and Electrical Glass FRP (S-GFRP and E-GFRP), Basalt FRP

(BFRP), Aramed FRP (AFRP) and Carbon FRP (CFRP). Comparison between tensile strength of those types is presented in Figure 2.11.

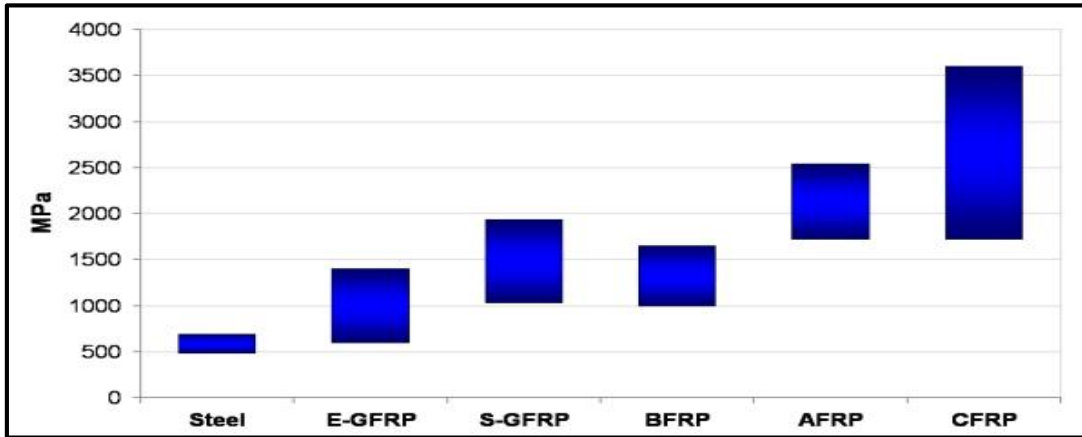


Figure 2.11: Range of tensile strength of various types of FRP against steel yield strength (ACI 440, 2008)

Generally, the fibers can have a high-tensile strength of 3500 MPa, while a typical polymeric matrix normally has a tensile strength of only 35 to 70 MPa. This matrix make the overall tensile capacity of FRP less than that of pure fibers as shown in Figure 2.12 (Campbell, 2010).

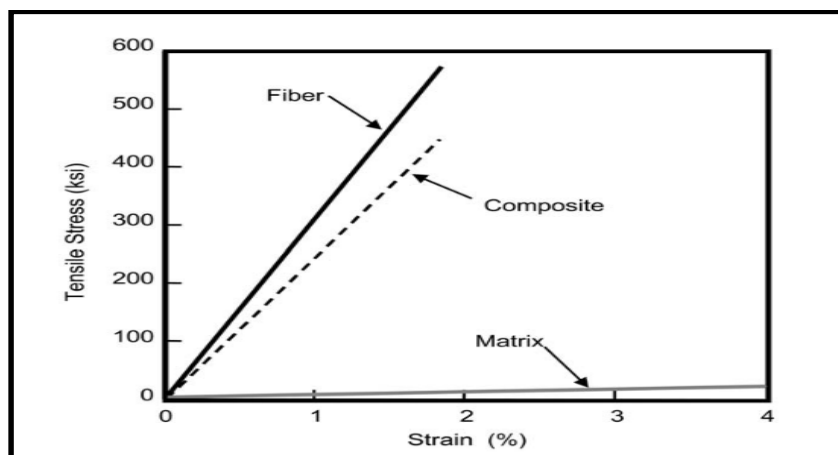


Figure 2.12: Comparison of tensile properties of fiber, matrix, and composite (Campbell, 2010).

Different methods of retrofitting RC joints using FRP are available. These methods include using sheets, laminates, strips or rebar.

Extensive research was conducted on using FRP in the strengthening and retrofitting of different structural elements. Sharif et al. (2015) conducted experimental investigation to study the effect of CFRP on the ratio between cracking load and yielding load of the continuous composite steel girders. The study aimed to maintain the composite action of the negative moment region. Three retrofitting schemes were used: First, CFRP sheets were used to maintain the composite action at the region of negative moment as shown in Figure 2.13. The second scheme, CFRP sheets wrapped at positive moment region as shown in Figure 2.14. In the third scheme, CFRP sheets were used at positive and negative moment in the continuous composite steel girders. RG girder was the control specimen without CFRP, while girders G1, G2 and G3 presented the first scheme of retrofitting with 1, 2 and 3 layers of CFRP, respectively. On the other hand, girder designated PGR showed second scheme of retrofitting. Moreover, girder G2R presented the third scheme of retrofitting with two layers of CFRP at negative moment and wrapping the concrete at positive moment region. Results of this investigation showed that using 1, 2 and 3 layers of CFRP at negative moment region, increases the cracking load to be 0.47, 0.75, and 0.79 of the service load for G1, G2 and G3, respectively compared to 0.86 for G2R. Also, results showed that when using CFRP only at positive moment regions, the ratio decrease from 0.47 to 0.38 due to increasing the yielding load and decreasing cracking load. However, when using CFRP at negative and

positive moment regions, the ratio increased from 0.38 to 0.82. Their findings could be summarized by the ability of CFRP to maintain composite action at negative moment region and ability of wrapping and confining concrete slab at the negative moment region.

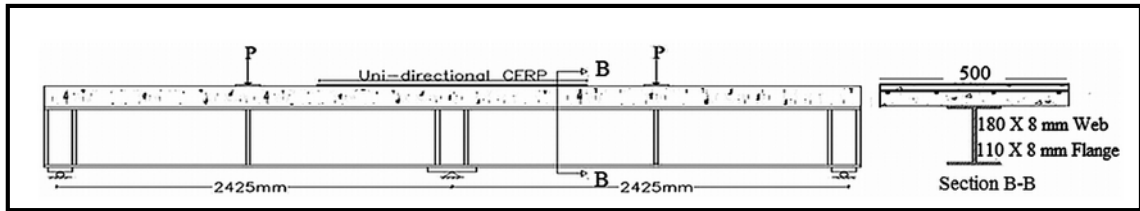


Figure 2.13: CFRP at negative moment in composite girder (Sharif et al., 2015)

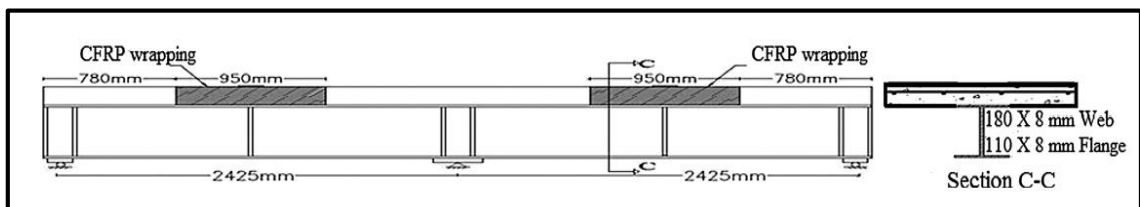


Figure 2.14: CFRP at positive moment in composite girder (Sharif et al., 2015)

Ghobarah and Said (2001) experimentally tested two full-scale specimens of exterior R.C beam column joint to study the effect of GFRP on the behavior of joint. Specimen T1 was a control joint with no shear reinforcement within the joint region as shown in Figure 2.15. After testing joints T1, the joint was strengthened using GFRP as shown in Figure 2.16, and then another test was conducted. The strengthened specimen is designated T1R. Both specimens were placed in the testing machine, then a constant axial load with value $0.2 A_g f_c$ was applied to the column and kept constant throughout the test, and after that, a reversal cycling displacements were applied to the free end of

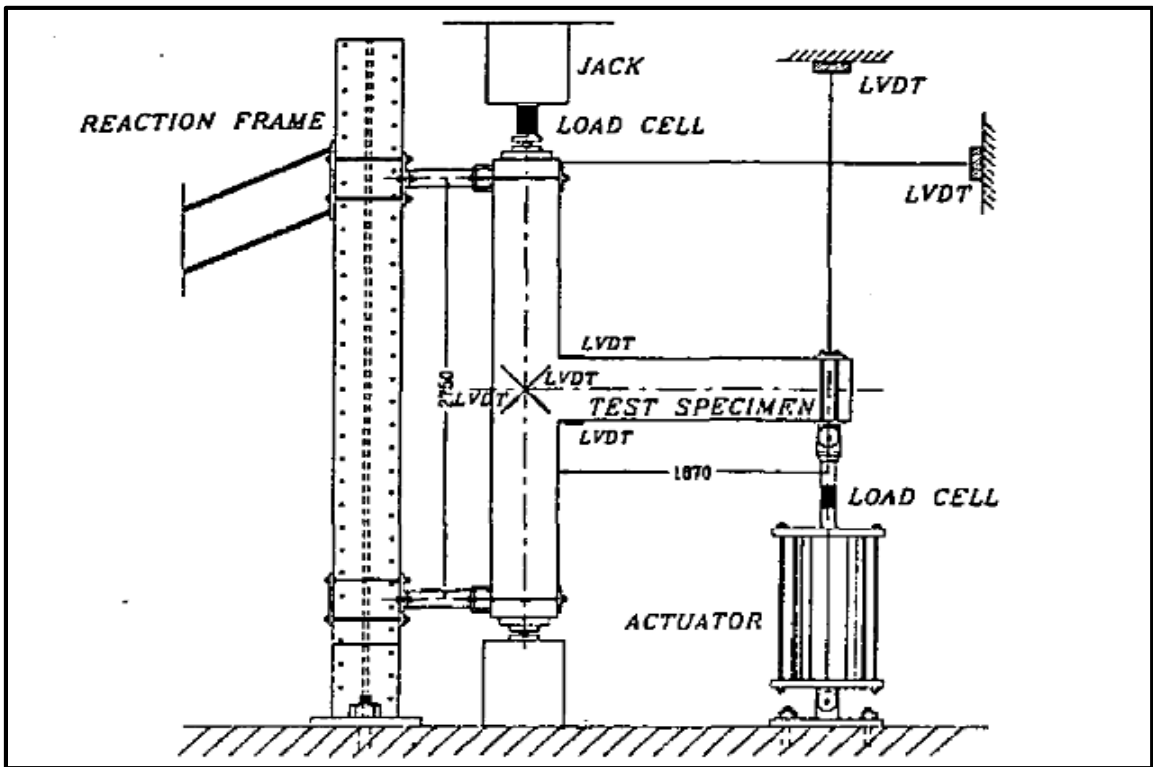


Figure 2.17: Test set-up (Ghobarah and Said, 2001)

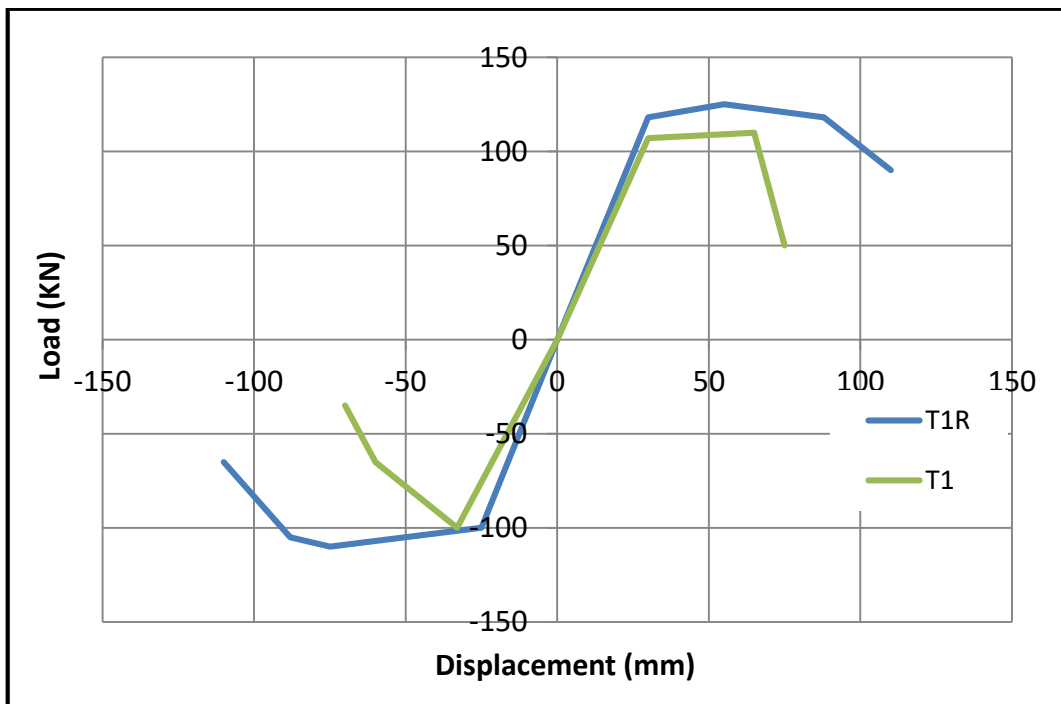


Figure 2.18: Load –deflection curve of specimens (Ghobarah and Said, 2001)

El-Amoury (2004) tested four full scale specimens. Control joint T-S1 and three joints with FRP: T-S1RR, T-S4R and T-S5. Control joint was designed according to pre-1970s codes to resist the gravity loads and light lateral loads. Dimensions and reinforcements of control joint are shown in Figure 2.19. After testing joints T-S1 T-S5 the spelled concrete was removed, a new concrete was poured in the joint area, then joint were prepared for retesting. These joints were renamed as T-S1RR and T-S4R. Techniques of retrofitting are shown in Figure 2.20. The specimens were placed in the testing machine as shown in Figure 2.21 and exposed to constant axial load on the column with value 600 kN. The results showed that the retrofitted specimens were more ductile than the un-retrofitted control specimen as shown in Figure 2.22

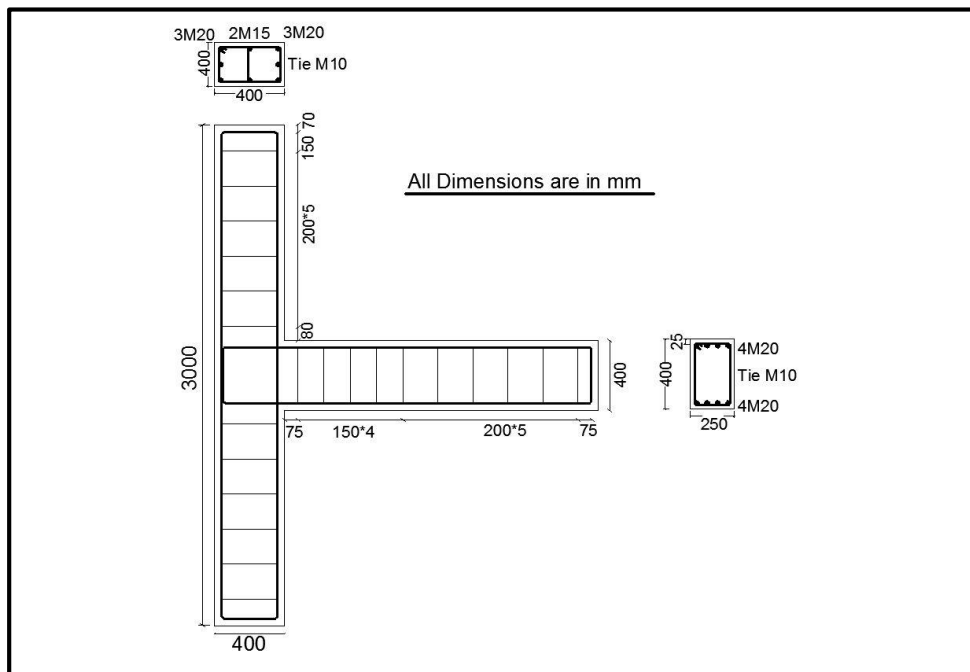


Figure 2.19: Reinforcement details control joint TS1 (El-Amoury, 2004)

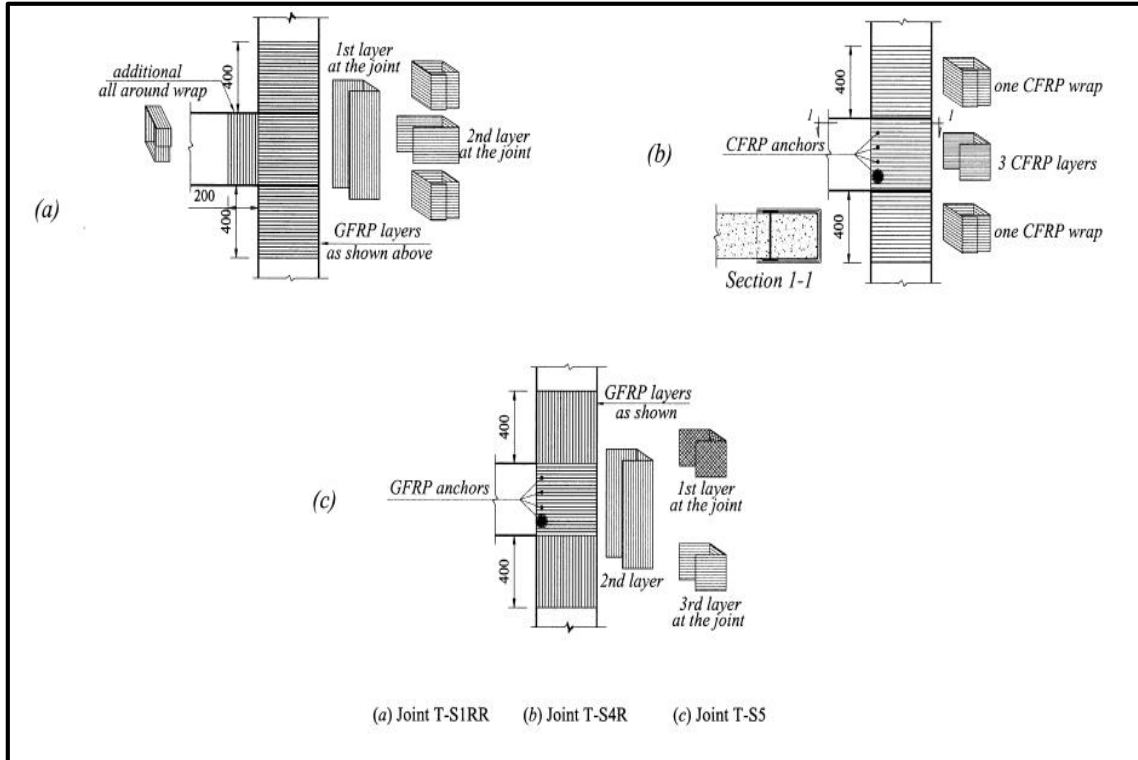


Figure 2.20: Proposed joint habitation scheme using FRP for specimens T-S1RR, T-S4R and T-S5 (El-Amoury, 2004)

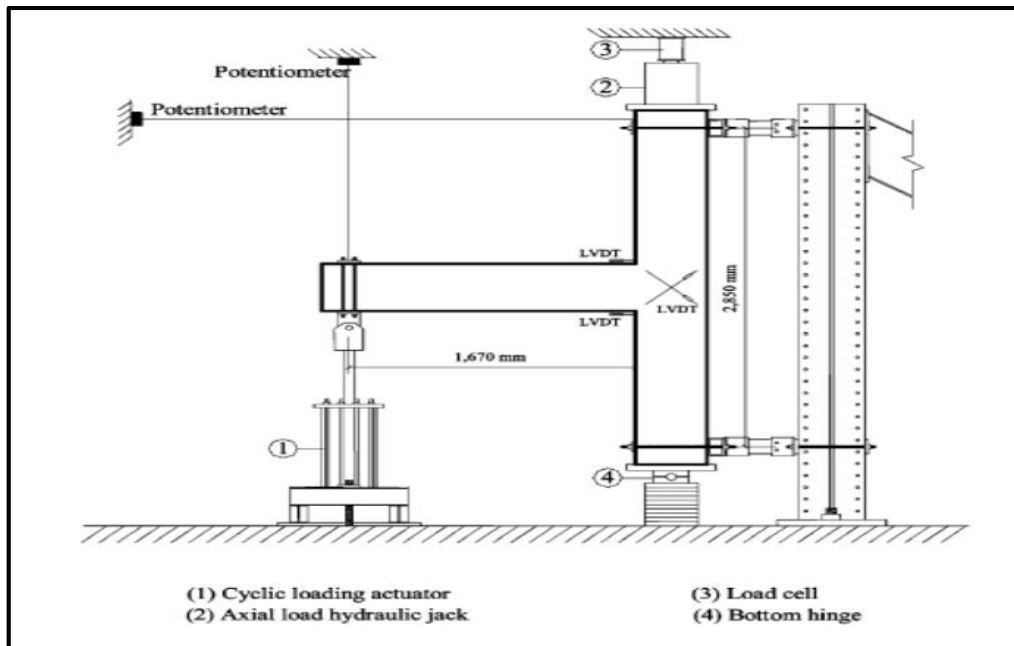


Figure 2.21: Test set-up (El-Amoury, 2004)

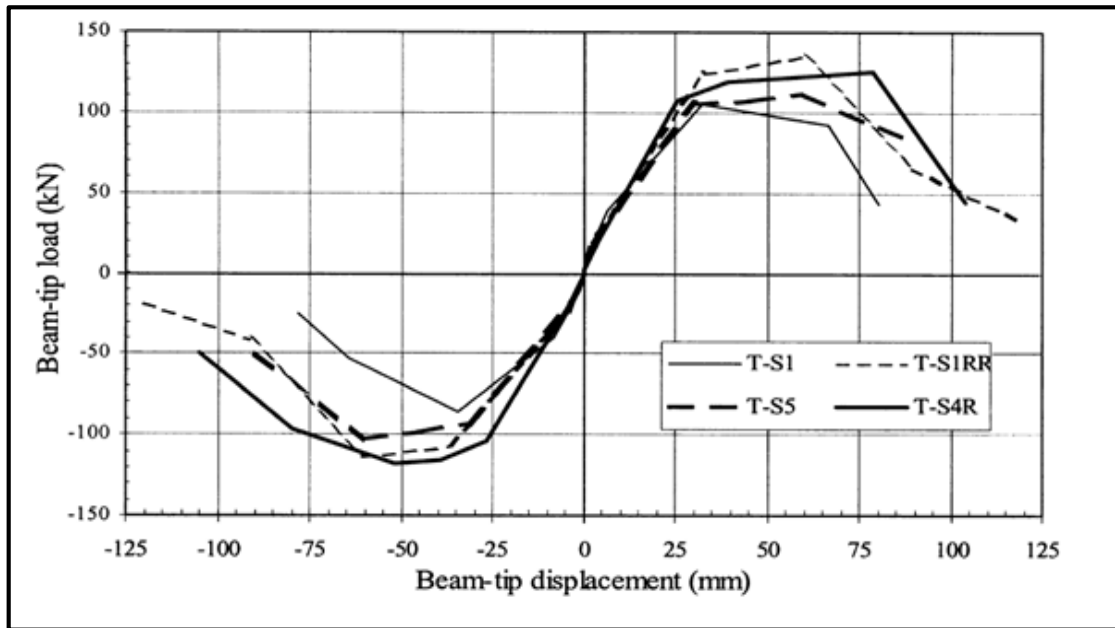


Figure 2.22: Load –deflection curve of specimens (El-Amoury, 2004)

Clyde et al. (2000) conducted experimental testing on a total of 4 half-scale specimens of exterior R.C beam-column joints. All specimens had the same dimensions and reinforcement details as shown in Figure 2.23. The differences between specimens are compressive strength and axial load on column as shown in Table 2.1. The specimens were subjected to constant axial load at column, and then tested under cyclic load at the beam tip. Results showed that there is a very slight variation in the peak lateral load sustained by each specimen. On the other hand, there is a distinct difference in ductility. The specimens with the lower axial load were 50% more ductile than the beam-column joints with higher column compression.

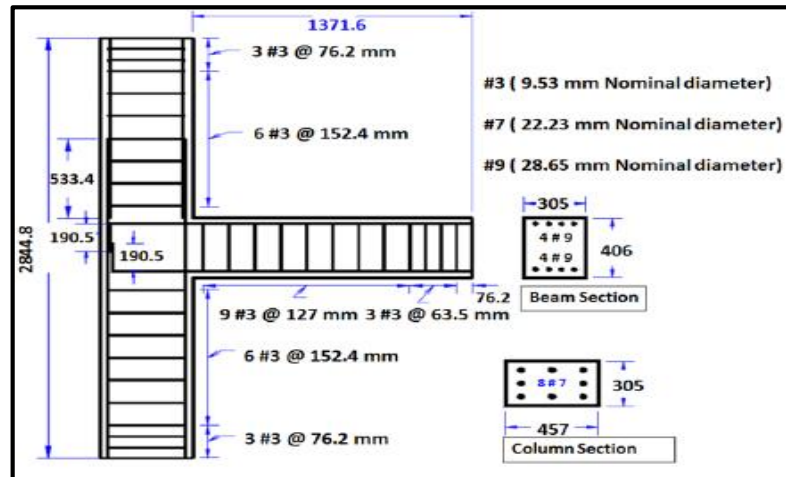


Figure 2.23: Dimensions and reinforcement details for the exterior R.C beam-column joint (Clyde et al., 2000)

Table 2.1: Properties of concrete and value of axial load at column for joints were tested by Clyde et al., (2000).

Test No.	Compressive concrete strength(f'_c)(MPa)	Axial load at column
2	46.2	$0.1f'_cA_g$
4	41	$0.25f'_cA_g$
5	37	$0.25f'_cA_g$
6	40.1	$0.1f'_cA_g$

Mahmoud et al. (2014) conducted experimental testing on a total of 10 half-scale specimens of exterior R.C beam-column joints. The details of control specimen are shown in Figure 2.24. Specimens are divided into three groups covering three possible configurations with different detailing of transverse reinforcement and different methods of retrofitting with CFRP as shown in Figure 2.25 and Figure 2.26. Results showed that using either CFRP fabric sheets or plates as strengthening material showed its efficiency in enhancing

the failure characteristics of the defected beam–column joints if the proper configuration was chosen. Also, using CFRP as a strengthening material led to increased ultimate capacity.

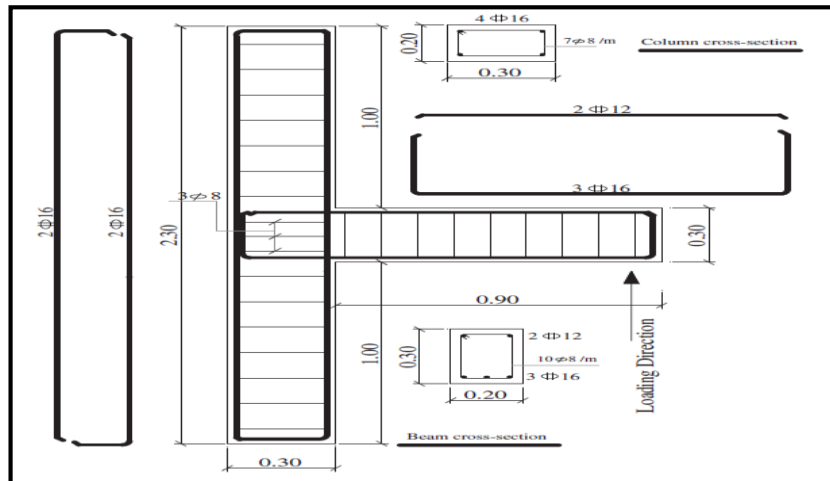


Figure 2.24: Dimensions and reinforcement details for the base control specimen (Mahmoud et al., 2014).

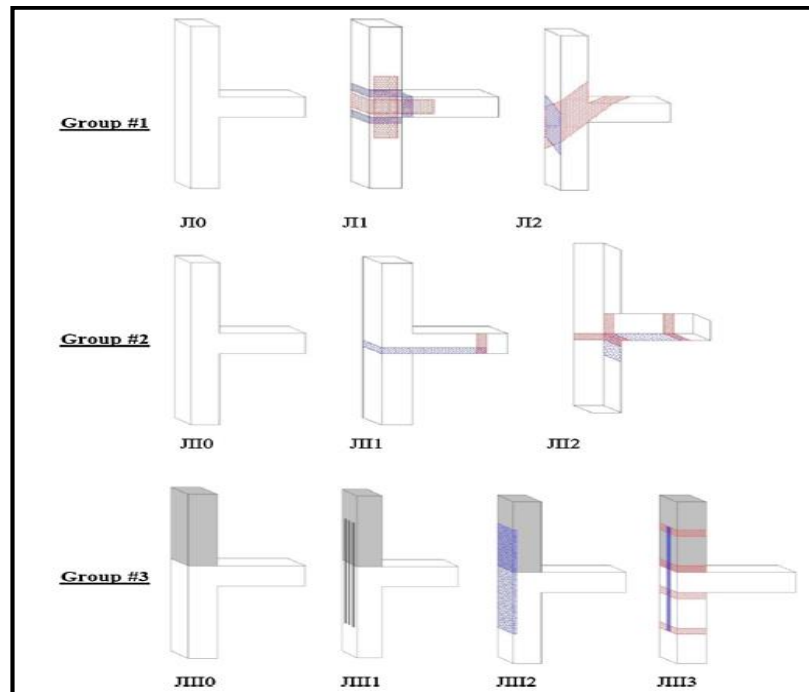


Figure 2.25: Schematic representation for the considered three groups (Mahmoud et al., 2014)

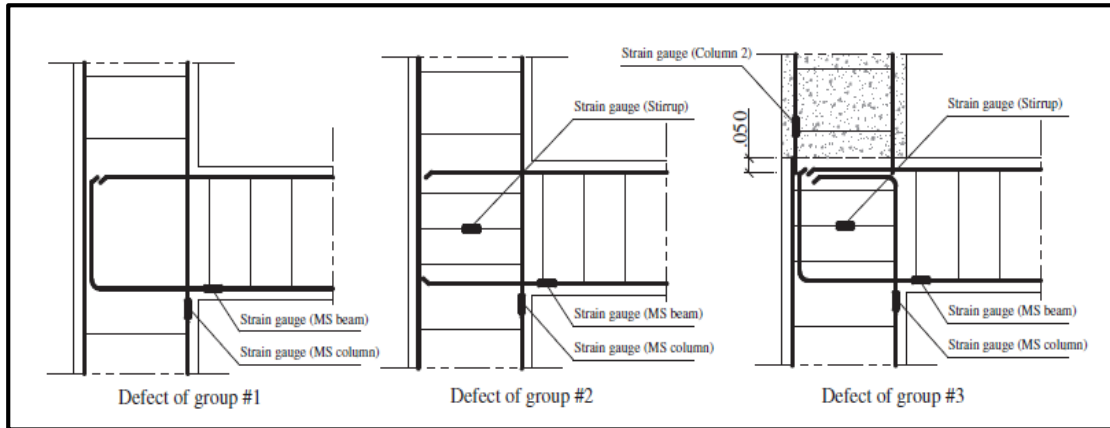


Figure 2.26: Details of joints in three groups (Mahmoud et al., 2014)

Al-Salloum et al. (2002) experimentally studied the effect of CFRP sheets on the ductility and strength of existing exterior R.C beam column joint which was designed in accordance to older ACI code (prior to 1970s). Half-scale specimen of exterior R.C beam column joint was constructed with dimensions and reinforcements as shown in Figure 2.27. Specimen was placed in the testing machine as shown in Figure 2.28. Then, it was exposed to cyclic lateral load, after damaging it; specimen was repaired through injecting epoxy into the cracks and externally bonding the specimens with CFRP sheets, as shown in Figure 2.29. Results show that CFRP sheets had improved the strength and the ductility of repaired specimen significantly. The strength of repaired specimen increased up to 75% with respect to its original (before repair) specimen. Also its ductility increased up to 40% with respect to its original specimen (before repair) as shown in Figure 2.30.

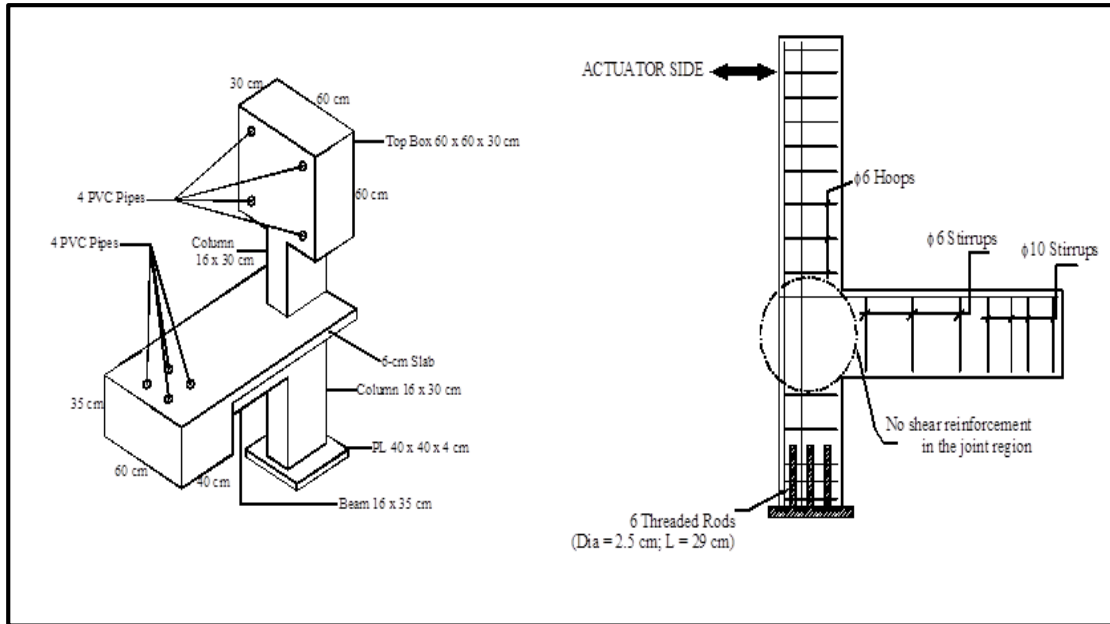


Figure 2.27: Dimensions and reinforcement details of all specimens (Al-Salloum et al., 2002)

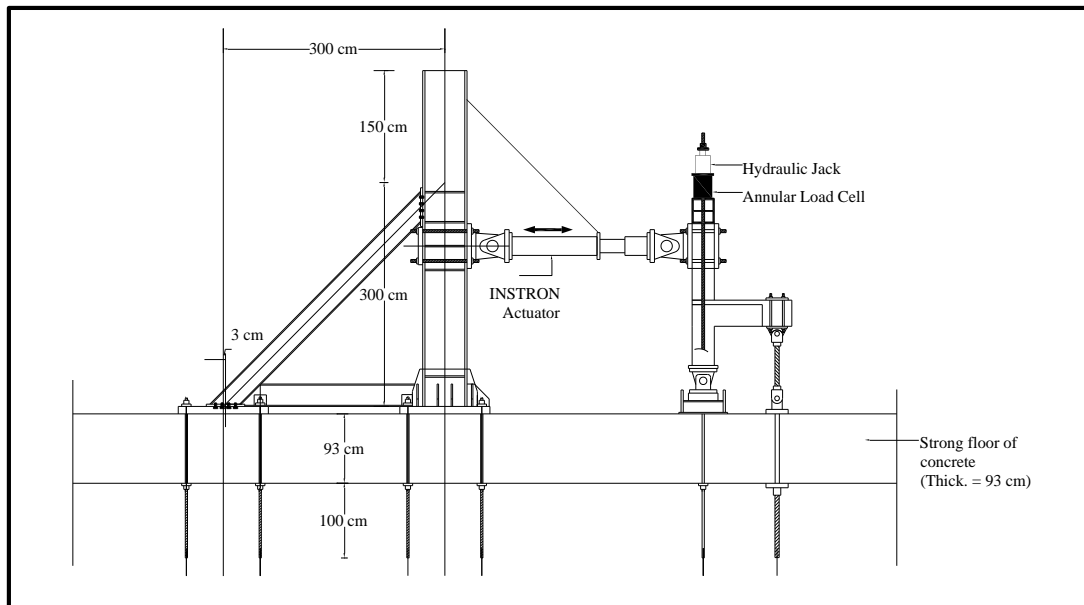


Figure 2.28: Test set-up (Al-Salloum et al., 2002)

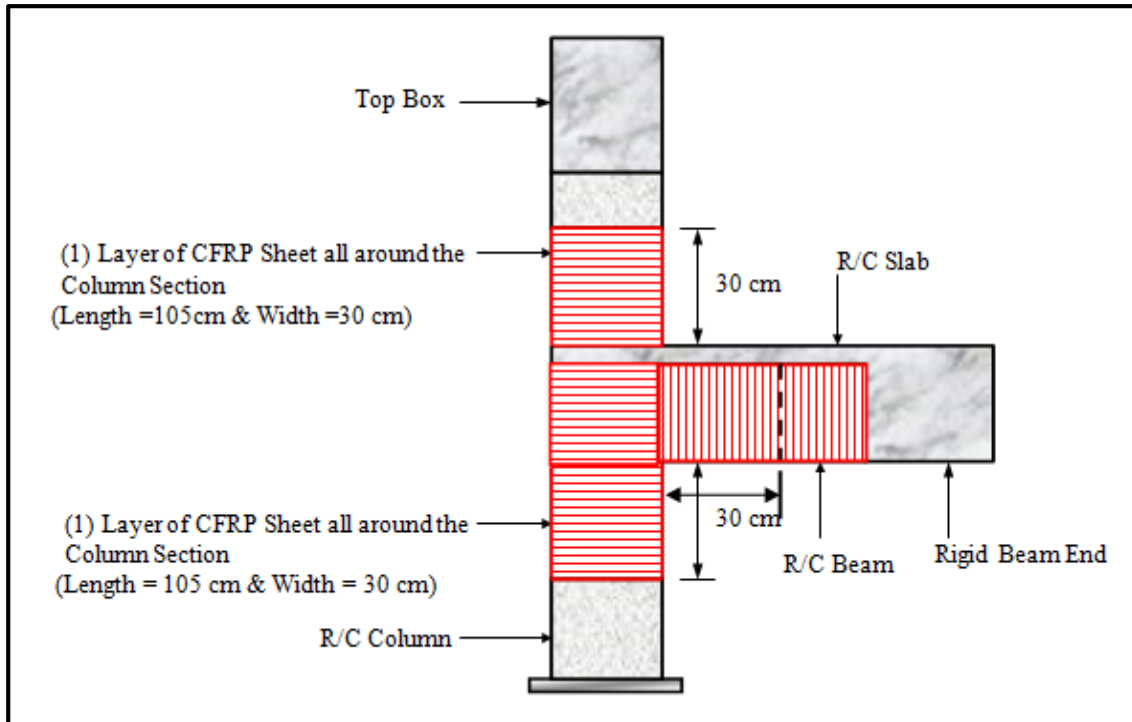


Figure 2.29: Schematic representation of FRP repaired specimen (Al-Salloum et al., 2002)

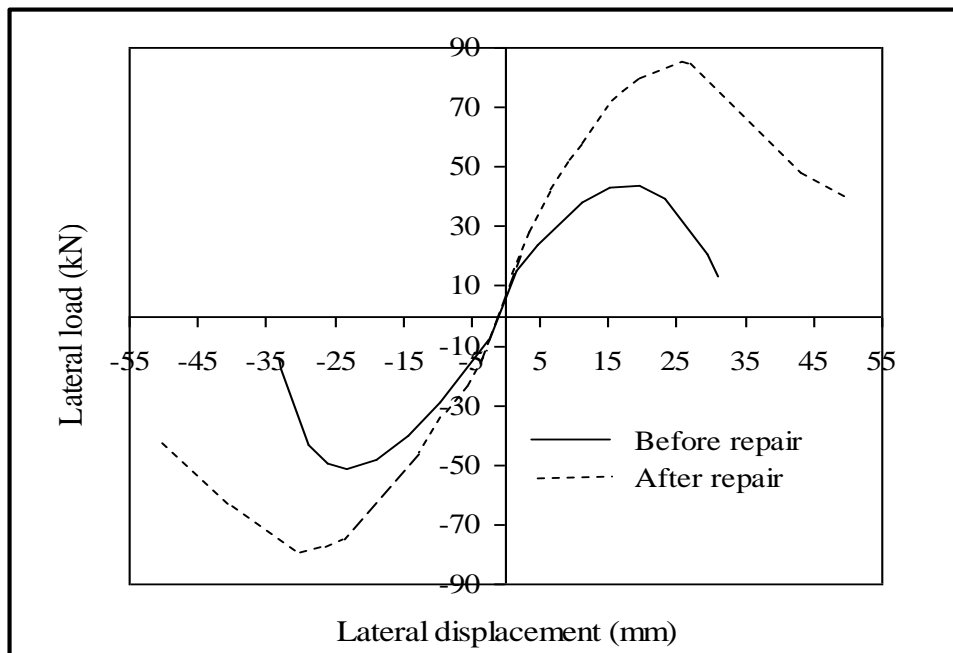


Figure 2.30: Load –displacement curves for specimen before and after repair (Al-Salloum et al., 2002)

2.4 Numerical investigation of strengthened structures using CFRP

Finite element (F.E.) offers attractive methodology of investigating structures effectively. Numerical investigation of the ability of CFRP sheets to maintain the composite action at the negative moment region for continuous composite girder was studied by Samaaneh et al. (2016). Results showed that the girder capacity and stiffness increase with the use of CFRP sheets bonded to the top of the concrete slab at the negative moment region. The increase in ultimate capacity is directly proportional to CFRP thickness up to certain thickness, when the negative moment capacity is close to the positive moment capacity. Numerical analysis of exterior beam-column joint was conducted by Bidgar and Bhattacharya (2014), and showed that the axial load on column makes a slight increase in the beam resisting moment capacity.

2.5 Summary

Based on the literature survey displayed in the previous sections, it is clear that many techniques and materials can be used to improve the behavior of R.C beam-column joint. One technique that could be used was steel jacketing. This technique was successfully used to improve strength and ductility of R.C beam column joint, but there were disadvantages in using this technique such as complicated working procedure and inner surface corrosion. The other techniques used to improve the behavior of joint was FRP strengthening. The use of FRP is a matter of adding low-weight, high tensile strength material to the structures. In addition, FRP has high

resistance against corrosion. At the same time, the use of FRP does not need concrete drilling and large volumes like other rehabilitation e.g. concrete jacketing.

After conducting a literature review on this subject, there are some important points that could be addressed:

- 1- Shear reinforcement within the joint is important to improve the ductility of these joints.
- 2- Steel jacketing such as wrapping around end of R.C beam and column has remarkable increase of ductility, but this technique required a complicated work, and suffers inner surface corrosion and heavy weight.
- 3- FRP technique may be considered better than steel jacketing due to high tensile strength, flexibility of application and resistance to corrosion. It should be noted that both strengthening techniques may require fire protection to improve their performance under fire conditions.
- 4- Two types of FRP may be used for retrofitting. Generally, sheets and wraps are used to resist shear and concrete confinement, while plates are used to resist flexure.
- 5- Axial force on column of a beam-column joint has a slight positive effect on the capacity of joint because this load reduces the cracks within the joint.

3 Modeling

3.1 Overview

Numerical investigation of structures offers an attractive technique of research due to low cost, quick results and ability to study several variables in depth. Therefore, a three-dimensional non-linear F.E. joint model is built using commercial software ABAQUS.

This chapter illustrates a general description of an R.C beam-column joint modeling, while the material parameters for this model will be shown in verification and parametric study chapters.

The modeling of the joint includes definition of materials, creation of parts, modeling of interfaces, selection of analysis regime, loading setup, boundary conditions and meshes as it will be discussed in the following subsections.

3.2 Material modeling

In this section, constitutive models for concrete and steel under compression and tension loads are presented. Also, a constitutive model for FRP lamina is included.

3.2.1 Concrete

Concrete is a non-homogenous material and hard to be modeled due to the change in material response at different stage of loading in both tension and compression. The effect of crushing and cracking on strength and stiffness of concrete can be modeled in different ways. One of these ways is to include

these effects in the stress-strain behavior of concrete in what is called the “Concrete Damaged Plasticity” model (CDP).

The CDP model available in ABAQUS software is used to model the complex nonlinear behavior of concrete. In this model, two main failure criteria are considered: tensile cracking and compressive crushing of the concrete material. Compression and tension behavior of concrete under uniaxial loading is shown in Figure 3.1.

The CDP allows capturing of strength and stiffness degradation through tension and compression damages parameters (d_t, d_c) of concrete as shown in Figure 3.1 (ABAQUS User Manual, 2013).

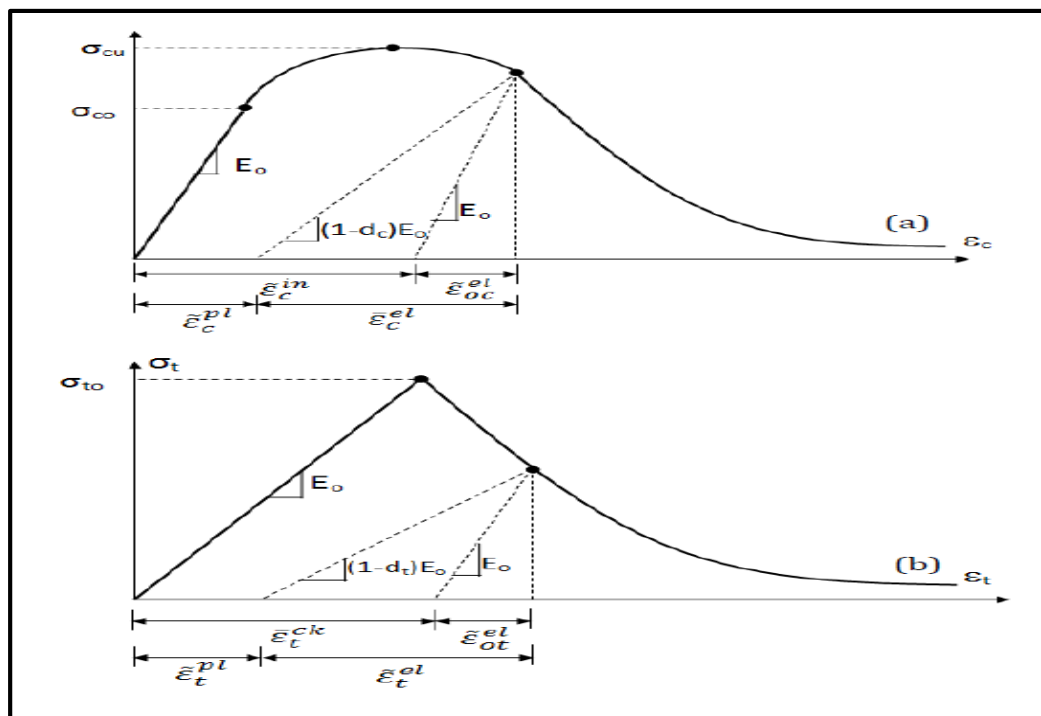


Figure 3.1: Response of concrete to uniaxial loading in (a) compression and (b) tension (ABAQUS User Manual, 2013)

As shown in Figure 3.1 the unloaded response of concrete specimen is weakened because the elastic stiffness of the material is damaged or

degraded due to cracks. The degradation of the elastic stiffness on the strain softening branch of the stress-strain curve is characterized by two damage variables, d_t and d_c , which can take values from zero to one. Zero represents the undamaged material where one represents total loss of strength. E_0 is the initial (undamaged) elastic stiffness of the material and $\varepsilon_c^{\sim pl}$, $\varepsilon_t^{\sim pl}$, $\varepsilon_c^{\sim in}$, $\varepsilon_t^{\sim in}$ are compressive plastic strain, tensile plastic strain, compressive inelastic strain and tensile inelastic strain respectively. The elastic relations under uniaxial tension (σ_t) and compression (σ_c) are taken into account in Equation (3.1) and Equation (3.3)

$$\sigma_t = (1 - d_t) \cdot E_0 \cdot (\varepsilon_t - \varepsilon_t^{\sim pl}) \quad (3.1)$$

$$\sigma_c = (1 - d_c) \cdot E_0 \cdot (\varepsilon_c - \varepsilon_c^{\sim pl}) \quad (3.2)$$

Where the effective tensile and compressive cohesion stress which are used to determine the yield point according to the yield function. The model makes use of the yield function according to Lubliner et al. (1989) with the modifications proposed by Lee and Fenves (1998). to account for different evolution of strength under tension and compression under multi-axial loading case. The yield function in 2-D plane stress (bi-axial) condition for

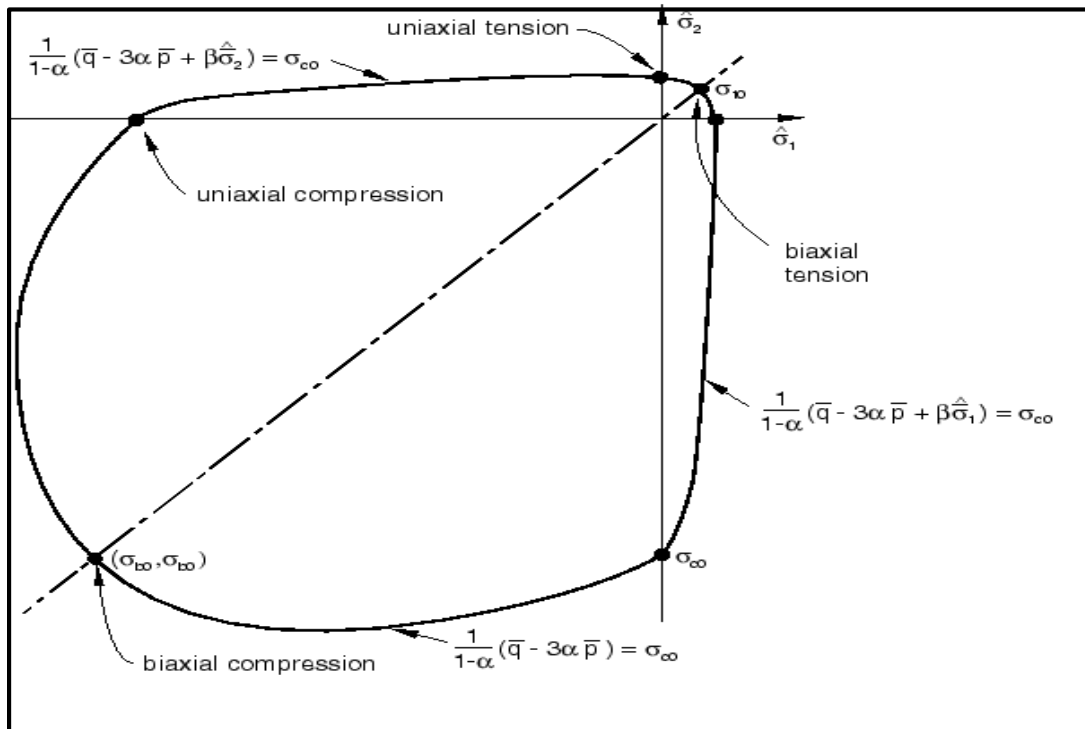


Figure 3.2: Yield surface in plane stress (ABAQUS User Manual, 2013)

Therefore, the material model captures the confinement effect that results from tri-axial stress data in concrete allowing improvement of compressive capacity in the case of hydrostatic stress state.

Uniaxial compression behavior

Generally, many researchers suggested equations that describe the behavior of concrete under uniaxial compression stress. However, most of these equations including the models suggested by Mander et al. (1988) and Yong et al. (1988) do not describe full stress-strain curve of concrete. For this reason, the stress-strain equation proposed by Saenz (1964) and validated by Asran et al. (2016) is used to define full behavior of concrete under uniaxial compressive stress as shown in Equation (3.3).

$$\sigma_c = \frac{E_c \varepsilon_c}{1 + (R + R_E - 2) \frac{\varepsilon_c}{\varepsilon_0} - (2R - 1) \left(\frac{\varepsilon_c}{\varepsilon_0}\right)^2 + R \left(\frac{\varepsilon_c}{\varepsilon_0}\right)^3} \quad (3.3)$$

$$E_c = 4700 \sqrt{f'_c} \quad (3.4)$$

$$R = \frac{R_E (R_\sigma - 1)}{(R_\varepsilon - 1)^2} - \frac{1}{R_\varepsilon} \quad (3.5)$$

$$R_E = \frac{E_c}{E_0} \quad (3.6)$$

$$R_\sigma = \frac{f'_c}{\sigma_f} \quad (3.7)$$

$$R_\varepsilon = \frac{\varepsilon_f}{\varepsilon_0} \quad (3.8)$$

$$E_0 = \frac{f'_c}{\varepsilon_0} \quad (3.9)$$

Where:

σ_c : Concrete compressive stress (MPa)

E_c : Modulus of elasticity of concrete (MPa)

E_0 : Secant modulus of concrete (MPa)

f'_c : Maximum compressive strength of concrete (MPa)

ε_c : Compression strain

ε_0 : Strain corresponding to f'_c which is equal approximately 0.0025 as reported by Hu (1989).

ε_f : Maximum strain.

σ_f : Stress at maximum strain (MPa).

R : Ratio relation

R_E : Modular ratio.

R_σ : Stress ratio, which is equal 4 as reported by Hu (1989).

R_ε : Strain ratio, which is equal 4 as reported by Hu (1989).

Tension behavior

The stress-strain curve for concrete under tension is tested experimentally by Sharif et al. (2015) for concrete 25MPa. The maximum tensile stress was reported as 2.9MPa corresponding to modulus of rupture of concrete which is equal $0.62\sqrt{f_c}$ according to ACI 318, after this load, the flexural capacity of concrete started to decrease until ultimate strain reach 0.003. Asran et al. (2016) used this equation for definition of tension behavior of concrete in ABAQUS, also assuming linear descending of tension. In this model, an assumption of maximum tensile strain of 0.003 under flexural test for all types of concrete is considered. This assumption is used due to lack of sufficient information about ultimate strain in tension of concrete from experimental tests which will be used for verification purpose.

Modeling of concrete needs many parameters according to CDP in order to capture the behavior of concrete accurately. These parameters are summarized below:

- 1- Young's Modulus (E_c): Modulus of elasticity of concrete (MPa).
Equation (3.4).
- 2- Poisson's Ratio (ν) : the amount of transversal elongation divided by the amount of axial elongation. A value of 0.2 is used in the model.
- 3- Dilation angle (internal friction angle). In other words, it is the angle measured in the p–q plane (hydrostatic pressure stress - Mises equivalent effective stress) at high confining pressure as shown in Figure 3.3 (ABAQUS User Manual, 2013). In simulations usually $\psi = 36^\circ$ or 40° is recommended by Kmiecik and Kaminski (2011).

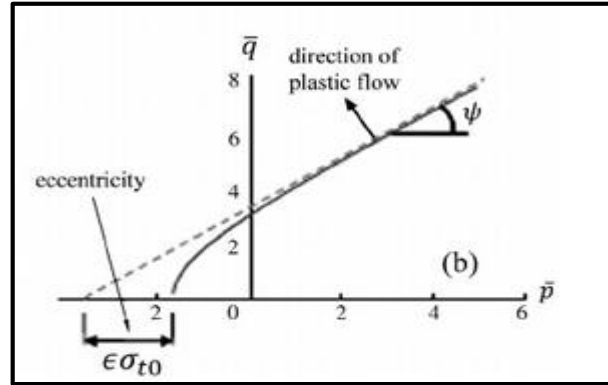


Figure 3.3: Dilatation angle and eccentricity (ABAQUS User Manual, 2013).

- 4- Eccentricity: parameter that defines the rate at which the flow potential function approaches the asymptote in p-q plane. The CDP model recommends assuming this value equal 0.1 (ABAQUS User Manual, 2013). When this value equals 0 then the surface in the meridian plan becomes straight line similar to the classic Drucker-Prager hypothesis as shown in Figure 3.3 (ABAQUS User Manual, 2013).
- 5- f_{b0}/f_{c0} : bi-axial compression stress divided by uni-axial compression stress. Kupfer (1969) conducted experimental test and obtained that this ratio is equal to 1.16.
- 6- K: represents the ratio of the distances between the hydrostatic axis and both the compression and the tension meridians in the deviatoric cross section which is equal 2/3 which is recommended by ABAQUS User Manual (2013). This factor is used to convert the shape of cross section of failure surface from circle to combination of three mutually tangent ellipses as shown in Figure 3.4 (ABAQUS User Manual, 2013). This shape was formulated by William and Warkne (1975).

compressive stiffness upon load reversal. The experimental observation in most quasi-brittle materials, including concrete, is that the compressive stiffness is recovered upon crack closure as the load changes from tension to compression. On the other hand, the tensile stiffness is not recovered as the load changes from compression to tension once crushing micro-cracks have developed. This behavior, which corresponds to $\omega_t = 0$ and $\omega_c = 1$, is the default used by ABAQUS. Uniaxial load cycle (tension-compression-tension) with default values for the stiffness recovery factors: to $\omega_t = 0$ and $\omega_c = 1$ as shown in Figure 3.5 (ABAQUS User Manual, 2013).

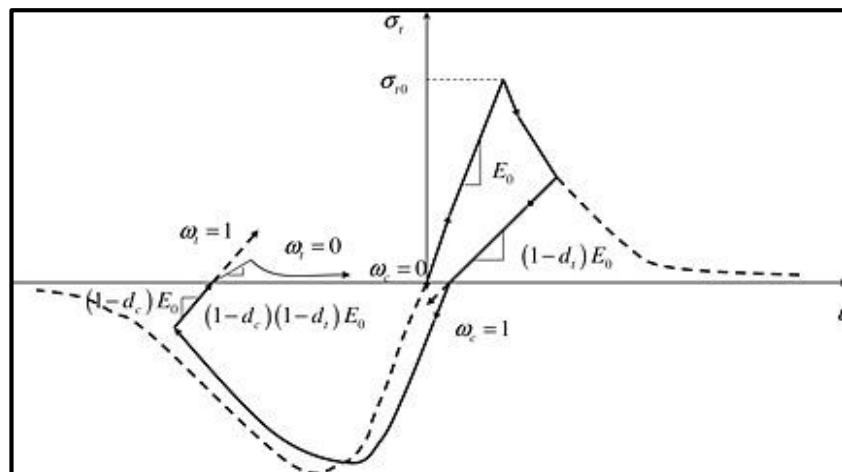


Figure 3.5: Uniaxial load cycle (tension-compression-tension) assuming default values for the stiffness recovery factors: to $\omega_t = 0$ and $\omega_c = 1$ (ABAQUS User Manual, 2013)

3.2.2 Steel

Generally, steel is initially linear-elastic for stress less than the initial yield stress. At ultimate tensile strain, the reinforcement begins to neck and

strength is reduced. At a maximum strain, the steel reinforcement fractures and load capacity is lost, Figure 3.6.

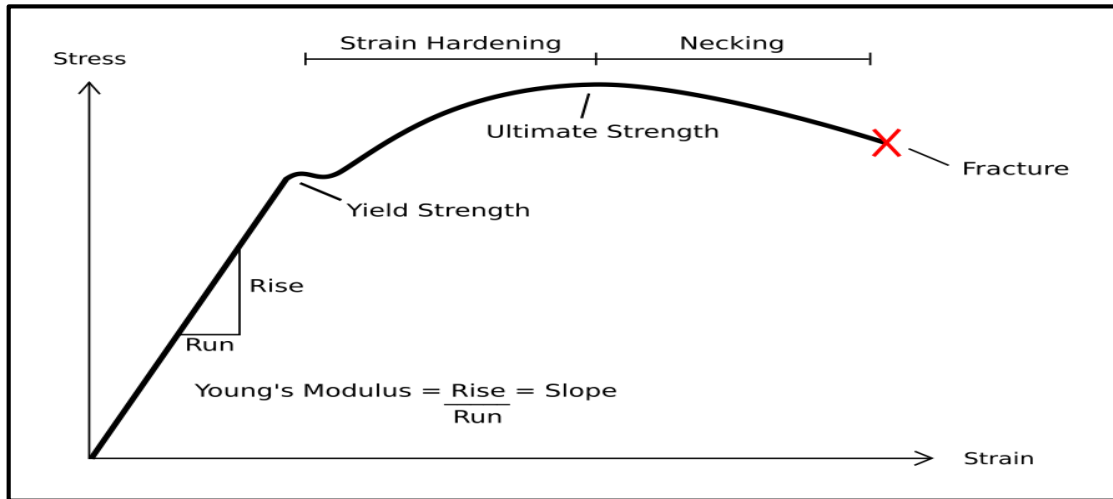


Figure 3.6: Typical stress-strain curve of steel

An isotropic behavior was used to model the reinforcement and loading plate. This means that the yield surface changes size uniformly in all directions such that the yield stress increases (or decreases) in all stress directions as plastic straining occurs.

3.2.3 Carbon Fiber-Reinforced Polymer (CFRP)

Unidirectional FRP sheets were assumed to strengthen the R.C beam-column joint model. The fibers provide both load carrying capacity and stiffness to the FRP composite sheet while the matrix is to ensure distribution of the load among all fibers and to protect the fibers themselves from the environment. The fiber behavior is assumed linear elastic up to failure with rupture failure. A lamina linear elastic element is used to model CFRP as shown in Figure 3.7.

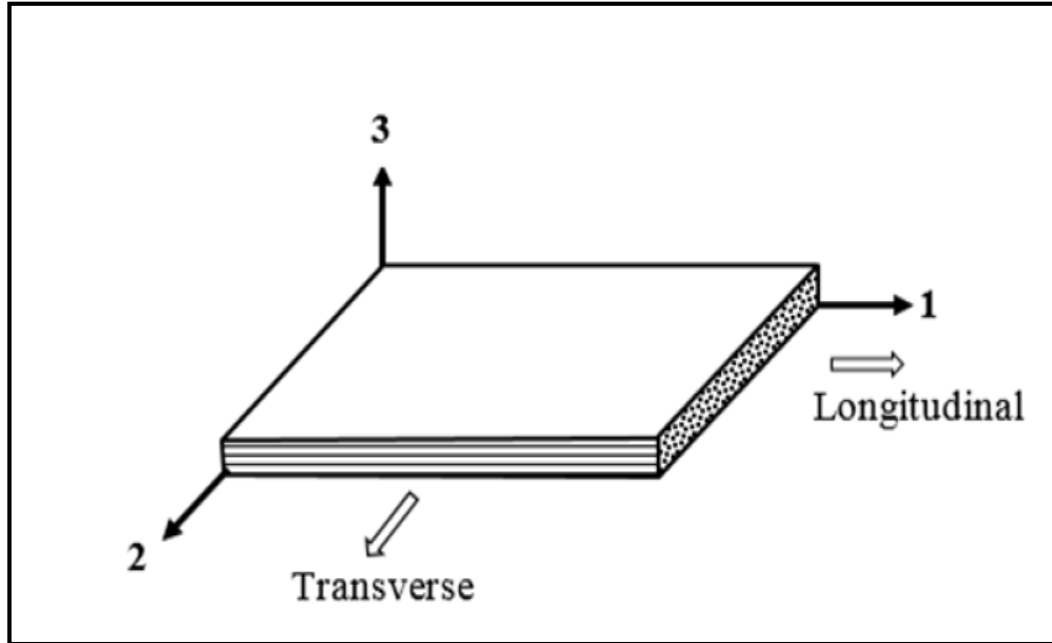


Figure 3.7: Schematic of unidirectional FRP lamina

The mechanical properties for the combined CFRP sheet and adhesive are evaluated using equations below as proposed by Mallick (1993). Those values will be discussed next chapter.

$$E_1 = E_f V_f + E_a (1 - V_f) \quad (3.10)$$

$$E_2 = E_f E_a / (E_a V_f + E_f (1 - V_f)) \quad (3.11)$$

$$G_{12} = G_{13} = G_f G_a / (G_a V_f + G_f (1 - V_f)) \quad (3.12)$$

$$G_{23} = E_2 / 2(1 + \nu_{23}) \quad (3.13)$$

$$\nu_{23} = \nu_f V_f + \nu_a (1 - V_f) \quad (3.14)$$

$$\sigma_{co} = V_f \sigma_u + ((1 - V_f) E_a / E_f) \sigma_u \quad (3.15)$$

where:

E_1 : Elastic modulus in the longitudinal direction

E_2 : Elastic modulus in the transverse direction

G_{12} and G_{13} : Plane shear modulus

G_{23} : Normal to the plane shear modulus

ν : Poisson's ratio

σ_{co} : Ultimate tensile strength

E_f : Elastic modulus of CFRP

V_f : Volume fraction of CFRP is provided by the manufacturer

E_a : Elastic modulus of adhesive material

G_f : Shear modulus of CFRP

G_a : Shear modulus of adhesive material

3.3 Modeling of interfaces

Different contact models could be used to model the interfacial region depending on the actual behavior and degree of accuracy. Tie contact is used between parts of beams and column. This type of contact is also used between loading plate and beam and this contact considers perfect bond between two surfaces to make the translational and rotational motion as well as all other active degrees of freedom equal for a pair of surfaces. At the same time, the contact between reinforcement and concrete is assumed perfectly bonded surfaces with no slip. This is justified by the enough development length of rebar and available friction between them, so embedded region contact is used to simulate the perfect bond. In this contact, the host elements are used to constrain the translation degrees of freedom of the embedded body. Cohesive contact is used to simulate the behavior of adhesive material between concrete and CFRP as will be discussed later. This contact can be used to model the delamination and slip at interfaces directly interns of traction versus separation.

3.4 Parameters for cohesive contact

Both separation-traction and force-slip constitutive curves are needed to model the cohesive behavior. Many models exist with various degrees of complexity. The linear-brittle model, developed by Neubauer and Rostasy (1999), does not consider the softening behavior, while Nakaba et al. (2001) and Savioa et al. (2003) considers softening by ascending and a descending branches of bond-slip curve. However, a bilinear bond-slip curve is presented by Monti et al (2003). Lu et al. (2005) proposed a “Precise model” which is very complicated model. All these models are shown in Figure 3.8.

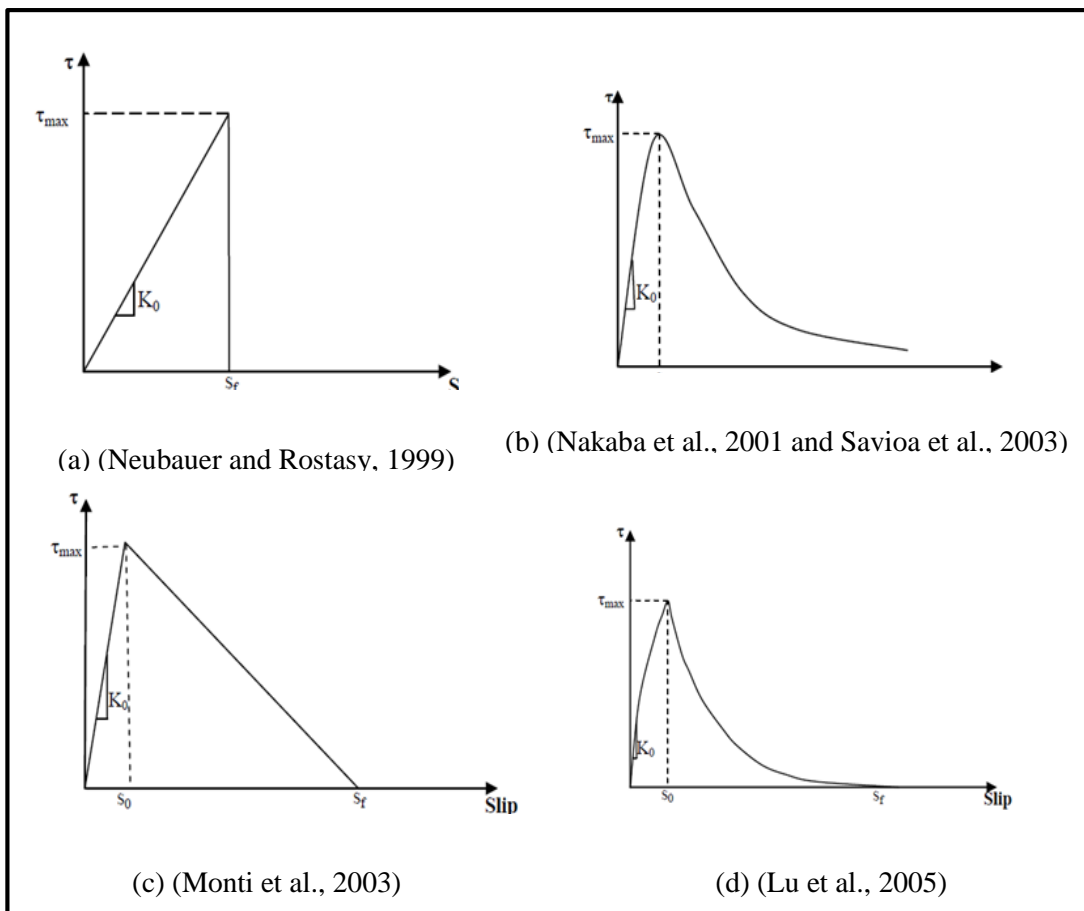


Figure 3.8: Bond-slip curves models

The initial shear stiffness (K_0) is proposed by many researchers. The initial stiffness according to Lu et al. (2005) was assumed to be related to the properties of the adhesive in contact with the concrete as well as the initial layer of the concrete substrate, as documented by Equation (3.16).

$$K_0 = \frac{1}{\frac{t_a}{G_a} + \frac{t_c}{G_c}} \quad (3.16)$$

Where:

K_0 : Initial shear stiffness

G_a : Shear modulus of adhesive

t_a : Adhesive thickness

G_c : Shear modulus of concrete

t_c : Initial layer of the concrete substrate thickness

Obaidat et al. (2011) developed an equation that relates adhesive thickness and shear modulus of adhesive with initial shear stiffness as shown in Equation (3.17). Also he developed an equation that relates shear modulus of adhesive and tensile strength of concrete with shear strength as shown in Equation (3.18). On the other hand, the maximum normal strength can be considered to be equal tensile strength of concrete (Obaidat et al., 2011). However, normal stiffness of cohesive zone is generally larger than the shear stiffness of cohesive zone, because the shear stiffness is related to shear modulus of adhesive not with tensile modulus of adhesive material. To be more conservative, normal stiffness will be considered equal to shear stiffness.

$$K_0 = 0.16 \frac{G_a}{t_a} + 0.47 \quad (3.17)$$

$$t_{max} = 1.46G_a^{0.165} f_{ct}^{1.033} \quad (3.18)$$

Where:

K_0 : Initial shear stiffness (GPa)

G_a : Shear modulus of adhesive (GPa)

t_a : Adhesive thickness (mm)

f_{ct} : Tensile strength of concrete (MPa)

t_{max} : Shear strength for cohesive interaction (MPa)

In this thesis, the model proposed by Neubauer and Rostasy (1999) is used to model the cohesive contact with shear stiffness and shear strength as proposed by Obaidat et al. (2011).

3.5 Analysis type, loading and boundary conditions

Pseudo-dynamic analysis is utilized to obtain the full behavior and to avoid convergence problem in ABAQUS. Therefore, load is applied with very large time steps in order to converge to the static solution. Using the dynamic analysis instead of static analysis helps in convergence of highly non-linear behavior of cohesive contact in ABAQUS.

Schematic view of boundary conditions and loads for the model are shown in Figure 3.9. The top end of the column is restrained by a rigid surface allowing the end to behave as pin, while the bottom end is restrained by a rigid surface allowing the end to behave as roller in the Y-direction. It should be noted that these rigid surfaces restrain the in-plane movement of the column ends. Such restraint conditions are generally assumed for similar cases in the literature (Chaudhari et al., 2014). A constant axial load (as

reported in experimental tests in the next chapter) is initially applied on column. This is followed by an incremental monotonic load applied at tip of beam. The beam load is applied through displacement control at rate of 2 mm/s at the tip of beam.

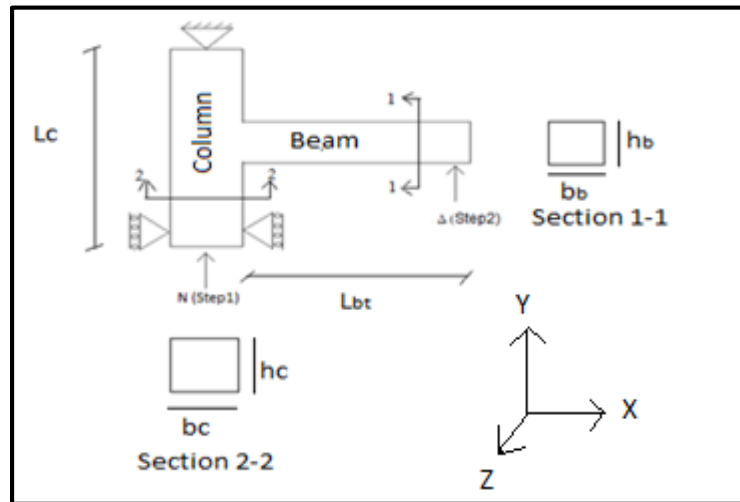


Figure 3.9: Location of loads and boundary conditions

3.6 Meshing type

The components of beam–column joint are meshed individually on part–by–part basis instead of using global or sweep mesh. Eight–noded linear brick element (C3D8R) is used to model the solid elements; concrete and loading plate. A 2–node linear 3–D truss element is used to model main and transfers reinforcement (T3D2), whereas 4–noded shell element (S4R) used to model CFRP as shown in Figure 3.10.

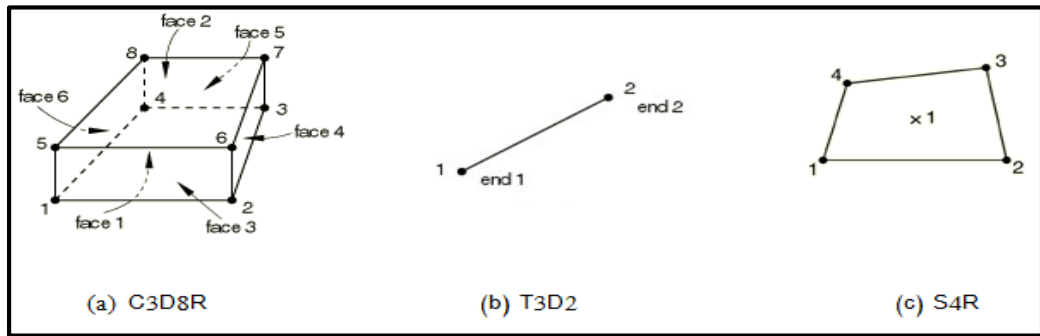


Figure 3.10: Finite Element Mesh Type

4 Model verification

4.1 Overview

To validate the results from the finite element model, data from experimental tests are used. However, there are many experiments concerning R.C beam-column joints. Many of these experiments were not reported in details and this makes it difficult to model them. A set of clearly reported experiments are selected to validate the results of F.E. models. Seven independent tests reported in the literature are used to establish the verification. One of them is an exterior R.C beam-column joint subjected to cyclic loading (displacement control) which was tested by Clyde et al. (2000). In addition, three of the exterior R.C beam-column joints are subjected to monotonic loading (load control) and tested by Mahmoud et al. (2014). The remaining three are the exterior R.C beam-column joints subjected to cyclic displacement and tested by El-Amory (2004).

4.2 Sensitivity study

In order to eliminate the effect of mesh size on the results, a sensitivity study was conducted. Materials parameters are assumed as reported by Clyde et al. (2000). Different global mesh sizes were considered (15 mm through 45mm). The results show that the resulting curves stabilize approximately for meshes of range sizes 15-35 mm as shown in Figure 4.1. However a mesh size of 15 mm is used in all subsequent models to prevent divergence error in ABAQUS which occurs in many models of 35/25 mesh sizes.

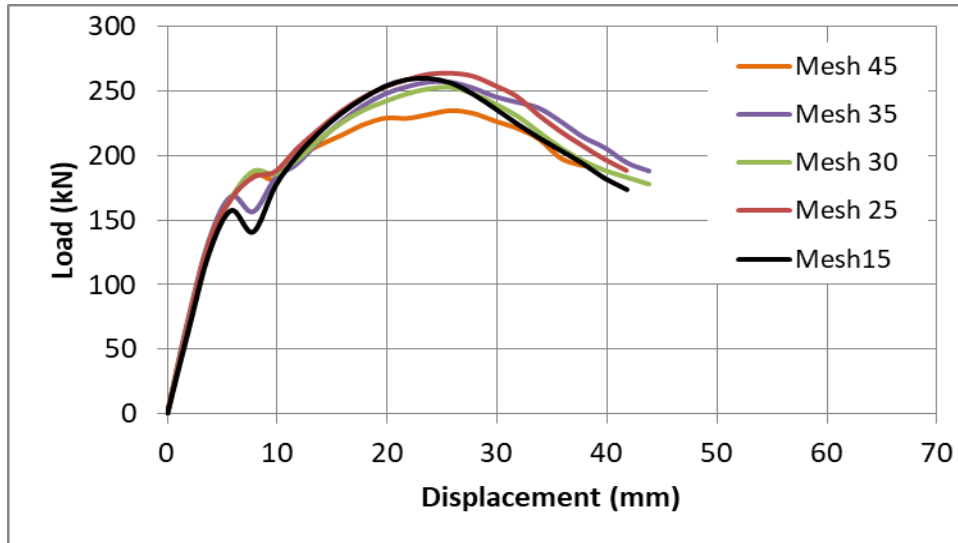


Figure 4.1: Effect of mesh size

4.3 Clyde et al. (2000) test

Dimensions and reinforcement details for tests done by Clyde et al. (2000) are illustrated in Chapter 2 in this thesis in Figure 2.23. The reported data on concrete property is the compressive strength only which is equal 46.2 MPa. Table 4.1 shows steel properties as reported by Clyde et al. (2000).

Table 4.1: Properties of reinforcement bars which were used by Clyde et al. (2000).

Bar name	Diameter (mm)	Cross sectional area (mm ²)	Yield strength (MPa)	Ultimate strength (MPa)
#9	28.65	645	454.4	746
#7	22.225	387	469.5	741.9
#3	9.525	71	427.5	654.3

The specimen was subjected to constant axial load ($0.1A_g f'_c$) at column, and then it is tested under cyclic load at the beam tip.

Table 4.2 shows the main parameters for defining the behavior of concrete model in ABAQUS. However, Figure 4.2a shows uniaxial compression

stress-inelastic strain curve of concrete, while Figure 4.2b shows tension stress-cracking strain curve of concrete with. Also, Figure 4.2c shows compression damage parameter versus inelastic strain curve, while Figure 4.2d shows tension damage parameter versus cracking strain curve.

Table 4.2: Parameters of concrete used in test of Clyde et al.(2000) ($f_c = 46.2\text{MPa}$)

$E_0(\text{MPa})$	ν	ψ	e	f_{b0}/f_{c0}	K
30165	0.2	36°	0.1	1.16	0.67

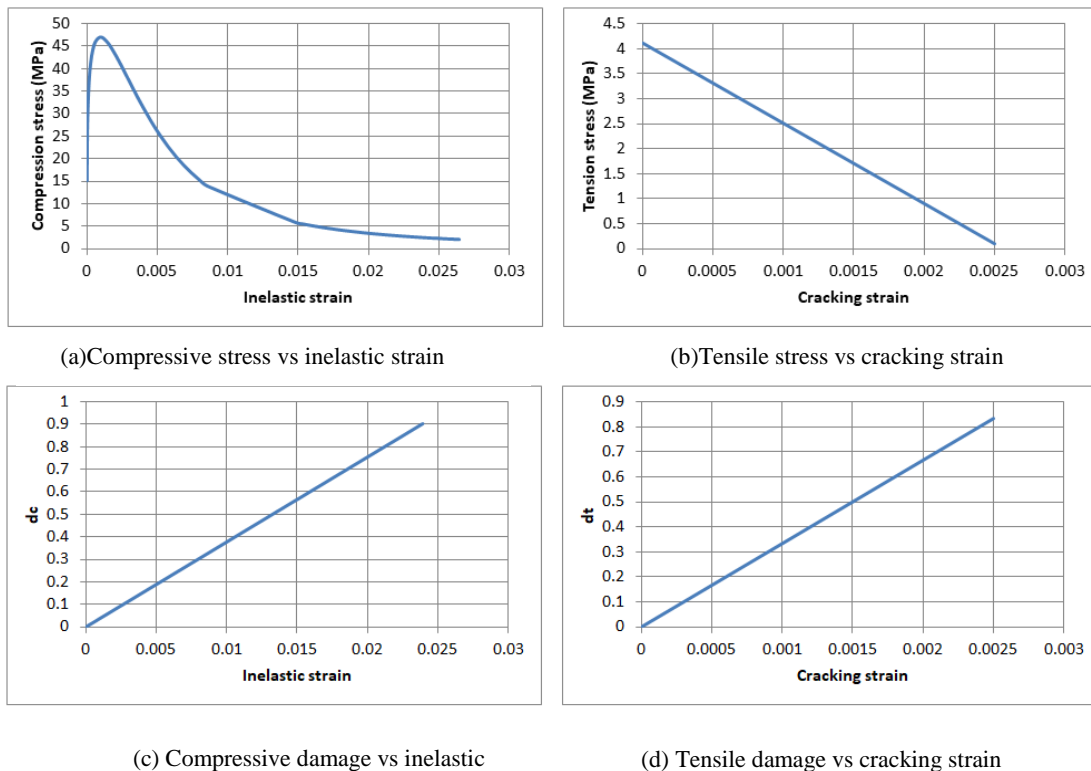


Figure 4.2: Curves needed for define CDP model in ABAQUS for test by Clyde et al. (2000)

Three types of steel are used in this model. The mechanical properties for each type are shown in previous Table 4.1. A bi-linear stress strain diagram is used for defining the steel with slope hardening equals $0.01E_s$ as assumed by Elmezaini and Ashour (2015) on their verification on R.C beam. The typical stress-plastic strain diagram for each type of bars is shown in Figure 4.3. All steels have Young's Modulus ($E = 205\text{GPa}$) and Poisson's Ratio ($\nu = 0.3$).

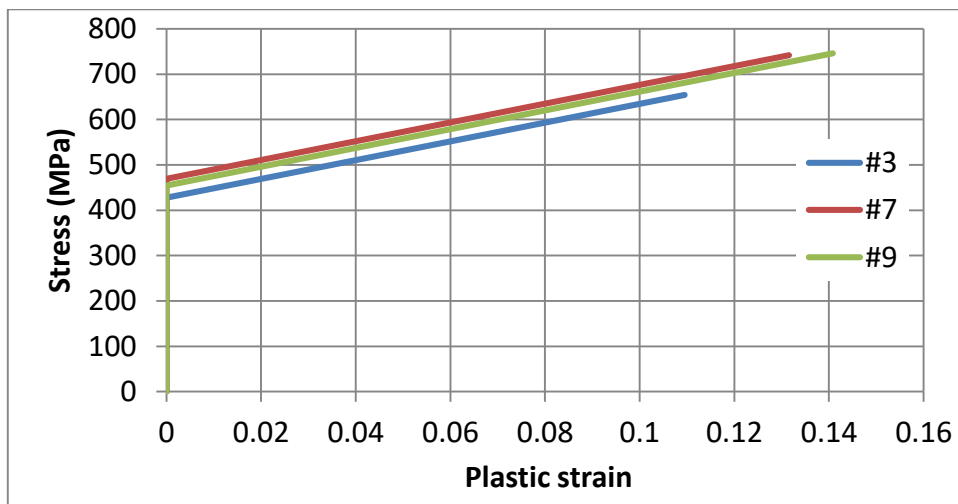


Figure 4.3: Stress –plastic strain diagram for steel which is used for test by Clyde et al. (2000).

In order to validate the accuracy and reliability of the numerical model, the numerical load-deflection curve due to monotonic loading is compared with the envelopes of the loading hysteresis loops from the experimental test conducted by Clyde et al. (2000). It should be noted that this method of comparison between numerical and experimental results was adopted by many researchers (Najafgholipour et al., 2017 and Alfarah et al., 2017). Comparison between F.E. and experimental results are shown in Figure 4.4.

It can be seen that the F.E. model captures the overall behavior quite satisfactorily.

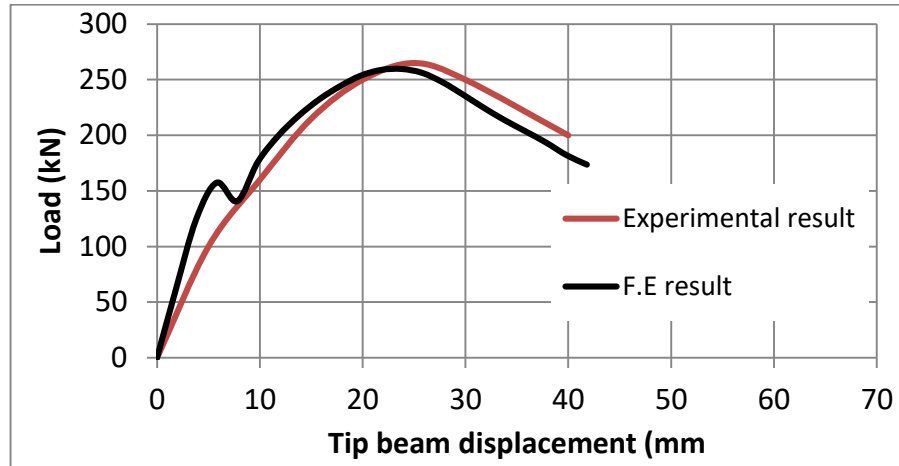


Figure 4.4: Comparison between experimental and F.E. results for test by Clyde et al. (2000).

4.4 Mahmoud et al. (2014) tests

Three specimens tested by Mahmoud et al. (2014) are chosen for the verification, two specimens (J0 and JI0) without CFRP, whereas the third specimen (JI1) with CFRP. The documented properties of steel, concrete, CFRP and epoxy are summarized in Tables 4.3 to 4.6, respectively.

Table 4.3: Properties of reinforcement bars used by Mahmoud et al. (2014)

Bar type	Diameter (mm)	Cross sectional area (mm ²)	Yield strength (MPa)
Ø16	16	200.96	400
Ø12	12	113.04	400
Ø8	8	50.24	240

Table 4.4: Properties of concrete for joints tested by Mahmoud et al. (2014)

Specimen	Compressive concrete strength (MPa)
J0	25.4
J10	24.8
J11	25.1

Table 4.5: Properties of FRP sheet used by Mahmoud et al. (2014)

Fiber type	Ultimate tensile strength (MPa)	Ultimate strain (%)	Modulus of elasticity (MPa)	Thickness (mm)
CFRP	3500	1.5	230000	0.13

Table 4.6 Properties of epoxy used by Mahmoud et al. (2014)

Epoxy type	Tensile strength (MPa)	Tensile modulus (MPa)	Ultimate elongation (%)
Epoxy for installing CFRP	30	21400	4.8

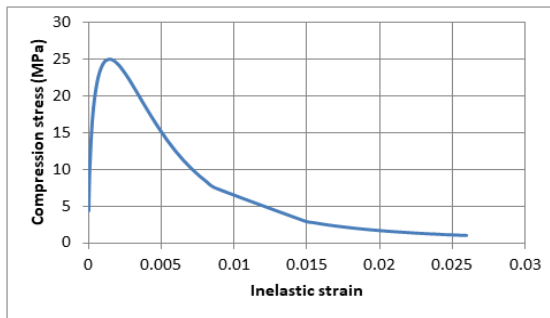
The specimens were tested monotonically under static load at the beam tip (load control). The load is increased at a rate of (5-10 kN/min) until failure, while a constant axial load of 200 kN was applied at column. Generally, the machine is stopped before failure to ensure its safety.

Table 4.7 shows the main parameters for defining the behavior of concrete model in ABAQUS for specimens J0, J10 and J11. As stated earlier, all specimens have approximately same compressive strength which is equal 25 MPa, so that, same stress-strain diagram is used for these specimens. Figure 4.5a shows uniaxial compression stress-inelastic strain curve of concrete, while Figure 4.5b shows tension stress-cracking strain curve of concrete. Also, Figure 4.5c shows compression damage parameter versus inelastic

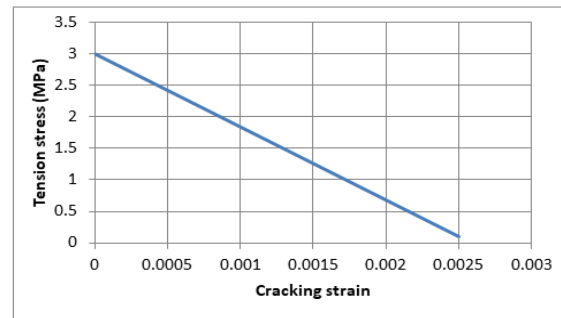
strain curve, while Figure 4.5d shows tension damage parameter versus cracking strain curve.

Table 4.7: Parameters of concrete for joints J0, JI0 and JI1 tested by Mahmoud et al. (2014)

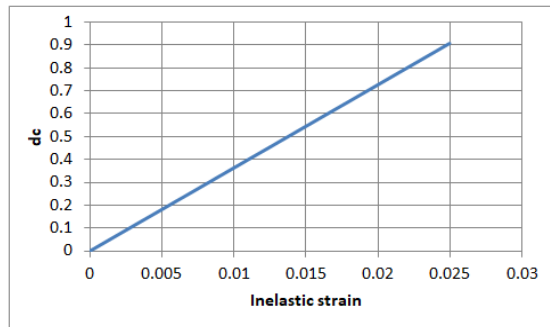
Joint ID	E_0 (MPa)	ν	ψ	e	f_{b0}/f_{c0}	K
J0	23500	0.2	36°	0.1	1.16	0.67
JI0	23500	0.2	36°	0.1	1.16	0.67
JI1	23500	0.2	36°	0.1	1.16	0.67



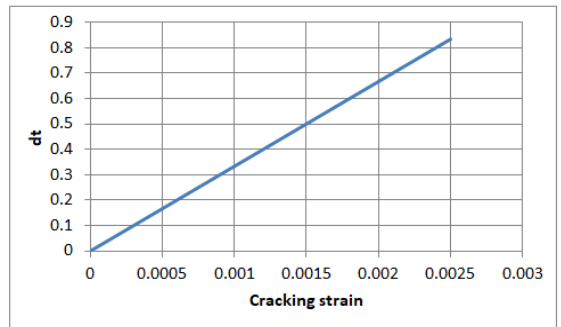
(a) Compressive stress vs inelastic strain



(b) Tensile stress vs cracking strain



(c) Compressive damage vs inelastic



(d) Tensile damage vs cracking strain

Figure 4.5: Definition of concrete parameters for CDP model in ABAQUS for joints J0, JI0 and JI1 tested by Mahmoud et al. (2014)

Two types of steel are used in this model. First type is for transverse steel and the other type for longitudinal reinforcement. However, there is no sufficient information about ultimate stress and strain of steel reinforcements

from experimental test, so that, stress-plastic strain curves which were reported by Sharif et al. (2015) as shown in Figure 4.6 are used for definition of steel reinforcements in this verification. Both steels have Young's Modulus ($E = 205\text{GPa}$) and Poisson's Ratio ($\nu = 0.3$).

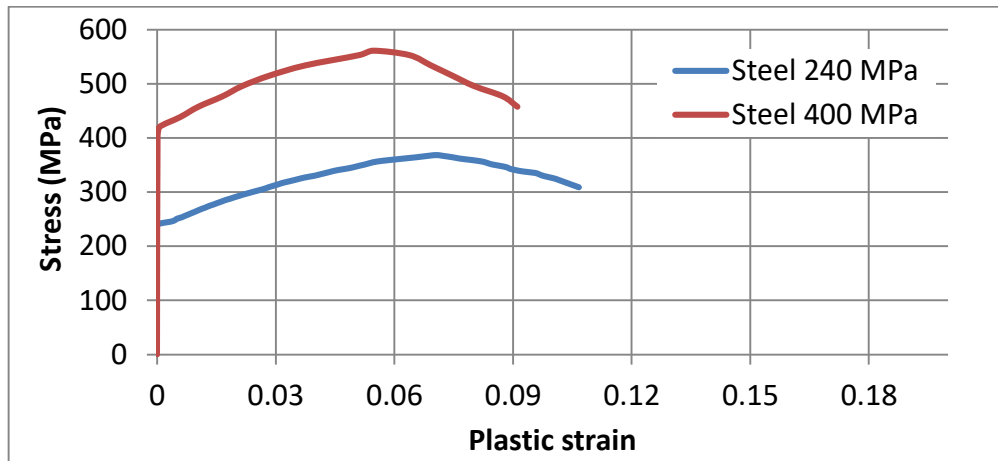


Figure 4.6: Stress vs plastic strain curves for steel 240 MPa and 400 MPa (Sharif et al., 2015)

Table 4.8 shows the input data for definition CFRP for joint JI1, also this table presents the normal and shear stiffness for cohesive interaction between beam and CFRP.

Table 4.8: Properties for combined CFRP with matrix and stiffness of interaction for specimen JI1 tested by Mahmoud et al. (2014)

Item	E1 (MPa)	E2 (MP)	Nu12	G12 (MPa)	G13 (MPa)	G23 (MPa)	Knn (N/mm ³)	Kss (N/mm ³)	Ktt (N/m ³)
Value	106509	33970	0.31	12400	12400	13065	1300	1300	1300

Numerical results are compared to experimental curves which were reported by Mahmoud et al. (2014) as shown in Figure 4.7 for joints J0, JI0 and JI1 respectively. However, Figure 4.8 shows the comparisons between tension

damage from the F.E. and experimental test for J0 and J11 at failure stage. This clearly shows that the F.E. model is able to predict the experimental cracks accurately.

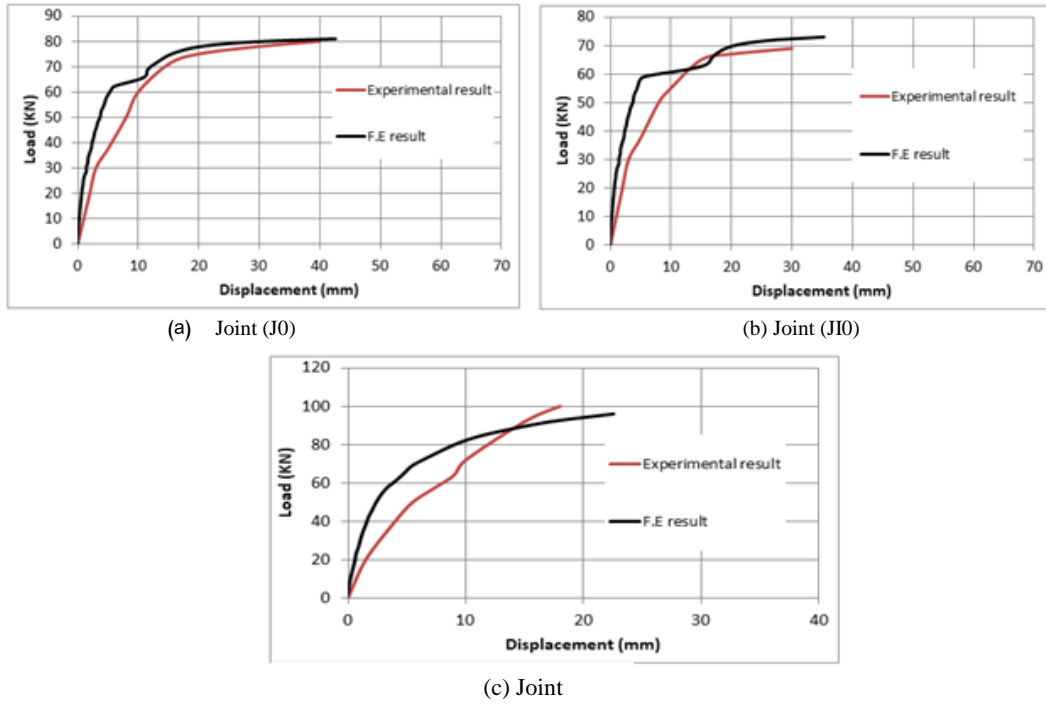
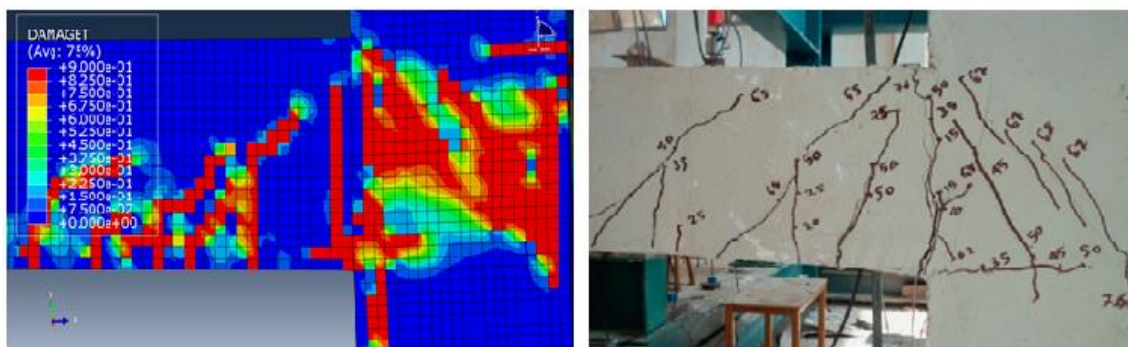
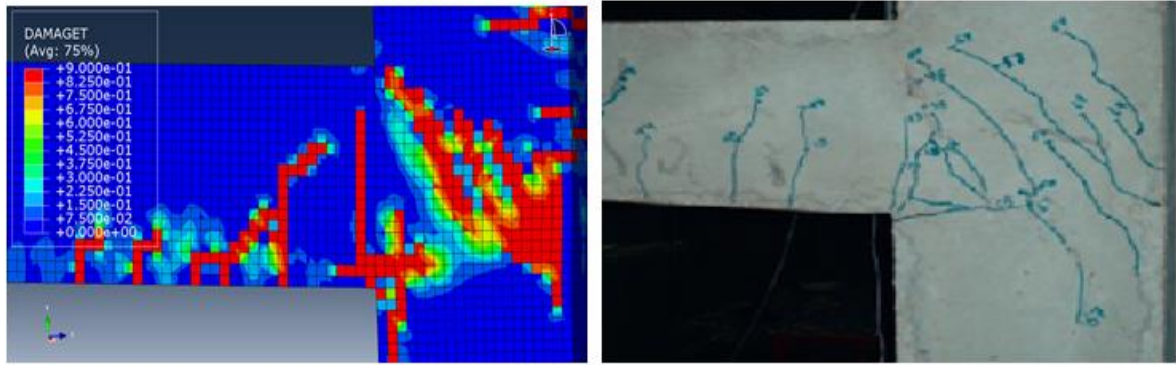


Figure 4.7: Comparison between experimental and F.E. results for joints J0, J10 and J11 tested by Mahmoud et al. (2014)



(a) Joint (J0)



(b) Joint (JI0)

Figure 4.8: Comparison between tension damage from F.E. and experimental test for joints J0 and JI0 tested by Mahmoud et al. (2014)

4.5 El-Amory (2004) tests

Three specimens tested by El-Amory (2004) are chosen for verification. The first specimen was without FRP (T-S1), while second and third specimens (T-S5 and T-S4R) were strengthened by GFRP and CFRP, respectively. The available information about steel, concrete, CFRP and epoxy are summarized in Tables 4.9 to 4.12, respectively.

Table 4.9: Properties of reinforcement bars used by El-Amoury (2004)

Bar Type	Diameter (mm)	Cross sectional area (mm ²)	Yield strength (MPa)	Ultimate strength (MPa)
M10	11.3	100.29	477	720
M15	16	201.06	409.5	617.5
M20	19.5	298.65	477	764

Table 4.10: Properties of concrete for joints tested by El-Amoury (2004)

Specimen	Compressive concrete strength (MPa) at 28-day	Compressive concrete strength (MPa) at test -day
T-S1	23.25	30.8
T-S4R	36.98	43.24
T-S5	32.59	36.66

Table 4.11: Properties of FRP sheets used by El-Amoury (2004)

Fiber type	Ultimate tensile strength (MPa)	Ultimate strain (%)	Modulus of elasticity (MPa)	Thickness (mm)
CFRP	3550	1.5	235000	0.165
GFRP	575	2.2	26100	1.3

Table 4.12: Properties of epoxy used by El-Amoury (2004)

Epoxy type	Tensile strength (MPa)	Tensile modulus (MPa)	Ultimate elongation (%)
Epoxy for installing CFRP	14	1138	5.3
Epoxy for installing GFRP	72.4	3180	5

Table 4.13 shows the main parameters for defining the behavior of concrete model in ABAQUS. However, Figure 4.9a shows uniaxial compression stress-inelastic strain curve of concrete, while Figure 4.9b shows uniaxial tension stress-cracking strain curve of concrete. Figure 4.9c shows compression damage parameter versus inelastic strain curve, while Figure

Table 4.13: Parameters of concrete for joints T-S1, T-S4R and T-S5 tested by El-Amoury (2004)

Joint ID	E0(MPa)	ν	ψ	e	f_{b0}/f_{c0}	K
T-S1	26169	0.2	36°	0.1	1.16	0.67
T-S4R	31176	0.2	36°	0.1	1.16	0.67
T-S5	28588	0.2	36°	0.1	1.16	0.67

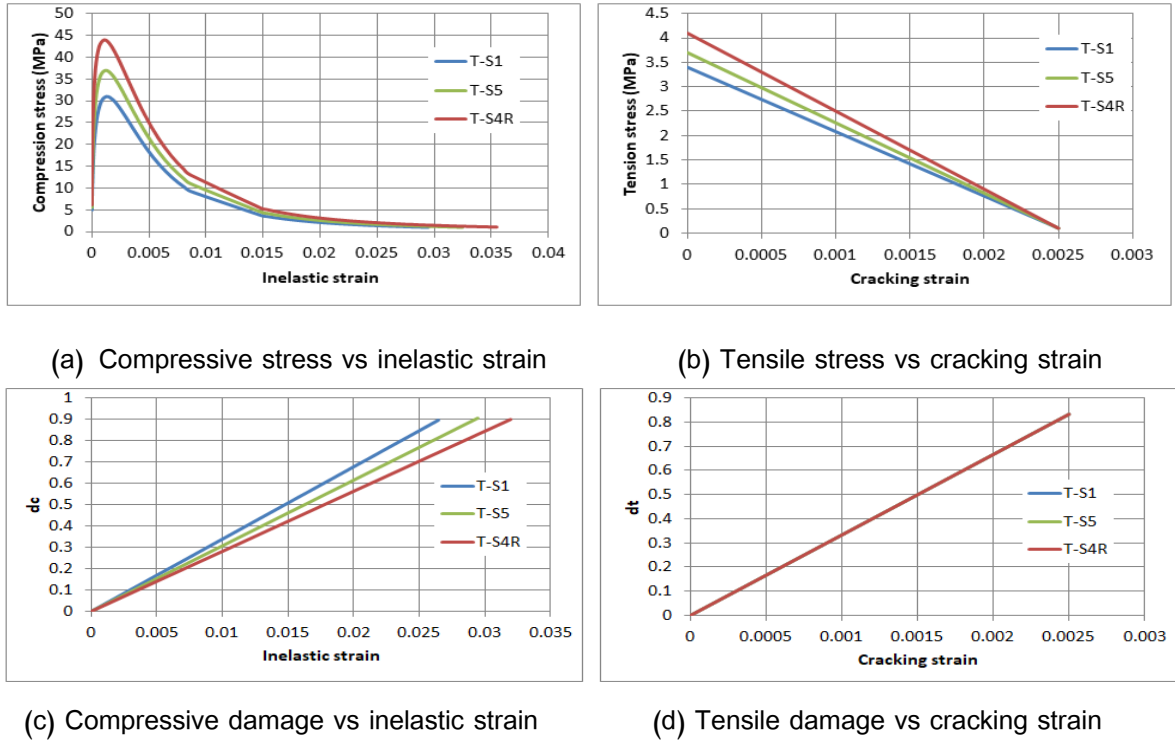


Figure 4.9: Definition of concrete parameters for CDP model in ABAQUS for joints T-S1, T-S4R and T-S5 tested by El-Amoury (2004)

Three types of steel are used in this model. The mechanical properties are shown in Table 4.9. A bi-linear stress strain diagram is used for defining the steel with assumed slope hardening equals $0.01E_s$. The typical stress-plastic strain diagram for each type of bars is shown in Figure 4.10. All steels assume Young's Modulus ($E = 205\text{GPa}$) and Poisson's Ratio ($\nu = 0.3$).

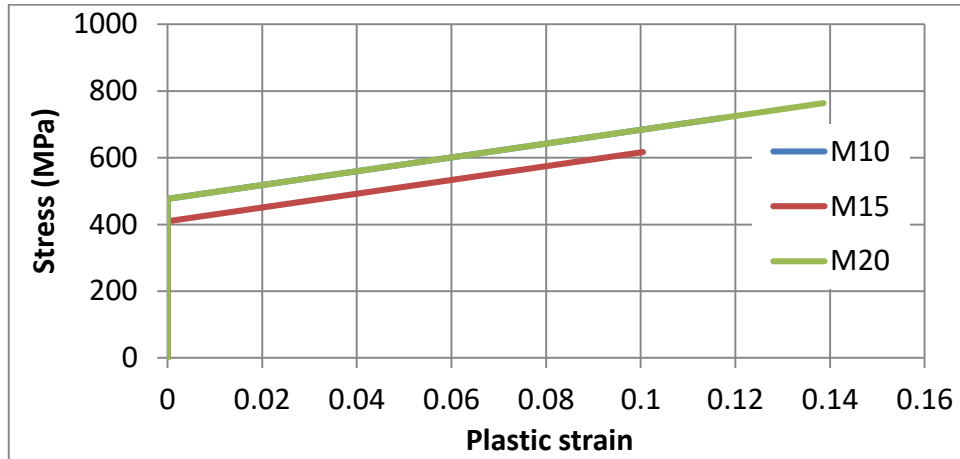


Figure 4.10: Stress –plastic strain diagram for steel which is used for modeling of joints T-S1, T-S4R and T-S5.

Table 4.14 shows the input data for definition CFRP and GFRP, also this table presents the normal and shear stiffness for cohesive interaction between beam and CFRP or GFRP.

Table 4.14: Properties for combined FRP with matrix and stiffness of interaction for specimens T-S5 and T-S4R tested by El-Amoury (2004)

Type of FRP	E1 (MPa)	E2 (MP)	Nu12	G12 (MPa)	G13 (MPa)	G23 (MPa)	Knn (N/mm ³)	Kss (N/mm ³)	Ktt (N/mm ³)
CFRP	96554	1916	0.31	750	750	750	515	515	515
GFRP	12531	4955	0.31	1800	1800	1800	600	600	600

Numerical load-deflection curves are compared to the experimental curves reported by El-Amoury (2004). Comparisons between load-deflection curves from ABAQUS and experimental test for specimens T-S1, T-S4R and T-S5 are shown in Figure 4.11. It can be seen that the F.E. model captures the descending branch quite satisfactory. However, for specimen T-S4R the variation between F.E. model and experiments is due to the fact that this specimen was re-strengthened with another type of concrete then re-tested.

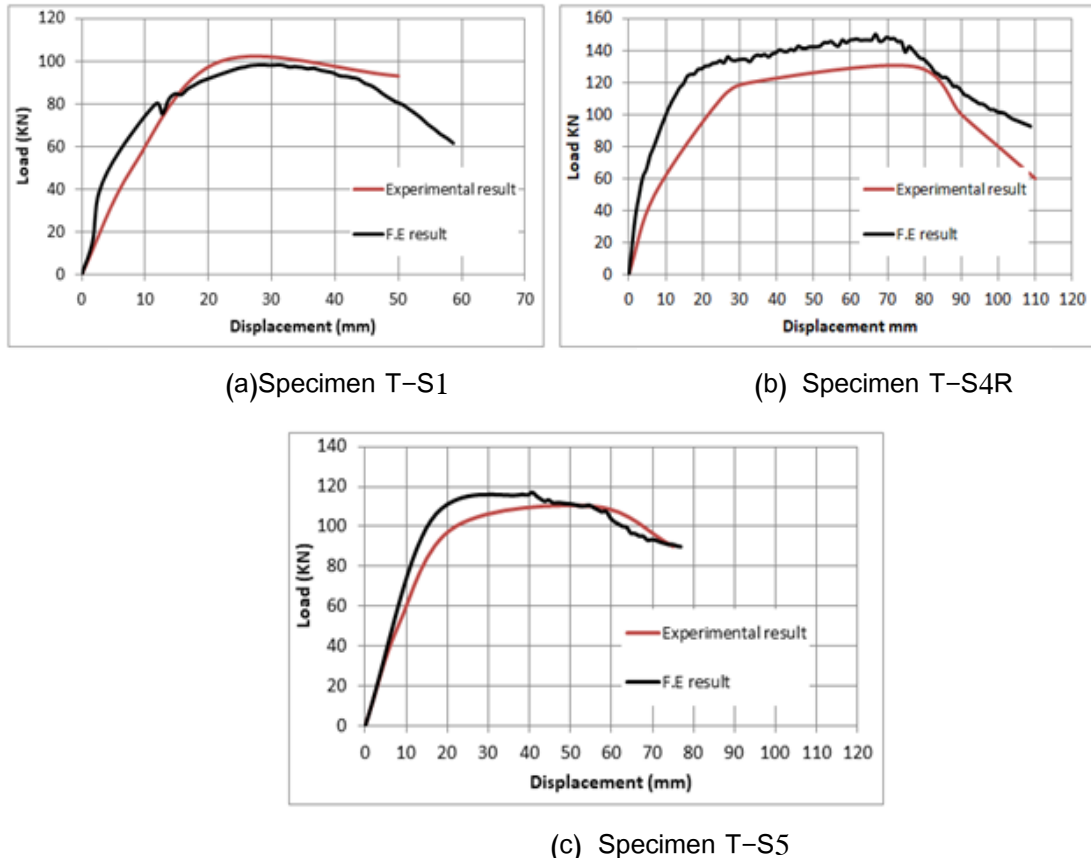


Figure 4.11: Comparison between experimental and F.E. results for joints T-S1, T-S4R and T-S5 tested by El-Amoury (2004)

Based on the above verifications, the F.E. model is able to predict the behavior of exterior R.C beam-column joint strengthened and not strengthened by FRP. This model will be used in the next section to investigate the behavior and ductility of exterior R.C beam-column joint. In this thesis, the parameters that are used for material modeling are the same as the materials used in the verification of tests by Mahmoud et al. (2014) as shown in this chapter. The only difference is the definition of steel. However, for design purpose, elastic-perfectly plastic model will be used in this thesis with yield strength of stirrups equals 285 MPa as reported by Sharif et al.(2015), this value is used to consider the worst case, while yield strength

of longitudinal reinforcement equal 420 MPa as reported by Sharif et al.(2015). These values are common in Palestine.

4.6 Parametric study

4.6.1 General

Parametric study is conducted to investigate the behavior of exterior R.C beam column joint strengthened by FRP. The behavior is affected by many parameters. These parameters include: relative moment of inertia of column to beam (G), amount of transverse steel in joint $(A_v/s)_J$, amount of transverse steel in beam $(A_v/s)_B$, longitudinal steel ratio (ρ), axial load on column (N), number of CFRP layers (n) and shear to moment ratio. However, some of these parameters are more significant than others. Also, due to computational limitations, four main parameters are investigated in this research. Those parameters have clear influence on the behavior which are relative inertia between column and beam (G), shear reinforcement in joint $(A_v/s)_J$, shear reinforcement in beam $(A_v/s)_B$ and the effect of CFRP will be considered, while the other variables (such as axial force, longitudinal steel ratio, number of CFRP layers and shear to moment ratio) are kept constant and may be investigated in future studies. The comparison will be made on the effect of these parameters on the ductility of exterior R.C beam column joint.

4.6.2 Parameter ranges

Total of 64 simulations have been conducted on RC joints with and without CFRP. The parameters are varied according to Table 4.15. The relative

inertia of column to beam range is assumed to vary from 0.512 to 4.63 where 0.512 represents weak column. The values of $(A_v/s)_B$ and $(A_v/s)_J$ ranged from 0.5 (representing minimum value) to 4.5 (representing maximum value). The generic overall model with its boundaries is shown in Figure 3.9. However, constant dimensions of beam-column joint are summarized in Table 4.16.

The layout of the CFRP is assumed as wraps around the beam member with only one layer of CFRP sheet. This schematic arrangement is selected as one of the effective strengthening techniques as stated by many researchers (Ghobarah et al., 1997, Sadone et al., 2012 and Al-Salloum et al., 2002). However, this arrangement of CFRP provides additional shear strength to the beam.

To simulate the service axial load in real structure, a compression force of 1050 kN is applied on column ($0.25 A_g f'_c$), where A_g : is the gross sectional area of column and f'_c is the compressive strength of concrete.

Each simulation is given a representative name. Generally, first symbol denotes the relative inertia, while second symbol denotes the amount of stirrups inside joint, third symbol denotes the amount of stirrups in beam; final symbol denotes the use of CFRP. For instance, simulation (G1-MaJ-MiB-0) means first relative inertia (0.512) with maximum amount of stirrups inside joint (4.5) and minimum amount of stirrups in beam (0.5) without CFRP. Another example is simulation (G3-MiJ-B1-1) means third relative inertia (4.63) with minimum amount of stirrups in joint (0.5) and amount of

stirrups in beam between maximum and minimum (1.13) with a layer of CFRP.

Table 4.15: Variable properties for all models

Model	h_b	G	$(AV/S)_J$	$(AV/S)_B$	CFRP (Yes /No)
G1-MaJ-MiB-0	0.5 m	0.5	4.5	0.5	No
G1-MaJ-B1B-0	0.5 m	0.5	4.5	1.13	No
G1-MaJ-B2B-0	0.5 m	0.5	4.5	3.14	No
G1-MaJ-MaB-0	0.5 m	0.97	4.5	4.5	No
G2-MaJ-MiB-0	0.4 m	0.97	4.5	0.5	No
G2-MaJ-B1B-0	0.4 m	0.97	4.5	1.13	No
G2-MaJ-B2B-0	0.4 m	0.97	4.5	3.14	No
G2-MaJ-MaB-0	0.4 m	0.97	4.5	4.5	No
G3-MaJ-MiB-0	0.24 m	4.83	4.5	0.5	No
G3-MaJ-B1B-0	0.24 m	4.83	4.5	1.13	No
G3-MaJ-B2B-0	0.24 m	4.83	4.5	3.14	No
G3-MaJ-MaB-0	0.24 m	4.83	4.5	4.5	No
G1-MiJ-MiB-0	0.5 m	0.5	0.5	0.5	No
G1-MiJ-B1B-0	0.5 m	0.5	0.5	1.13	No
G1-MiJ-B2B-0	0.5 m	0.5	0.5	3.14	No
G1-MiJ-MaB-0	0.5 m	0.97	0.5	4.5	No
G2-MiJ-MiB-0	0.4 m	0.97	0.5	0.5	No
G2-MiJ-B1B-0	0.4 m	0.97	0.5	1.13	No
G2-MiJ-B2B-0	0.4 m	0.97	0.5	3.14	No
G2-MiJ-MaB-0	0.4 m	0.97	0.5	4.5	No
G3-MiJ-MiB-0	0.24 m	4.83	0.5	0.5	No
G3-MiJ-B1B-0	0.24 m	4.83	0.5	1.13	No
G3-MiJ-B2B-0	0.24 m	4.83	0.5	3.14	No
G3-MiJ-MaB-0	0.24 m	4.83	0.5	4.5	No
G1-MaJ-MiB-1	0.5 m	0.5	4.5	0.5	Yes
G1-MaJ-B1B-1	0.5 m	0.5	4.5	1.13	Yes
G1-MaJ-B2B-1	0.5 m	0.5	4.5	3.14	Yes
G1-MaJ-MaB-1	0.5 m	0.97	4.5	4.5	Yes
G2-MaJ-MiB-1	0.4 m	0.97	4.5	0.5	Yes
G2-MaJ-B1B-1	0.4 m	0.97	4.5	1.13	Yes
G2-MaJ-B2B-1	0.4 m	0.97	4.5	3.14	Yes
G2-MaJ-MaB-1	0.4 m	0.97	4.5	4.5	Yes
G3-MaJ-MiB-1	0.24 m	4.83	4.5	0.5	Yes

G3-MaJ-B1B-1	0.24 m	4.83	4.5	1.13	Yes
G3-MaJ-B2B-1	0.24 m	4.83	4.5	3.14	Yes
G3-MaJ-MaB-1	0.24 m	4.83	4.5	4.5	Yes
G1-MiJ-MiB-1	0.5 m	0.5	0.5	0.5	Yes
G1-MiJ-B1B-1	0.5 m	0.5	0.5	1.13	Yes
G1-MiJ-B2B-1	0.5 m	0.5	0.5	3.14	Yes
G1-MiJ-MaB-1	0.5 m	0.97	0.5	4.5	Yes
G2-MiJ-MiB-1	0.4 m	0.97	0.5	0.5	Yes
G2-MiJ-B1B-1	0.4 m	0.97	0.5	1.13	Yes
G2-MiJ-B2B-1	0.4 m	0.97	0.5	3.14	Yes
G2-MiJ-MaB-1	0.4 m	0.97	0.5	4.5	Yes
G3-MiJ-MiB-1	0.24 m	4.83	0.5	0.5	Yes
G3-MiJ-B1B-1	0.24 m	4.83	0.5	1.13	Yes
G3-MiJ-B2B-1	0.24 m	4.83	0.5	3.14	Yes
G3-MiJ-MaB-1	0.24 m	4.83	0.5	4.5	Yes
C1-MaJ-X1B-0	0.36 m	1.37	4.5	1.74	No
C1-MaJ-X0B-0	0.36 m	1.37	4.5	0.78	No
C2-MaJ-X1B-0	0.29 m	2.62	4.5	1.74	No
C2-MaJ-X0B-0	0.29 m	2.62	4.5	0.78	No
C1-MiJ-X1B-0	0.36 m	1.37	0.5	1.74	No
C1-MiJ-X0B-0	0.36 m	1.37	0.5	0.78	No
C2-MiJ-X1B-0	0.29 m	2.62	0.5	1.74	No
C2-MiJ-X0B-0	0.29 m	2.62	0.5	0.78	No
C1-MaJ-X1B-1	0.36 m	1.37	4.5	1.74	Yes
C1-MaJ-X0B-1	0.36 m	1.37	4.5	0.78	Yes
C2-MaJ-X1B-1	0.29 m	2.62	4.5	1.74	Yes
C2-MaJ-X0B-1	0.29 m	2.62	4.5	0.78	Yes
C1-MiJ-X1B-1	0.36 m	1.37	0.5	1.74	Yes
C1-MiJ-X0B-1	0.36 m	1.37	0.5	0.78	Yes
C2-MiJ-X1B-1	0.29 m	2.62	0.5	1.74	Yes
C2-MiJ-X0B-1	0.29 m	2.62	0.5	0.78	Yes

Table 4.16: Constant dimensions of beam-column models

Dimension name	Value (m)
Total length of beam (L_{bt})	0.9
Total length of column (L_c)	2.3
Width of beam(b_b)	0.4
Width of colum(b_c)	0.4
Depth of column(h_c)	0.4

5 Results and discussion

5.1 Overview

This chapter presents the main results of all parameterized models that were mentioned in Chapter 5. Load-deflection curves for all cases will be discussed, and will be used later to estimate the ductility. All values will be fitted to simple practical equations for conceptual design use.

5.2 General behavior

The general features of a typical load-deflection curve of an R.C beam-column joint is shown in Figure 5.1. The behavior of the beam-column joint is initially linear elastic up to the development of beam cracks close to the beam-column interface (tension zoon). This could be noticed by a simple drop of the load-deflection curve. Tension force is resisted later by the tension reinforcement where the beam continues elastically up to the yielding of tension steel. Beyond this stage, the behavior is controlled by reinforcement details and strengthening techniques. Based on that, brittle shear failure or ductile flexural failure may happen.

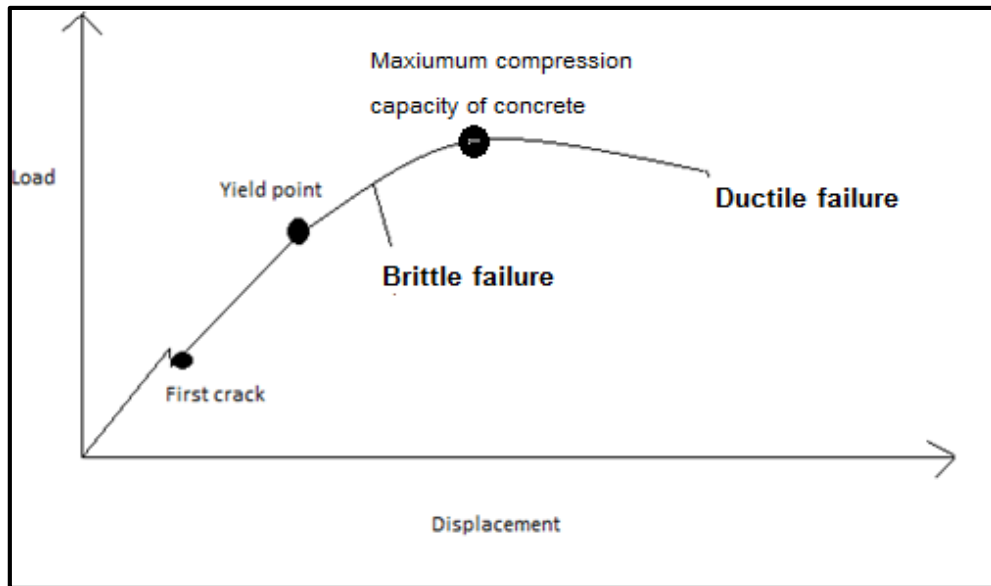


Figure 5.1: Typical load –deflection curve for joints

5.3 Failure criteria

In order to calculate the rotational ductility of the joint from the resulting load-deflection curves, a criterion is needed to specify the yield and ultimate deflections. First, the yield deflection is taken to be the stage at which tensile steel starts to yield. The ultimate deflection is considered to be the instance when the load-deflection curve goes below 85% of the peak capacity (Park and Paulay, 1975). This criterion is applied for all curves regardless of the nature of failure.

The rotational ductility is then defined as the ultimate deflection divided by the yield deflection.

5.4 Results and discussion

In total, 64 simulations have been conducted on exterior R.C beam-column joints with and without CFRP. These models include different parameters as

estimated in Chapter 5. This section presents a discussion of the effect of each parameter on the ductility.

5.4.1 Effect of column stirrups

Load-deflection curve for the model (G1-MaJ-MaB) with maximum stirrups in column ($(A_v/s)_c = 4.5$) is compared with the same model but without stirrups in column ($(A_v/s)_c = 0$) in Figure 5.2. Results show that there is no significant effect of column stirrups on the strength and ductility of the joint, because the failure does not happen in the column.

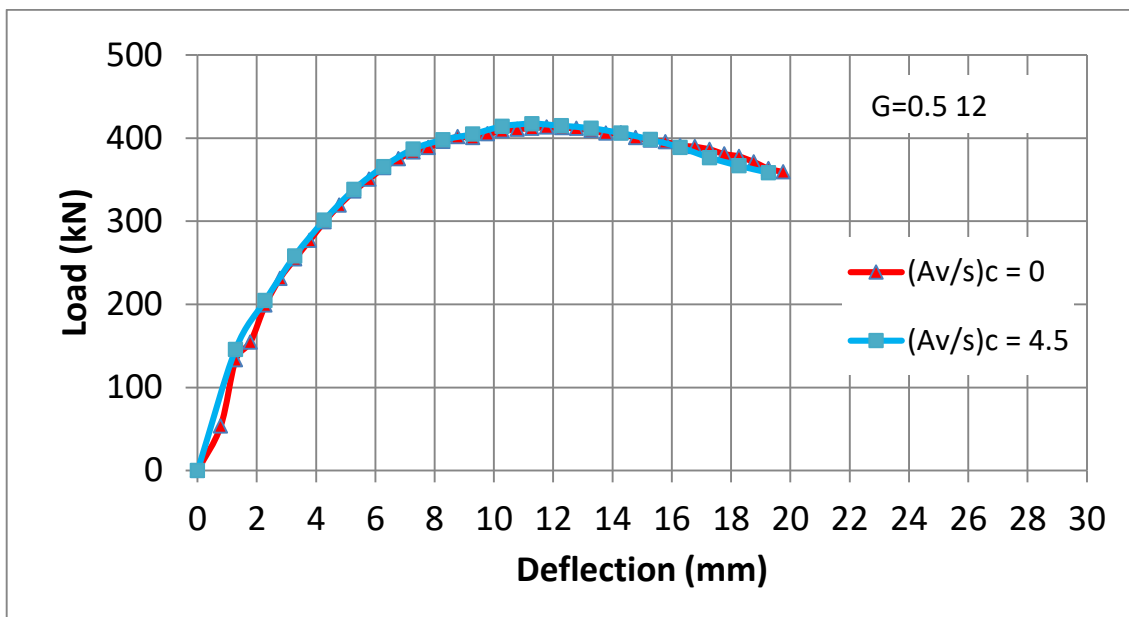


Figure 5.2: Effect of column stirrups on the ductility

5.4.2 Effect of joint stirrups continuity $(A_v/s)_j$

The resulting curves for cases without CFRP are shown in Figures 5.3 to 5.5 which present the effect of joints stirrups continuity for models with relative inertia (G) equals 0.512, 1 and 4.63, respectively. Results show that, stirrups

continuity inside the joint increases the capacity remarkably for models with G equals 0.512 which are dominated by shear failure of joint or beam. However, small effect of stirrups continuity inside the joint for G equals 1, while there is no effect of stirrups continuity inside the joint for G equals 4.63, since the flexural capacity of the beam is less than shear capacity of joint. However, ductility decreases when using minimum shear reinforcement in beam and maximum shear reinforcement in the joint. This is logical because the load-deflection curve becomes stiffer due to strengthening of joint, and then sudden failure happens in the beam due to shear. The same behavior happens for models with CFRP, but the ductility remains approximately constant for models with CFRP because no shear failure happens in the beam. This is shown in Figures 5.6 to 5.8 which present the effect of joints stirrups continuity for models with relative inertia (G) equals 0.512, 1 and 4.63, respectively.

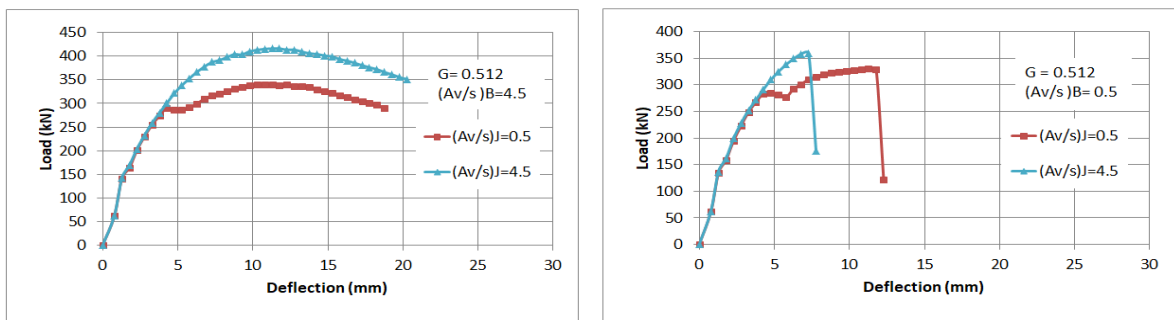


Figure 5.3: Effect of joints stirrups continuity on strength and ductility of joints with G equals 0.512 without CFRP

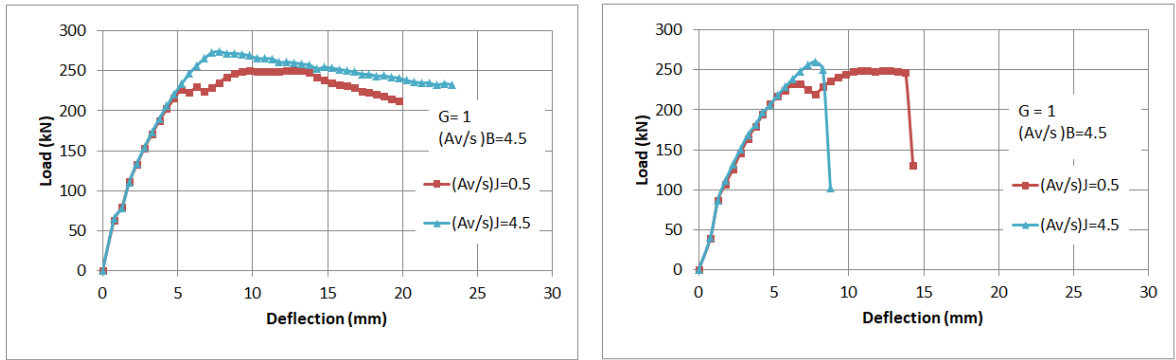


Figure 5.4: Effect of joints stirrups continuity on strength and ductility of joints with G equals 1 without CFRP

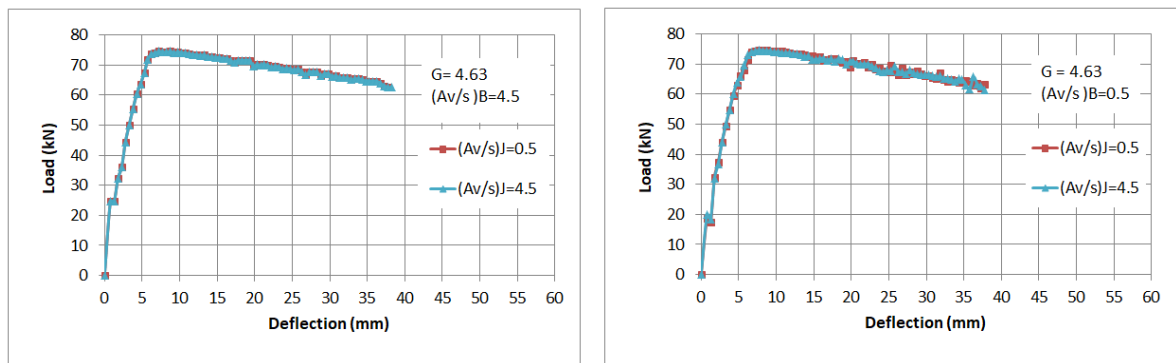


Figure 5.5: Effect of joints stirrups continuity on strength and ductility of joints with G equals 4.63 without CFRP

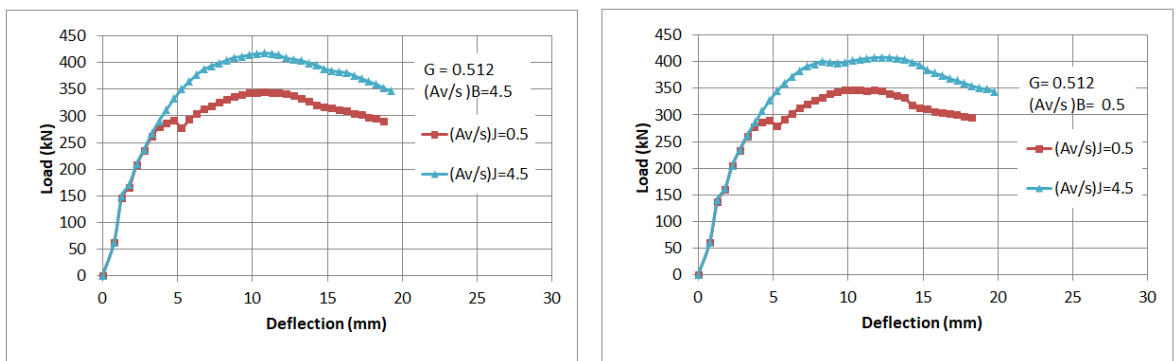


Figure 5.6: Effect of joints stirrups continuity on strength and ductility of joints with G equals 0.512 strengthened with CFRP

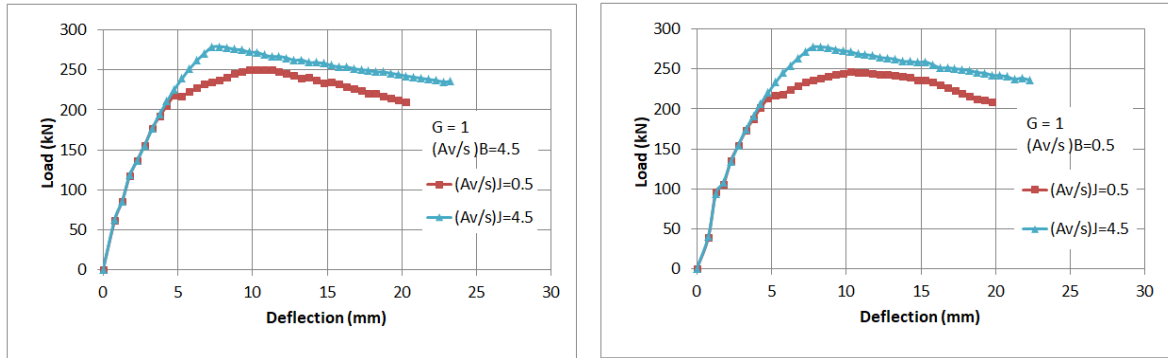


Figure 5.7: Effect of joints stirrups continuity on strength and ductility of joints with G equals 1 strengthened with CFRP

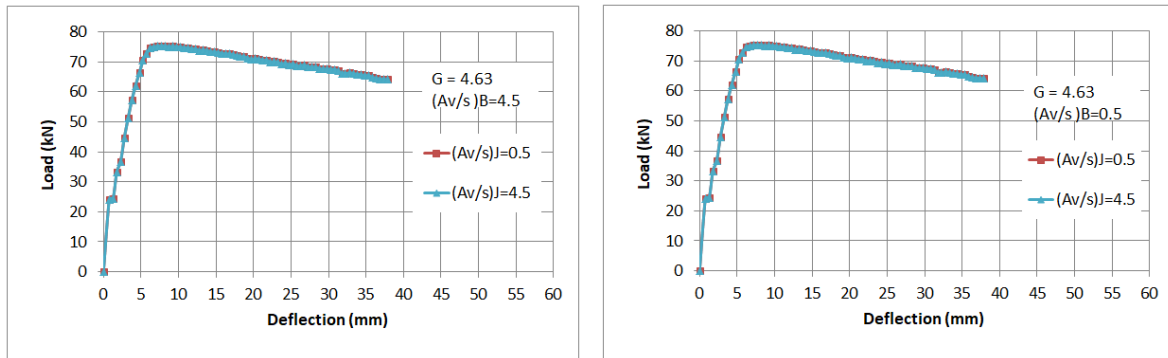


Figure 5.8: Effect of joints stirrups continuity on strength and ductility of joints with G equals 4.63 strengthened with CFRP

5.4.3 Effect of relative inertia (G)

The resulting curves for cases without CFRP are shown in Figures 5.9 and 5.10 which present the effect of relative inertia for models with $(Av/s)_J$ equals 4.5 and 0.5, respectively. Results show that, generally, as the relative inertia decreases, the ultimate capacity increases and the ductility decreases. This is logical because decreasing G means larger beam. This trend also exists for the case of using CFRP as shown in Figures 5.11 and 5.12 which present the effect of relative inertia for models with $(Av/s)_J$ equals 4.5 and

0.5, respectively. However, by using CFRP, the shear failure which is predicted to happen in beam converts to flexure failure in beam or shear failure in joint depending on the amount of stirrups continuity inside the joint.

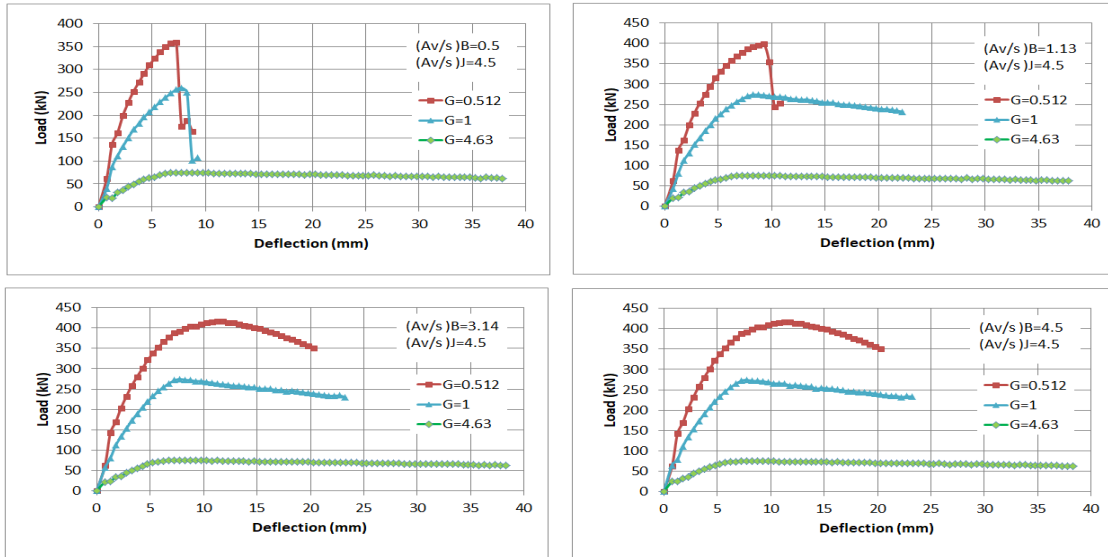


Figure 5.9: Effect of relative inertia on strength and ductility of joints with maximum $(Av/s)_J$ without CFRP

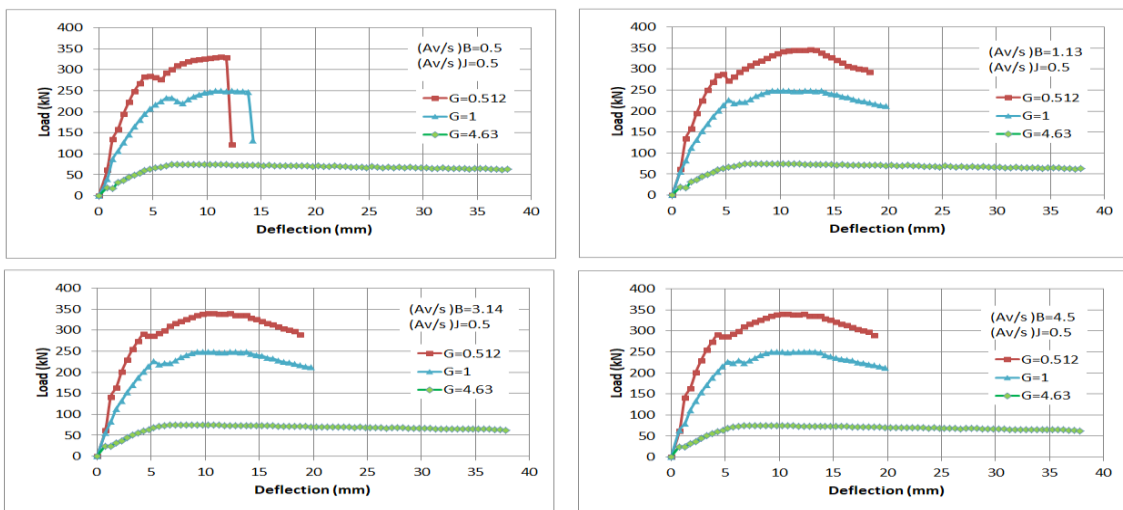


Figure 5.10: Effect of relative inertia on strength and ductility of joints with minimum $(Av/s)_J$ without CFRP

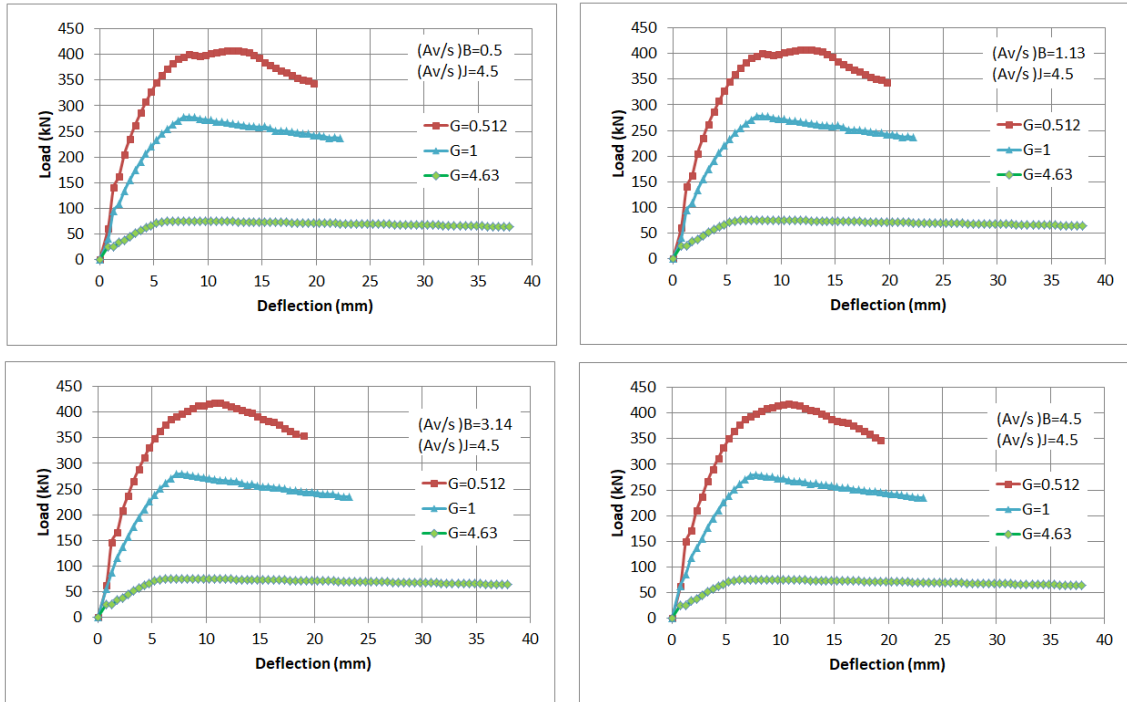


Figure 5.11: Effect of relative inertia on strength and ductility of joints with maximum $(Av/s)_J$ strengthened with CFRP

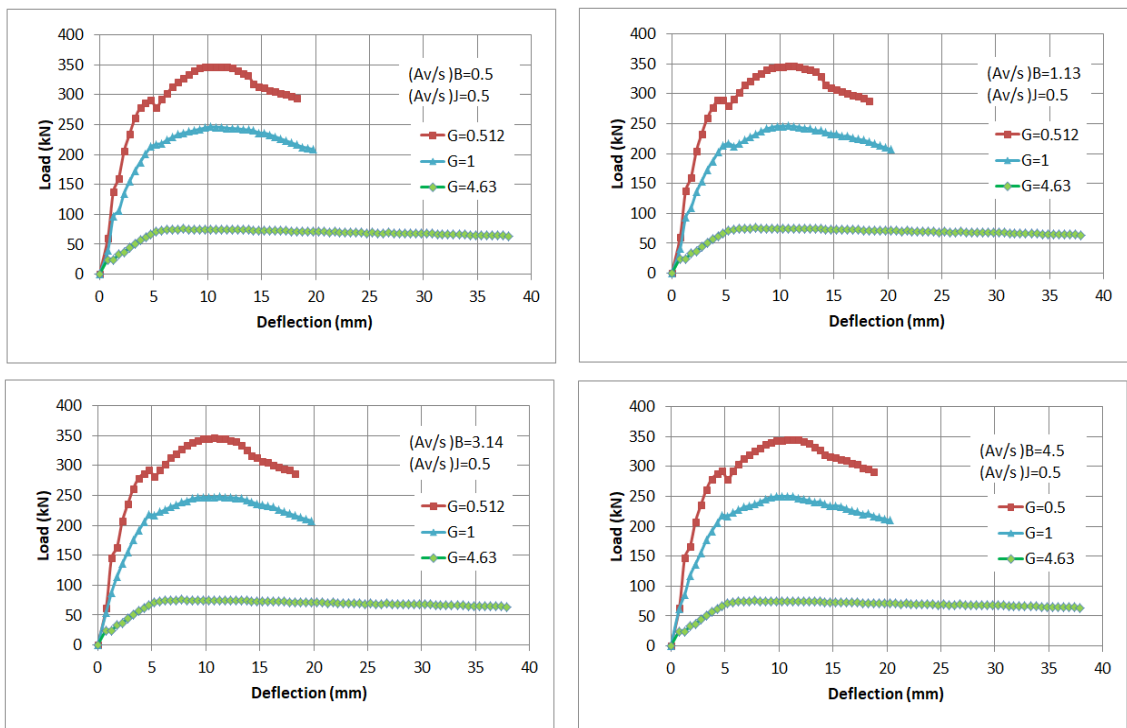


Figure 5.12: Effect of relative inertia on strength and ductility of joints with minimum $(Av/s)_J$ strengthened with CFRP

5.4.4 Effect of beam stirrups $(A_v/s)_B$

Load-deflection curves for cases without CFRP are shown in Figures 5.13 and 5.14 which present the effect of beams stirrups for models with $(A_v/s)_J$ equals 4.5 and 0.5, respectively. Generally, it can be seen that for small values of $(A_v/s)_B$ in cases of maximum $(A_v/s)_J$, the failure is dominated by shear in beam and therefore it is a brittle failure. As the value of $(A_v/s)_B$ increases, the ductility increases mainly due to shear strengthening. On the other hand, in cases of minimum $(A_v/s)_J$, as the value of $(A_v/s)_B$ increases, the failure becomes shear failure in the joint. This is due to strong beam-weak joint for this case.

The results show that the ductility increases with increasing the transverse steel up to a certain maximum value of $(A_v/s)_B$. Increasing $(A_v/s)_B$ beyond this maximum value causes no significant effect on ductility. This maximum value of $(A_v/s)_B$ depends on the relative inertia (G) and amount of stirrups inside the joint $(A_v/s)_J$. The maximum value of $(A_v/s)_B$ for each case of relative inertia are summarized in Table 5.1. This trend does not happen when using CFRP, because using CFRP converts brittle failure to ductile failure as shown in Figures 5.15 and 5.16, which present the effect of beams stirrups for models with $(A_v/s)_J$ equals 4.5 and 0.5, respectively. The effect of CFRP will be discussed in the next section.

Table 5.1: Maximum value of $(A_v/s)_B$ beyond which it has no effect on ductility

G	$(A_v/s)_J$ (mm^2/mm)	Fixed value of $(A_v/s)_B$ (mm^2/mm)
0.512	0.5	1.13
	4.5	3.14
1	0.5	1.13
	4.5	1.13
4.63	0.5	0.5
	4.5	0.5

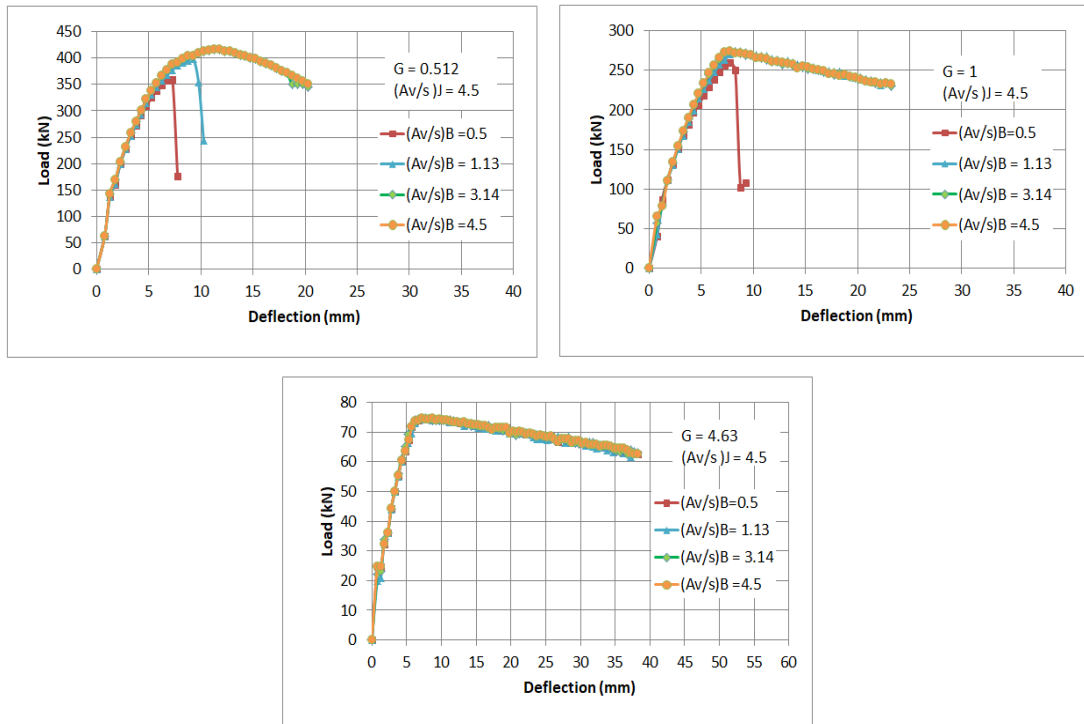


Figure 5.13: Effect of beams stirrups on strength and ductility of joints with maximum $(A_v/s)_J$ without CFRP

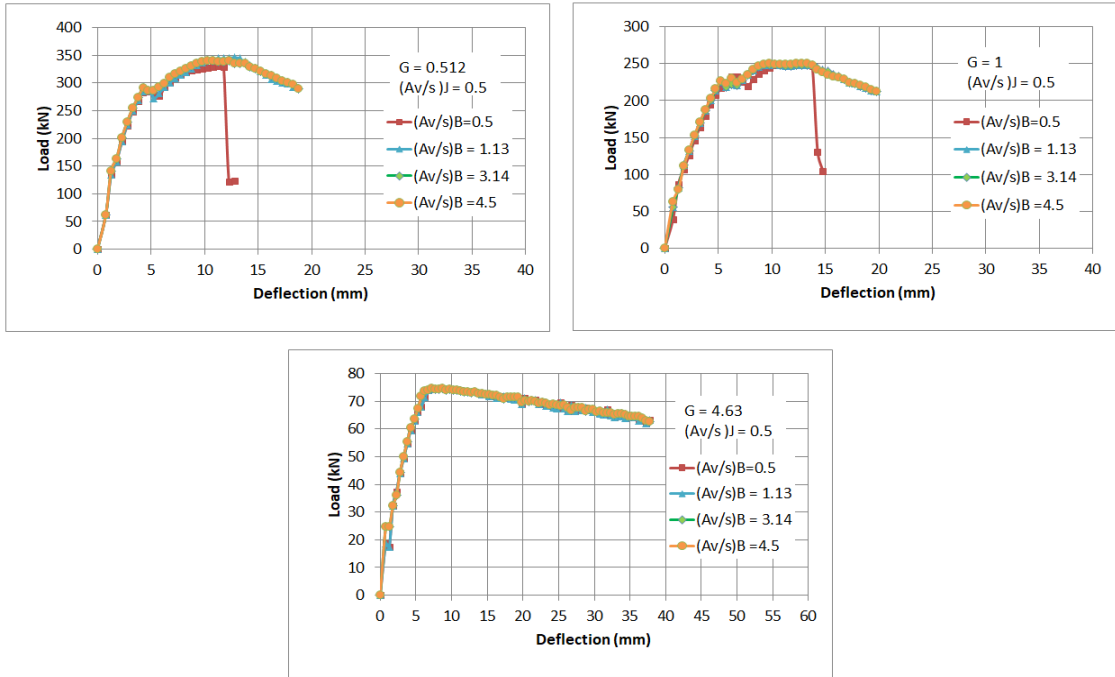


Figure 5.14: Effect of beams stirrups on strength and ductility of joints with minimum $(A_v/s)_J$ without CFRP

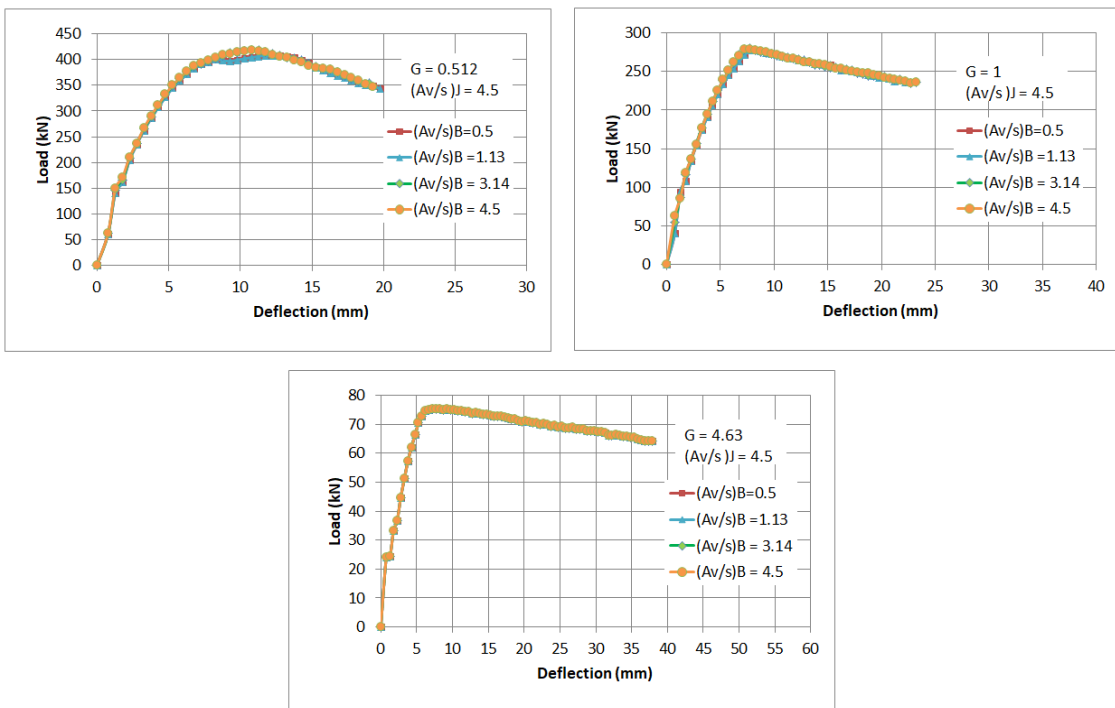


Figure 5.15: Effect of beams stirrups on strength and ductility of joints with maximum $(A_v/s)_J$ strengthened with CFRP

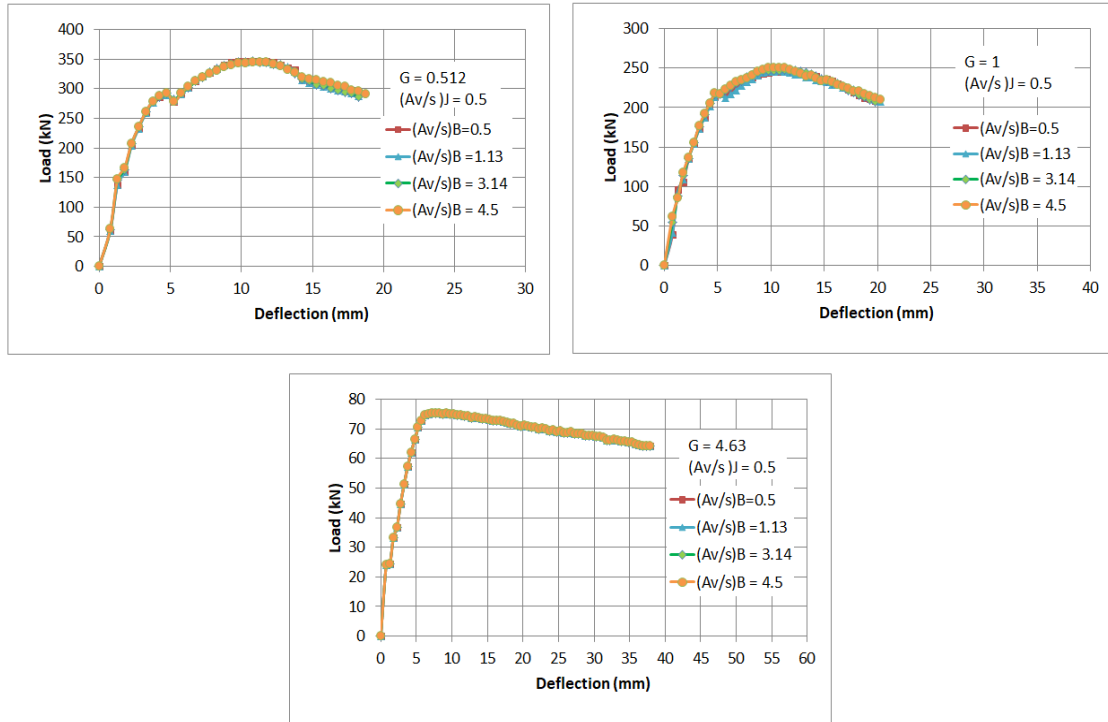
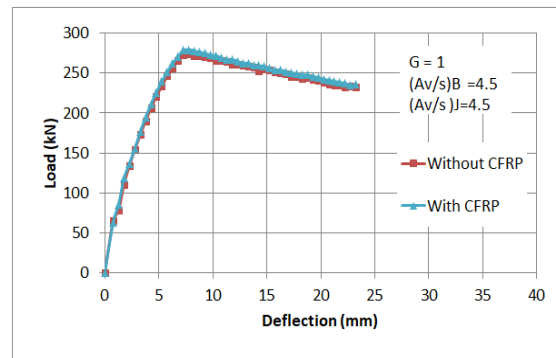
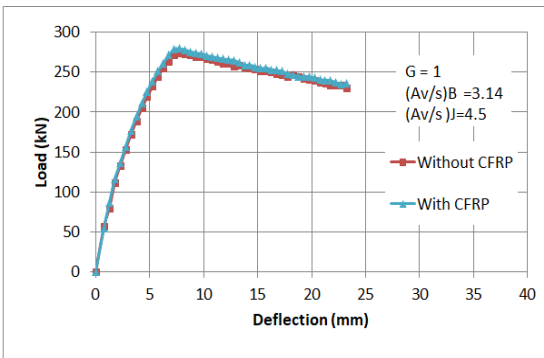
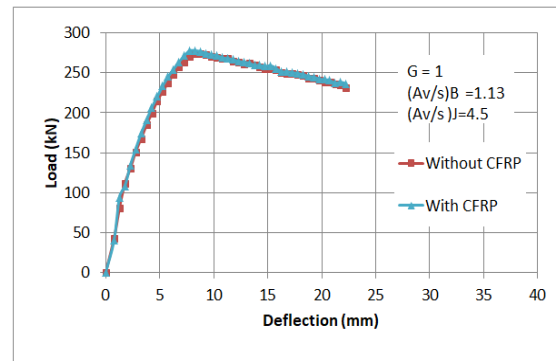
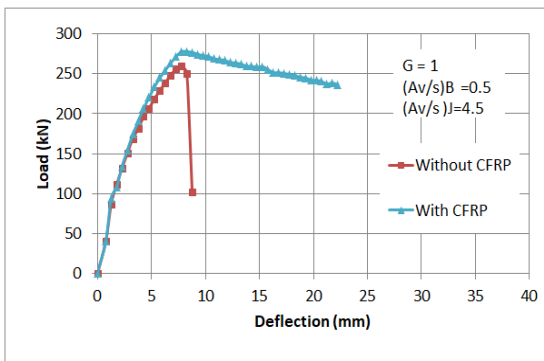
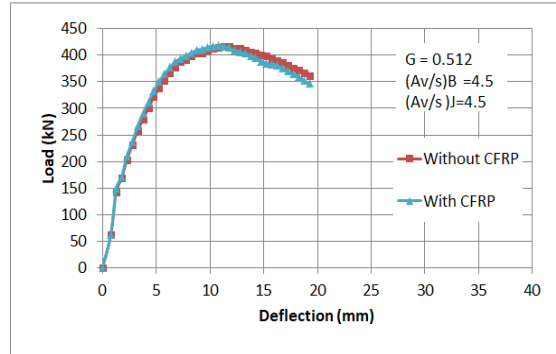
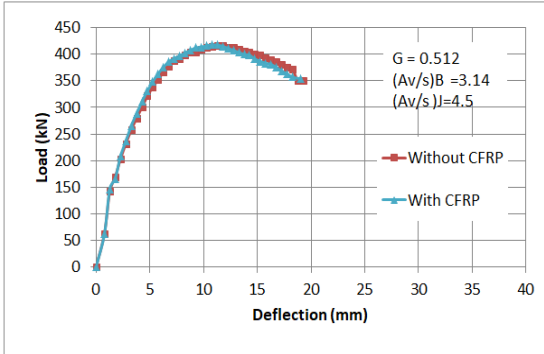
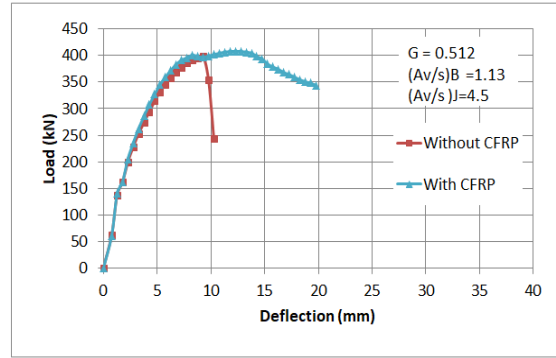
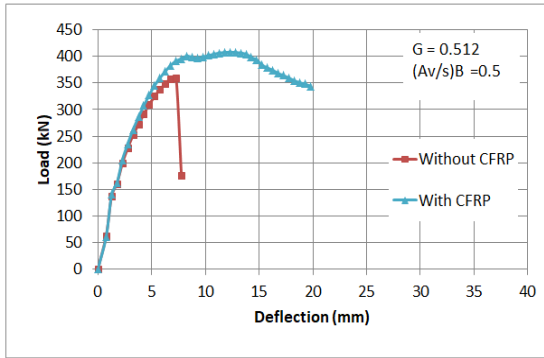


Figure 5.16: Effect of beams stirrups on strength and ductility of joints with minimum $(Av/s)_J$ strengthened with CFRP

5.4.5 Effect of using CFRP

Generally, CFRP is used to strengthen the joints and prevent brittle failure. The curves for the cases with maximum and minimum $(Av/s)_J$ are shown in Figures 5.17 and 5.18, respectively. Results show that, generally, using CFRP converts the brittle failure to a ductile failure. However, there is no effect of CFRP when models reach maximum confinement due to beam stirrups or when failure happens inside the joint. On the other hand, the effect of CFRP is remarkable for models that are dominated by shear failure of beam. For instance, Figure 5.19 shows the cracks at failure before and after wrapping CFRP for joint P1-MaJ-MiB.



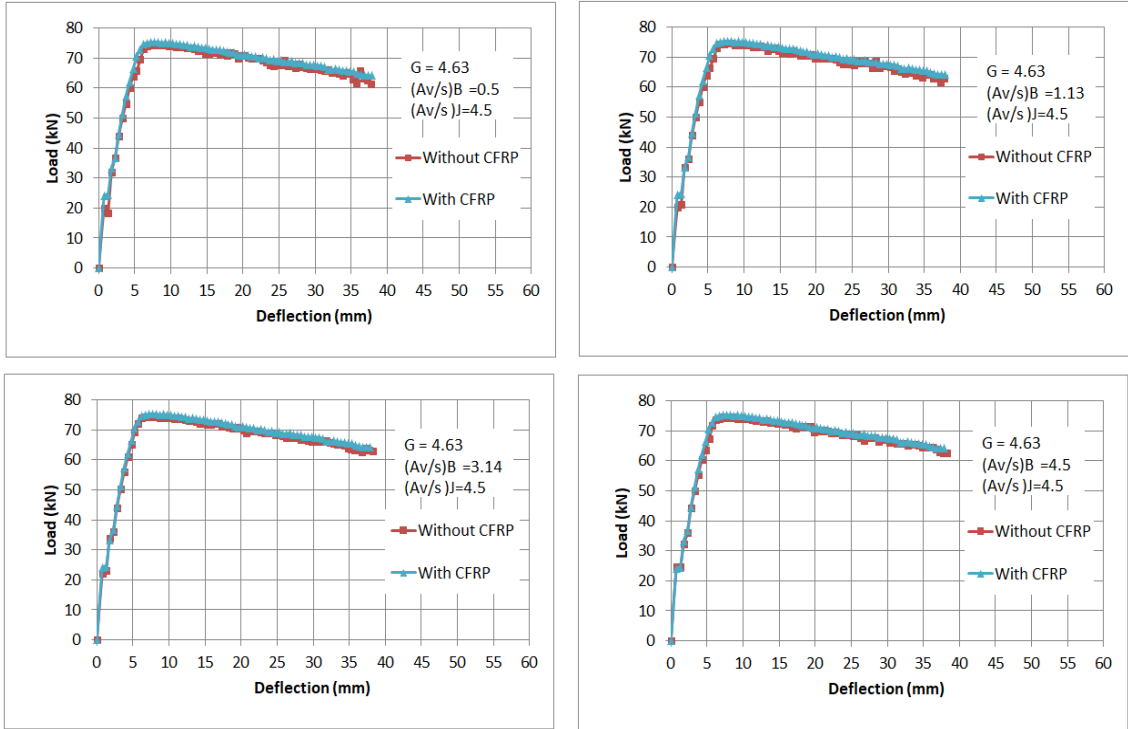
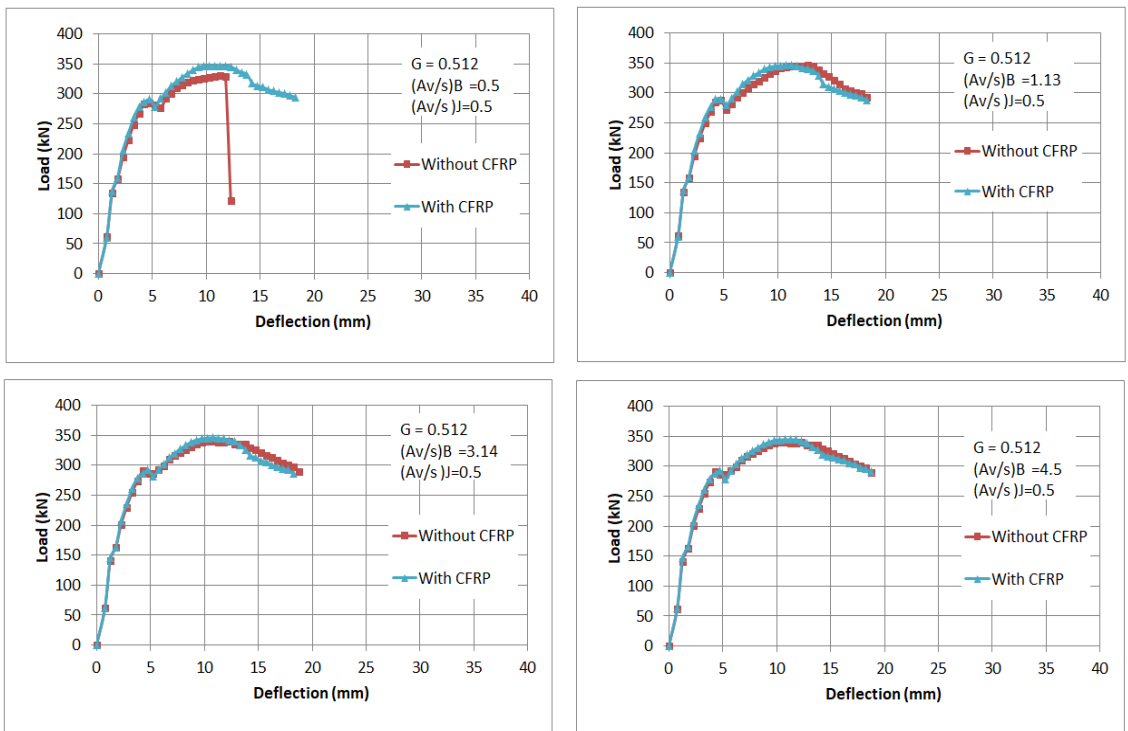


Figure 5.17: Effect of CFRP on strength and ductility of joints with maximum $(Av/s)_J$



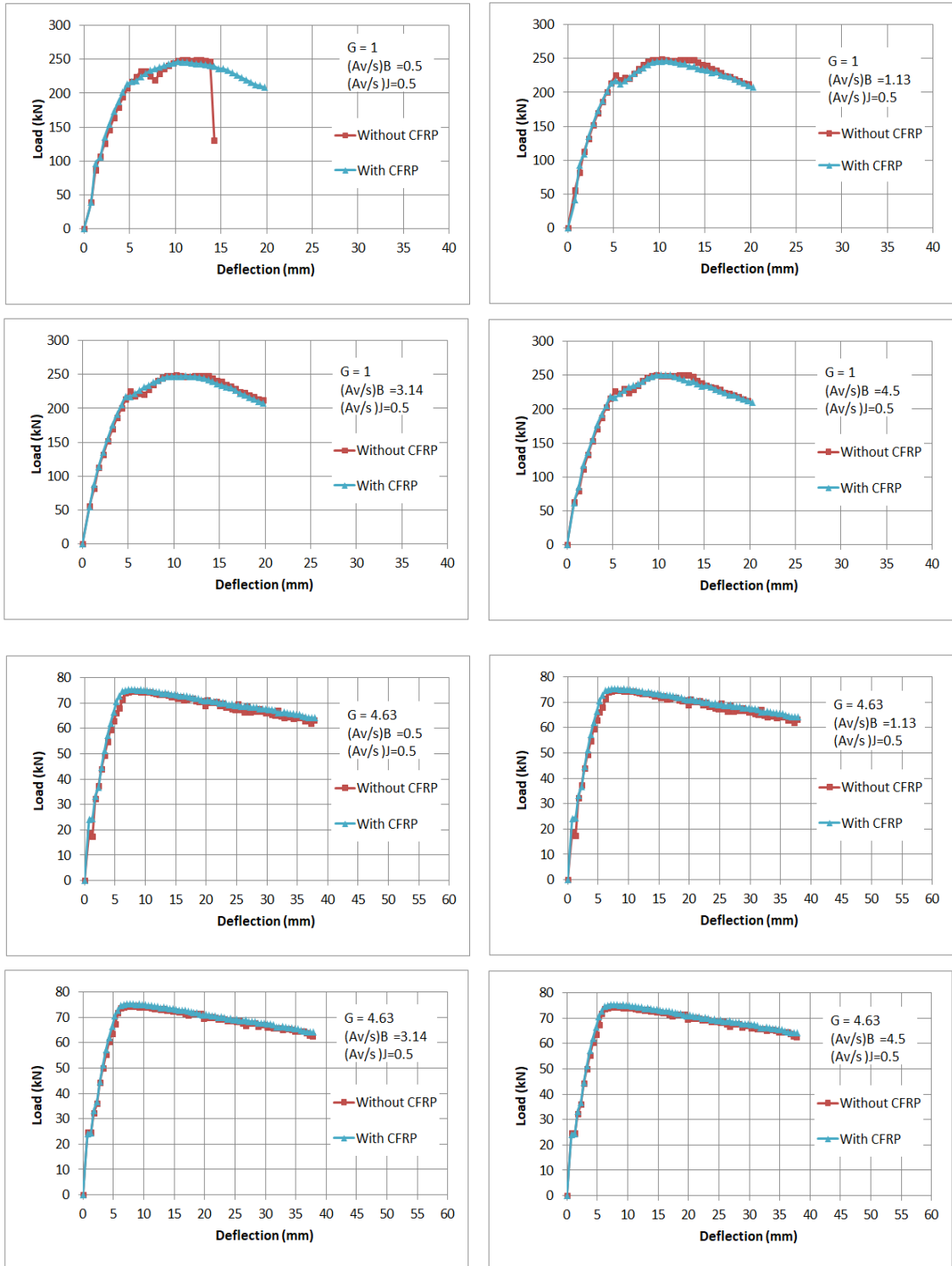


Figure 5.18: Effect of CFRP on strength and ductility of joints with minimum $(Av/s)_j$

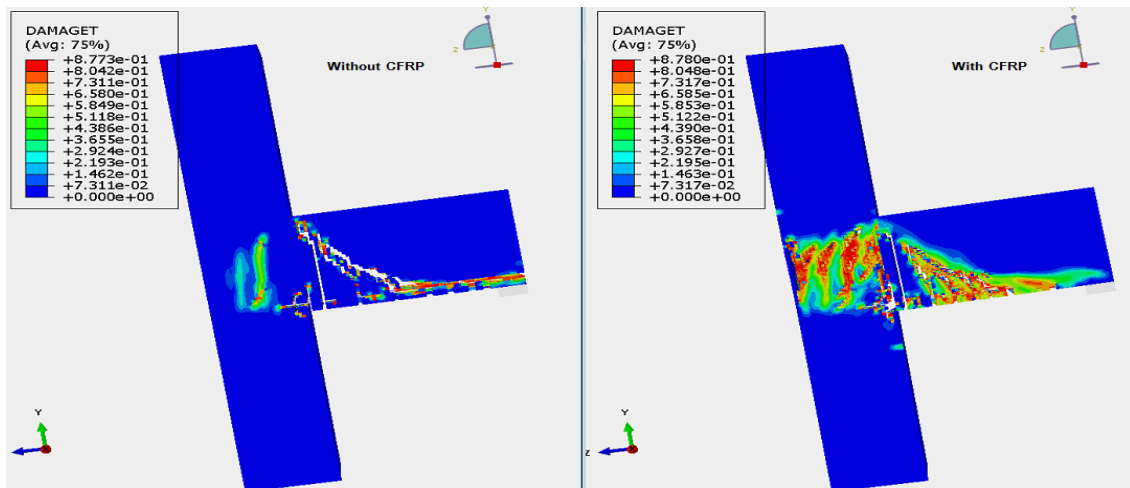


Figure 5.19: Cracks at failure before (G1-MaJ-MiB-0) and after (G1-MaJ-MiB-1) wrapping CFRP

5.5 Failure modes

Different types of failure modes happen in the simulated exterior R.C beam-column joints. Failure mode is controlled by many parameters such as amount of shear reinforcement inside joint $(A_v/s)_j$, amount of shear reinforcement in beam $(A_v/s)_B$, relative inertia between beam and column (G) , and method of wrapping of CFRP.

Generally, the types of failure can be divided into two categories. The first is ductile failure, another one is brittle failure. These failure modes will be illustrated in this section with clear examples.

5.5.1 Ductile failure

Ductile failure includes one of the following cases:

1- Crushing of concrete at compression zone of the beam after yielding of tension beam bars. This failure mode is called flexural failure in the beam (FB-D). For instance, model (G3-MaJ-MaB-0) illustrates a good example on FB-D failure. The obtained F.E. response of this joint is shown in Figure 5.20 and the general features (marked from 1 to 4) can be clearly seen on the curve.

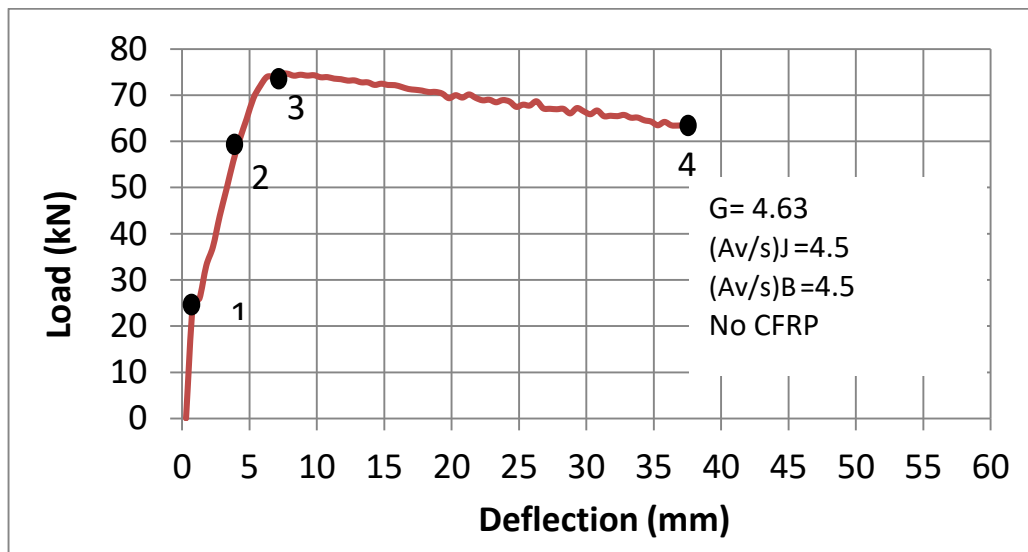


Figure 5.20: Load –deflection curve for joint (G3-MaJ-MaB-0) with stages of behaviors

The typical sequence of failure of the behavior is marked on the curve as follows:

Point (1) represents tensile cracking of beam. A 3D view of the axial stress (S33) in beam at this stage is shown in Figure 5.21.

Point (2) represents yielding of steel. A 3D view of the longitudinal stress in steel at this limit is shown in Figure 5.22.

Point (3) represents maximum Tri-axial compressive capacity of concrete at top layer of compression zone in beam. At this point, the compression stress starts to decrease as shown in Figure 5.23.

Point (4) represents flexure failure of joint due to crushing of beam concrete. Beyond this point, the joint is no longer capable of resisting imposed rotations. Distribution of plastic strain clearly shows that the type of failure is flexural failure due to damage of concrete at compression zone of beam as shown in Figure 5.24. Compression damage of concrete at this stage is shown in Figure 5.25.

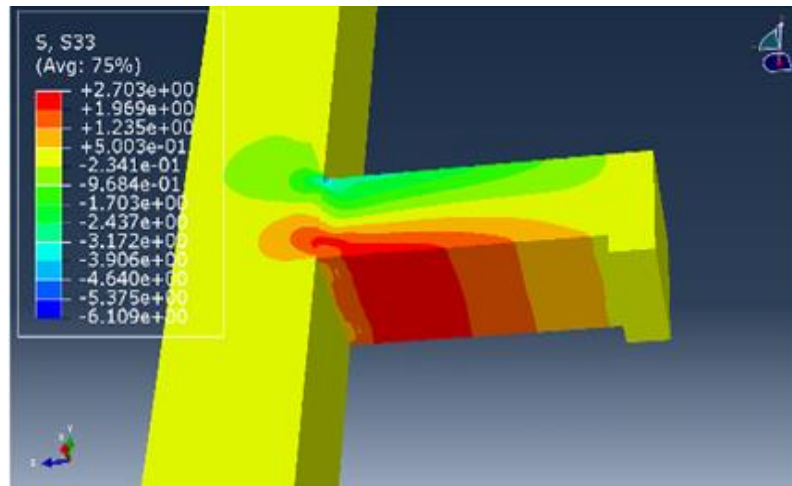


Figure 5.21: Cracking of beam for joint (G3-MaJ-MaB-0) (Normal stress in MPa)

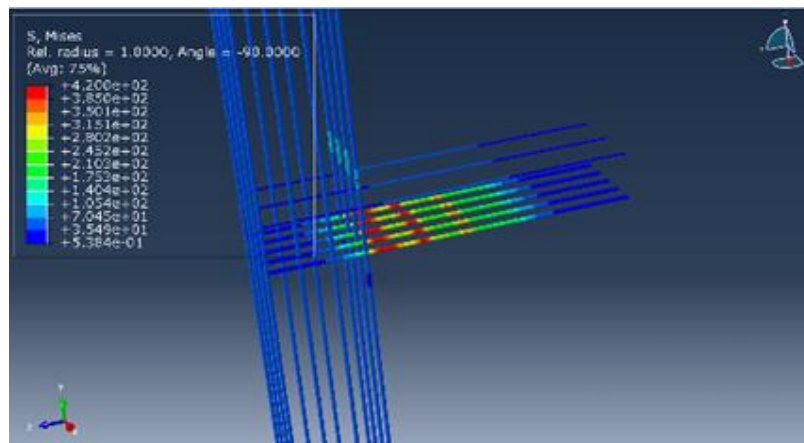


Figure 5.22: Yielding of steel for joint (G3-MaJ-MaB-0) (Tensile stress in MPa)

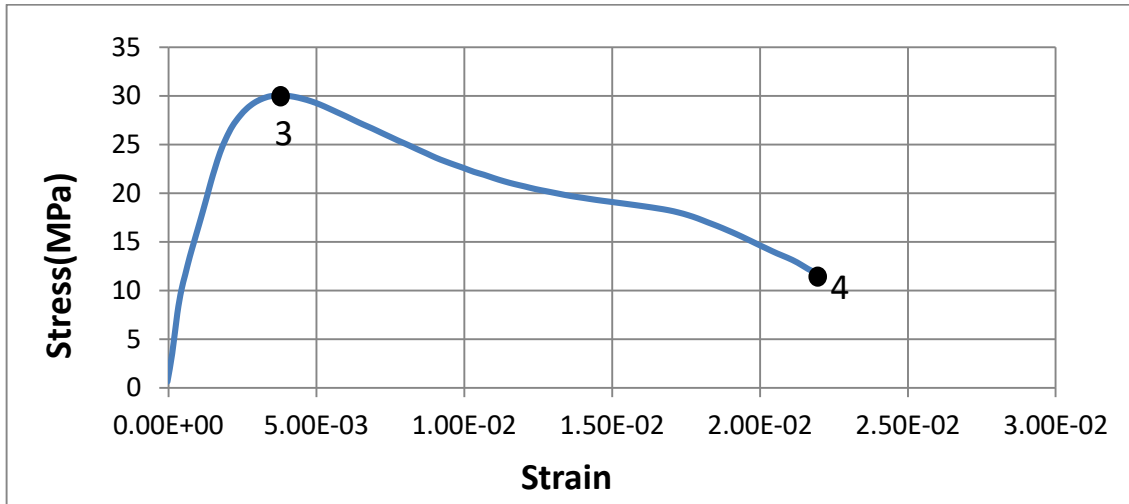


Figure 5.23: F.E. resulting stress strain curve for points in the compression zone of beam for joint (G3-MaJ-MaB-0)

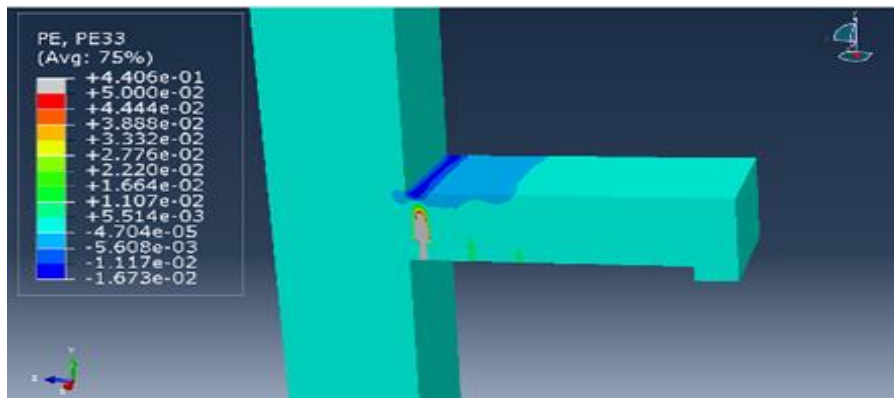


Figure 5.24: Plastic Strain distribution at beam for joint (G3-MaJ-MaB-0)

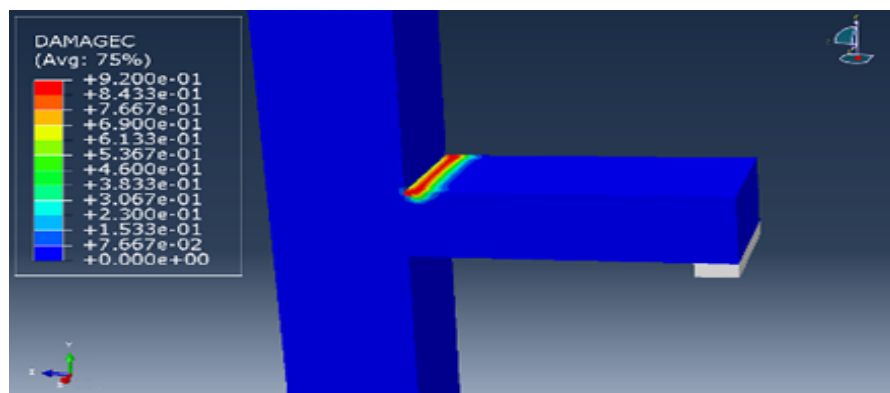


Figure 5.25: Compression damage of Concrete for joint (G3-MaJ-MaB-0)

2- Shear failure of joint (SJ-D). This type happens for models with the following conditions: ($G \leq 1$, $(A_v/s)_J = 0.5$ (minimum) and $(A_v/s)_B > 0.5$ for models without CFRP, but $(A_v/s)_B \geq 0.5$ for models with CFRP). Model (G1-MiJ-MaB-0) demonstrates a good example on this type of failure, the obtained F.E. response of this joint is shown in Figure 5.26.

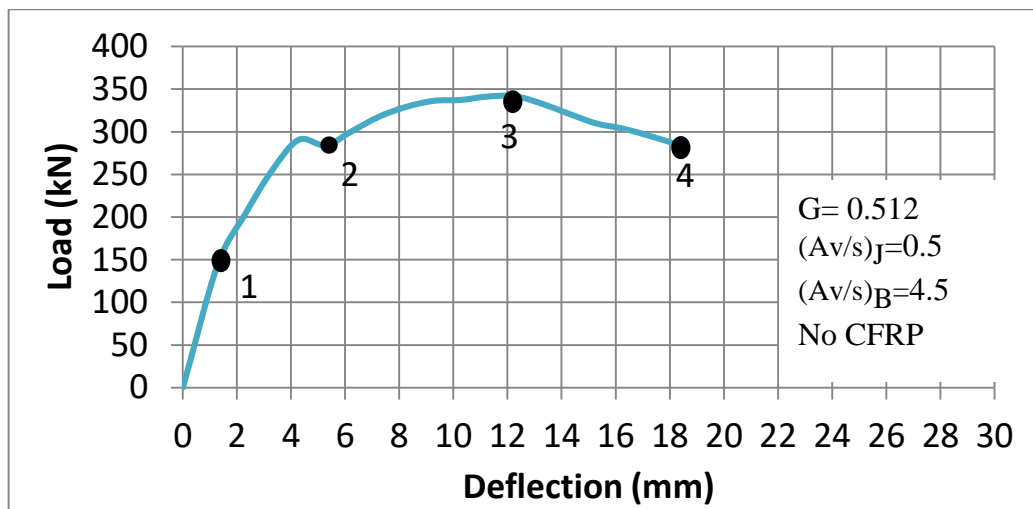


Figure 5.26: Load –deflection curve for joint (G1-MiJ-MaB-0) with stages of behaviors

The typical sequence of failure of the behavior is marked on the curve as follows:

Point (1) represents tensile cracking of beam. A 3D view of the axial stress (S33) in beam at this stage is shown in Figure 5.27.

Point (2) represents yielding of steel. A 3D view of the longitudinal stress in steel at this limit is shown in Figure 5.28.

Point (3) represents reaching ultimate compression stress at top layer of beam as shown in Figure 5.29. This is followed by shear failure of joint.

Point (4) represents complete diagonal shear failure in the joint. Figure 5.30 illustrates the tension damage of concrete which indicates that shear failure happens inside joint.

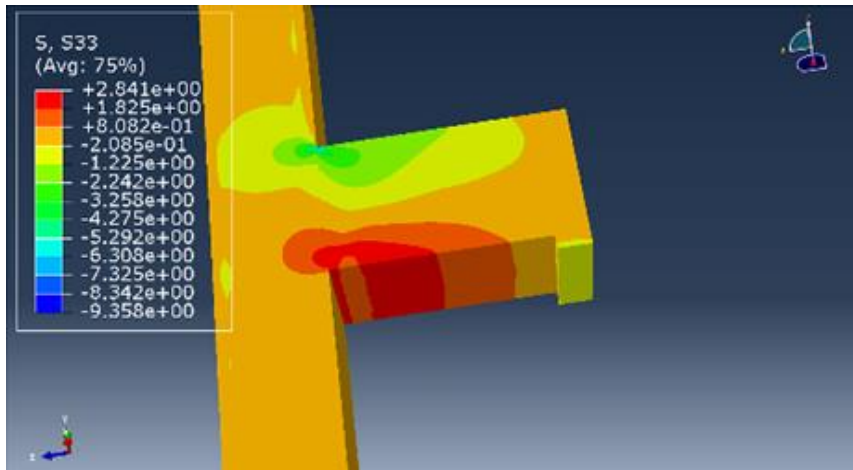


Figure 5.27: Cracking of beam for joint (G1-MiJ-MaB-0) (Normal stress in MPa)

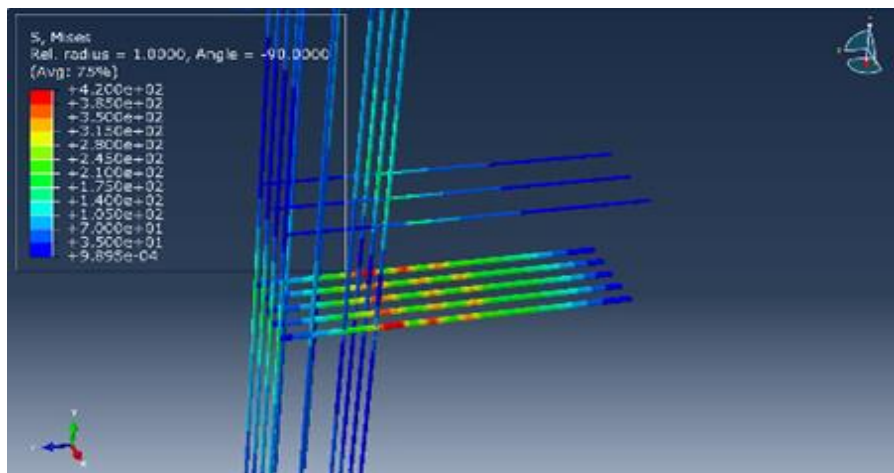


Figure 5.28: Yielding of steel for joint (G1-MiJ-MaB-0) (Tensile stress in MPa)

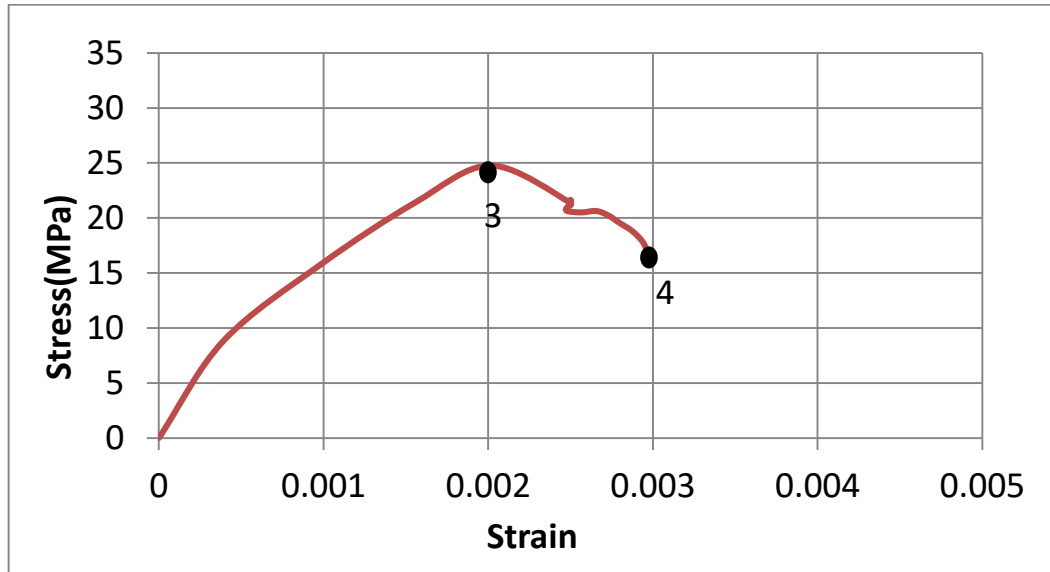


Figure 5.29: F.E. resulting Stress strain curve for points in the compression zone of beam for joint (G1-MiJ-MaB-0)

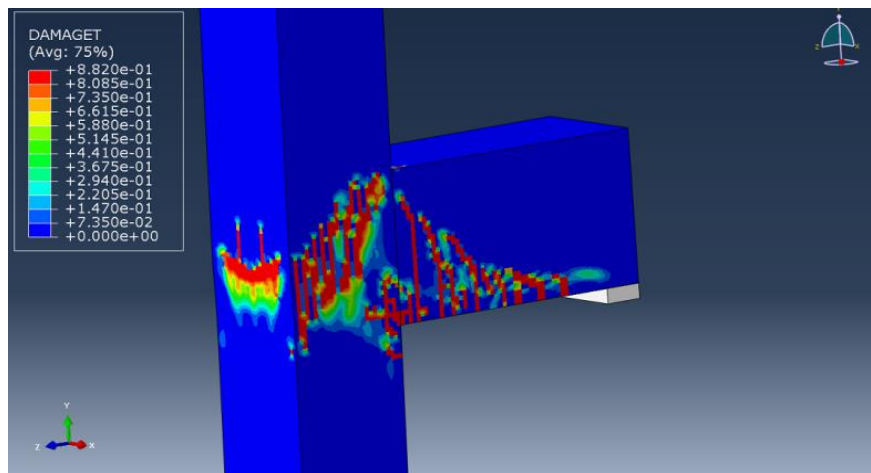


Figure 5.30: Tension damage of concrete beam for joint (G1-MiJ-MaB-0)

5.5.2 Brittle failure

Brittle failure includes one of the following:

- 1- Shear failure in the beam (SB-B). This type of failure happens for the following conditions (for $G = 0.512$, $(Av/s)_J = 4.5$ (maximum) and $(Av/s)_B \leq 1.13$ and for $G=1$, $(Av/s)_J = 4.5$ and $(Av/s)_B = 0.5$). This type

of failure could be avoided by using CFRP. Model (G1-MaJ-MiB-0) demonstrates a good example on the shear failure of beam, the obtained F.E. response of this joint is shown in Figure 5.31.

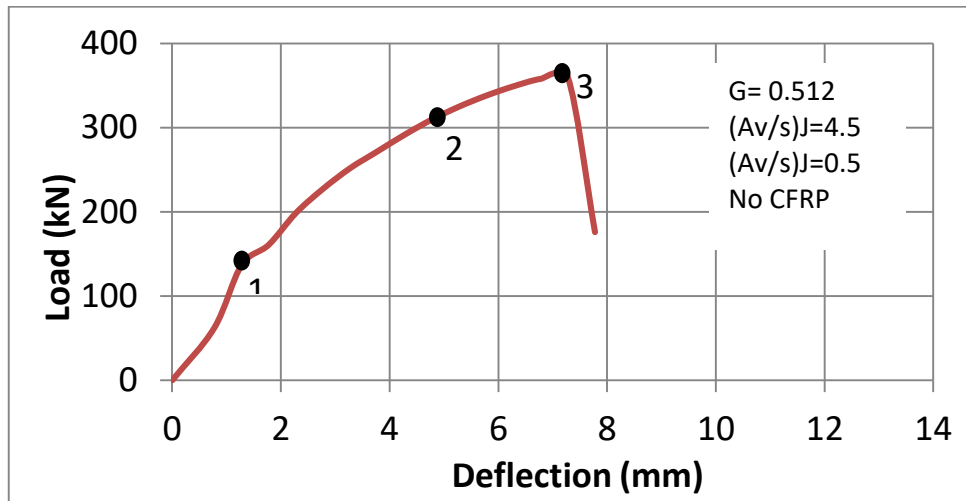


Figure 5.31: Load –deflection curve for joint (G1-MaJ-MiB-0) with stages of behaviors

The typical sequence of failure of the behavior is marked on the curve as follows:

Point (1) represents tensile cracking of beam. A 3D view of the axial stress (S33) in beam at this stage is shown in Figure 5.32.

Point (2) represents yielding of steel. A 3D view of the longitudinal stress in steel at this limit is shown in Figure 5.33.

Point (3) represents shear failure of beam due to insufficient strength of stirrups to resist shear force. Figure 5.34 illustrates the tension damage of concrete which indicates shear failure of beam.

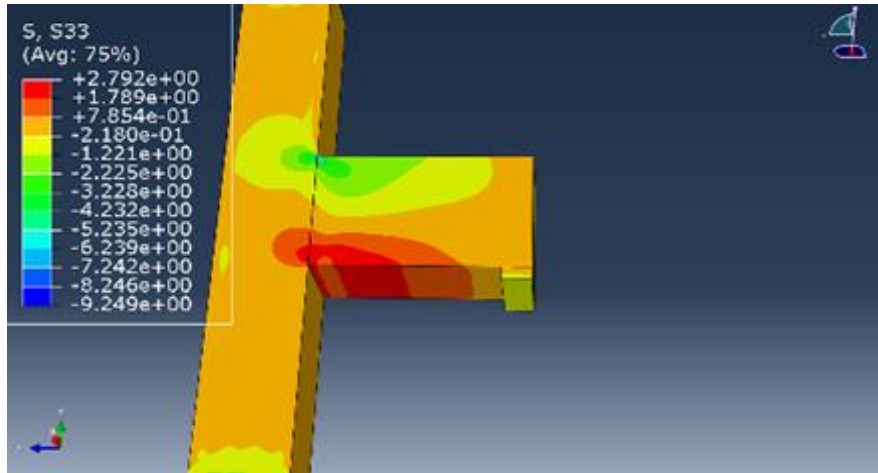


Figure 5.32: Cracking of beam for joint (G1-MaJ-MiB-0) (Normal stress in MPa)

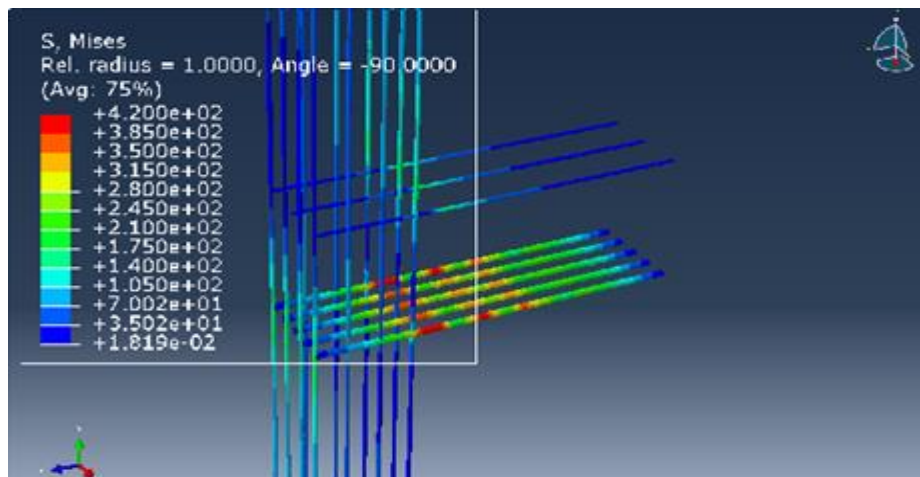


Figure 5.33: Yielding of steel for joint (G1-MaJ-MiB-0) (Tensile stress in MPa)

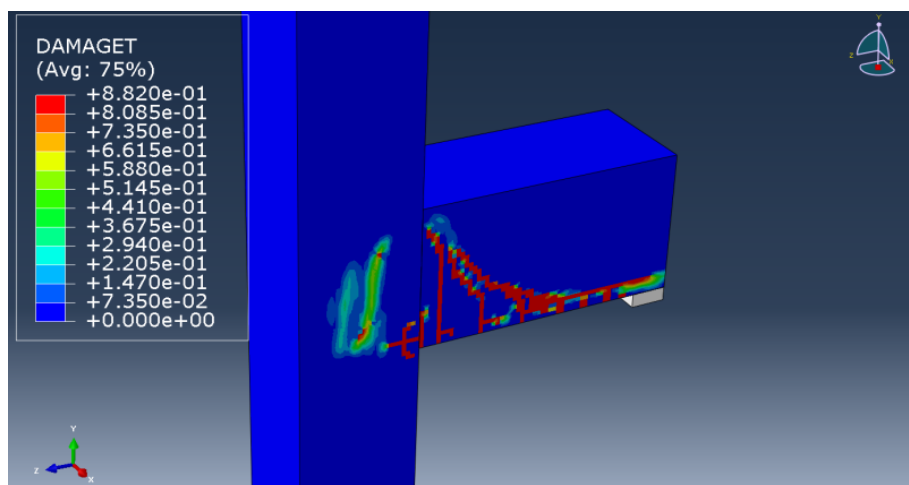


Figure 5.34: Complete tension damage of concrete beam for joint (G1-MaJ-MiB-0)

2- Shear failure of joint and beam simultaneously (SJSB-B). This type is developed for $G \leq 1$, $(A_v/s)_J = 0.5$ and $(A_v/s)_B = 0.5$. The sequence of failure is similar to (SB-B) but with shear failure happening in beam and joint at the same time. Model (G1-MiJ-MiB-R) demonstrates a good example on this type of failure. The obtained F.E. response of this joint is shown in Figures 5.35 to 5.37.

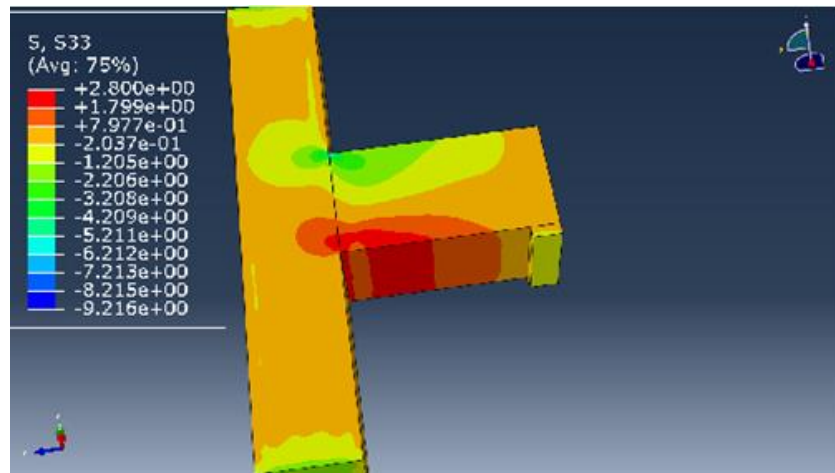


Figure 5.35: Cracking of beam for joint (G1-MiJ-MiB-R) (Normal stress in MPa)

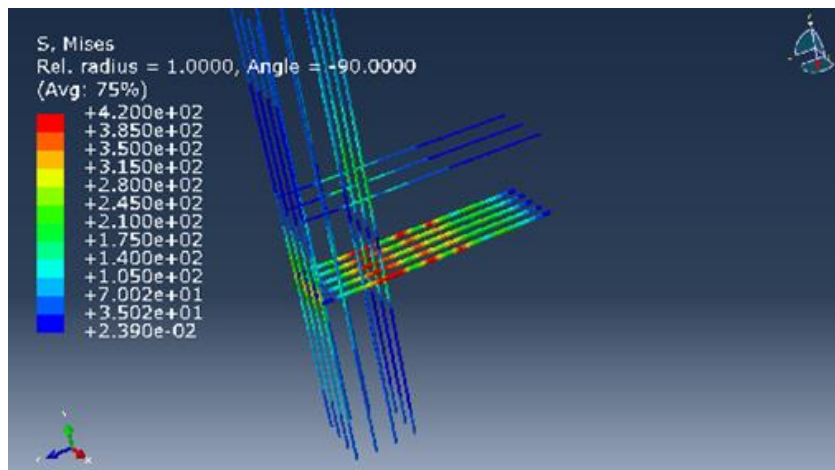


Figure 5.36: Yielding of steel for joint (G1-MiJ-MiB-R) (Tensile stress in MPa)

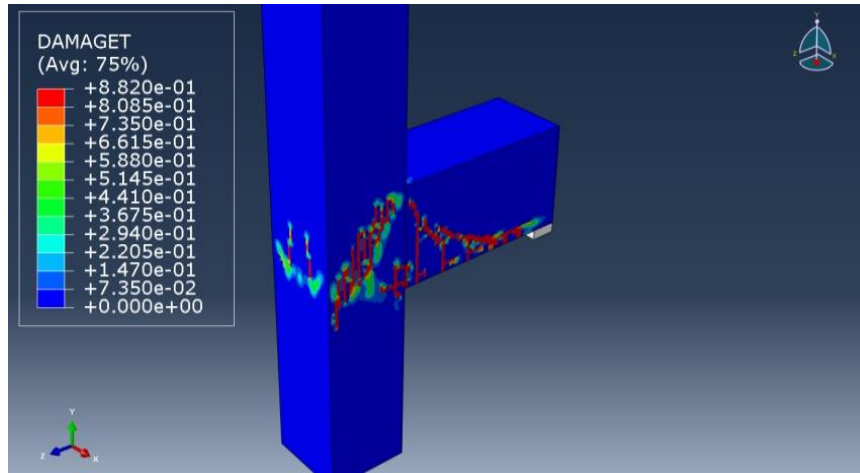


Figure 5.37: Complete tension damage of concrete beam for joint (G1-MiJ-MiB-R)

Table 5.2 summarizes the main features for all curves which are developed from F.E. These main features include; yield force (P_y), Peak force (P_p), force which goes under 85% of the peak force (P_c), deflection at yield force (Δ_y), deflection at peak force (Δ_p) and deflection at load criteria (ultimate deflection) (Δ_u). Also this table summarizes the failure mode for all joints.

Table 5.2: Summary of F.E. results

Model	P_y (kN)	P_p (kN)	P_c (kN)	Δ_y (mm)	Δ_p (mm)	Δ_u (mm)	Ductility ($\frac{\Delta_u}{\Delta_y}$)	Failure mode
G1-MaJ-MiB-0	350	360	306	6.28	7.8	7.8	1.24	SB-B
G1-MaJ-B1B-0	360	400	340	6.28	8.7	10.27	1.64	SB-B
G1-MaJ-B2B-0	366.4	416.2	353.77	6.28	10.2	20.27	3.23	FB-D
G1-MaJ-MaB-0	366.5	417	354.45	6.28	10.2	20.3	3.23	FB-D
G2-MaJ-MiB-0	210	260.2	221.17	5	7.4	8.8	1.76	SB-B
G2-MaJ-B1B-0	220	274	232.9	5	7.4	22.26	4.45	FB-D
G2-MaJ-B2B-0	230	274.5	233.325	5	7.4	23	4.6	FB-D
G2-MaJ-MaB-0	230	275	233.75	5	7.4	23	4.6	FB-D
G3-MaJ-MiB-0	69	74.5	63.325	5.2	7.5	37.8	7.27	FB-D
G3-MaJ-B1B-0	69	74.8	63.58	5.2	7.5	38	7.31	FB-D
G3-MaJ-B2B-0	69	75	63.75	5.2	7.5	38.3	7.37	FB-D
G3-MaJ-MaB-0	69	75	63.75	5.2	7.5	38.5	7.4	FB-D
G1-MiJ-MiB-0	310	330.1	280.585	6.5	10.2	13.1	1.95	SJSB-B
G1-MiJ-B1B-0	310	347	294.95	6.7	10.2	18.266	2.73	SJ-D
G1-MiJ-B2B-0	315	347	294.95	6.7	10.2	18.76	2.8	SJ-D
G1-MiJ-MaB-0	315	347	294.95	6.7	10.2	18.77	2.8	SJ-D
G2-MiJ-MiB-0	220	249	211.65	5	9	14.5	2.9	SJSB-B
G2-MiJ-B1B-0	225	249	211.65	5	9	19.76	4	SJ-D
G2-MiJ-B2B-0	225	249	211.65	5	9	19.8	4	SJ-D
G2-MiJ-MaB-0	225	250.6	213.01	5	9	19.81	4	SJ-D
G3-MiJ-MiB-0	69	74.5	63.325	5.2	7.5	37.78	7.27	FB-D
G3-MiJ-B1B-0	69	74.5	63.325	5.2	7.5	37.78	7.27	FB-D

G3-MiJ-B2B-0	69	74.5	63.325	5.2	7.5	38	7.31	FB-D
G3-MiJ-MaB-0	69	74.5	63.325	5.2	7.5	38	7.31	FB-D
G1-MaJ-MiB-1	370	408	346.8	6.28	7.8	19	3.03	FB-D
G1-MaJ-B1B-1	370	408.5	347.225	6.28	8.7	19	3.03	FB-D
G1-MaJ-B2B-1	370	417.6	354.96	6.28	10.2	19.5	3.1	FB-D
G1-MaJ-MaB-1	370	418	355.3	6.28	10.2	19.5	3.1	FB-D
G2-MaJ-MiB-1	230	277	235.45	5	7.4	22.25	4.45	FB-D
G2-MaJ-B1B-1	230	277	235.62	5	7.4	22.25	4.45	FB-D
G2-MaJ-B2B-1	230	279	237.15	5	7.4	23.25	4.65	FB-D
G2-MaJ-MaB-1	230	280	238	5	7.4	23.25	4.65	FB-D
G3-MaJ-MiB-1	70	75	63.75	5.2	7.5	38	7.31	FB-D
G3-MaJ-B1B-1	70	75	63.75	5.2	7.5	38	7.31	FB-D
G3-MaJ-B2B-1	70	75	63.75	5.2	7.5	38.4	7.38	FB-D
G3-MaJ-MaB-1	70	75	63.75	5.2	7.5	38.7	7.44	FB-D
G1-MiJ-MiB-1	302	347	294.95	6.7	10.2	18.25	2.72	SJ-D
G1-MiJ-B1B-1	302	347	294.95	6.7	10.2	18.25	2.72	SJ-D
G1-MiJ-B2B-1	302	347	294.95	6.7	10.2	18.7	2.79	SJ-D
G1-MiJ-MaB-1	302	347	294.95	6.7	10.2	18.7	2.79	SJ-D
G2-MiJ-MiB-1	216	246	209.1	5	9	19.7	3.94	SJ-D
G2-MiJ-B1B-1	216	247	209.95	5	9	20	4	SJ-D
G2-MiJ-B2B-1	216	248	210.8	5	9	20.2	4.04	SJ-D
G2-MiJ-MaB-1	216	250	212.5	5	9	20.4	4.08	SJ-D
G3-MiJ-MiB-1	70	75	63.75	5.2	7.5	38	7.31	FB-D
G3-MiJ-B1B-1	70	75	63.75	5.2	7.5	38	7.331	FB-D
G3-MiJ-B2B-1	70	75	63.75	5.2	7.5	38.4	7.38	FB-D
G3-MiJ-MaB-1	70	75	63.75	5.2	7.5	38.7	7.44	FB-D

5.6 Data fitting

After conducting the previous simulations and confirming the reasonability of the results, it is desired to have equations that can be used to predict the ductility of exterior R.C beam-column joint with and without CFRP.

MATLAB software is used to develop such equations using the multivariable fitting tool. The procedure that is used in the fitting is as follows: First, a data set containing results from the parametric study was used to fit the equations by minimizing the norm of error between equation and data points. Then the equations are simplified. After that, another independent set of F.E. simulation data are used to verify the fitted equations. The primary variables for the equation were selected to be the relative inertia (G), shear reinforcement in beam $(A_v/S)_B$ and shear reinforcement in joint $(A_v/S)_J$ with and without CFRP for a constant longitudinal reinforcement ratio ($\rho = 1\%$) for beam and column.

5.6.1 Ductility equation for exterior R.C beam-column joint without CFRP

Generally, two equations of ductility are proposed due to large variations in the ductility of joints due to the variable effect of shear failure in beam and other types of failure. First equation is for joints with brittle failure while the other for ductile failure. However, to predict which failure mode will happen; ACI 318 code equations for shear and bending capacities are used and compared. The equations are shown below.

$$P_{av} = V_{acb} + V_{asb} \quad (5.1)$$

$$V_{acb} = \frac{1}{6} \sqrt{f_c} b_w d \quad (\text{ACI-318}) \quad (5.2)$$

$$V_{asb} = \frac{A_v}{s} f_y d \quad (\text{ACI-318}) \quad (5.3)$$

$$M_{af} = b_w d^2 \rho f_y \left(1 - \frac{\rho f_y}{1.7 f_c}\right) \quad (\text{ACI-318}) \quad (5.4)$$

$$P_{af} = \frac{M_{af}}{L_t} \quad (5.5)$$

$$\Upsilon = \frac{P_{av}}{P_{af}} \quad (5.6)$$

Where

P_{av} : Approximated shear capacity of beam (N)

V_{acb} : Approximated shear capacity of concrete beam (N)

V_{asb} : Approximated shear capacity of stirrups in beam (N).

f_c : Compressive strength of concrete (MPa).

b_w : Width of cross section (mm).

d : Effective depth of cross section of beam (mm).

A_v : Area of stirrups that resist shear force in beam (mm²).

s : Spacing between stirrups in beam (mm).

f_y : yield stress of stirrups (MPa).

M_{af} : Approximated moment capacity of beam (N.mm).

ρ : Longitudinal reinforcement ratio.

P_{af} : Approximated flexural load capacity of beam (N)

L_t : total length of beam (mm) and is taken to be 900 mm in this thesis.

Υ : Factor for perdition the type of failure. (For brittle failure, $\Upsilon \leq 1$ while $\Upsilon > 1$ for ductile failure).

Multivariable surface fitting was done in MATLAB as shown in Figures 5.38 and 5.39 for brittle and ductile failure, respectively. As a result of these fittings, the surface equations were obtained, as a function of three variables:

the relative stiffness (G), transverse steel in beam $(A_v/s)_B$ and transverse steel in joint $(A_v/s)_J$. The relation between ductility and both variables (G) and $(A_v/s)_B$ is in direct relation, while it is in inverse relation between ductility and $(A_v/s)_J$ as shown in Equations (5.7) and (5.8). The resulting equations are bounded by the maximum and minimum values (D_{max} , D_{min}) of ductility as obtained by this study.

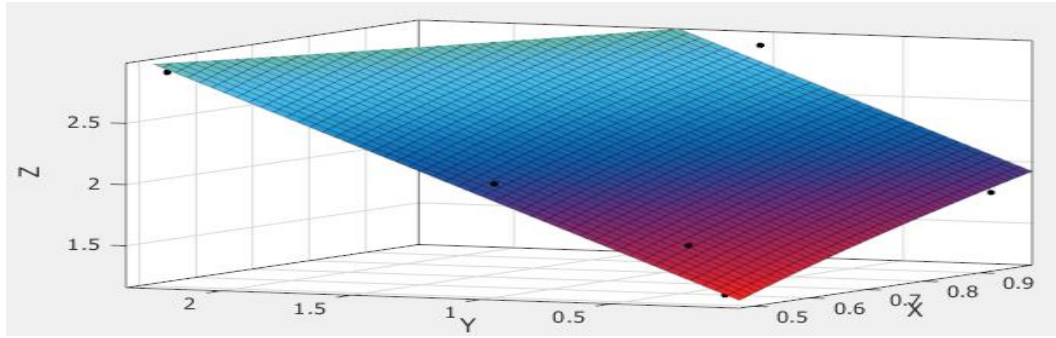


Figure 5.38: Surface ductility fitting for joints without CFRP with brittle failure

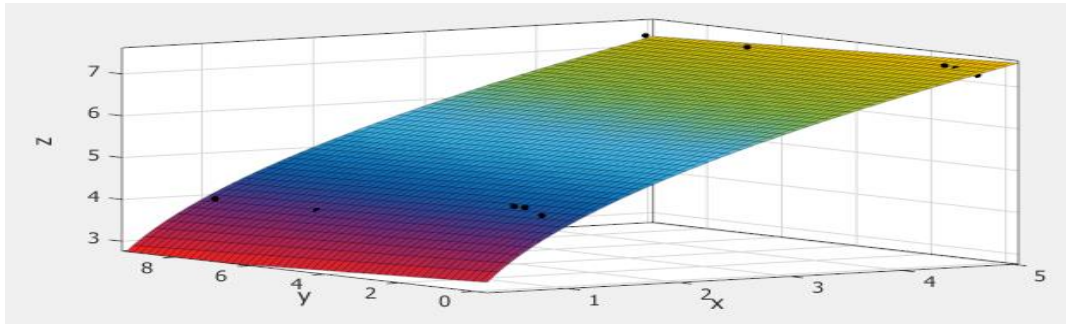


Figure 5.39: Surface ductility fitting for joints without CFRP with ductile failure

The final equation from this surface fitting is:

$$D_{min} \leq D_0 = -0.50 + 2.40\sqrt{G} + 0.70 \frac{\left(\frac{A_v}{s}\right)_B}{\left(\frac{A_v}{s}\right)_J} \leq D_{max}, \quad \text{for } \gamma \leq 1 \quad (5.7)$$

$$D_{min} \leq D_0 = 1.0 + 3.0\sqrt{G} + 0.010 \frac{\left(\frac{A_v}{s}\right)_B}{\left(\frac{A_v}{s}\right)_J} \leq D_{max}, \quad \text{for } \gamma > 1 \quad (5.8)$$

Where

D_0 : Ductility of exterior reinforced beam- column joint without CFRP

D_{max} : Maximum ductility of exterior reinforced beam- column joint without CFRP, and is taken equal to 7.5

D_{min} : Minimum ductility of exterior reinforced beam- column joint without CFRP, and is taken equal to 1.3

G : Relative gross inertia of column to beam (IC/IB)

S: spacing between stirrups.

A_v : area of stirrups that resist shear force.

Ductility of all models was calculated again by using Equations (5.7) and (5.8) and compared to ductility from ABAQUS as shown in Table 5.3.

Table 5.3: Comparing ABAQUS results and equation results for joints without CFRP

Model	Ductility (ABAQUS)	Ductility (Equations 5.7&5.8)	Relative error = 100%. $\frac{D_{ABAQUS} - D_{Equation}}{D_{ABAQUS}}$
G1-MaJ-MiB-0	1.24	1.3	-4.84
G1-MaJ-B1B-0	1.64	1.4	14.63
G1-MaJ-B2B-0	3.23	3.15	2.47
G1-MaJ-MaB-0	3.23	3.15	2.47
G2-MaJ-MiB-0	1.76	1.98	-12.5
G2-MaJ-B1B-0	4.45	4	10.11
G2-MaJ-B2B-0	4.6	4	13.04
G2-MaJ-MaB-0	4.6	4.01	12.83
G3-MaJ-MiB-0	7.27	7.45	-2.48
G3-MaJ-B1B-0	7.31	7.46	-2.05
G3-MaJ-B2B-0	7.37	7.46	-1.22
G3-MaJ-MaB-0	7.4	7.46	-0.81
G1-MiJ-MiB-0	1.95	1.92	1.54
G1-MiJ-B1B-0	2.73	2.8	-2.56
G1-MiJ-B2B-0	2.8	3.2	-14.3
G1-MiJ-MaB-0	2.8	3.23	-15
G2-MiJ-MiB-0	2.9	2.5	13.8
G2-MiJ-B1B-0	4	4.02	-0.5
G2-MiJ-B2B-0	4	4.06	-1.5
G2-MiJ-MaB-0	4	4.09	-2.25
G3-MiJ-MiB-0	7.27	7.46	-2.61
G3-MiJ-B1B-0	7.27	7.48	-2.9
G3-MiJ-B2B-0	7.31	7.52	-2.87
G3-MiJ-MaB-0	7.31	7.54	-3.15

For further verification, an independent set of data points was generated by ABAQUS to check the validity of the Equations 5.7 and 5.8. Ductility of eight independent models with geometry and reinforcement details as shown in the Appendix is calculated by ABAQUS software and compared with results from Equations (5.7) and (5.8). The properties of these models are shown in Table 5.4. The values of variables (G) , and $(AV/s)_B$ are selected to be within the range of earlier parameters.

Table 5.4: Properties of random joints without CFRP

Model	b_b	h_b	G	$(AV/S)_J$	$(AV/S)_B$	CFRP (Yes /No)
C1-MaJ-X1B-0	0.4m	0.36 m	1.37	4.5	1.74	No
C1-MaJ-X0B-0	0.4m	0.36 m	1.37	4.5	0.78	No
C2-MaJ-X1B-0	0.4m	0.29 m	2.62	4.5	1.74	No
C2-MaJ-X0B-0	0.4m	0.29 m	2.62	4.5	0.78	No
C1-MiJ-X1B-0	0.4m	0.36 m	1.37	0.5	1.74	No
C1-MiJ-X0B-0	0.4m	0.36 m	1.37	0.5	0.78	No
C2-MiJ-X1B-0	0.4m	0.29 m	2.62	0.5	1.74	No
C2-MiJ-X0B-0	0.4m	0.29 m	2.62	0.5	0.78	No

Load deflection curves of these models are shown in Figure 5.40

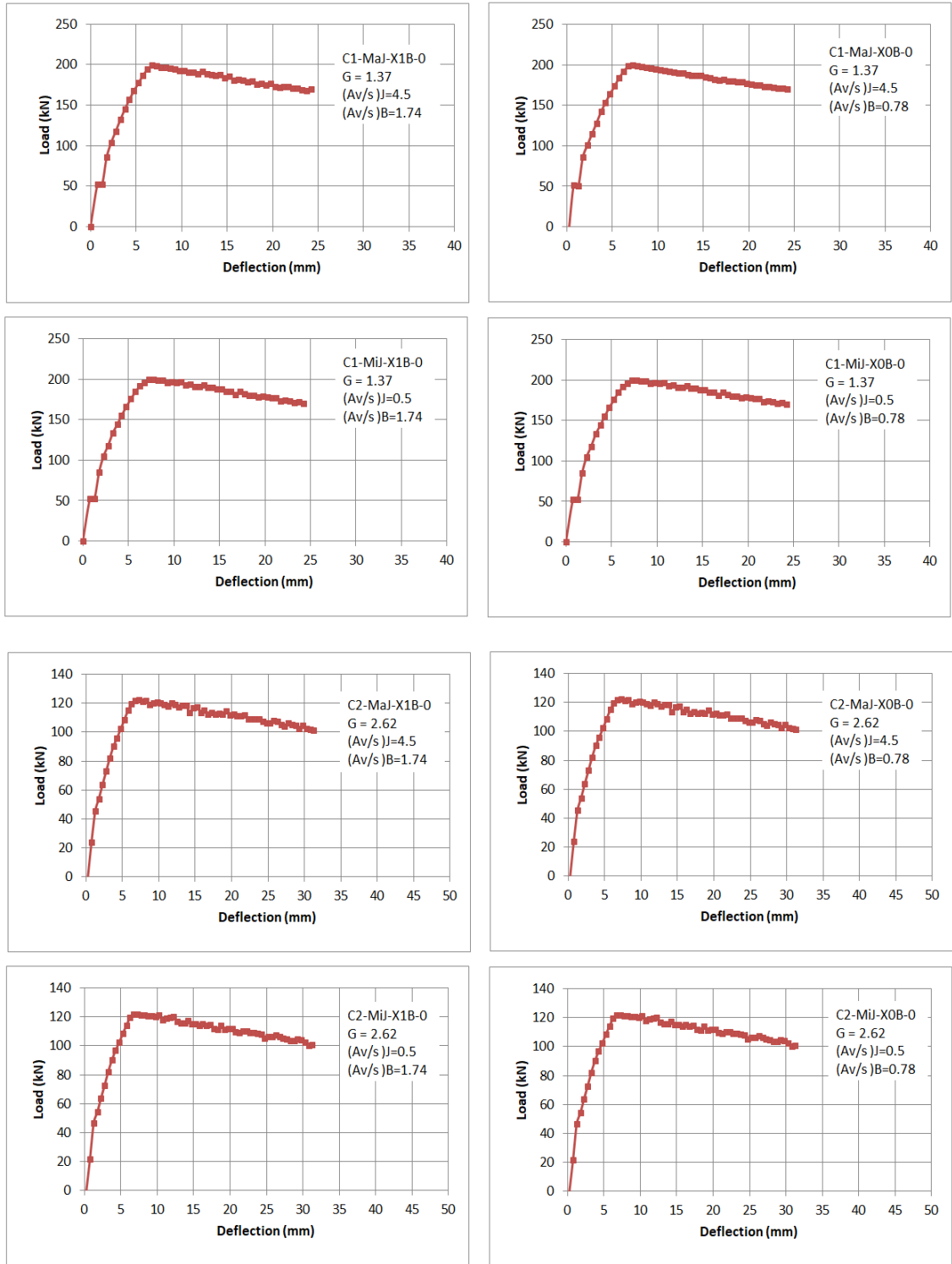


Figure 5.40: Load deflection curves for independent models without CFRP

Conclusion of results for these models as shown in Table 5.5

Table 5.5: Results of independent models without CFRP

Model	P_y (kN)	P_p (kN)	P_c (kN)	Δ_y (mm)	Δ_p (mm)	Δ_u (mm)	Ductility ($\frac{\Delta_u}{\Delta_y}$)
C1-MaJ-X1B-R	177	199	169.15	5.1	6.8	24.26	4.76
C1-MaJ-X0B-R	177	199	169.15	5.1	6.8	24.25	4.75
C2-MaJ-X1B-R	108	122	103.7	5.1	6.8	31	6.08
C2-MaJ-X0B-R	108	121	102.85	5.1	6.8	30	5.88
C1-MiJ-X1B-R	177	199	169.15	5.1	6.8	24.26	4.76
C1-MiJ-X0B-R	177	199	169.15	5.1	6.8	24.25	4.75
C2-MiJ-X1B-R	108	122	103.7	5.1	6.8	31	6.08
C2-MiJ-X0B-R	108	121	102.85	5.1	6.8	30	5.88

The comparisons between ABAQUS ductility and ductility from Equations (5.7) and (5.8) for these independent models are shown in Table 5.6.

Table 5.6: Comparing ABAQUS results and equation results for independent models without CFRP

Model	Ductility (ABAQUS)	Ductility (Equations 5.7 & 5.8)	Relative error = $100\% \cdot \frac{D_{ABAQUS} - D_{Equation}}{D_{ABAQUS}}$
C1-MaJ-X1B-0	4.76	4.52	5.04
C1-MaJ-X0B-0	4.75	4.51	5.05
C2-MaJ-X1B-0	6.08	5.86	3.62
C2-MaJ-X0B-0	5.88	5.86	0.34
C1-MiJ-X1B-0	4.76	4.55	4.4
C1-MiJ-X0B-0	4.75	4.53	4.63
C2-MiJ-X1B-0	6.08	5.89	3.13
C2-MiJ-X0B-0	5.88	5.87	0.2

As shown in Figures 5.41 and 5.42 that the relation between relative error and each variable of these equations has a random distribution. This means that the fit optimally provides random error in values. The relation between ductility from ABAQUS and ductility from Equations 5.7 and 5.8 is shown in Figure 5.43. This figure shows that the maximum percent of error is 15%.

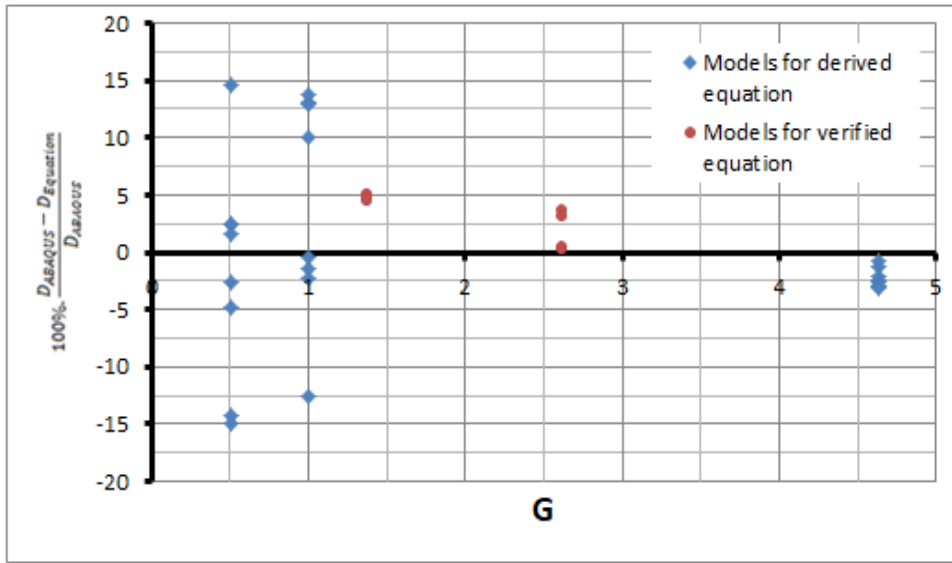


Figure 5.41: Relative errors as a function of relative stiffness (G) for models without CFRP

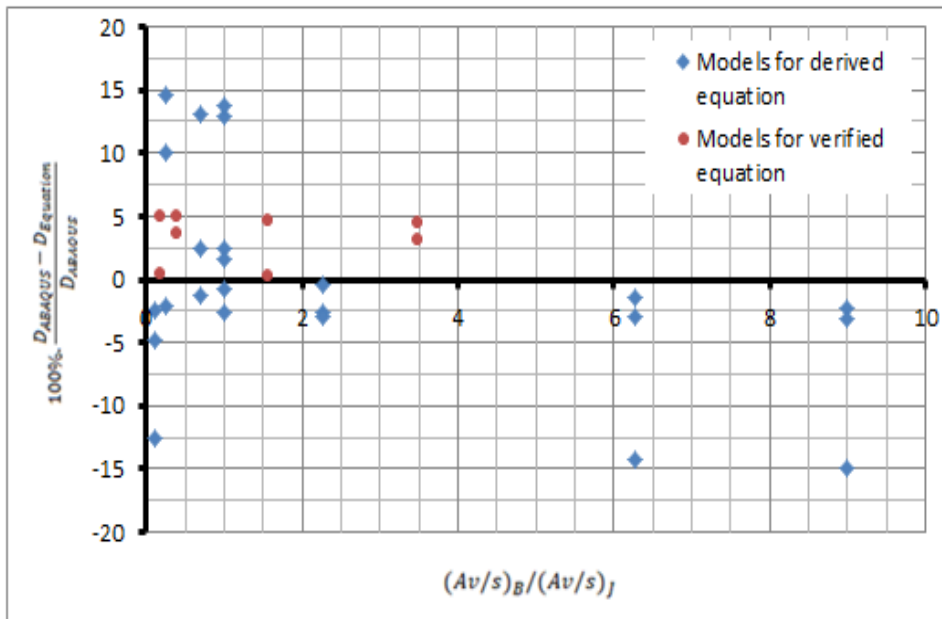


Figure 5.42: Relative errors as a function of transverse steel (Av/s) for models without CFRP

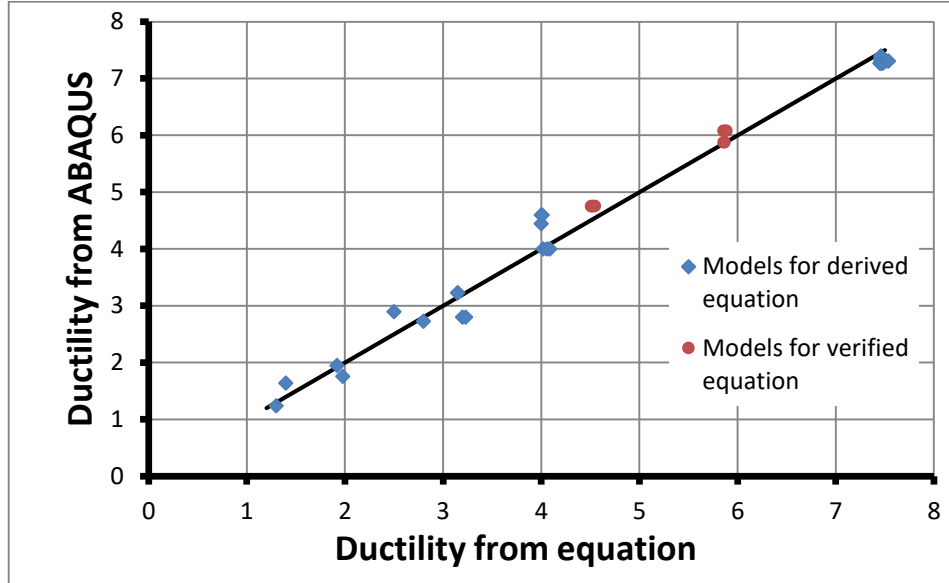


Figure 5.43: Relation between ABAQUS ductility and ductility from equations (5.7) and (5.8) for models without CFRP

5.6.2 Ductility equation for exterior reinforced beam-column joint with CFRP

Multivariable surface fitting was done in MATLAB as shown in Figure 5.44. As a result of this fitting, the surface equation was obtained, as a function of three variables: the relative stiffness (G), transverse steel in beam $(A_v/s)_B$ and transverse steel in joint $(A_v/s)_J$. The relation between ductility and both variables (G) and $(A_v/s)_B$ is in direct proportion, while it is in inverse proportion between ductility and $(A_v/s)_J$ as shown in Equation (5.9). The resulting equation are bounded by the maximum and minimum values (D_{F-max}, D_{F-min}) of ductility as obtained by this study.

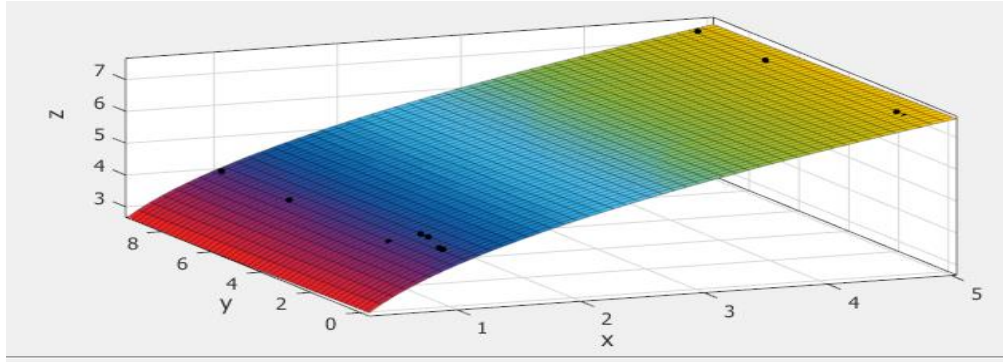


Figure 5.44: Surface ductility fitting for joints with CFRP

The final equation from this fitting is:

$$D_{F-min} \leq D_{FRP} = 1.0 + 3.0\sqrt{G} + 0.010 \frac{\left(\frac{Av}{s}\right)_B}{\left(\frac{Av}{s}\right)_J} \leq D_{F-max} \quad (5.9)$$

Where

D_{FRP} : Ductility of exterior reinforced beam- column joint with CFRP

D_{F-max} : Maximum ductility of exterior reinforced beam- column joint with CFRP, and is taken equal to 7.5

D_{F-min} : Minimum ductility of exterior reinforced beam- column joint with CFRP, and is taken equal to 3.

Ductility of all models was calculated again by using Equation (5.9) and compared to ductility from ABAQUS as shown in Table 5.7

Table 5.7: Comparing ABAQUS results and equation results for joint with CFRP

Model	Ductility (ABAQUS)	Ductility (equation 5.9)	Relative error = $100\% \cdot \frac{D_{ABAQUS} - D_{Equation}}{D_{ABAQUS}}$
G1-MaJ-MiB-1	3.03	3.15	-4
G1-MaJ-B1B-1	3.03	3.15	-4
G1-MaJ-B2B-1	3.1	3.15	-1.61
G1-MaJ-MaB-1	3.1	3.15	-1.61
G2-MaJ-MiB-1	4.45	4	10.11
G2-MaJ-B1B-1	4.45	4	10.11
G2-MaJ-B2B-1	4.65	4	14
G2-MaJ-MaB-1	4.65	4.01	13.76
G3-MaJ-MiB-1	7.31	7.45	-1.92
G3-MaJ-B1B-1	7.31	7.46	-2.05
G3-MaJ-B2B-1	7.38	7.46	-1.08
G3-MaJ-MaB-1	7.44	7.46	-0.27
G1-MiJ-MiB-1	2.72	3.15	-15
G1-MiJ-B1B-1	2.72	3.15	-15
G1-MiJ-B2B-1	2.79	3.2	-14.69
G1-MiJ-MaB-1	2.79	3.2	-14.69
G2-MiJ-MiB-1	3.94	4.01	-1.78
G2-MiJ-B1B-1	4	4.02	-0.5
G2-MiJ-B2B-1	4.04	4.06	-0.5
G2-MiJ-MaB-1	4.08	4.09	-0.25
G3-MiJ-MiB-1	7.31	7.46	-2.05
G3-MiJ-B1B-1	7.331	7.48	-2.03
G3-MiJ-B2B-1	7.38	7.52	-1.89
G3-MiJ-MaB-1	7.44	7.54	-1.34

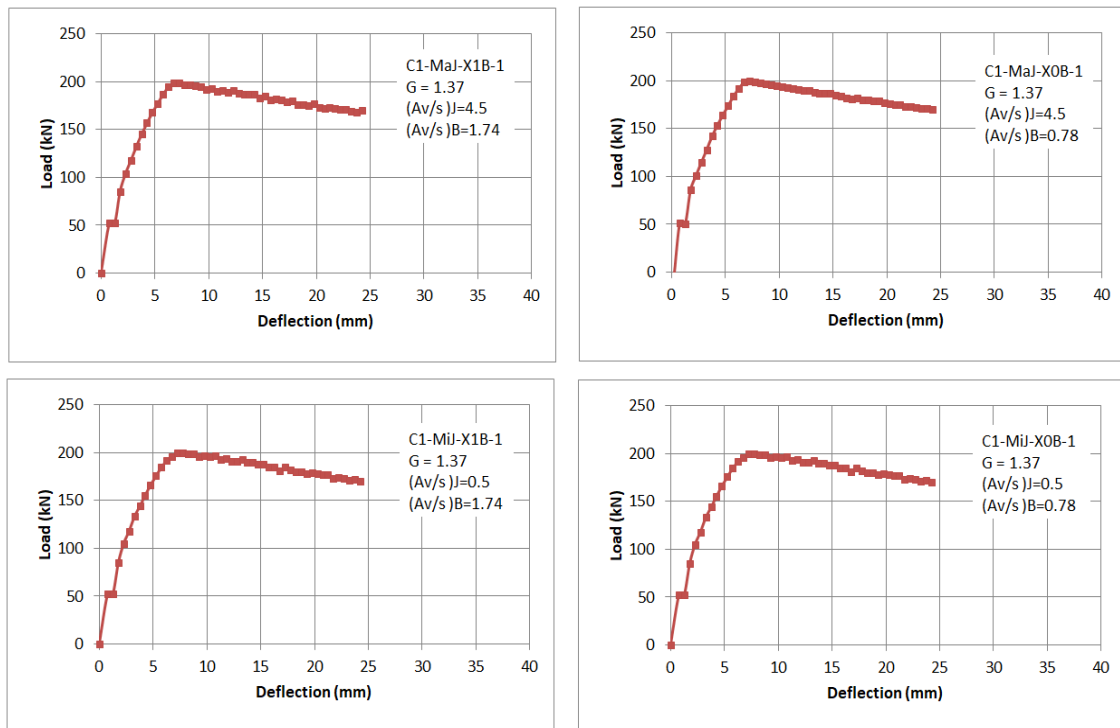
For further verification, an independent set of data points was generated by ABAQUS to check the validity of the Equation (5.9). Ductility of eight independent models with geometry and reinforcement details as shown in the Appendix is calculated by ABAQUS software and compared with results from Equation (5.9). The properties of these models are shown in Table 5.8.

The values of variables (G), and $(AV/s)_B$ are selected to be within the range of earlier parameters.

Table 5.8: Properties of random joints with CFRP

Model	b_b	h_b	G	$(AV/s)_J$	$(AV/s)_B$	CFRP (Yes /No)
C1-MaJ-X1B-1	0.4 m	0.36 m	1.37	4.5	1.74	Yes
C1-MaJ-X0B-1	0.4 m	0.36 m	1.37	4.5	0.78	Yes
C2-MaJ-X1B-1	0.4 m	0.29 m	2.62	4.5	1.74	Yes
C2-MaJ-X0B-1	0.4 m	0.29 m	2.62	4.5	0.78	Yes
C1-MiJ-X1B-1	0.4 m	0.36 m	1.37	0.5	1.74	Yes
C1-MiJ-X0B-1	0.4 m	0.36 m	1.37	0.5	0.78	Yes
C2-MiJ-X1B-1	0.4 m	0.29 m	2.62	0.5	1.74	Yes
C2-MiJ-X0B-1	0.4 m	0.29 m	2.62	0.5	0.78	Yes

Load deflection curves of these models are shown in Figure 5.45



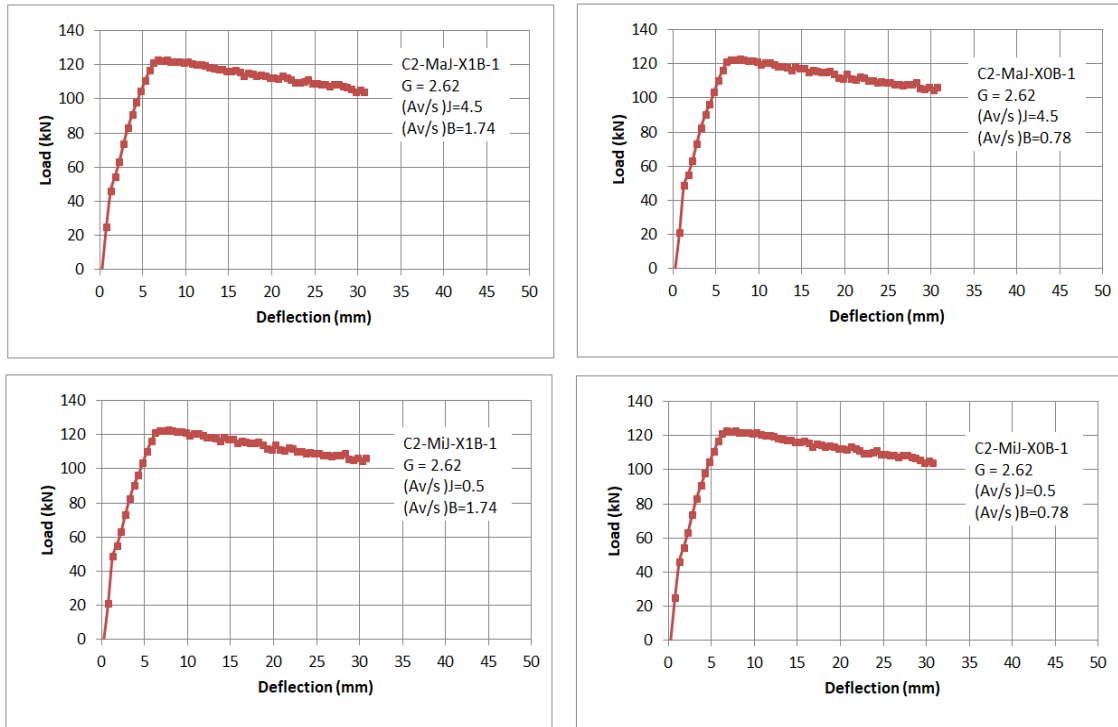


Figure 5.45: Load deflection curves for independent models with CFRP

Conclusion of results for these models is shown in Table 5.9.

Table 5.9: Results of independent models with CFRP

Model	P_y (kN)	P_P (kN)	P_c (kN)	Δ_y (mm)	Δ_p (mm)	Δ_u (mm)	Ductility $\left(\frac{\Delta_u}{\Delta_y}\right)$
C1-MaJ-X1B-1	180	202.3	171.955	5.1	6.8	25.2	4.94
C1-MaJ-X0B-1	180	202	171.7	5.1	6.8	25	4.9
C2-MaJ-X1B-1	106	122.7	104.295	5.1	6.8	31	6.08
C2-MaJ-X0B-1	106	122.6	104.21	5.1	6.8	30	5.9
C1-MiJ-X1B-1	180	202.3	171.955	5.1	6.8	25.2	4.94
C1-MiJ-X0B-1	180	202.3	171.955	5.1	6.8	25	4.92
C2-MiJ-X1B-1	106	122.7	104.295	5.1	6.8	31	6.08
C2-MiJ-X0B-1	106	122.6	104.21	5.1	6.8	30	5.88

The comparisons between ABAQUS ductility and ductility from equation (5.9) for these independent models are shown in Table 5.10.

Table 5.10: Comparing ABAQUS results and equation results for independent models with CFRP

Model	Ductility (ABAQUS)	Ductility (Equation 5.9)	Relative error = $100\% \cdot \frac{D_{\text{ABAQUS}} - D_{\text{Equation}}}{D_{\text{ABAQUS}}}$
C1-MaJ-X1B-1	4.94	4.52	8.5
C1-MaJ-X0B-1	4.9	4.51	7.96
C2-MaJ-X1B-1	6.08	5.86	3.62
C2-MaJ-X0B-1	5.9	5.86	0.68
C1-MiJ-X1B-1	4.94	4.55	7.89
C1-MiJ-X0B-1	4.92	4.53	7.93
C2-MiJ-X1B-1	6.08	5.89	3.13
C2-MiJ-X0B-1	5.88	5.87	0.17

As shown in Figures 5.46 and 5.47 that the relation between relative error and each variable of this equation has a random distribution. This means that the fit optimally provides random error in values. The relation between ductility from ABAQUS and ductility from Equation (5.9) is shown in Figure 5.48. This figure shows the maximum percent of error is 15%.

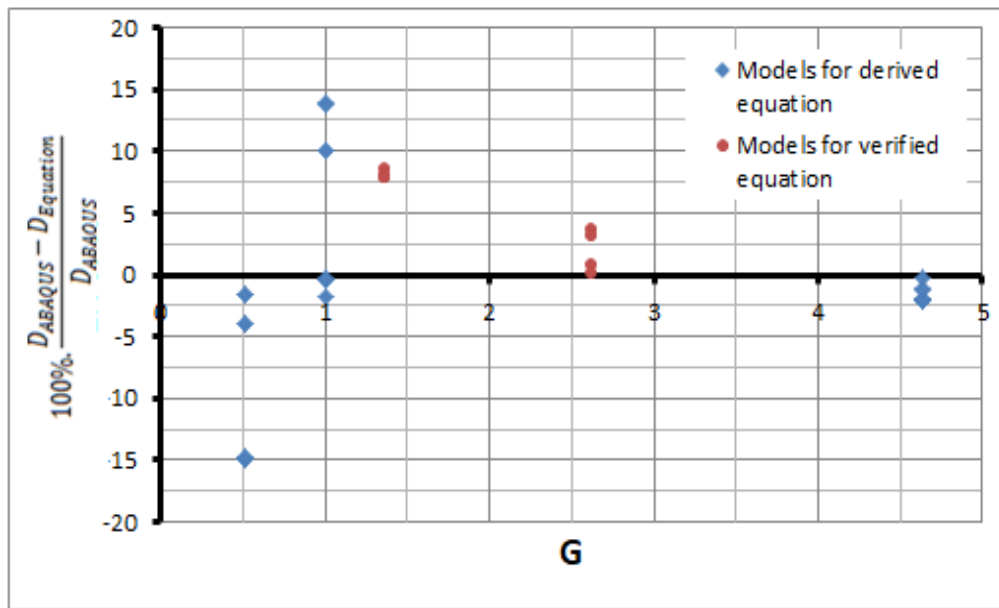


Figure 5.46: Relative errors as a function of relative stiffness (G) for models with CFRP

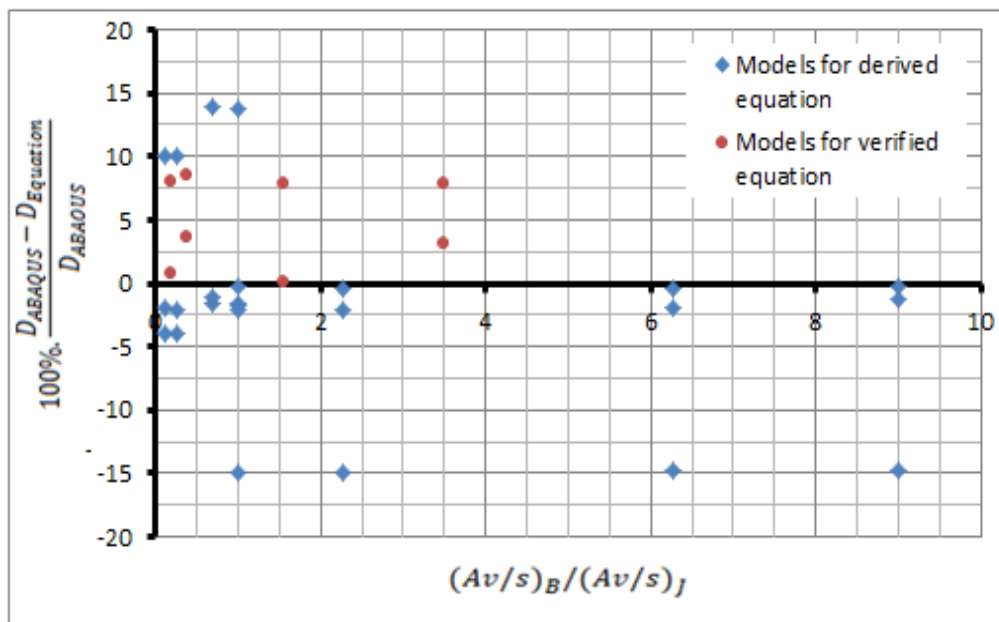


Figure 5.47: Relative errors as a function of transverse steel (Av/s) for models with CFRP

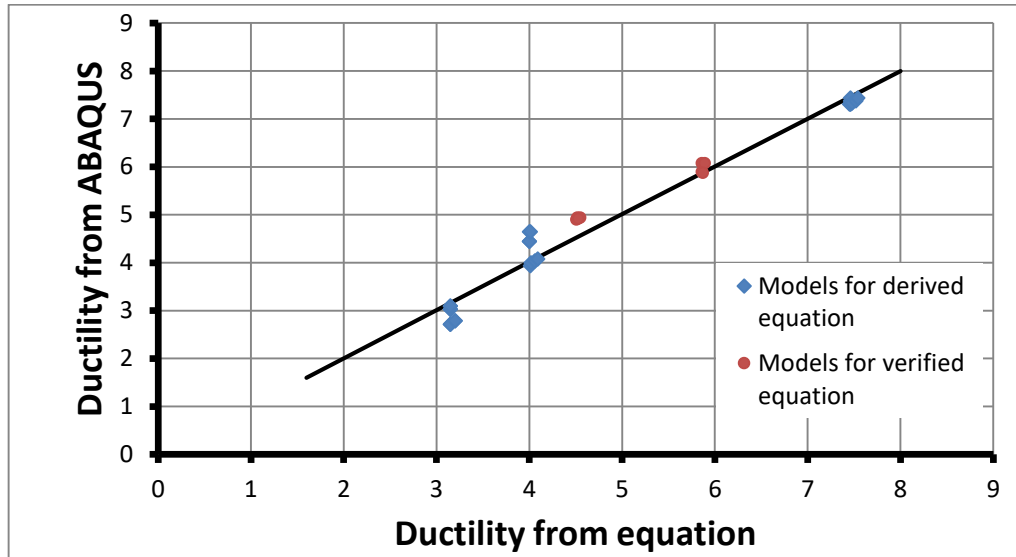


Figure 5.48: Relation between ABAQUS ductility and ductility from equation (5.9) for models with CFRP

5.7 Limitations of proposed equations

As shown before, for all cases, the maximum percent of error is less than 15%. Equations 5.7, 5.8 and 5.9 can be used with the following limitations:

- 1- These equations can be used for exterior R.C beam-column joints only.
- 2- Ratio between moment and shear loads on joint approximately equals 1.
- 3- Relative inertia (G) between 0.512 until to 4.63 (these values are common and realistic).
- 4- Flexural steel ratio for beam and column is 1% (this value is common and realistic).
- 5- Axial load on column equal $0.25A_g f_c$ (this value is common).
- 6- No axial force in beam.
- 7- One layer of CFRP.

6 Analytical verification

6.1 Overview

This chapter proposes an analytical verification for the behavior of exterior R.C beam-column joint subjected to monotonic loading at tip of beam. Yield and ultimate points in the load-deflection curve will be calculated analytically and compared with ABAQUS results. In the following sections the model and the approach to find these points is discussed.

6.2 Yield and ultimate moments capacity for beam

Yield and ultimate moments are calculated at critical section in beam at column face as shown in the model used for analytical solution in Figure 6.1 In the figure, L_{be} is the distance between applied load and column face (This value is constant and equals to 840 mm). However, the yield moment is taken as the moment corresponding to the first yield of the bottom beam longitudinal bars, while the ultimate moment is taken as the moment corresponding to the crushing of concrete at top face of beam. This crushing happens when stress-strain curve goes below 85% of the peak stress (ACI 318).

The theoretical yield and ultimate moments are calculated assuming linear strain distribution in the concrete. Also, linear stresses distributions along beam cross section are assumed to calculate yield moment, while the theoretical ultimate moment values are calculating from basic principles of sectional analysis by using the stress-strain curve used in ABAQUS.

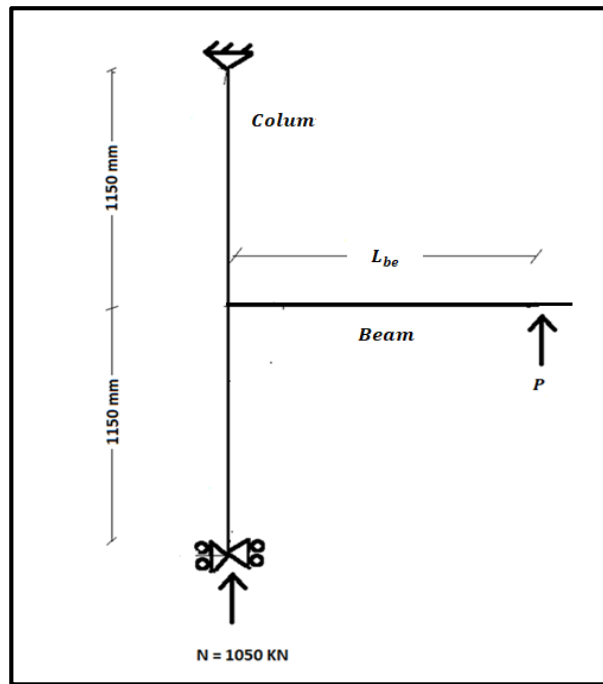


Figure 6.1: Model of beam-column joint for analytical solution

6.2.1 Methodology of calculating yield force

The theoretical yield moment is calculated using sectional analysis as shown in Figure 6.2.

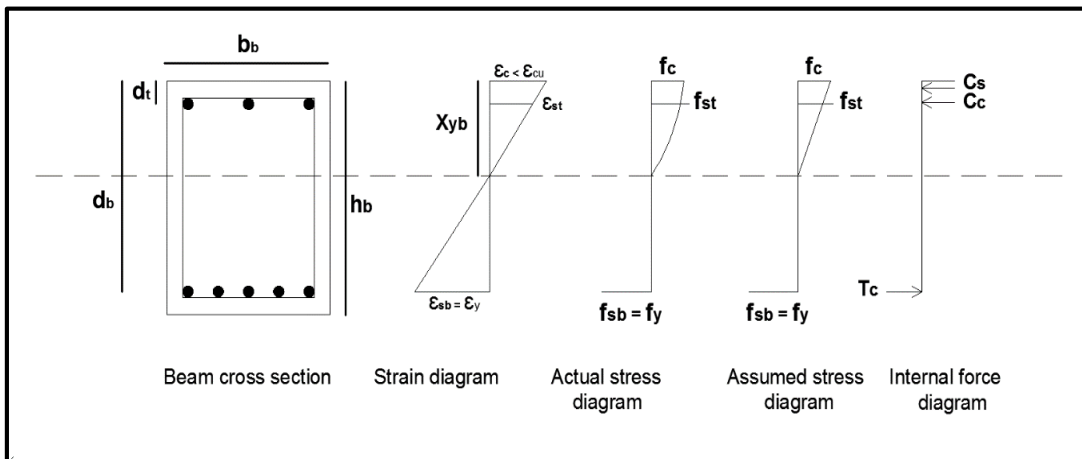


Figure 6.2: Stress, strain and force distributions along cross section of beam at yield stage

To calculate yield moment, we must determine location of neutral axis (x_{yb}) by the following equations.

Equilibrium equation:

$$C_c + C_s = T_s \quad (6.1)$$

$$C_c = 0.5x_{yb}f_c b_b \quad (6.2)$$

$$C_s = A_{st}f_{st} \quad (6.3)$$

$$T_s = A_{sb}f_{sb} = A_{sb}f_y \quad (6.4)$$

Where

b_b : Width of beam

h_b : Full depth of beam

d_b : Effective depth of beam

d_t : Cover (distance from the centroid of longitudinal bars and surface of concrete)

x_{yb} : Depth of neutral axis at yield stage which is calculated from top surface of beam

ε_c : Strain in concrete

ε_{cu} : Strain of concrete at crushing stage

ε_{st} : Strain in top longitudinal reinforcements.

ε_{sb} : Strain in bottom longitudinal reinforcements.

ε_y : Yield strain in bottom longitudinal reinforcements.

f_c : Stress in concrete

f_{st} : Stress in top longitudinal reinforcements.

f_{sb} : Stress in bottom longitudinal reinforcements.

f_y : Yield stress in bottom longitudinal reinforcements.

C_s : Compression force provided by top longitudinal reinforcements

C_c : Compression force provided by concrete.

T_s : Tension force provided by bottom longitudinal reinforcements

A_{st} : Area of top longitudinal reinforcements.

A_{sb} : Area of bottom longitudinal reinforcements.

Compatibility in strain diagram between concrete and bottom steel

$$\left[\frac{\varepsilon_c}{\varepsilon_y} = \frac{x_{yb}}{d_b - x_{yb}} \right] = \left[\left(\frac{E_s E_c}{E_s E_c} \right) \frac{\varepsilon_c}{\varepsilon_y} = \frac{x_{yb}}{d_b - x_{yb}} \right] = \left[n \frac{f_c}{f_y} = \frac{x_{yb}}{d_b - x_{yb}} \right], \text{ then } x_{yb} = \frac{f_c}{f_c + \frac{f_y}{n}} d_b \quad (6.5)$$

Where

E_c : Modulus of elasticity of concrete

E_s : Modulus of elasticity of steel

n : Modular ratio $\left(\frac{E_s}{E_c} \right)$

Compatibility in strain diagram between concrete and top steel

$$\left[\frac{\varepsilon_c}{\varepsilon_{st}} = \frac{x_{yb}}{x_{yb} - d_t} \right] = \left[\left(\frac{E_s E_c}{E_s E_c} \right) \frac{\varepsilon_c}{\varepsilon_{st}} = \frac{x_{yb}}{x_{yb} - d_t} \right] = \left[n \frac{f_c}{f_{st}} = \frac{x_{yb}}{x_{yb} - d_t} \right], \text{ then } f_{st} = \frac{n f_c (1 - \frac{d_t}{x_{yb}})}{n} \quad (6.6)$$

From these equations we can find the position of neutral axis (x_{yb}), then the

yield moment capacity of the beam (M_{yb}) can be determined

$$M_{yb} = 0.5 x_{yb} f_c b_b \left(\frac{2}{3} x_{yb} \right) + A_{st} f_{st} (x_{yb} - d_t) + A_{sb} f_y (d_b - x_{yb}) \quad (6.7)$$

Dividing the yield moment by the moment arm to the critical section at the

column face (L_{be}), the yield force (P_{yb}) can be calculated as

$$P_{yb} = \frac{M_{yb}}{L_{be}} \quad (6.8)$$

6.2.2 Methodology of calculating ultimate force

The theoretical ultimate moment is calculated from basic principle of sectional analysis by using actual stress-strain curve for concrete compressive strength is 25MPa as shown in Figure 6.3.

As mentioned before, ultimate moment is the moment corresponding to the crushing of concrete at top face of beam; this crushing happens when stress-strain curve goes below 85% of the peak stress (ACI 318). However, Figure 6.4 shows the stress, strain and force distributions along cross section of the beam.

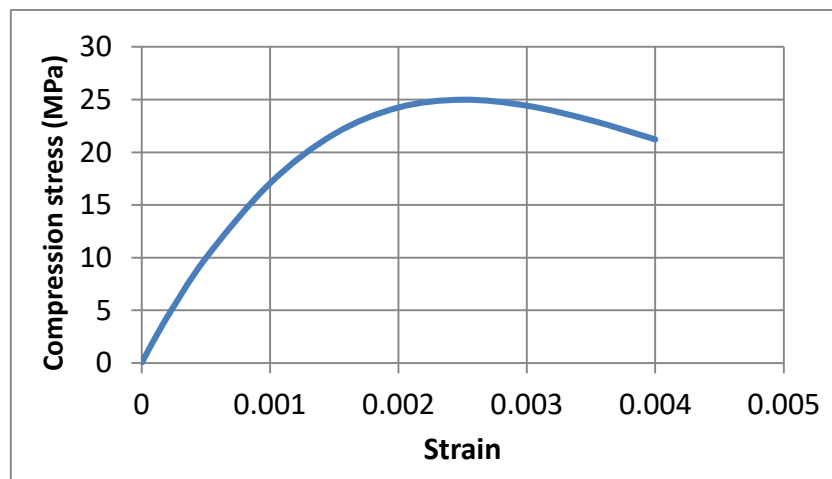


Figure 6.3: stress strain curve of concrete 25MPa

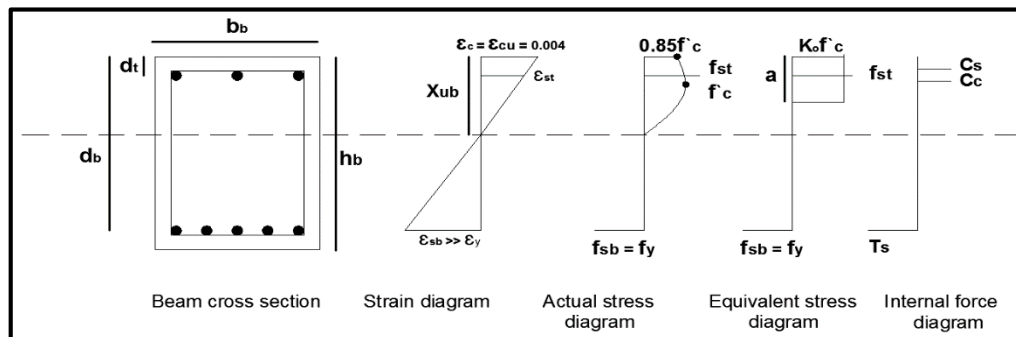


Figure 6.4: Stress, strain and force distributions along cross section of column at ultimate stage

Where

x_{ub} : Depth of neutral axis at ultimate stage which is calculated from top surface of beam.

f_c : Compressive stress of concrete.

a : Depth of compressive block of concrete.

K_0 : Factor for conversion the actual stress of concrete to equivalent stress

First of all, we must calculate factor (K_0) to convert the actual stress diagram to equivalent stress diagram. The following procedure is done to find this factor.

The equation of stress –strain as obtained from excel software is

$$f_c = 5 * 10^8 * \varepsilon_c^3 - 7 * 10^6 * \varepsilon_c^2 + 23225 * \varepsilon_c + 0.0026 \quad (6.9)$$

Then the centroid of this curve (ε_n) is

$$\varepsilon_n = \frac{\int_0^{0.004} f_c \varepsilon_c d\varepsilon_c}{\int_0^{0.004} f_c d\varepsilon_c} = 0.00219 \quad (6.10)$$

at $x = x_{ub}$ (from bottom to top) $\rightarrow \varepsilon_c = 0.004$

at $x = rx_{ub}$ (from bottom to top) $\rightarrow \varepsilon_c = 0.00219$

$$r = \frac{0.00219}{0.004} = 0.54 \text{ (from bottom to top)} \quad (6.11)$$

$$(1 - r)x_{ub} = 0.5a \rightarrow \frac{a}{x_{ub}} = \frac{1-r}{0.5} = \beta = 0.9 \quad (6.12)$$

$$\left(\int_0^{0.004} f_c d\varepsilon_c \right) \frac{x_{ub}}{0.004} = K_0 f_c \beta x_u b_b \rightarrow K_0 = 0.76 \quad (6.13)$$

To calculate the ultimate moment, we must determine location of neutral axis (x_{ub}) by the following equations.

Equilibrium equation:

$$C_c + C_s = T_s \quad (6.14)$$

$$C_c = 0.76 f_c \beta x_{ub} b_b \quad (6.15)$$

$$C_s = A_{st} f_{st} \quad (6.16)$$

$$T_s = A_{sb}f_{sb} = A_{sb}f_y \quad (6.17)$$

Compatibility in strain diagram between concrete and top steel

$$\left[\frac{\varepsilon_{cu}}{\varepsilon_{st}} = \frac{x_{ub}}{x_{ub}-d_t} \right] = \left[\left(\frac{E_s}{E_s} \right) \frac{\varepsilon_{cu}}{\varepsilon_{st}} = \frac{x_{ub}}{x_{ub}-d_t} \right] = \left[E_s \frac{\varepsilon_{cu}}{f_{st}} = \frac{x_{ub}}{x_{ub}-d_t} \right], \text{ then } f_{st} E_s \varepsilon_{cu} \left(1 - \frac{d_t}{x_{ub}} \right) \quad (6.18)$$

From these equations we can find the position of neutral axis (x_{ub}), then the ultimate moment capacity of the beam (M_{ub}) can be determined

$$M_{ub} = 0.76f_c \cdot 0.9x_{ub}b_b \left(\frac{a}{2} \right) + A_{st}f_{st}(a - d_t) + A_{sb}f_y (d - a) \quad (6.19)$$

Dividing the ultimate moment by the moment arm to the critical section at the column face (L_{be})

$$P_{ub} = \frac{M_{ub}}{L_{be}} \quad (6.20)$$

6.3 Beam shear capacity

Many equations that predict the shear capacity of R.C beam exist in literatures. Zsutty (1971), provides more accurate prediction of the shear capacity of beams through Equation (6.22). Many studies suggested that Zsutty (1971) equation is more appropriate and simple to predict the shear strength of both short and long beams as it takes into account size effect and longitudinal steel effect as shown in Equation (6.22) (Reddy et al., 2010). While ACI 318 code predicts the shear capacity of stirrups as shown in Equation (6.23). On the other hand, the shear strength of FRP fabric V_{fb} is calculated using the equation proposed by Khalifa et al. (1998) as shown in Equation (6.24).

$$V_b = V_{cb} + V_{sb} + V_{fb} \quad (6.21)$$

$$V_{cb} = f \left(2.2 \sqrt[3]{f_c' \rho \frac{d}{a}} \right) b_w d \quad (6.22)$$

$$f = 1 \quad \text{for } \frac{a}{d} \geq 2.5 \quad f = \left(2.5 \frac{d}{a} \right) \quad \text{for } \frac{a}{d} < 2.5$$

$$V_{sb} = \frac{Av}{s} f_y d \quad (6.23)$$

$$V_{fb} = n R f_{fu} t_e d_b (\sin \theta + \cos \theta) \quad (6.24)$$

Where

V_b : Shear capacity of R.C beam (N).

V_{cb} : Shear capacity of concrete beam (N).

V_{sb} : Shear capacity of stirrups in beam (N).

V_{fb} : Shear capacity of FRP (N)

f_c' : Compressive strength of concrete (MPa).

b_w : Width of cross section (mm).

d : Effective depth of cross section of beam (mm).

$\frac{a}{d}$: Shear span to depth ratio.

ρ : Longitudinal reinforcement ratio.

Av : Area of stirrups that resist shear force in beam (mm²).

s : Spacing between stirrups in beam (mm).

f_y : yield stress of stirrups (MPa).

n : Number of FRP layers

R : Ratio of effective strain to ultimate strain and it can be taken 0.21 as reported by El-Amory (2004) and Tran (2014).

f_{fu} : Ultimate strength of FRP (MPa)

t_e : Thickness of FRP (mm)

θ : Fiber orientation, this angle is measured from horizontal axis

Maximum external load that causes shear failure in beam is V_b

$$P_{sb} = V_b \quad (6.25)$$

6.4 Joint Shear capacity

Several proposals are currently available for evaluating the shear strength V_{jh} of RC joints. Those formulae are generally based on the sum of two basic contributions V_{ch} and V_{sh} related to concrete and steel stirrups, respectively:

$$V_{jh} = V_{cj} + V_{sj} \quad (6.26)$$

ACI 318 code predicts the shear capacity of R.C joint according to location of joints. However, shear strength of concrete and stirrups are shown in Equations (6.27) and (6.28), respectively.

$$V_{cj} = (0.083\gamma\sqrt{f_c})b_j h_c \quad (6.27)$$

$$V_{sj} = \frac{Av}{s} f_y dj \quad (6.28)$$

Where

V_{jh} : Shear capacity of R.C joint (N).

V_{cj} : Shear strength provided by concrete (N)

V_{sj} : Shear strength provided by stirrups (N).

f_c : Compressive strength of concrete (MPa).

Av : Area of stirrups that resist shear force in joint (mm²).

s : Spacing between stirrups in joint (mm).

f_y : yield stress of stirrups (MPa).

b_j : Effective joint width (mm)

h_c : Depth of the column (mm)

γ : Factor depends on the location of joint. This factor equals 12 for exterior R.C joints with continues column (ACI 318).

$$T_s - V_c = V_j h \quad (6.29)$$

$$\frac{M_j}{j} - \frac{M_j}{L_c} = V_j h \rightarrow M_j = \frac{V_j h}{\frac{1}{j} - \frac{1}{L_c}} \quad (6.30)$$

$$P_j = \frac{M_j}{L_{be} + \frac{h_c}{2}} \quad (6.31)$$

Where

j : Distance between the compressive/tensile force couple in the beam
(7/8d) (Li and Sanada, 2017).

P_j : Maximum load that can be applied at beam before failure of joint due to shear stress

h_c : Width of column

6.5 Yield moment capacity for column

For all our cases, the external moment on column is less than its yield capacity. This means no flexural failure happens in column. The theoretical yield moment values are calculated assuming linear strain and stress distribution in the concrete as shown in Figure 6.5.

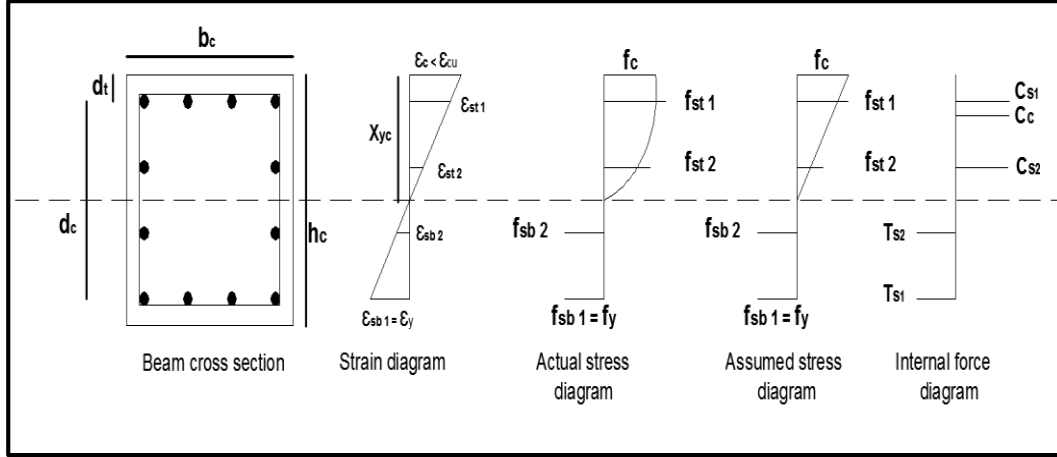


Figure 6.5: Stress, strain and force distributions along cross section of column at yield stage

To calculate yield moment, we must determine the location of neutral axis (x_{yc}) by the following equations.

Equilibrium equation:

$$C_c + C_{s1} + C_{s2} = T_{s1} + T_{s2} + P \quad (6.32)$$

$$C_c = 0.5x_{yc}f_c b_c \quad (6.33)$$

$$C_{s1} = A_{st1}f_{st1} \quad (6.34)$$

$$C_{s2} = A_{st2}f_{st2} \quad (6.35)$$

$$T_{s1} = A_{sb1}f_{sb1} = A_{sb1}f_y \quad (6.36)$$

$$T_{s2} = A_{sb2}f_{sb2} \quad (6.37)$$

Compatibility in strain diagram

$$\left[\frac{\varepsilon_c}{\varepsilon_y} = \frac{x_{yc}}{d_c - x_{yc}} \right] = \left[\left(\frac{E_S E_C}{E_S E_C} \right) \frac{\varepsilon_c}{\varepsilon_y} = \frac{x_{yc}}{d_c - x_{yc}} \right] = \left[n \frac{f_c}{f_y} = \frac{x_{yc}}{d_c - x_{yc}} \right], \text{ then } f_c = \frac{f_y}{n} \left(\frac{x_{yc}}{d_c - x_{yc}} \right) \quad (6.38)$$

$$\left[\frac{\varepsilon_{st1}}{\varepsilon_y} = \frac{x_{yc} - d_t}{d_c - x_{yc}} \right] = \left[\left(\frac{E_S}{E_S} \right) \frac{\varepsilon_{st1}}{\varepsilon_y} = \frac{x_{yc} - d_t}{d_c - x_{yc}} \right] = \left[\frac{f_{st1}}{f_y} = \frac{x_{yc} - d_t}{d_c - x_{yc}} \right], \text{ then } f_{st1} = f_y \left(\frac{x_{yc} - d_t}{d_c - x_{yc}} \right) \quad (6.39)$$

$$\left[\frac{\varepsilon_{st2}}{\varepsilon_y} = \frac{x_{yc} - (d_t + s)}{d_c - x_{yc}} \right] = \left[\left(\frac{E_S}{E_S} \right) \frac{\varepsilon_{st2}}{\varepsilon_y} = \frac{x_{yc} - (d_t + s)}{d_c - x_{yc}} \right] = \left[\frac{f_{st2}}{f_y} = \frac{x_{yc} - (d_t + s)}{d_c - x_{yc}} \right], \text{ then } f_{st2} = f_y \left(\frac{x_{yc} - (d_t + s)}{d_c - x_{yc}} \right) \quad (6.40)$$

$$\left[\frac{\varepsilon_{sb2}}{\varepsilon_y} = \frac{(d_c - x_{yc}) - s}{d_c - x_{yc}} \right] = \left[\left(\frac{E_S}{E_S} \right) \frac{\varepsilon_{sb2}}{\varepsilon_y} = \frac{(d_c - x_{yc}) - s}{d_c - x_{yc}} \right] \\ = \left[\frac{f_{sb2}}{f_y} = \frac{(d_c - x_{yc}) - s}{d_c - x_{yc}} \right], \text{ then } \\ f_{sb2} = f_y \left(\frac{(d_c - x_{yc}) - s}{d_c - x_{yc}} \right) \quad (6.41)$$

From these equations we can find the position of neutral axis (x_{yc}), then the yield moment can be determined

$$M_{yc} = 0.5x_{yc}f_c b_c \left(\frac{2}{3}x_{yc} \right) + A_{st1}f_{st1}(x_{yc} - d_t) + A_{st2}f_{st2}(x_{yc} - (d_t + s)) + A_{sb1}f_y(d_c - x_{yc}) + A_{sb2}f_{sb2}(d_c - x_{yc} - s) + P\left(\frac{h_c}{2} - x_{yc}\right) \quad (6.42)$$

Where

b_c : Width of column

h_c : Full depth of column

d_c : Effective depth of column

x_{yc} : Depth of neutral axis at yield stage which is calculated from compression surface of column

ε_{st1} : Strain in the first top longitudinal reinforcements.

ε_{st2} : Strain in the second top longitudinal reinforcements.

ε_{sb1} : Strain in the first bottom longitudinal reinforcements.

ε_{sb2} : Strain in the second bottom longitudinal reinforcements.

f_{st1} : Stress in the first top longitudinal reinforcements.

f_{st2} : Stress in the second top longitudinal reinforcements.

f_{sb1} : Stress in the first bottom longitudinal reinforcements.

f_{sb2} : Stress in the second bottom longitudinal reinforcements.

C_{s1} : Compression force provided by first top longitudinal reinforcements

C_{s2} : Compression force provided by second top longitudinal reinforcements

T_{s1} : Tension force provided by first bottom longitudinal reinforcements

T_{s2} : Tension force provided by second bottom longitudinal reinforcements

s : Spacing between longitudinal reinforcements in column.

6.6 Yield and ultimate deflections

Virtual work method is used for calculating the yield and ultimate deflections. Generally, three main types of deflections happen in these joints, namely: flexure, shear and axial deflections. However, the compression damage parameter will be neglected in hand calculations because not all sections reach the same damage at the same time.

$$\Delta_f = \int_0^l m_v k dx = \frac{1}{E_c I_e} \int_0^l m_v M_r dx \quad (6.43)$$

$$\Delta_s = \frac{\mathcal{F}}{G_c A} \int_0^l v_v V_r dx \quad (6.44)$$

$$\Delta_a = \frac{1}{E_c A} \int_0^l n_v N_r dx \quad (6.45)$$

$$\mathcal{F} = \frac{6}{5} \left(\frac{I_g}{I_e} \right)^2 \quad \text{for rectangular cross section} \quad (6.46)$$

$$I_e = \left(\frac{M_{cr}}{M_y} \right)^3 I_g + \left(1 - \left(\frac{M_{cr}}{M_y} \right)^3 \right) I_{cr} \quad (ACI - 318) \quad (6.47)$$

$$M_{cr} = \frac{f_r I_g}{y_b} \quad (6.48)$$

$$f_r = 0.62 \sqrt{f_c} \quad (6.49)$$

$$I_g = \frac{BH^3}{12} \quad (6.50)$$

$$I_{cr} = \frac{Bx_n^3}{3} + (n - 1)A_{st}(x_n - d_t)^2 + nA_{sb}(d - x_n) \quad (ACI - 318)$$

(6.51)

Where

Δ_f : Flexural deflection

l : Length of element

m_v : Virtual moment

k : Curvature

M_r : Real moment

I_e : Effective moment of inertia of cross section

Δ_s : shear deflection

\mathcal{F} : Shear shape factor

A : Area of cross section

v_v : Virtual shear force

V_r : Real shear force

Δ_a : Axial deflection

n_v : Virtual axial force

N_r : Real axial force

I_g : Gross moment of inertia

M_{cr} : Cracked moment

f_r : Modulus of rupture

y_b : Depth of natural axis before cracking which is equal approximately $(\frac{H}{2})$ for rectangular cross section.

B : Width of cross section

H : Depth of cross section

x_n : Depth of neutral axis from top at certain stage

6.6.1 Methodology for calculating flexural deflection

To calculate flexural deflection, first of all we must determine yield curvature and ultimate curvature for beam and column. In our cases, column exposed to moment less than yield capacity for all cases, so that; yield curvature of column is enough to calculate yield and ultimate flexural deflection for joints. Figures 7.6a and 7.6b show moment diagram at yield stage and ultimate stage for typical joint respectively, while Figures 6.7a and 6.7b show curvature diagram at yield stage and ultimate stage for typical joint, respectively, also Figures 6.8 shows virtual moment diagram for 1 unit load at tip of beam (position of needed deflection). The symbol (L_b) is the distance between applied load to critical section.

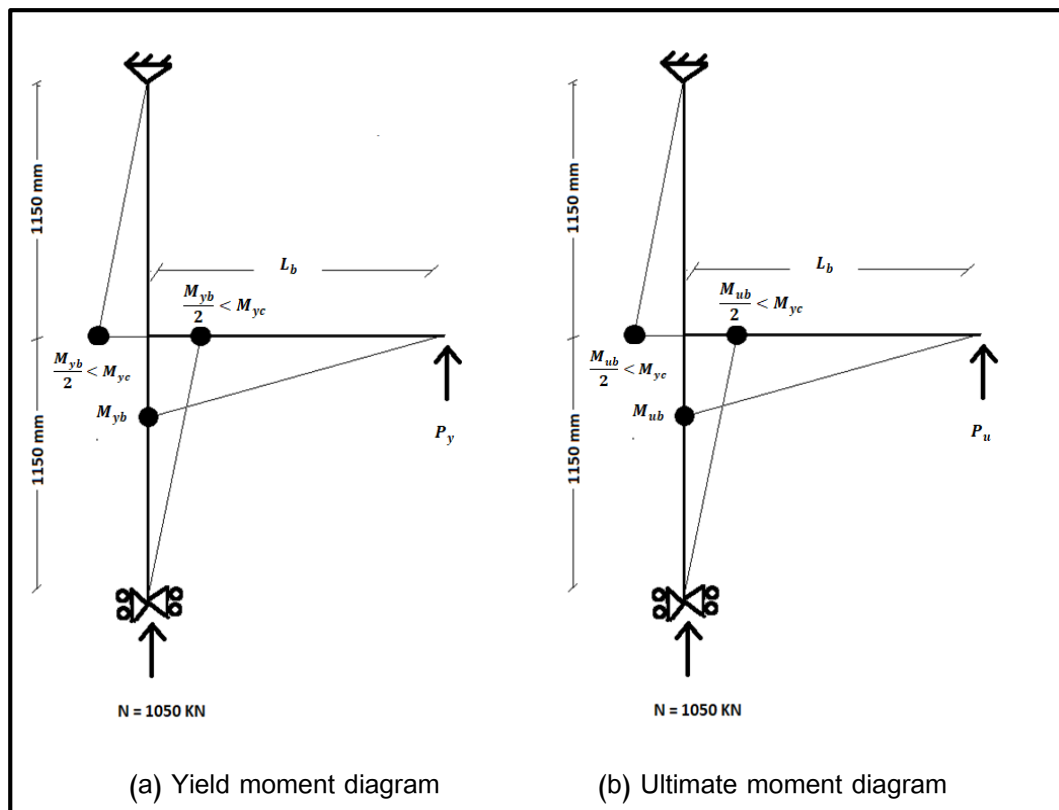


Figure 6.6: Yield and ultimate moment diagrams for typical joint

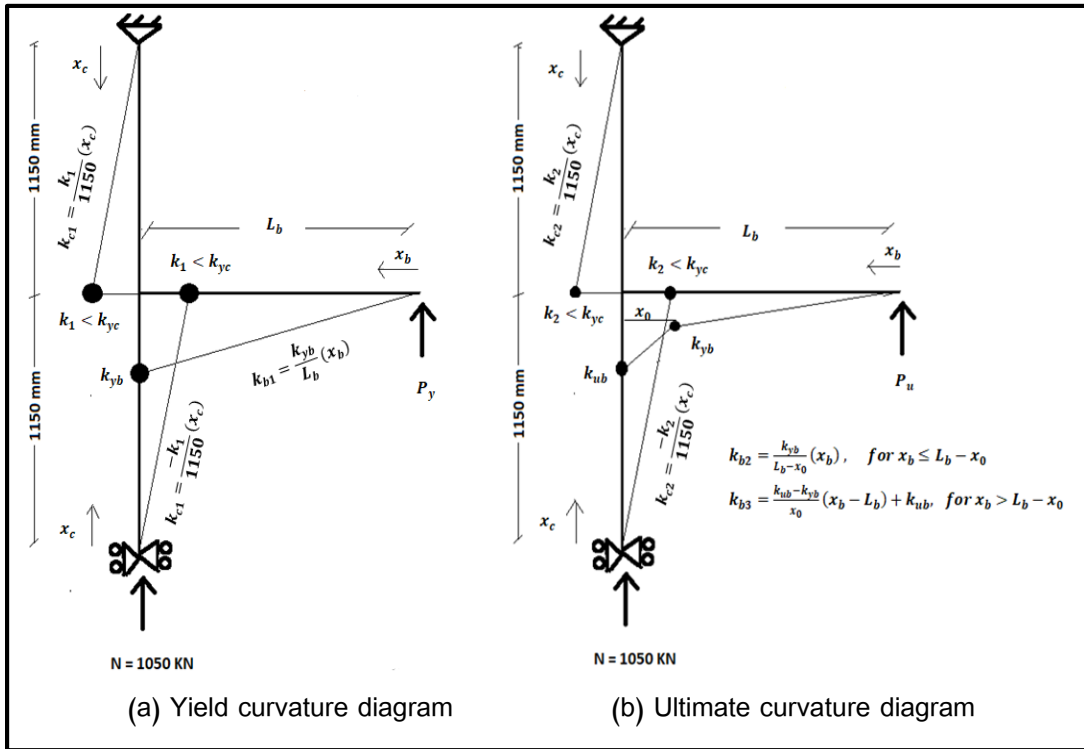


Figure 6.7: Yield and ultimate curvature diagrams for typical joint

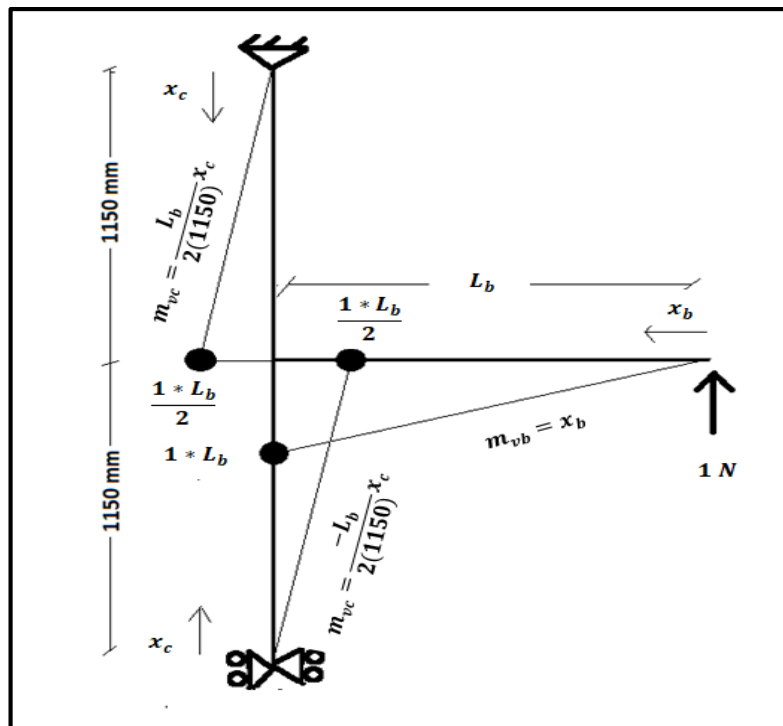


Figure 6.8: Virtual moment diagram for typical joint

$$\Delta_{fy} = \int_0^{L_b} m_{vb} k_{b1} dx_b + 2 \int_0^{1150} m_{vc} k_{c1} dx_c \quad (6.52)$$

$$\Delta_{fu} = \int_0^{L_b - x_0} m_{vb} k_{b2} dx_b + \int_{L_b - x_0}^{L_b} m_{vb} k_{b3} dx_b + 2 \int_0^{1150} m_{vc} k_{c2} dx_c \quad (6.53)$$

$$k_{yb} = \frac{\varepsilon_y}{d_b - x_{yb}} \quad (6.54)$$

$$k_{ub} = \frac{\varepsilon_{cu}}{x_{ub}} \quad (6.55)$$

$$k_{yc} = \frac{\varepsilon_y}{d_c - x_{yc}} \quad (6.56)$$

$$k_1 = \frac{M_{yb} k_{yc}}{2M_{yc}} \quad (6.57)$$

$$k_2 = \frac{M_{ub} k_{yc}}{2M_{yc}} \quad (6.58)$$

Where:

Δ_{fy} : Yield flexural deflection

L_b : Length at critical section

m_{vb} : Virtual moment equation along beam

k_{b1} : Curvature equation along beam at yield stage

m_{vc} : Virtual moment equation along column

k_{c1} : Curvature equation along column at yield stage

Δ_{fu} : Ultimate flexural deflection

k_{b2}, k_{b3} : Curvature equations along beam at ultimate stage

k_{c2} : Curvature equation along beam at ultimate stage

x_0 : Length of plastic hinge ($x_0 = L_b - L_b \frac{M_{yb}}{M_{ub}}$)

k_{yb} : Yield curvature of beam cross section

k_{ub} : Ultimate curvature of beam cross section

k_{yc} : Yield curvature of column cross section

k_1 : Maximum curvature of column at yield stage

k_{21} : Maximum curvature of column at ultimate stage

6.6.2 Methodology for calculating shear deflection

To calculate shear deflection, the same method in flexural deflection is used. But the integration will be between actual shear and virtual shear diagrams divided by (G.A). Figures 6.9a and 6.9b show shear diagram at yield stage and ultimate stage for typical joint, respectively, while Figure 6.10 shows virtual shear diagram for 1 unit load at tip of beam (position of needed deflection).however, assume no cracks happen in the column due to high compression axial force on column, so that, the shear shape factor of column can be taken as 1.2. On the other hand, for beam, the shear shape factor at ultimate load can be considered same factor at yield load because the ultimate load and yield load closed to each other.

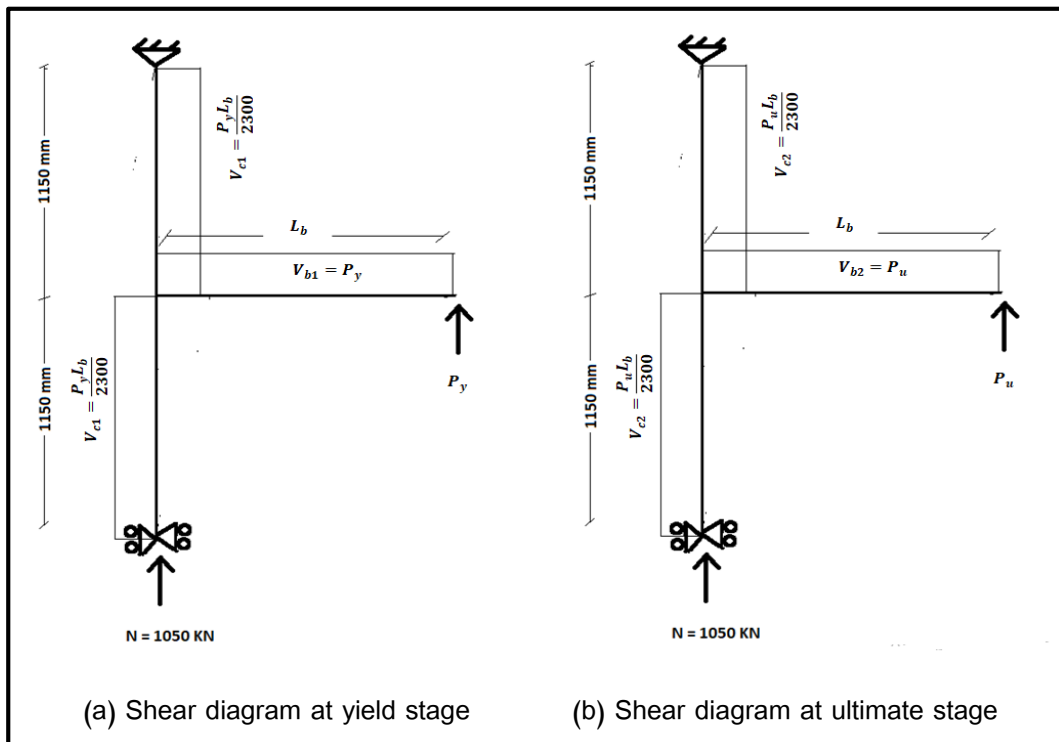


Figure 6.9: shear diagrams at yield and ultimate stages for typical joint

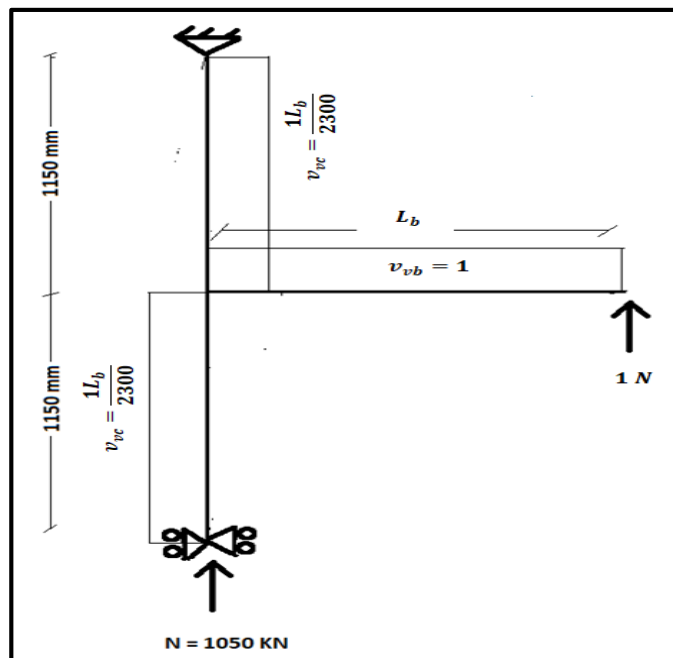


Figure 6.10: Virtual shear diagram for typical joint

$$\Delta_{sy} = \frac{\mathcal{F}_b}{G_c A_b} \int_0^{L_b} v_{vb} V_{b1} dx_b + 2 \frac{\mathcal{F}_c}{G_c A_c} \int_0^{1150} v_{vc} V_{c1} dx_c \quad (6.59)$$

$$\Delta_{su} = \frac{\mathcal{F}_b}{G_c A_b} \int_0^{L_b} v_{vb} V_{b2} dx_b + 2 \frac{\mathcal{F}_c}{G_c A_c} \int_0^{1150} v_{vc} V_{c2} dx_c \quad (6.60)$$

Where:

Δ_{sy} : Shear deflection at yield stage

\mathcal{F}_b : Shear shape factor of beam.

A_b : Gross area for beam cross section

v_{vb} : Virtual shear equation along beam

V_{b1} : Shear equation along beam at yield stage

\mathcal{F}_c : Shear shape factor of column.

v_{vc} : Virtual shear equation along column

V_{c1} : Shear equation along column at yield stage

Δ_{su} : Shear deflection at ultimate stage

V_{b2} : Shear equation along beam at ultimate stage

V_{c2} : Shear equation along column at ultimate stage

6.6.3 Methodology for calculating axial deflection

To calculate the axial deflection, using the same previous procedure, but the integration will be between actual axial and virtual axial diagrams divided by (E.A). Figures 6.11a and 6.11b show axial diagram at yield stage and ultimate stage for typical joint, respectively, while Figures 6.12 shows virtual shear diagram for 1 unit load at tip of beam (position of needed deflection).

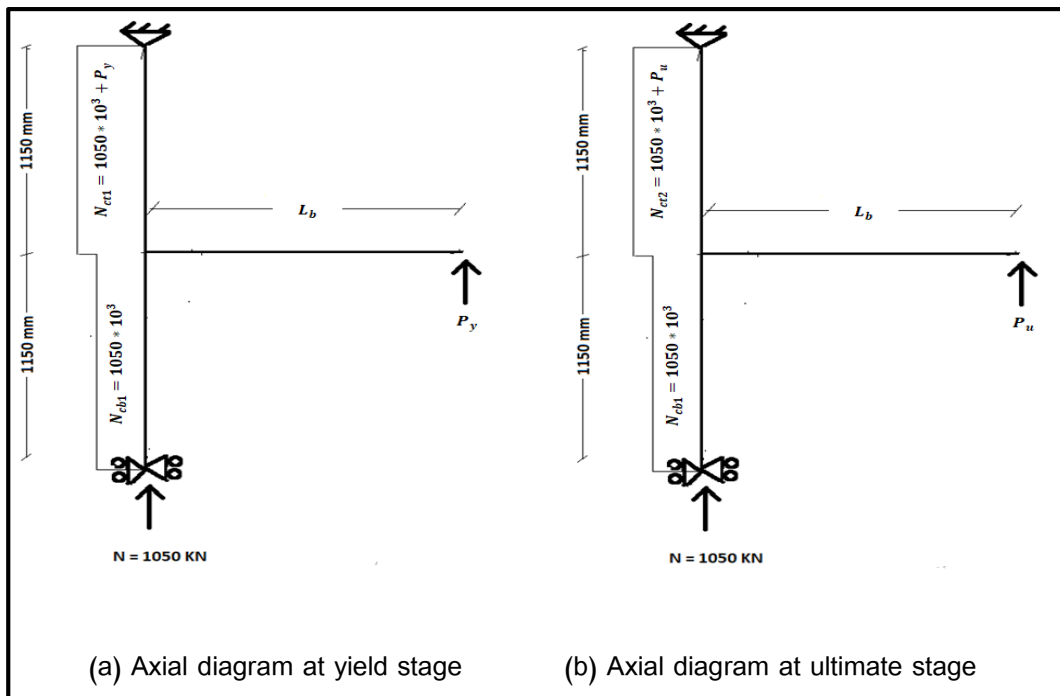


Figure 6.11: Axial diagrams at yield and ultimate stages for typical joint

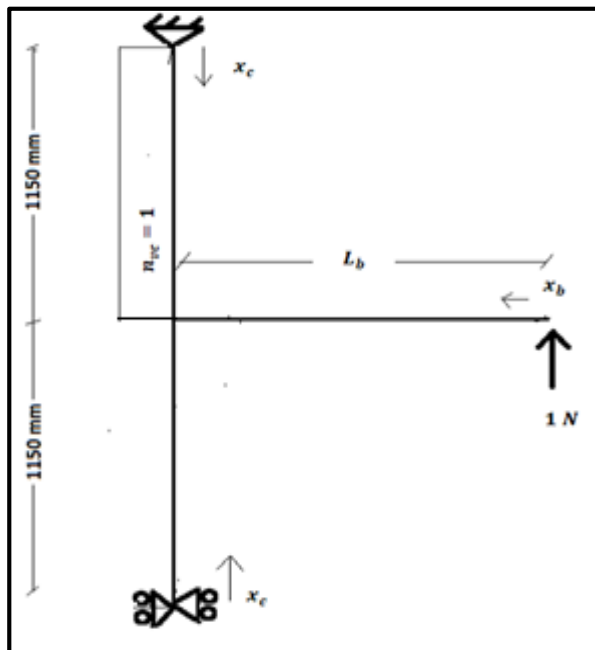


Figure 6.12: Virtual axial diagram for typical joint

$$\Delta_{ay} = \frac{1}{E_c A_c} \int_0^{1150} n_{vc} N_{ct1} dx_b + \frac{1}{E_c A_c} \int_0^{1150} n_{vc} N_{cb1} dx_b \quad (6.61)$$

$$\Delta_{au} = \frac{1}{E_c A_c} \int_0^{1150} n_{vc} N_{ct2} dx_b + \frac{1}{E_c A_c} \int_0^{1150} n_{vc} N_{cb1} dx_b \quad (6.62)$$

Where:

Δ_{ay} : Axial deflection at yield stage

n_{vc} : Virtual axial equation along column

N_{ct1} : Axial equation along top column at yield stage

N_{cb1} : Axial equation along bottom column at yield and ultimate stage

Δ_{au} : Axial deflection at ultimate stage

N_{ct2} : Axial equation along top column at ultimate stage

6.7 Analytical results

The results from analytical solution are calculated as discussed in previous sections and then are compared with ABAQUS results as shown in Table 6.1. However, Table 6.2 illustrates deflection from each type (flexure, shear and axial deflections) for all models.

Table 6.1: Comparisons between ABAQUS results and analytical results

Model	P_y (KN) (ABAQUS)	P_y (KN) (Analytically)	P_P (KN) (ABAQUS)	P_P (KN) (Analytically)	Δ_y (mm) (ABAQUS)	Δ_y (mm) (Analytically)	Δ_P (mm) (ABAQUS)	Δ_P (mm) (Analytically)
G1-MaJ-MiB-0	350	*N.Y	360	325	6.28	N.Y	7.8	5.5
G1-MaJ-B1B-0	360	385	400	398	6.28	5.88	8.7	5.88
G1-MaJ-B2B-0	366.4	385	416.2	402	6.28	5.88	10.2	6.5
G1-MaJ-MaB-0	366.5	385	417	402	6.28	5.88	10.2	6.5
G2-MaJ-MiB-0	210	N.Y	260.2	200	5	N.Y	7.4	4.63
G2-MaJ-B1B-0	220	250	274	260	5	5.03	7.4	5.6
G2-MaJ-B2B-0	230	250	274.5	260	5	5.03	7.4	5.6
G2-MaJ-MaB-0	230	250	275	260	5	5.03	7.4	5.6
G3-MaJ-MiB-0	69	68.3	74.5	70	5.2	5.06	7.5	5.5
G3-MaJ-B1B-0	69	68.3	74.8	70	5.2	5.06	7.5	5.5
G3-MaJ-B2B-0	69	68.3	75	70	5.2	5.06	7.5	5.5
G3-MaJ-MaB-0	69	68.3	75	70	5.2	5.06	7.5	5.5
G1-MiJ-MiB-0	310	N.Y	330.1	325	6.5	N.Y	10.2	5.5
G1-MiJ-B1B-0	310	314	347	365	6.7	7.32	10.2	9.96
G1-MiJ-B2B-0	315	314	347	365	6.7	7.32	10.2	9.96
G1-MiJ-MaB-0	315	314	347	365	6.7	7.32	10.2	9.96
G2-MiJ-MiB-0	220	N.Y	249	200	5	N.Y	9	4.63
G2-MiJ-B1B-0	225	250	249	260	5	5.03	9	5.6
G2-MiJ-B2B-0	225	250	249	260	5	5.03	9	5.6
G2-MiJ-MaB-0	225	250	250.6	260	5	5.03	9	5.6
G3-MiJ-MiB-0	69	68.3	74.5	70	5.2	5.06	7.5	5.5
G3-MiJ-B1B-0	69	68.3	74.5	70	5.2	5.06	7.5	5.5

G3-MiJ-B2B-0	69	68.3	74.5	70	5.2	5.06	7.5	5.5
G3-MiJ-MaB-0	69	68.3	74.5	70	5.2	5.06	7.5	5.5
G1-MaJ-MiB-1	370	385	408	402	6.28	5.88	7.8	6.5
G1-MaJ-B1B-1	370	385	408.5	402	6.28	5.88	8.7	6.5
G1-MaJ-B2B-1	370	385	417.6	402	6.28	5.88	10.2	6.5
G1-MaJ-MaB-1	370	385	418	402	6.28	5.88	10.2	6.5
G2-MaJ-MiB-1	230	250	277	260	5	5.03	7.4	5.6
G2-MaJ-B1B-1	230	250	277	260	5	5.03	7.4	5.6
G2-MaJ-B2B-1	230	250	279	260	5	5.03	7.4	5.6
G2-MaJ-MaB-1	230	250	280	260	5	5.03	7.4	5.6
G3-MaJ-MiB-1	70	68.3	75	70	5.2	5.06	7.5	5.5
G3-MaJ-B1B-1	70	68.3	75	70	5.2	5.06	7.5	5.5
G3-MaJ-B2B-1	70	68.3	75	70	5.2	5.06	7.5	5.5
G3-MaJ-MaB-1	70	68.3	75	70	5.2	5.06	7.5	5.5
G1-MiJ-MiB-1	302	314	347	365	6.7	7.32	10.2	9.96
G1-MiJ-B1B-1	302	314	347	365	6.7	7.32	10.2	9.96
G1-MiJ-B2B-1	302	314	347	365	6.7	7.32	10.2	9.96
G1-MiJ-MaB-1	302	314	347	365	6.7	7.32	10.2	9.96
G2-MiJ-MiB-1	216	250	246	260	5	5.03	9	5.6
G2-MiJ-B1B-1	216	250	247	260	5	5.03	9	5.6
G2-MiJ-B2B-1	216	250	248	260	5	5.03	9	5.6
G2-MiJ-MaB-1	216	250	250	260	5	5.03	9	5.6
G3-MiJ-MiB-1	70	68.3	75	70	5.2	5.06	7.5	5.5
G3-MiJ-B1B-1	70	68.3	75	70	5.2	5.06	7.5	5.5
G3-MiJ-B2B-1	70	68.3	75	70	5.2	5.06	7.5	5.5
G3-MiJ-MaB-1	70	68.3	75	70	5.2	5.06	7.5	5.5

C1-MaJ-X1B-0	177	181	199	186	5.1	4.71	6.8	5.26
C1-MaJ-X0B-0	177	181	199	186	5.1	4.71	6.8	5.26
C2-MaJ-X1B-0	108	111	122	114	5.1	4.74	6.8	5.28
C2-MaJ-X0B-0	108	111	121	114	5.1	4.74	6.8	5.28
C1-MiJ-X1B-0	177	181	199	186	5.1	4.71	6.8	5.26
C1-MiJ-X0B-0	177	181	199	186	5.1	4.71	6.8	5.26
C2-MiJ-X1B-0	108	111	122	114	5.1	4.74	6.8	5.28
C2-MiJ-X0B-0	108	111	121	114	5.1	4.74	6.8	5.28
C1-MaJ-X1B-1	180	181	202.3	186	5.1	4.71	6.8	5.26
C1-MaJ-X0B-1	180	181	202	186	5.1	4.71	6.8	5.26
C2-MaJ-X1B-1	106	111	122.7	114	5.1	4.74	6.8	5.28
C2-MaJ-X0B-1	106	111	122.6	114	5.1	4.74	6.8	5.28
C1-MiJ-X1B-1	180	181	202.3	186	5.1	4.71	6.8	5.26
C1-MiJ-X0B-1	180	181	202.3	186	5.1	4.71	6.8	5.26
C2-MiJ-X1B-1	106	111	122.7	114	5.1	4.74	6.8	5.28
C2-MiJ-X0B-1	106	111	122.6	114	5.1	4.74	6.8	5.28

*N.Y: No yield in longitudinal beam steel reinforcement

Table 6.2: Yield and ultimate flexure, shear, axial deflections analatically

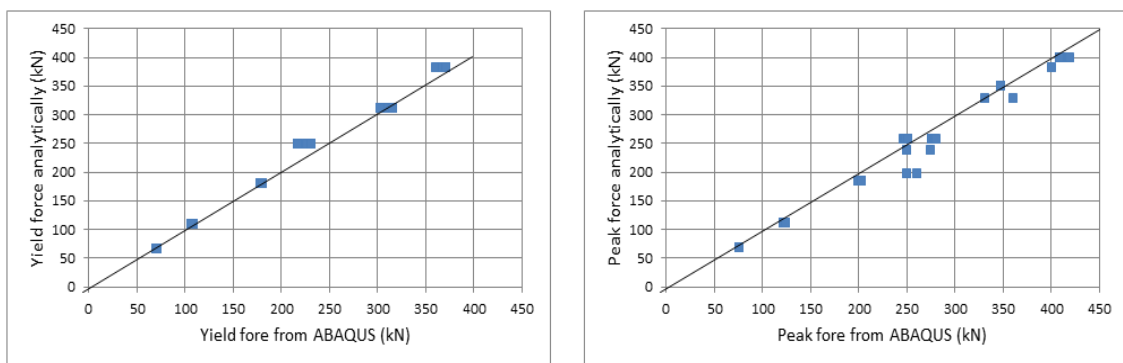
Model	Yield				Ultimate			
	Δ_{fy} (mm)	Δ_{sy} (mm)	Δ_{ay} (mm)	Δ_y (mm)	Δ_{fu} (mm)	Δ_{su} (mm)	Δ_{au} (mm)	Δ_u (mm)
G1-MaJ-MiB-0	*N.Y	N.Y	N.Y	N.Y	4.3	0.77	0.42	5.5
G1-MaJ-B1B-0	4.53	0.91	0.44	5.88	4.53	0.91	0.44	5.88
G1-MaJ-B2B-0	4.53	0.91	0.44	5.88	5.14	0.93	0.43	6.5
G1-MaJ-MaB-0	4.53	0.91	0.44	5.88	5.14	0.93	0.43	6.5
G2-MaJ-MiB-0	N.Y	N.Y	N.Y	N.Y	3.61	0.64	0.38	4.63
G2-MaJ-B1B-0	3.9	0.74	0.39	5.03	4.4	0.78	0.4	5.6
G2-MaJ-B2B-0	3.9	0.74	0.39	5.03	4.4	0.78	0.4	5.6
G2-MaJ-MaB-0	3.9	0.74	0.39	5.03	4.4	0.78	0.4	5.6
G3-MaJ-MiB-0	4.1	0.62	0.34	5.06	4.53	0.63	0.34	5.5
G3-MaJ-B1B-0	4.1	0.62	0.34	5.06	4.53	0.63	0.34	5.5
G3-MaJ-B2B-0	4.1	0.62	0.34	5.06	4.53	0.63	0.34	5.5
G3-MaJ-MaB-0	4.1	0.62	0.34	5.06	4.53	0.63	0.34	5.5
G1-MiJ-MiB-0	N.Y	N.Y	N.Y	N.Y	4.3	0.77	0.42	5.5
G1-MiJ-B1B-0	6	0.92	0.4	7.32	8.5	1.04	0.42	9.96
G1-MiJ-B2B-0	6	0.92	0.4	7.32	8.5	1.04	0.42	9.96
G1-MiJ-MaB-0	6	0.92	0.4	7.32	8.5	1.04	0.42	9.96
G2-MiJ-MiB-0	N.Y	N.Y	N.Y	N.Y	3.61	0.64	0.38	4.63
G2-MiJ-B1B-0	3.9	0.74	0.39	5.03	4.4	0.78	0.4	5.6
G2-MiJ-B2B-0	3.9	0.74	0.39	5.03	4.4	0.78	0.4	5.6

G2-MiJ-MaB-0	3.9	0.74	0.39	5.03	4.4	0.78	0.4	5.6
G3-MiJ-MiB-0	4.1	0.62	0.34	5.06	4.53	0.63	0.34	5.5
G3-MiJ-B1B-0	4.1	0.62	0.34	5.06	4.53	0.63	0.34	5.5
G3-MiJ-B2B-0	4.1	0.62	0.34	5.06	4.53	0.63	0.34	5.5
G3-MiJ-MaB-0	4.1	0.62	0.34	5.06	4.53	0.63	0.34	5.5
G1-MaJ-MiB-1	4.53	0.91	0.44	5.88	5.14	0.93	0.43	6.5
G1-MaJ-B1B-1	4.53	0.91	0.44	5.88	5.14	0.93	0.43	6.5
G1-MaJ-B2B-1	4.53	0.91	0.44	5.88	5.14	0.93	0.43	6.5
G1-MaJ-MaB-1	4.53	0.91	0.44	5.88	5.14	0.93	0.43	6.5
G2-MaJ-MiB-1	3.9	0.74	0.39	5.03	4.4	0.78	0.4	5.6
G2-MaJ-B1B-1	3.9	0.74	0.39	5.03	4.4	0.78	0.4	5.6
G2-MaJ-B2B-1	3.9	0.74	0.39	5.03	4.4	0.78	0.4	5.6
G2-MaJ-MaB-1	3.9	0.74	0.39	5.03	4.4	0.78	0.4	5.6
G3-MaJ-MiB-1	4.1	0.62	0.34	5.06	4.53	0.63	0.34	5.5
G3-MaJ-B1B-1	4.1	0.62	0.34	5.06	4.53	0.63	0.34	5.5
G3-MaJ-B2B-1	4.1	0.62	0.34	5.06	4.53	0.63	0.34	5.5
G3-MaJ-MaB-1	4.1	0.62	0.34	5.06	4.53	0.63	0.34	5.5
G1-MiJ-MiB-1	6	0.92	0.4	7.32	8.5	1.04	0.42	9.96
G1-MiJ-B1B-1	6	0.92	0.4	7.32	8.5	1.04	0.42	9.96
G1-MiJ-B2B-1	6	0.92	0.4	7.32	8.5	1.04	0.42	9.96
G1-MiJ-MaB-1	6	0.92	0.4	7.32	8.5	1.04	0.42	9.96
G2-MiJ-MiB-1	3.9	0.74	0.39	5.03	4.4	0.78	0.4	5.6
G2-MiJ-B1B-1	3.9	0.74	0.39	5.03	4.4	0.78	0.4	5.6
G2-MiJ-B2B-1	3.9	0.74	0.39	5.03	4.4	0.78	0.4	5.6

G2-MiJ-MaB-1	3.9	0.74	0.39	5.03	4.4	0.78	0.4	5.6
G3-MiJ-MiB-1	4.1	0.62	0.34	5.06	4.53	0.63	0.34	5.5
G3-MiJ-B1B-1	4.1	0.62	0.34	5.06	4.53	0.63	0.34	5.5
G3-MiJ-B2B-1	4.1	0.62	0.34	5.06	4.53	0.63	0.34	5.5
G3-MiJ-MaB-1	4.1	0.62	0.34	5.06	4.53	0.63	0.34	5.5
C1-MaJ-X1B-0	3.61	0.73	0.37	4.71	4.14	0.75	0.37	5.26
C1-MaJ-X0B-0	3.61	0.73	0.37	4.71	4.14	0.75	0.37	5.26
C2-MaJ-X1B-0	3.74	0.65	0.35	4.74	4.26	0.67	0.35	5.28
C2-MaJ-X0B-0	3.74	0.65	0.35	4.74	4.26	0.67	0.35	5.28
C1-MiJ-X1B-0	3.61	0.73	0.37	4.71	4.14	0.75	0.37	5.26
C1-MiJ-X0B-0	3.61	0.73	0.37	4.71	4.14	0.75	0.37	5.26
C2-MiJ-X1B-0	3.74	0.65	0.35	4.74	4.26	0.67	0.35	5.28
C2-MiJ-X0B-0	3.74	0.65	0.35	4.74	4.26	0.67	0.35	5.28
C1-MaJ-X1B-1	3.61	0.73	0.37	4.71	4.14	0.75	0.37	5.26
C1-MaJ-X0B-1	3.61	0.73	0.37	4.71	4.14	0.75	0.37	5.26
C2-MaJ-X1B-1	3.74	0.65	0.35	4.74	4.26	0.67	0.35	5.28
C2-MaJ-X0B-1	3.74	0.65	0.35	4.74	4.26	0.67	0.35	5.28
C1-MiJ-X1B-1	3.61	0.73	0.37	4.71	4.14	0.75	0.37	5.26
C1-MiJ-X0B-1	3.61	0.73	0.37	4.71	4.14	0.75	0.37	5.26
C2-MiJ-X1B-1	3.74	0.65	0.35	4.74	4.26	0.67	0.35	5.28
C2-MiJ-X0B-1	3.74	0.65	0.35	4.74	4.26	0.67	0.35	5.28

*N.Y: No yield in longitudinal beam steel reinforcement

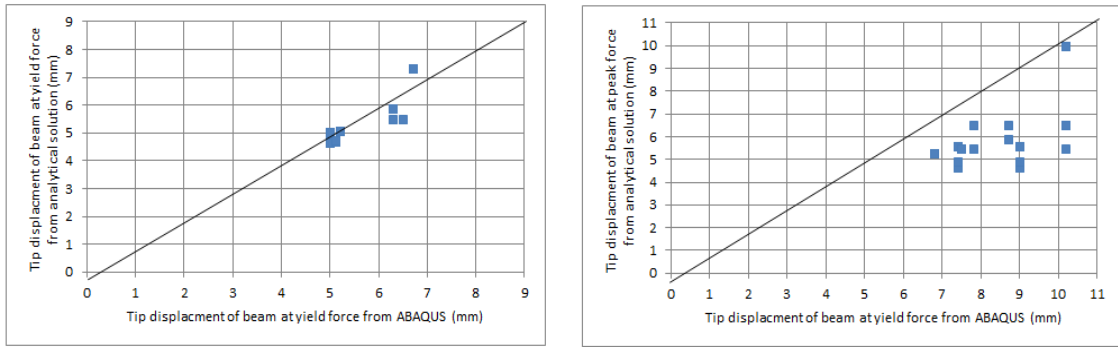
As shown in Figures 6.13a and 6.13b that the yield force and peak force which are computed analytically are close enough to the ABAQUS results. Also, the tip beam deflections at yield stage are close to ABAQUS results as shown in Figure 6.14a. In contrast, there is clear variation between analytical solution and ABAQUS results for tip beam deflections at peak load as shown in Figure 6.14b. This difference can be attributed to the simplification assumptions used in the virtual method; particularly the distribution of real curvatures and strains. Tip beam deflections at peak load from analytical solution always less than ABAQUS results because, for most cases, the assumed length between applied loads to critical section is smaller than its real value (to the center of the joint).



(a) Yield stage

(b) Peak stage

Figure 6.13: Comparisons between ABAQUS results and analytical results for yield and peak forces



(a) Yield stage

(b) Peak stage

Figure 6.14: Comparisons between ABAQUS results and analytical results for tip beam deflections at yield and peak forces

7 Conclusions and recommendations

7.1 Overview

In this thesis, three-dimensional (3-D) non-linear finite element (F.E.) model of an exterior R.C beam-column joint is verified and then used to study the ductility of beam-column joint under various parameters. A set of simplified equations to predict the ductility is also proposed. In the following sections, we summarize the main findings and results of the study.

7.2 Research findings

Based on this study, the following conclusions are summarized:

- 1- Using CFRP wraps converts the brittle failure to ductile failure. However, there is no effect of CFRP when models reach maximum confinement due to beam stirrups or when failure happens inside the joint. On the other hand, the effect of CFRP wrapping is significant for models that are dominated by only shear failure of beam.
- 2- Results show that, stirrups continuity inside the joint increase the capacity and ductility for models dominated by shear failure. This behavior also happens for models with CFRP, but with small increase in ductility.
- 3- As relative stiffness ratio decreases, the ultimate capacity increase and the ductility decrease. This is logical because decreasing of G means larger beam. This trend also exists for the case of using CFRP.

- 4- Ductility increases with increasing the transverse steel up to a certain maximum value of $(A_v/s)_B$ which can be called a fixed value. Increasing $(A_v/s)_B$ beyond this maximum value causes no significant effect on ductility. This value depends on the relative inertia (G) and amount of stirrups inside the joint $(A_v/s)_J$. This trend does not happen when using CFRP, because using CFRP converts brittle failure to ductile failure.

7.3 Proposed equations

Based on statistical regression and fitting of data generated by ABAQUS F.E. models, the following equations can be used to predict the ductility of the exterior R.C beam-column joints subjected to the limitations below.

These equations are:

$$D_{min} \leq D_0 = -0.50 + 2.40\sqrt{G} + 0.70 \frac{\left(\frac{A_v}{s}\right)_B}{\left(\frac{A_v}{s}\right)_J} \leq D_{max}, \quad \text{for } \Upsilon \leq 1 \quad (5.7)$$

$$D_{min} \leq D_0 = 1.0 + 3.0\sqrt{G} + 0.010 \frac{\left(\frac{A_v}{s}\right)_B}{\left(\frac{A_v}{s}\right)_J} \leq D_{max}, \quad \text{for } \Upsilon > 1 \quad (5.8)$$

$$D_{F-min} \leq D_{FRP} = 1.0 + 3.0\sqrt{G} + 0.010 \frac{\left(\frac{A_v}{s}\right)_B}{\left(\frac{A_v}{s}\right)_J} \leq D_{F-max} \quad (5.9)$$

Where

Υ : Factor for perdition the type of failure. (For brittle failure, $\Upsilon \leq 1$ while $\Upsilon > 1$ for ductile failure).

D_0 : Ductility of exterior reinforced beam- column joint without CFRP.

D_{max} : Maximum ductility of exterior reinforced beam- column joint without CFRP, and is taken equal to 7.5.

D_{min} : Minimum ductility of exterior reinforced beam- column joint without CFRP, and is taken equal to 1.3

G : Relative gross inertia of column to beam (IC/IB)

D_{FRP} : Ductility of exterior reinforced beam- column joint with CFRP

D_{F-max} : Maximum ductility of exterior reinforced beam- column joint with CFRP, and is taken equal to 7.5

D_{F-min} : Minimum ductility of exterior reinforced beam- column joint with CFRP, and is taken equal to 3

S: spacing between stirrups in mm.

A_v : area of stirrups that resist shear force.

These equations can be used in many cases to conceptually predict the behavior of the structure in a simplified nonlinear analysis process.

It must be noted that the previously mentioned equations have limitations that must be considered when used. These equations are valid under the following limitations:

- 1- These equations can be used for exterior R.C beam-column joints only
- 2- Ratio between external moment and shear loads on joint approximately equals 1.
- 3- Relative inertia (G) between 0.512 until to 4.63 (these values are common and realistic).
- 4- Flexural steel ratio for beam and column is 1% (this value is common and realistic).
- 5- Axial load on column equal $0.25A_g f_c$ (this value is common).
- 6- No axial force in beam.
- 7- One layer of CFRP.

7.4 Future work

As mentioned before, this thesis focuses on the exterior R.C beam-column joint without secondary beams, it is recommended to consider the effect of secondary beams and other types of joints in any further studies.

Furthermore, the axial force in beam is unfortunately not included in this research. It is highly recommended to study the effect of the axial force in beam and joint on the ductility of exterior R.C beam-column joint.

Also, the external moment to shear ratio (M/V) at critical section in beam approximately equals 1.0. It is recommended to study the effect of this ratio on the ductility.

Finally, one layer of CFRP wraps is used on the beam sides, and assumed the ratio of longitudinal reinforcements is 1 % in beam and column. It is recommended to study the effect of number of layers and other configurations of CFRP and ratio of longitudinal reinforcements on the ductility of exterior R.C beam-column joint.

References

- 1- **ABAQUS version 6.13.** (2013). [Computer software]. Assault Systems. Waltham. MA.
- 2- **ABAQUS: ABAQUS Analysis User's Manual Version 6.13.** (2013). Assault Systems.
- 3- ACI-ASCE (1985). *Recommendations for Design of Beam-Column Joints in Monolithic Reinforced Concrete Structures*. Committee report 352R-85. American Concrete Institute, **ACI Journal**, Vol. 82, No. 3, pp. 266-284.
- 4- ACI (2008a). *Guide for the Design and Construction of Externally Bonded FRP Systems for Strengthening Concrete Structures*. Committee report 440.2R-08, **American Concrete Institute**, Detroit, Michigan, 76 pages
- 5- ACI (2008). *Building Code Requirements for Structural Concrete*. Committee report 318-08, American Concrete Institute, Detroit, Michigan, 473 pages.
- 6- Al-Salloum, Y. A., Al-Sayed, S. H., Al-Musallam, T. H., and Siddiqui, N. A. (2002). *Seismic Performance of Shear Deficient Exterior RC Beam-Column Joints Repaired Using CFRP Composites*. **Saudi Engineering Conference**.
- 7- Asran, G., EL-Esnawi, H., and Fayed, S. (2016). *Numerical Investigation of RC Exterior Beam Colum Connections under Monotonic Loads*. **Journal of Mechanical and Civil Engineering**, Vol .13, No. 1, pp. 60-67.

- 8- Bidgar, S. T., and Bhattacharya, P. (2014). *Nonlinear Finite Element Analysis of Reinforced Concrete Exterior Beam Column Joint Subjected to Monotonic Loading*. **RTCET STM J**, Vol. 4, No. 2, pp. 1-10.
- 9- Campbell, F. C. (2010). **Structural Composite Materials**. ASM international, USA.
- 10- CSA A23.3. (1994). **Design of Concrete Structures**. Canadian Standard Association, Rexdale, Ontario, Canada, 220 pages.
- 11- Clyde, C., Pantelides, C.P., and Reaveley R.D. (2000). *Performance Based Evaluation of Exterior Reinforced Concrete Building Joints for Seismic Excitation*. PEER Report 2000/05 Pacific Earthquake Research Center, College of Engineering University of California, Berkeley.
- 12- El-Amoury, A. T. (2004). *Seismic Rehabilitation of Concrete Frame Beam-Column Joints*. Ph.D. Thesis, McMaster University, Ontario, Canada.
- 13- Elmezaini, N., and Ashour, M. (2015). *Nonlinear Analysis of Concrete Beams Strengthened with Steel Fiber-Reinforced Concrete Layer*. **Journal of Engineering Research and Technology**, Vol. 2, No. 3, pp.181-188.
- 14- Chaudhari, S. V., Mukane, K. A., and Chakrabarti, M. A. (2014). *Comparative study on Exterior RCC Beam Column Joint Subjected to Monotonic Loading*. **International Journal of Computer Applications**, Vol.102, No.3, pp. 34-39.

- 15- Ghojarah, A., Aziz, T. S., and Biddah, A. (1996). *Seismic Rehabilitation of Reinforced Concrete Beam-Column Connections. Journal of Earthquake Spectra*, Vol. 12, No. 4, pp. 761-780.
- 16- Ghojarah, A., Biddah, A., and Mahgoub, M. (1997). *Rehabilitation of Reinforced Concrete Columns Using Corrugated Steel Jacketing. Journal of Earthquake Engineering*, Vol. 1, No. 4, pp. 651-673.
- 17- Ghojarah, A., and Said, A. (2001). *Seismic Rehabilitation of Beam-Column Joints Using FRP Laminates. Journal of Earthquake Engineering*, Vol. 5, No. 1, pp. 113-129.
- 18- Ghojarah, A., and Said, A. (2002). *Shear Strengthening of Beam-Column Joints. Journal of Engineering structures*, Vol. 24, No. 7, pp. 881-888.
- 19- Jing, L. I., Pam, H. J., and Francis, T. K. (2004). *New Details of HSC Beam-Column Joints for Regions of Low to Moderate Seismicity. In 13th World Conference on Earthquake Engineering*, Vancouver, Canada, No. 449.
- 20- Kaliluthin, A. K., Kothandaraman, S., and Suhail-Ahamed, T. S. (2014). *A Review on Behavior of Reinforced Concrete Beam-Column Joint. International Journal of Innovative Research in Science, Engineering and Technology*, Vol. 3, No. 4, pp.11299-11312.
- 21- Khalifa, A., Gold, W. J., Nanni, A., and MI, A. A. (1998). *Contribution of Externally Bonded FRP to Shear Capacity of RC Flexural Members. Journal of composites for construction*, Vol. 2, No. 4, pp. 195–202.

- 22- Kmiecik, P., and Kamiński, M. (2011). *Modeling of reinforced concrete structures and composite structures with concrete strength degradation taken into consideration*. **Archives of civil and mechanical engineering Journal**, Vol. 11, No. 3, pp. 623–636.
- 23- Kupfer, H., Hilsdorf, H.K., and Rüsç, H. (1969). *Behavior of Concrete Under Biaxial Stresses*. **ACI Journal of structural Divisions**, Vol. 66, No. 8, pp. 656–666.
- 24- Lee, J., and Fenves, G. L. (1998). *Plastic-Damage Model for Cyclic Loading of Concrete Structures*. **Journal of engineering mechanics**, Vol. 124, No. 8, pp. 892–900.
- 25- Li, Y., and Sanada, Y. (2017). *Seismic Strengthening of Existing RC Beam-Column Joints by Wing Walls*. **Earthquake Engineering & Structural Dynamics**, Vol. 46, No. 12, pp. 1987-2008.
- 26- Lubliner, J., Oliver, J., Oller, S., and Onate, E. (1989). *A Plastic-Damage Model for Concrete*. **International Journal of solids and structures**, Vol. 25, No. 3, pp. 299–326.
- 27- Lu, X. Z., Teng, J. G., Ye, L. P., and Jiang, J. J. (2005). *Bond-Slip Models for FRP Sheets/Plates Bonded to Concrete*. **Journal of Engineering structures**, Vol. 27, No. 6, pp. 920–937.
- 28- Mahmoud, M. H., Afefy, H. M., Kassem, N. M., and Fawzy, T. M. (2014). *Strengthening of Defected Beam–Column Joints Using CFRP*. **Journal of advanced research**, Vol. 5, No. 1, pp. 67–77.
- 29- Mallick, P.K. (1993). **Fiber-Reinforced Composites**. Marcel Dekker, New York.

- 30- Mander, J. B., Priestley, M. J., and Park, R. (1988). *Theoretical Stress-Strain Model for Confined Concrete*. **Journal of structural engineering**, Vol. 114, No. 8, pp. 1804-1826.
- 31- Monti, M., Renzelli, M., and Luciani, P. (2003). *FRP Adhesion in Uncracked and Cracked Concrete Zones*. In *Fiber-Reinforced Polymer Reinforcement for Concrete Structures: (in 2 Volumes)* pp. 183-192.
- 32- Najafgholipour, M. A., Dehghan, S. M., Dooshabi, A., and Niroomandi, A. (2017). *Finite Element Analysis of Reinforced Concrete Beam-Column Connections with Governing Joint Shear Failure Mode*. **Latin American Journal of Solids and Structures**, Vol. 14, No.7, pp. 1200-1225.
- 33- Nakaba, K., Kanakubo, T., Furuta, T., and Yoshizawa, H. (2001). *Bond Behavior Between Fiber-Reinforced Polymer Laminates and Concrete*. **Structural Journal**, Vol. 98, No. 3, pp. 359–367.
- 34- Neubauer, U., and Rostasy, F. S. (1999). *Bond Failure of Concrete Fiber Reinforced Polymer Plates at Inclined Cracks—Experiments and Fracture Mechanics Model*. **Proc., 4th Int. Symp. on Fiber-Reinforced Polymer Reinforcement for Reinforced Concrete Structures**, SP-188, American Concrete Institute, Farmington Hills, Mich., pp. 369–382.
- 35- Obaidat, Y. T., Heyden, S., and Dahlblom, O. (2011). *Bond Action Between FRP and Concrete—A New Model*. *Structural Retrofitting of Concrete Beams Using FRP*, pp. 107.

- 36- Park, R., and Paulay, T. (195). **Reinforced Concrete Structures**. John Wiley and sons, New York.
- 37- Reddy, S. L., Rao, R. N., and Rao, G. T. (2010). *Shear Resistance of High Strength Concrete Beams Without Shear Reinforcement*. **International journal of civil and structural engineering**, Vol. 1, No. 1, pp. 101.
- 38- Sadone, R., Quiertant, M., Mercier, J., and Ferrier, E. (2012). *Experimental Study on RC Columns Retrofitted by FRP and Subjected to Seismic Loading*. In **6th International Conference on FRP Composites in Civil Engineering CICE**, Rome, Italy,
- 39- Samaaneh, M. A., Sharif, A. M., Baluch, M. H., and Azad, A. K. (2016). *Numerical Investigation of Continuous Composite Girders Strengthened with CFRP*. **Journal of Steel and Composite Structures**, Vol. 21, No. 6, pp. 1307–1325.
- 40- Saenz, L. P. (1964). *Equation for the Stress-Strain Curve of Concrete*. **ACI Journal**, Vol. 61, No. 9, pp. 1229–1235.
- 41- Savoia, M., Ferracuti, B., and Mazzotti, C. (2003). *Nonlinear Bond-Slip Law for FRP-Concrete Interface*. In **Proc. of 6th international symposium on FRP reinforcement for concrete structures**, Singapore: World Scientific Publications.
- 42- Sharif, A. M., Samaaneh, M. A., Azad, A. K., and Baluch, M. H. (2015). *Use of CFRP to Maintain Composite Action for Continuous Steel–Concrete Composite Girders*. **Journal of Composites for Construction**, Vol. 20, No. 4.

- 43- Siva Chidambaram. K.R, and Thirugnanam.G.S. (2012). *Comparative Studies on Behavior of Reinforced Beam-Column Joints with Reference to Anchorage Detailing*. **Journal of Civil Engineering Research**, Vol. 2, No.4, pp. 12-17.
- 44- Tran, M. T. (2014). *The Shear Strength of As-Built and Fiber Reinforced Polymer-A Strengthened Exterior Reinforced Concrete Beam-Column Connections Under Seismic Loading*. Thesis, University of Wollongong, Australia.
- 45- Uma, S. R., and Prasad, A. M. (1996). *Seismic Behavior of Beam Column Joints in Reinforced Concrete Moment Resisting Frames*. Department of Civil Engineering, Indian Institute of technology Madras, Chennai, Document No.IITK-GSDMA-EQ31-V1.0.
- 46- Wahalathantri, B. L., Thambiratnam, D. P., Chan, T. H. T., and Fawzia, S. (2011). *Material Model for Flexural Crack Simulation in Reinforced Concrete Elements Using ABAQUS*. In **Proceedings of the First International Conference on Engineering, Designing and Developing the Built Environment for Sustainable Wellbeing**, pp. 260-264.
- 47- WILLAM, K. J. (1975). *Constitutive Model for the Triaxial Behavior of Concrete*. **International association for bridge and structural engineering proceedings**, Vol. 19, pp. 1-30.
- 48- Yong, Y. K., Nour, M. G., and Nawy, E. G. (1988). *Behavior of Laterally Confined High-Strength Concrete Under Axial Loads*. **Journal of Structural Engineering**, Vol. 114, No.2, pp.332-351.

- 49- Zsutty, T. (1971). *Shear Strength Prediction for Separate Categories of Simple Beam Tests*. In **Journal Proceedings**, Vol. 68, No. 2, pp. 138-143.

Appendix

Detailing's of joints are shown below for all models without CFRP wrapping. This is indicated with number "0" at the end of the names of these models. In addition, a typical model wrapped with CFRP is shown in Figure A.33. This is indicated with number "1" at the end of the names of these models.

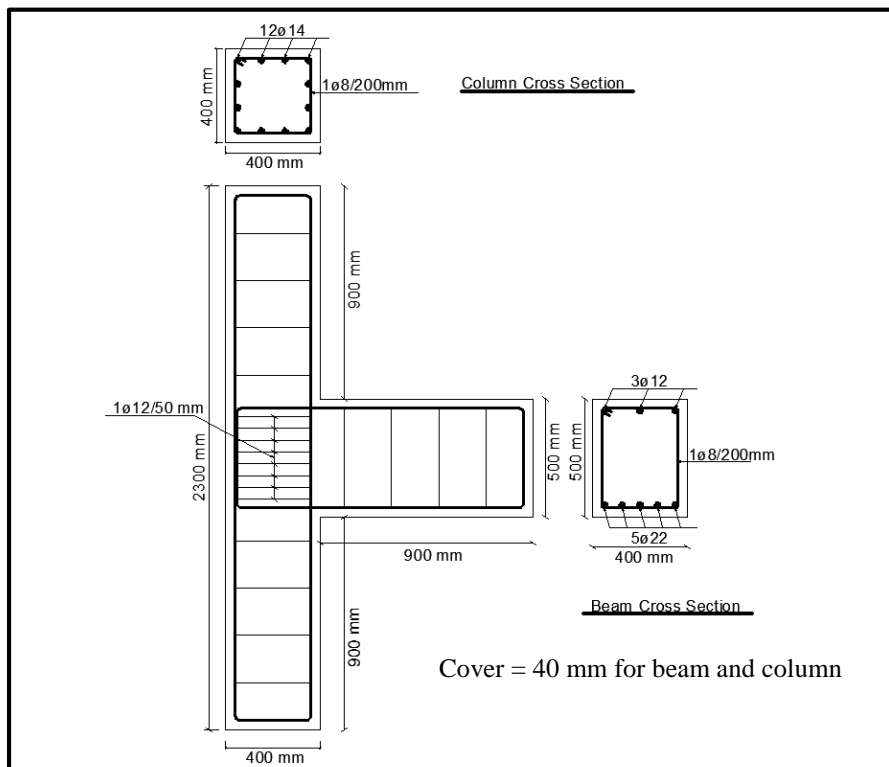


Figure A. 1: G1-MaJ-MiB-0

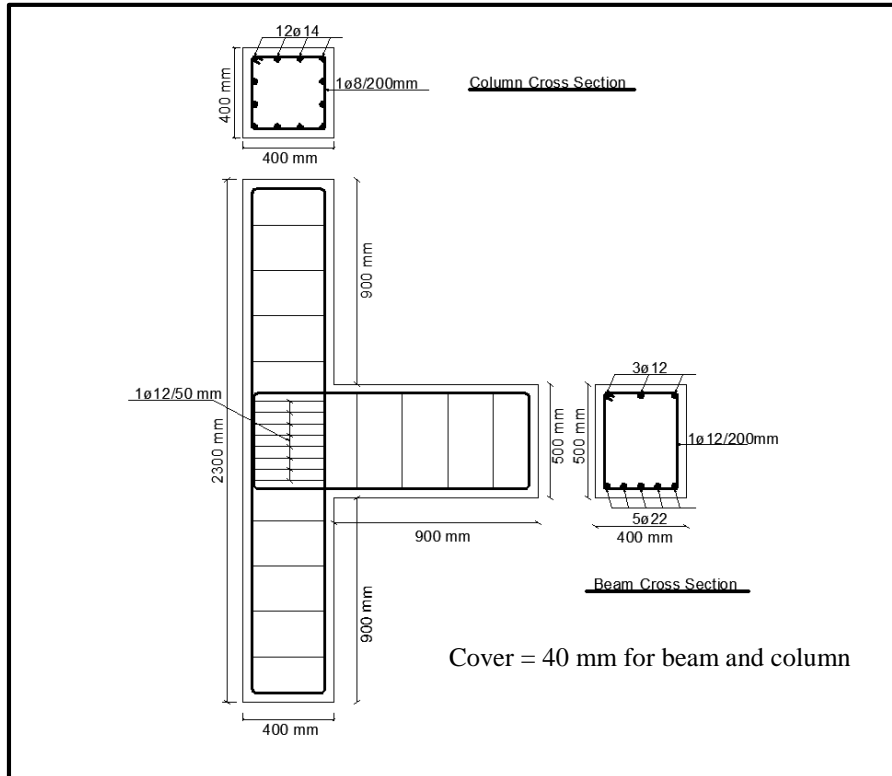


Figure A. 2: G1-MaJ-B1B-0

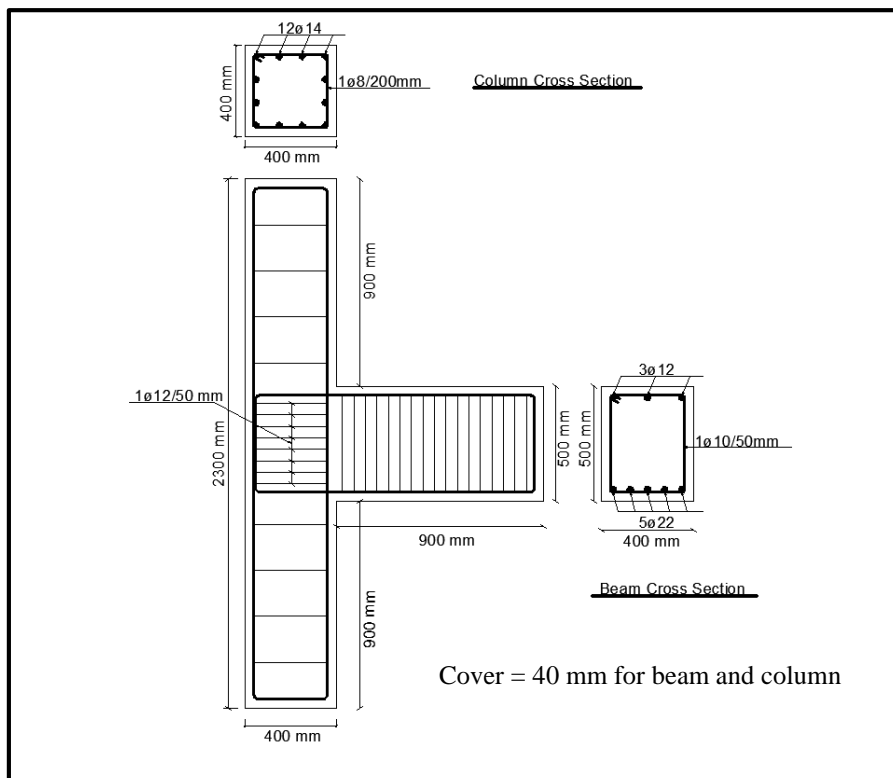


Figure A. 3: G1-MaJ-B2B-0

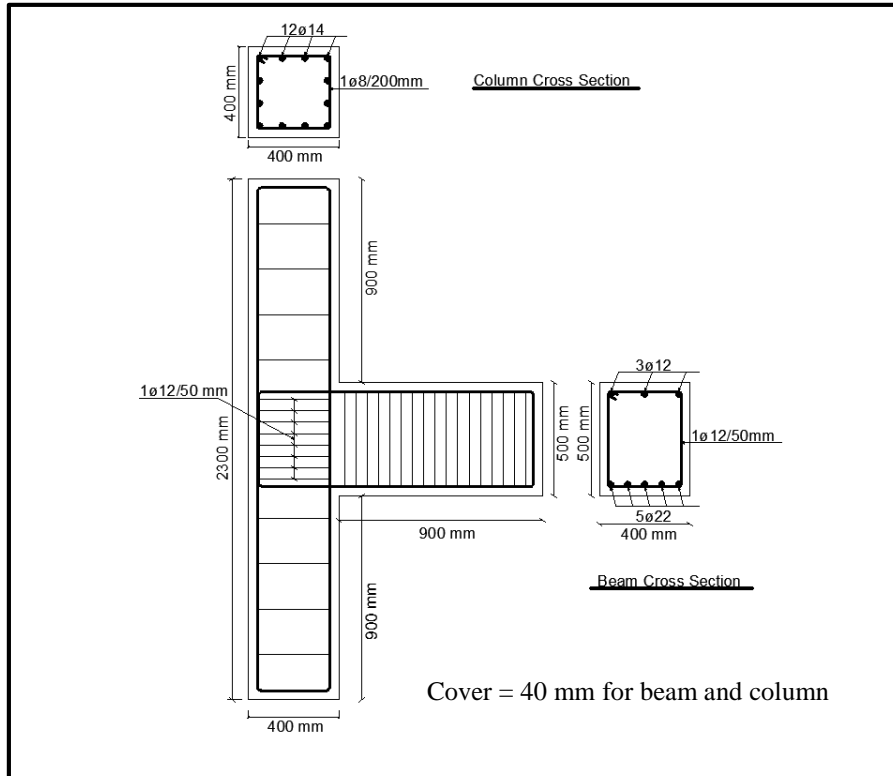


Figure A. 4: G1-MaJ-MaB-0

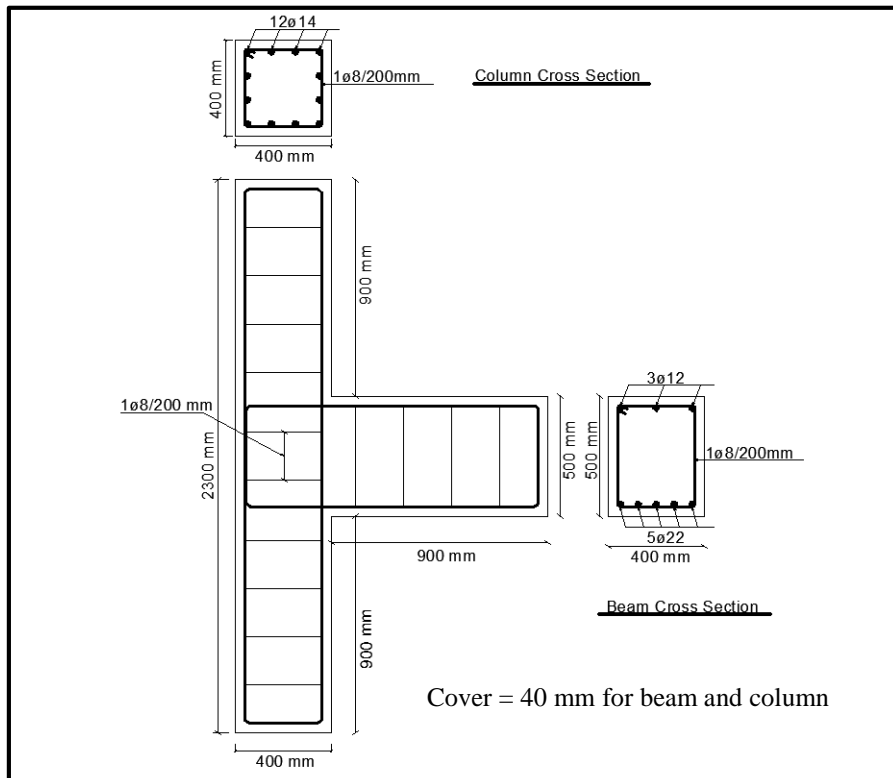


Figure A. 5: G1-MiJ-MiB-0

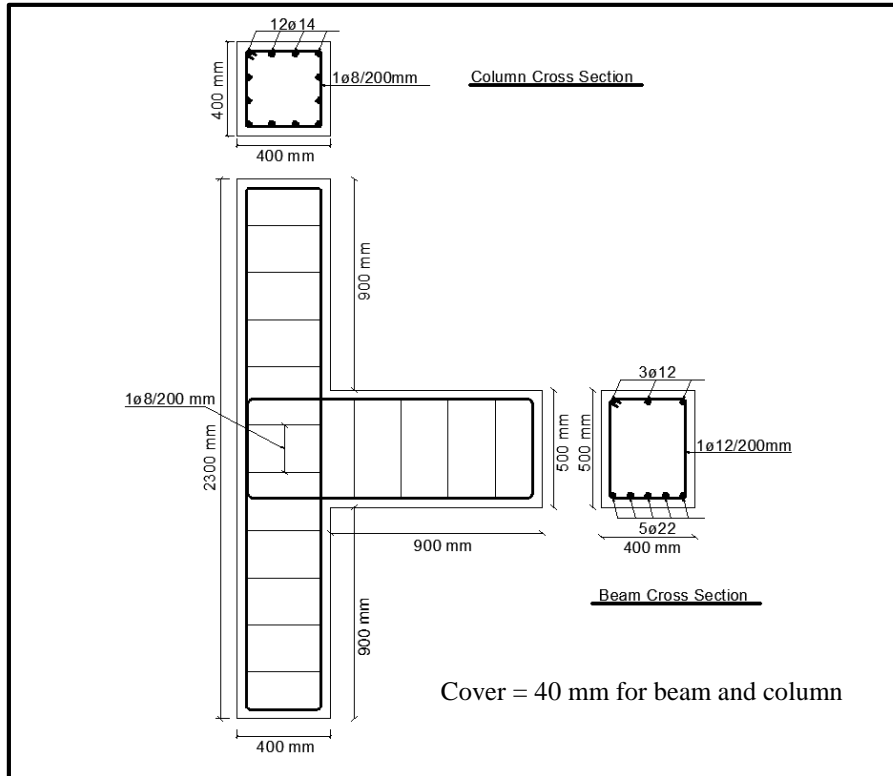


Figure A. 6: G1-MiJ-B1B-0

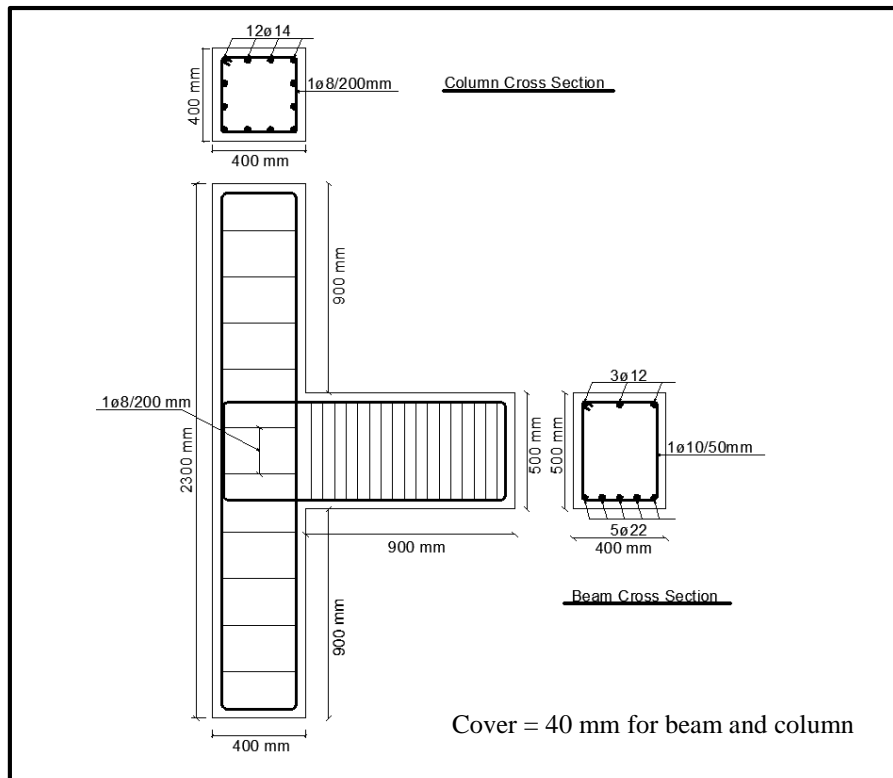


Figure A. 7: G1-MiJ-B2B-0

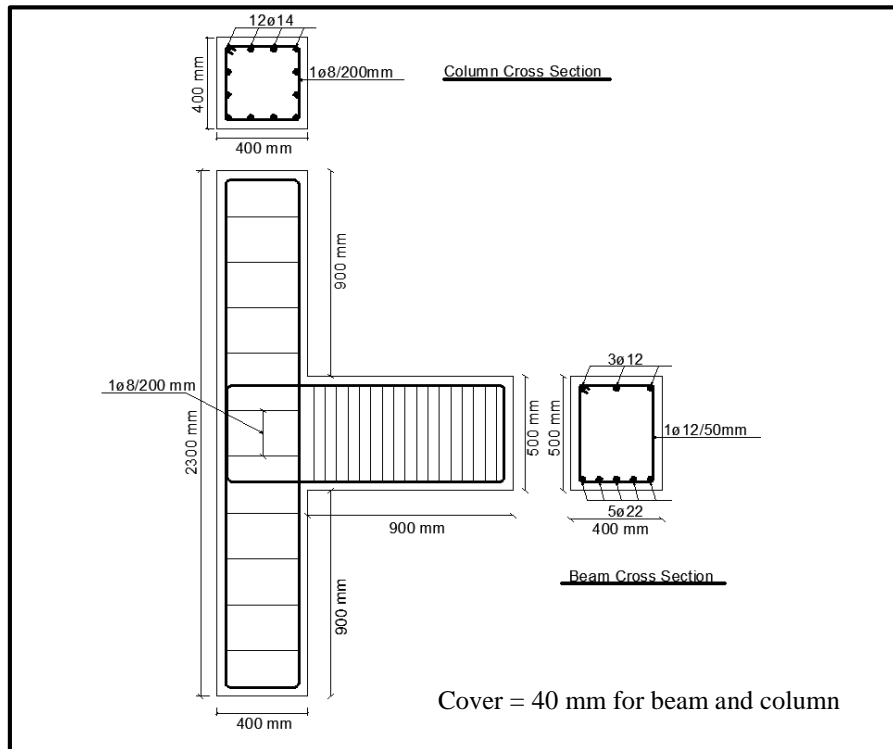


Figure A. 8: G1-MiJ-MaB-0

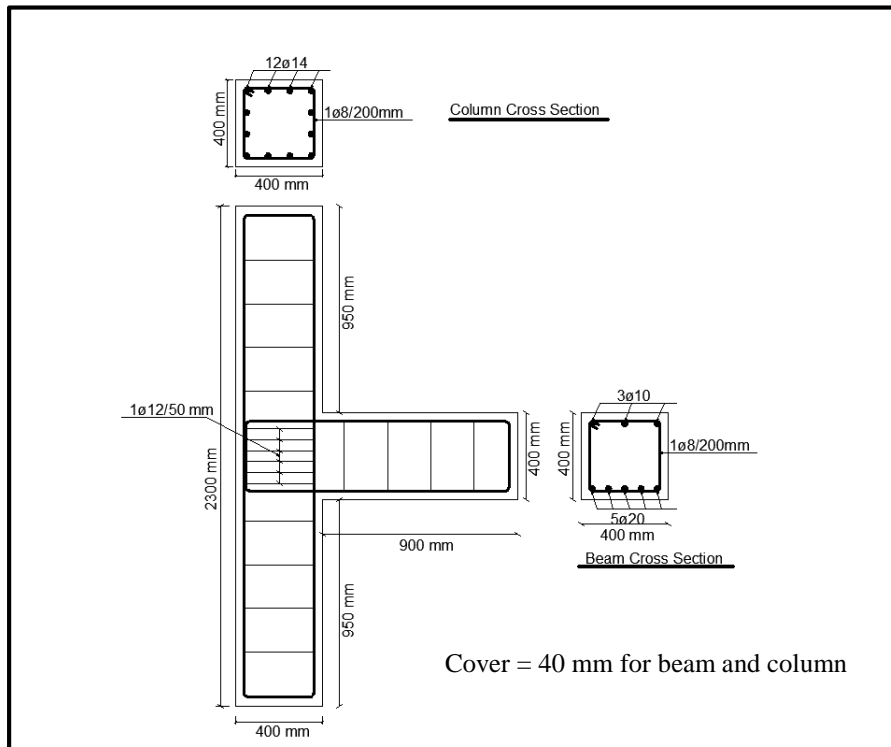


Figure A. 9: G2-MaJ-MiB-0

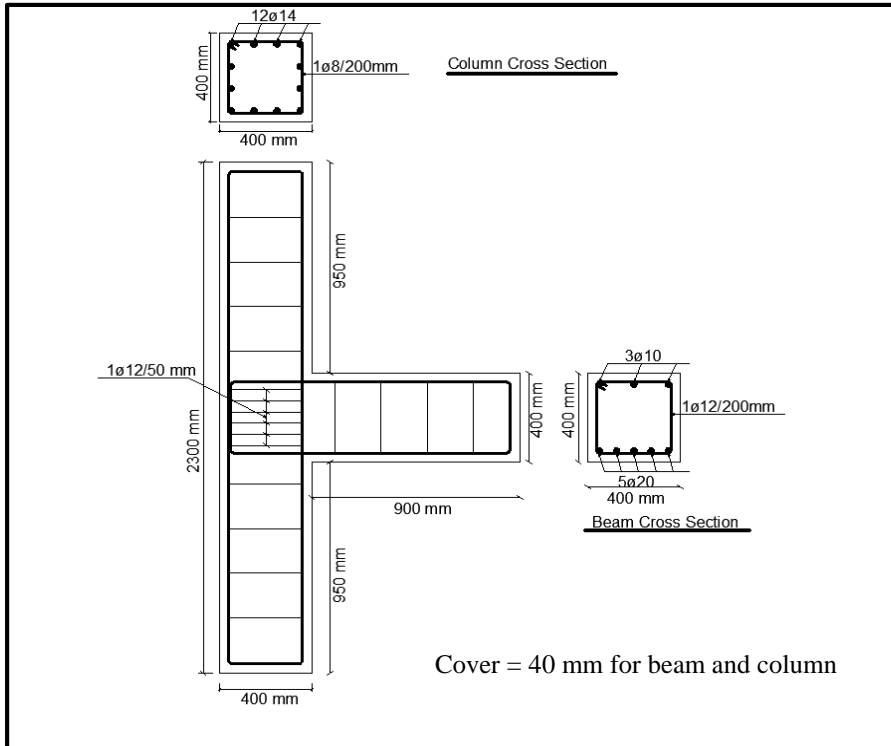


Figure A. 10: G2-MaJ-B1B-0

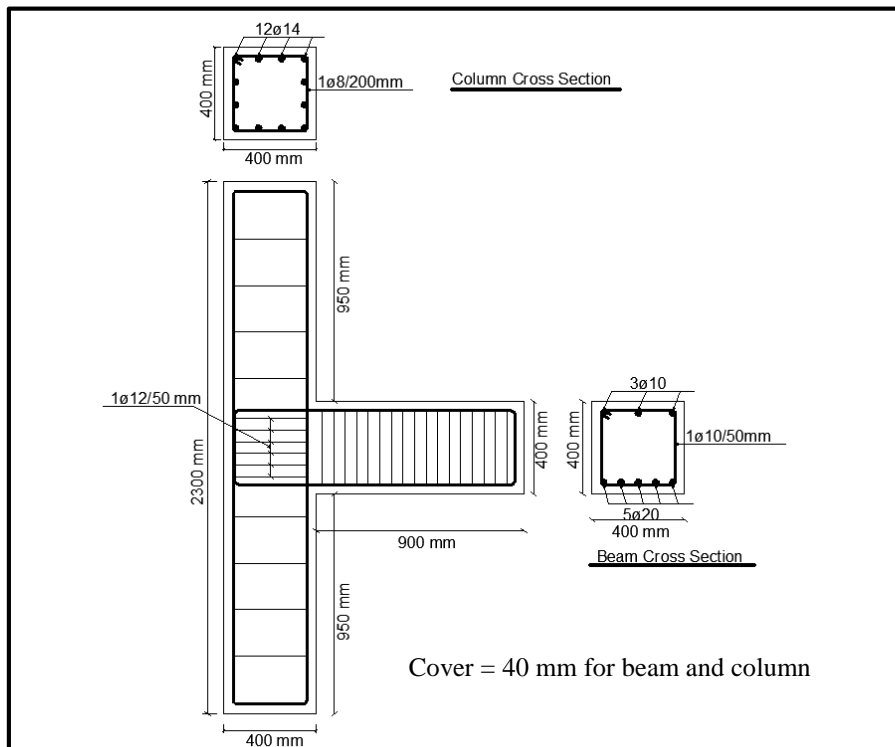


Figure A. 11: G2-MaJ-B2B-0

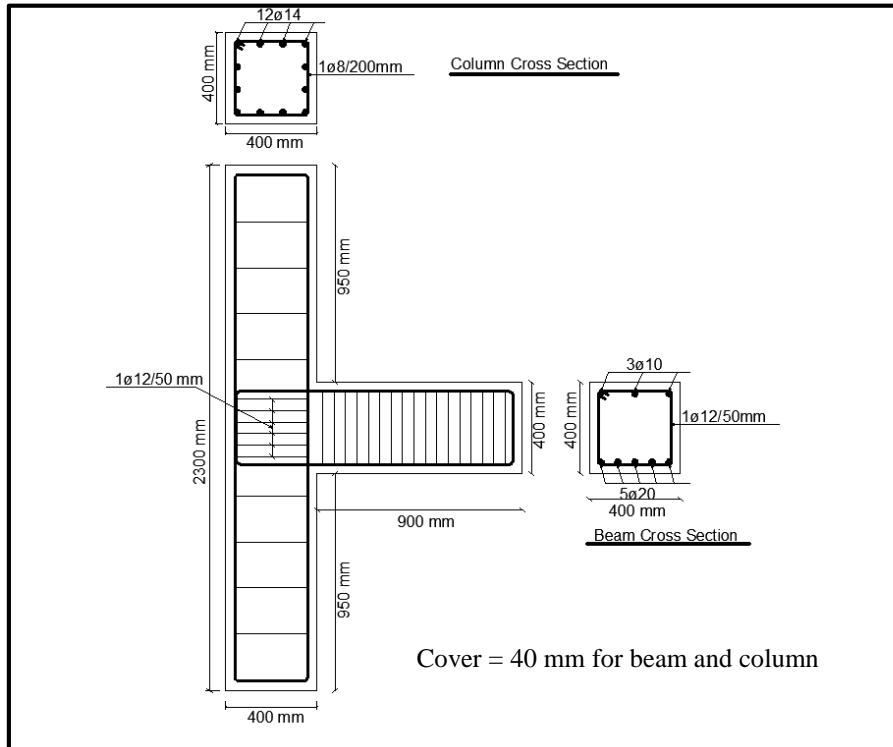


Figure A. 12: G2-MaJ-B2B-0

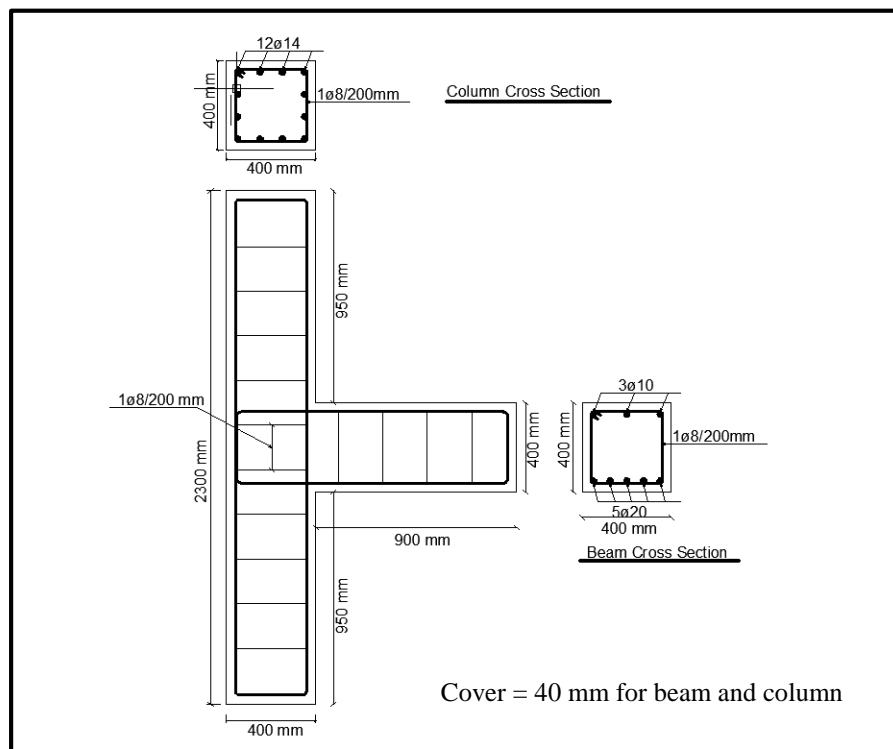


Figure A. 13: G2-MiJ-MiB-0

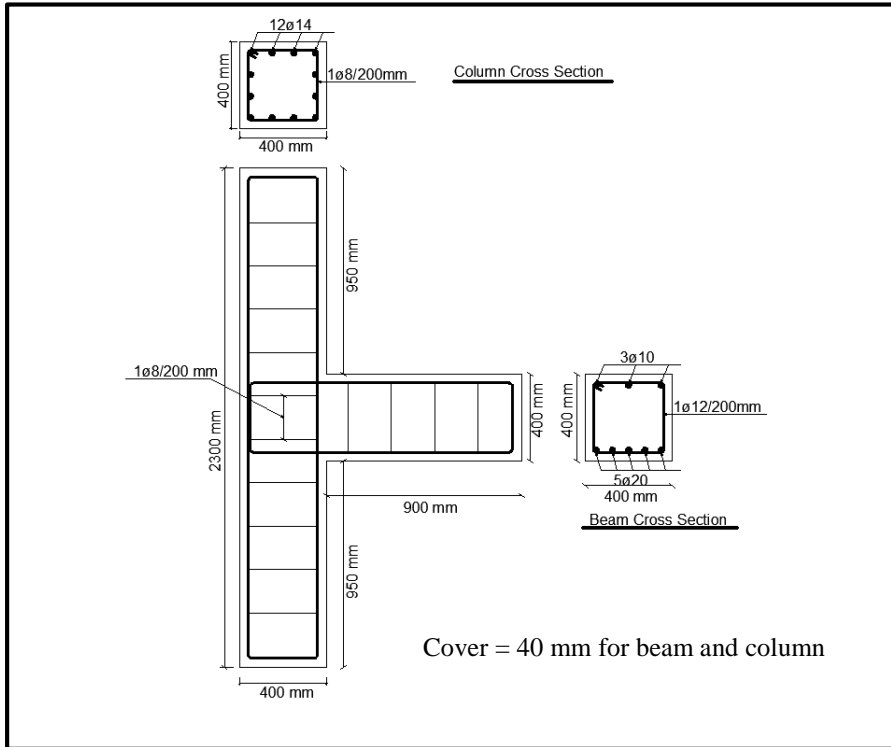


Figure A. 14: G2-MiJ-B1B-0

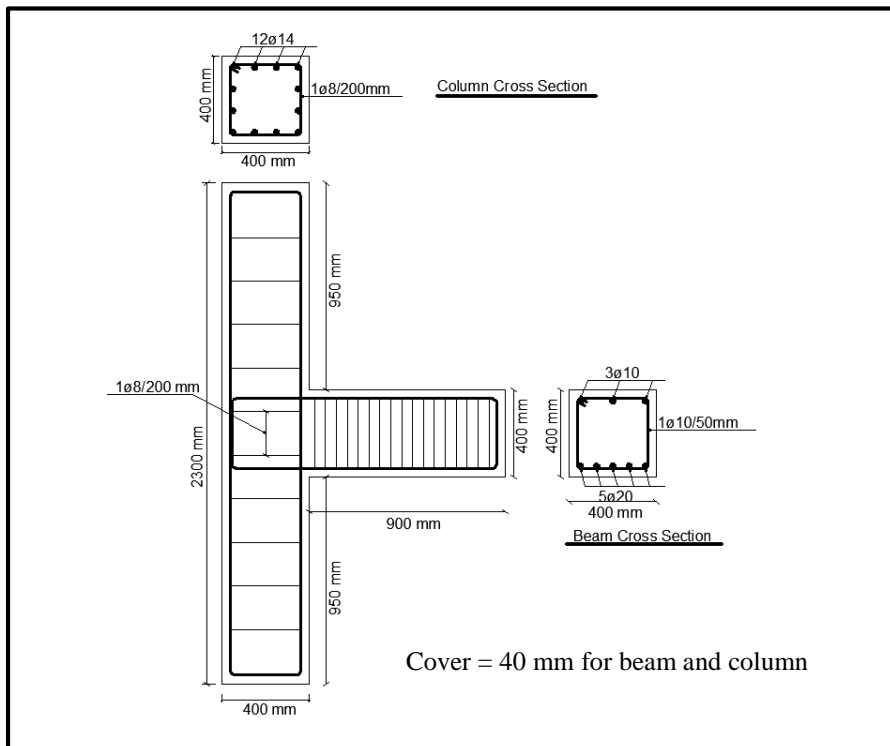


Figure A. 15: G2-MiJ-B2B-0

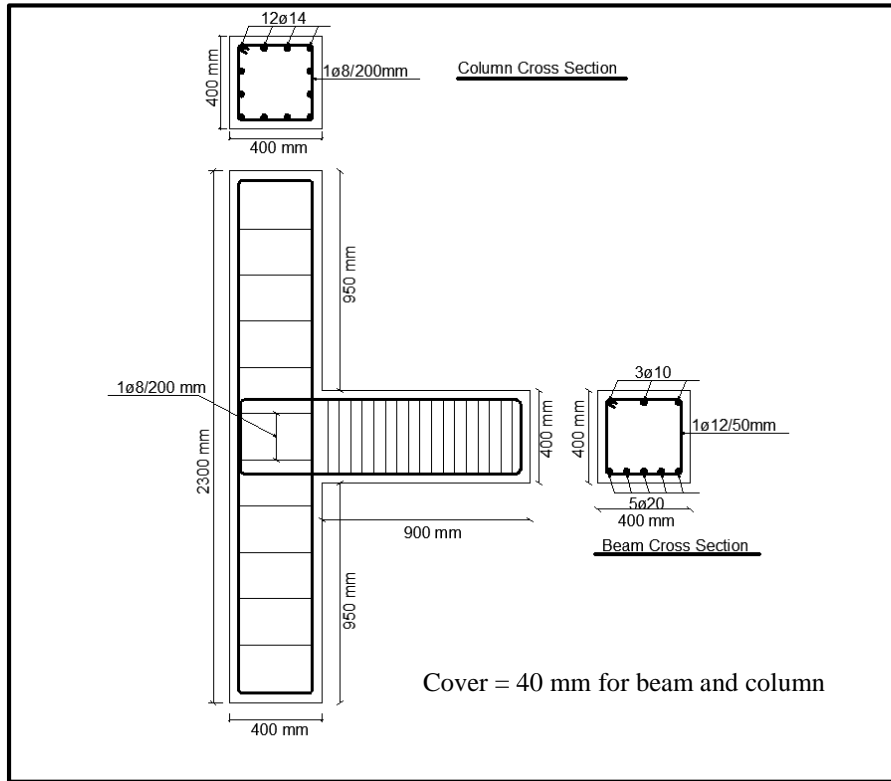


Figure A. 16: G2-MiJ-B2B-0

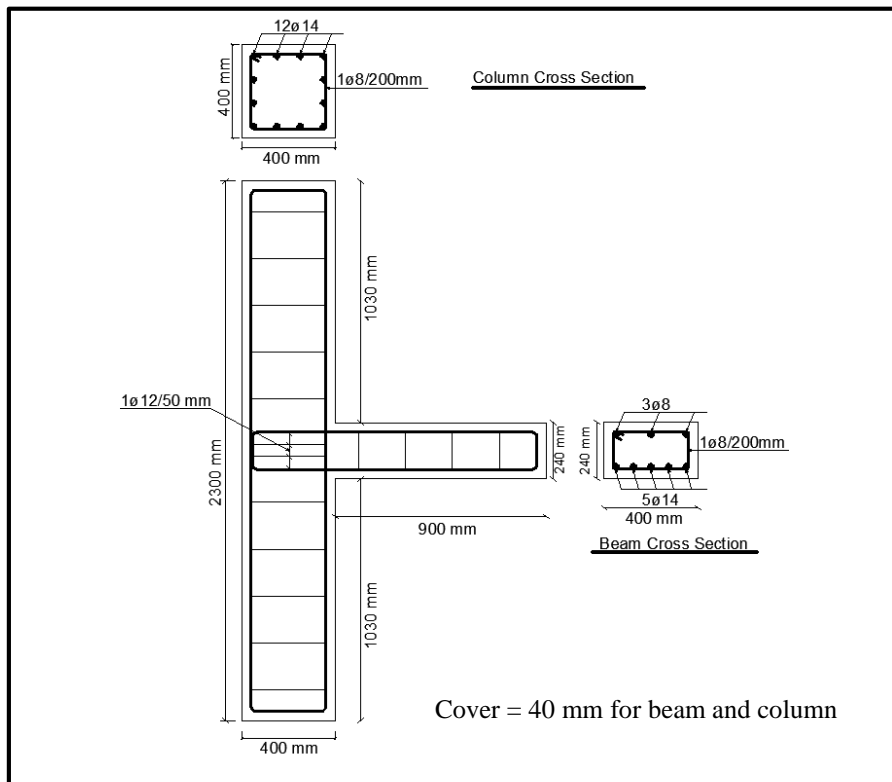


Figure A. 17: G3-MaJ-MiB-0

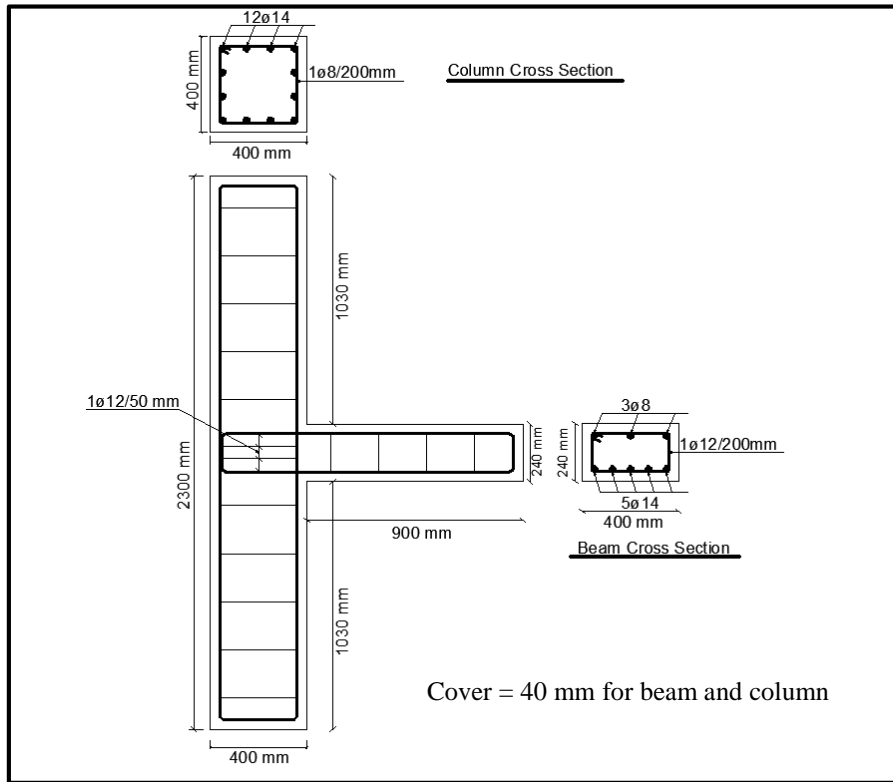


Figure A. 18: G3-MaJ-B1B-0

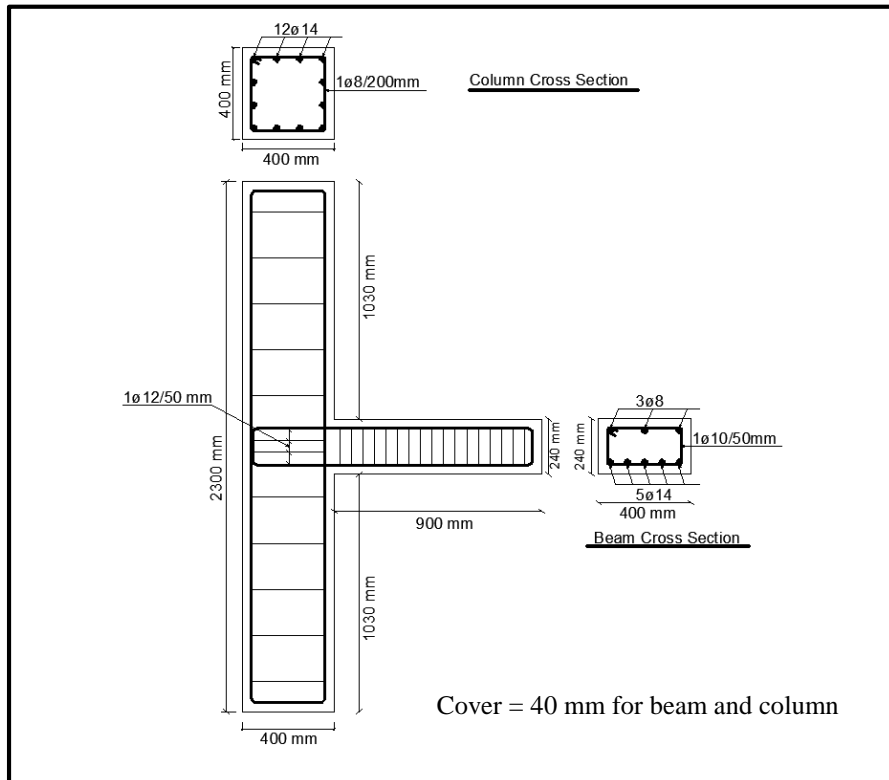


Figure A. 19: G3-MaJ-B2B-0

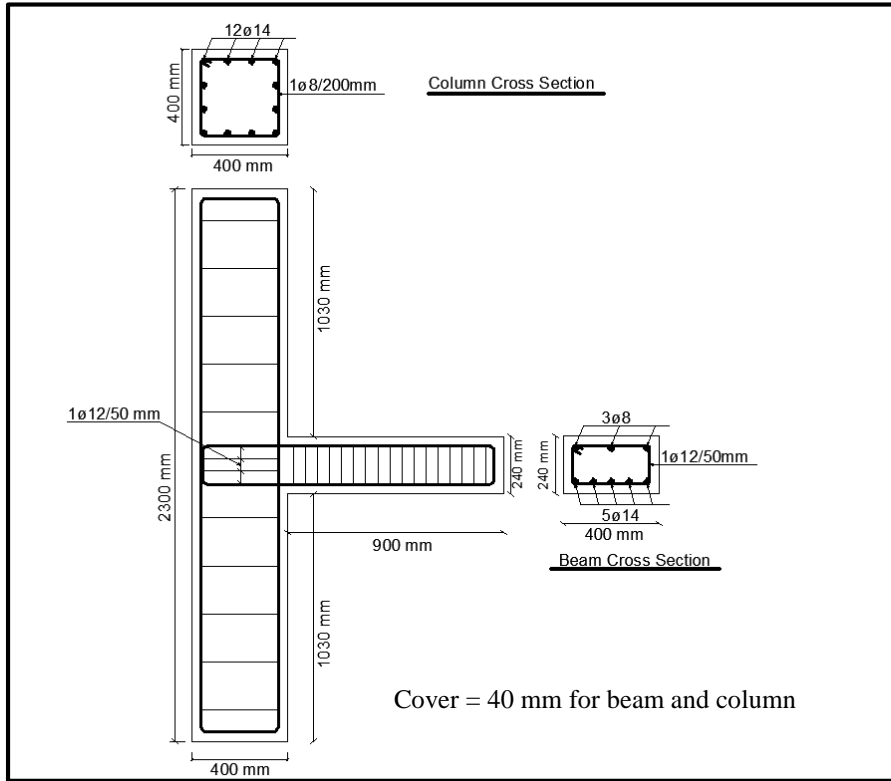


Figure A. 20: G3-MaJ-MaB-0

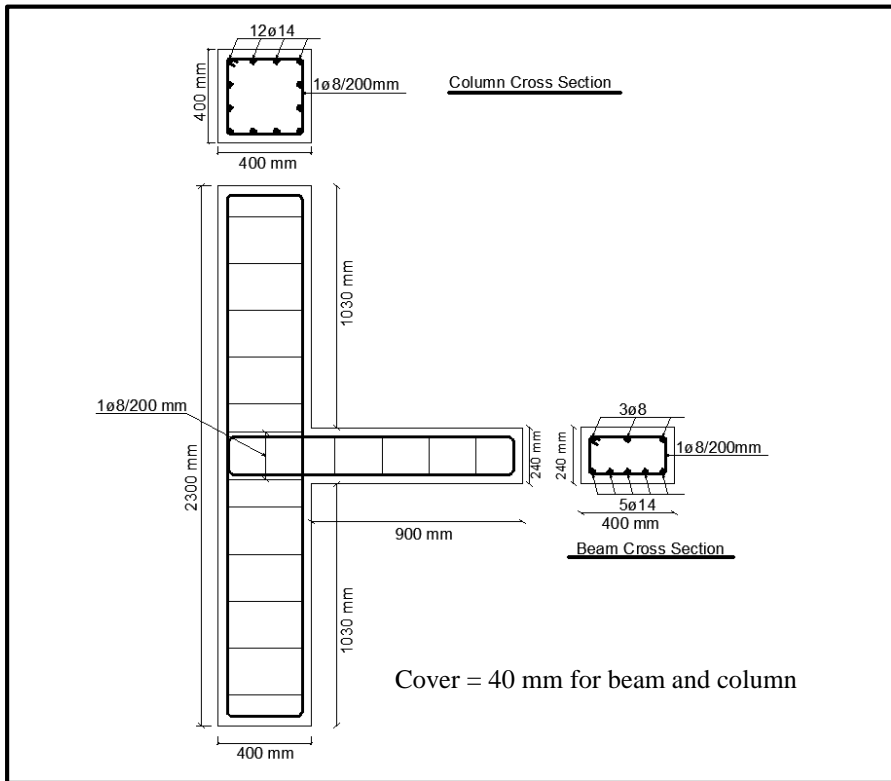


Figure A. 21: G3-MiJ-MiB-0

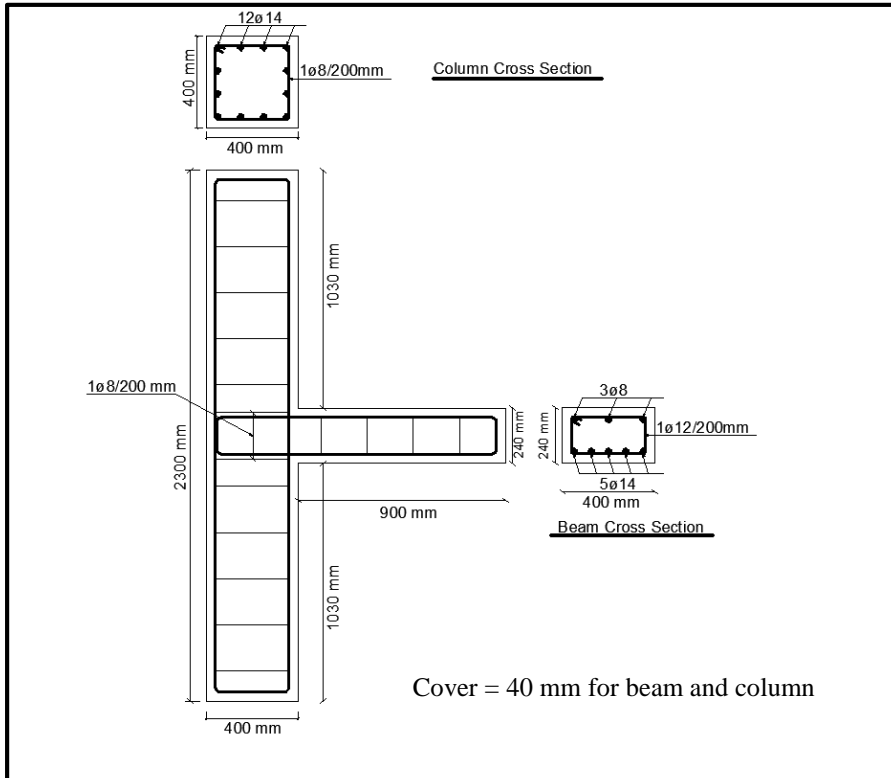


Figure A. 22: G3-MiJ-B1B-0

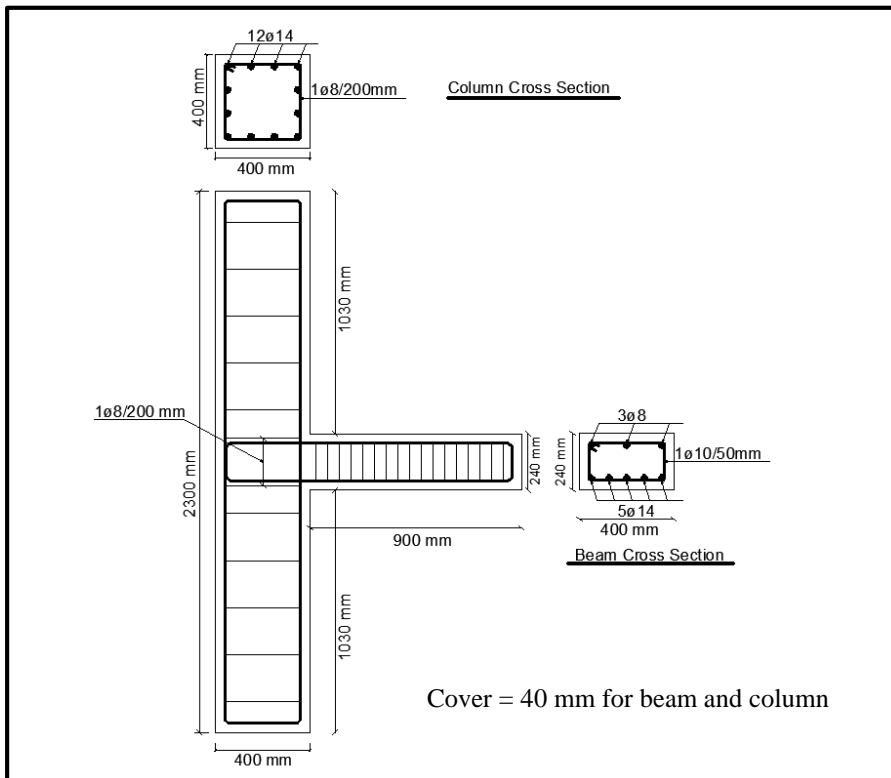


Figure A. 23: G3-MiJ-B2B-0

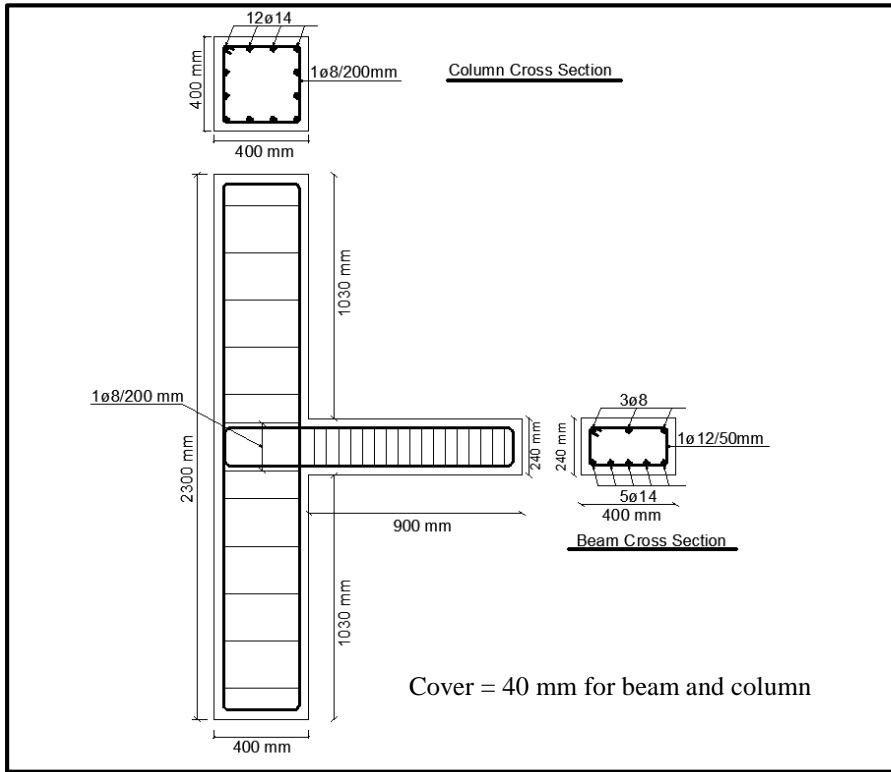


Figure A. 24: G3-MiJ-MaB-0

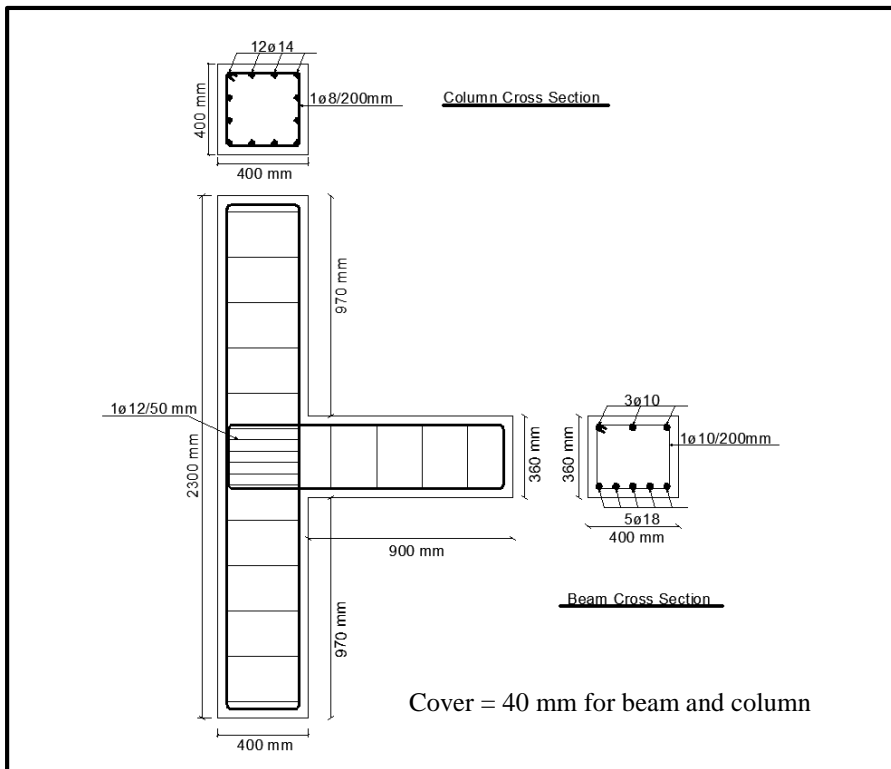


Figure A. 25: C1-MaJ-X0B-0

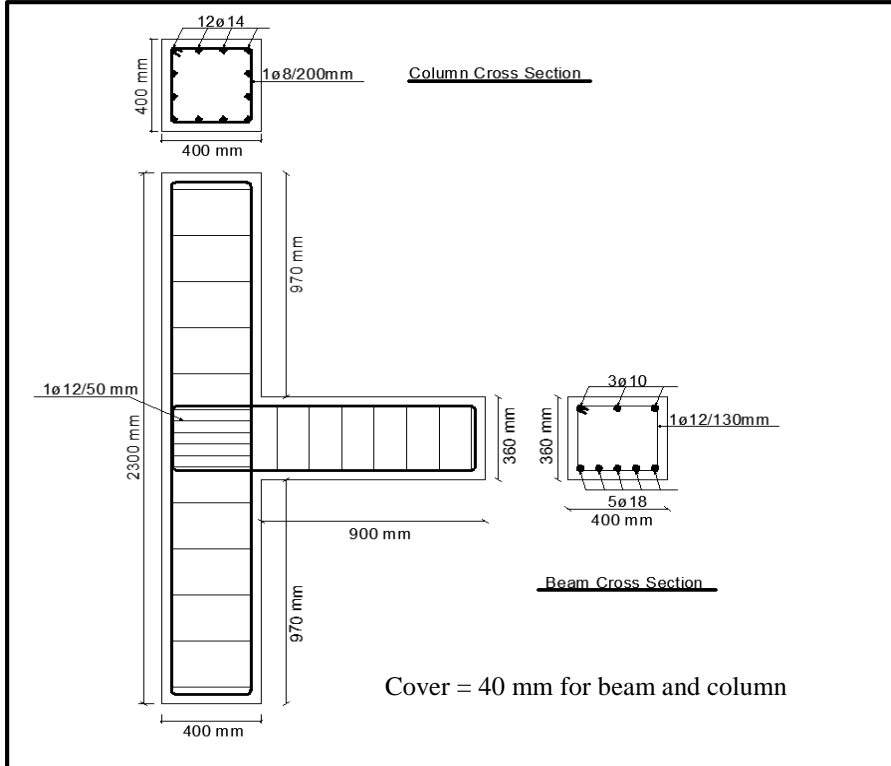


Figure A. 26: C1-MaJ-X1B-0

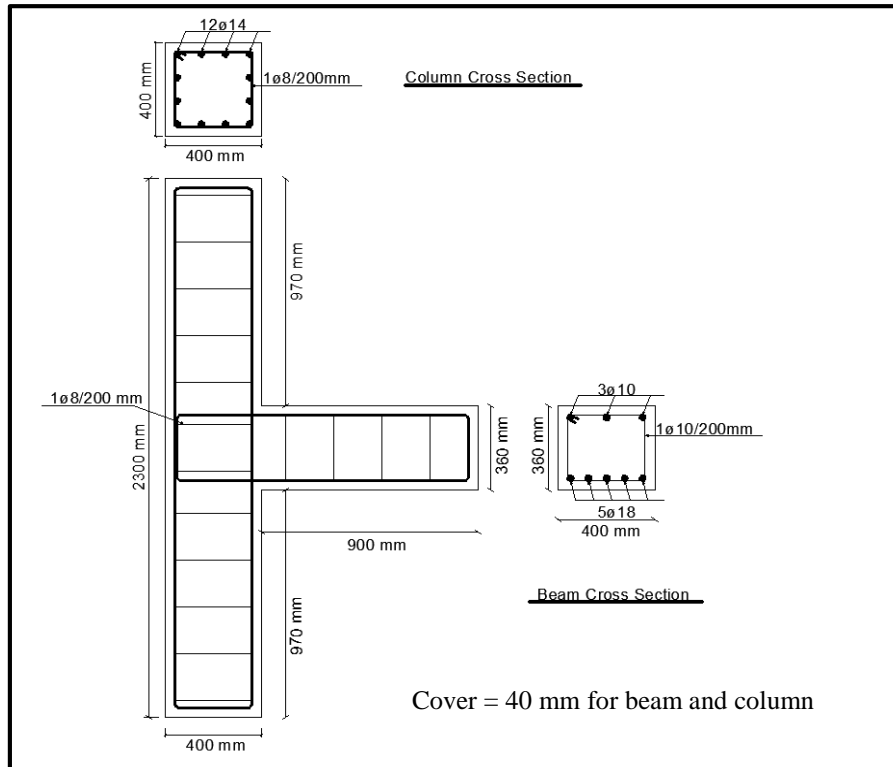


Figure A. 27: C1-MiJ-X0B-0

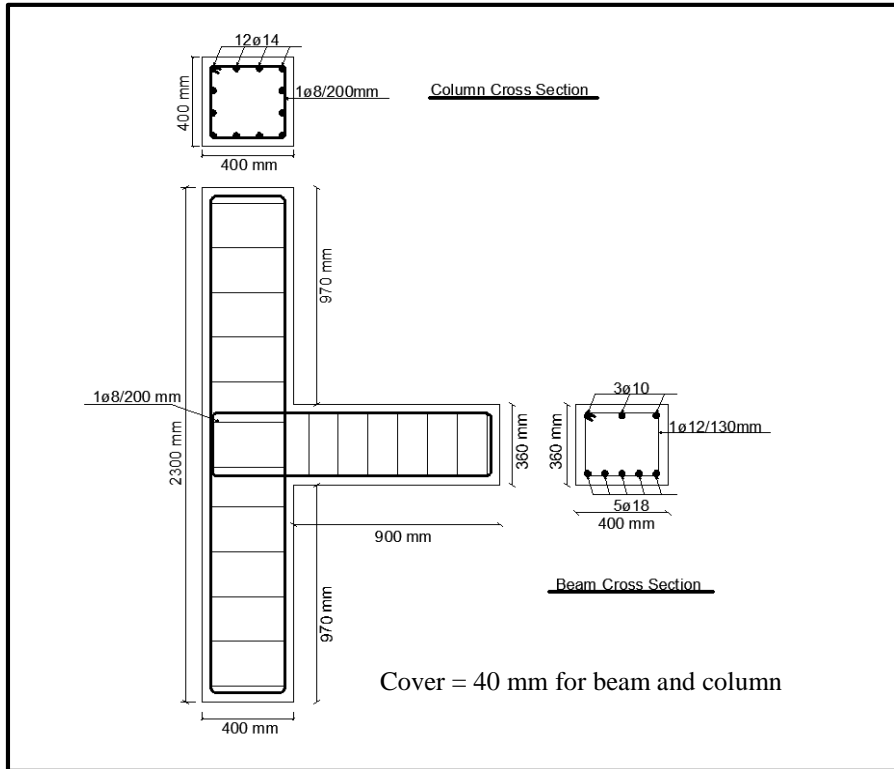


Figure A. 28: C1-MiJ-X1B-0

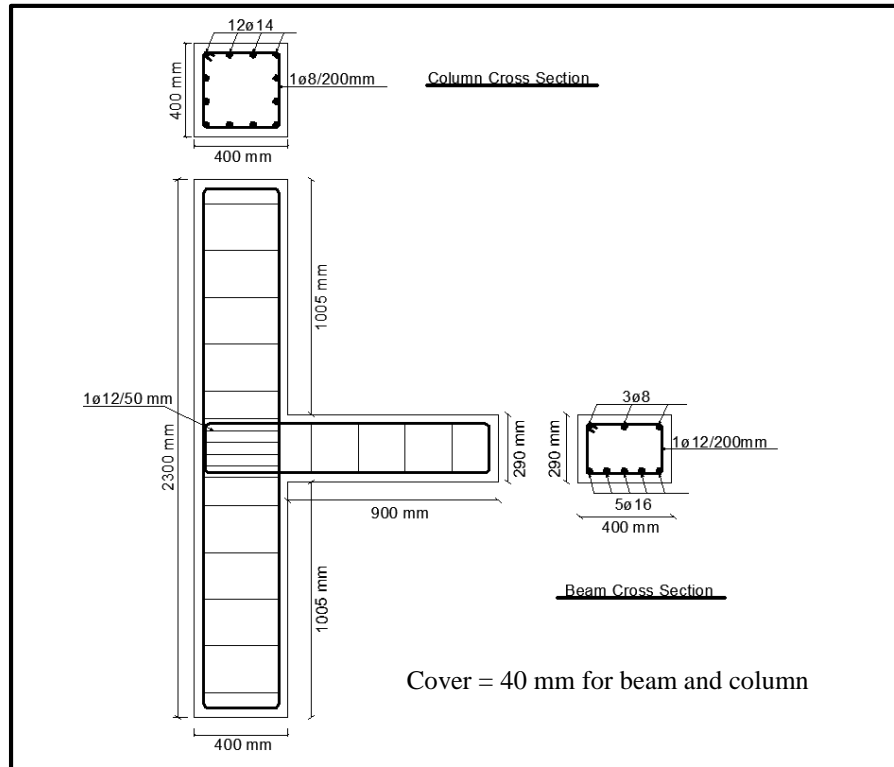


Figure A. 29: C2-MaJ-X0B-0

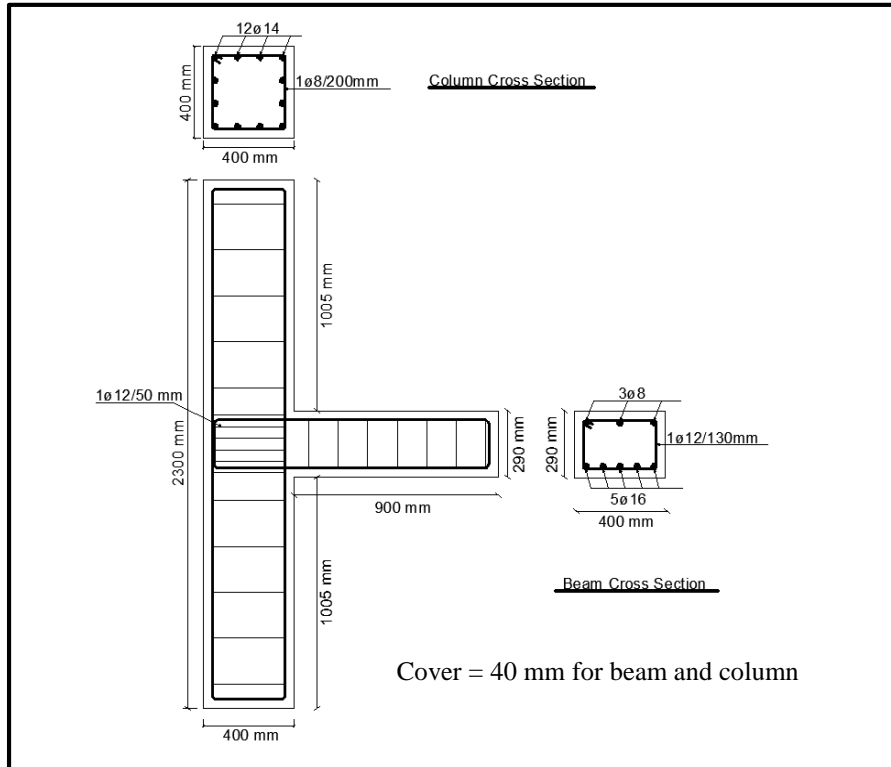


Figure A. 30: C2-MaJ-X1B-0

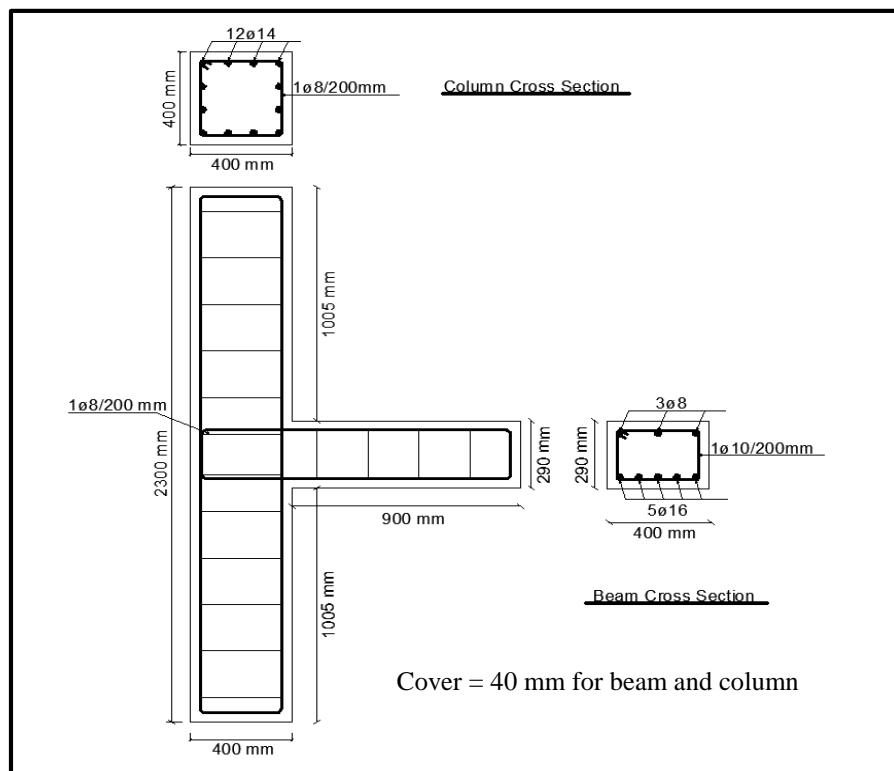


Figure A. 31: C2-MiJ-X0B-0

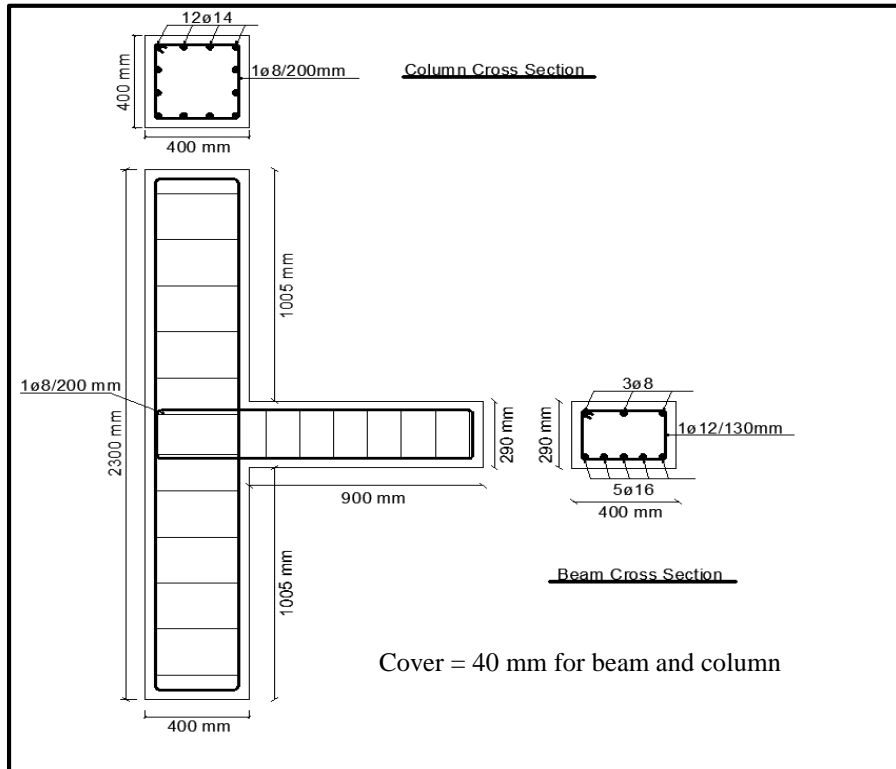


Figure A. 32: C2-MiJ-X1B-0

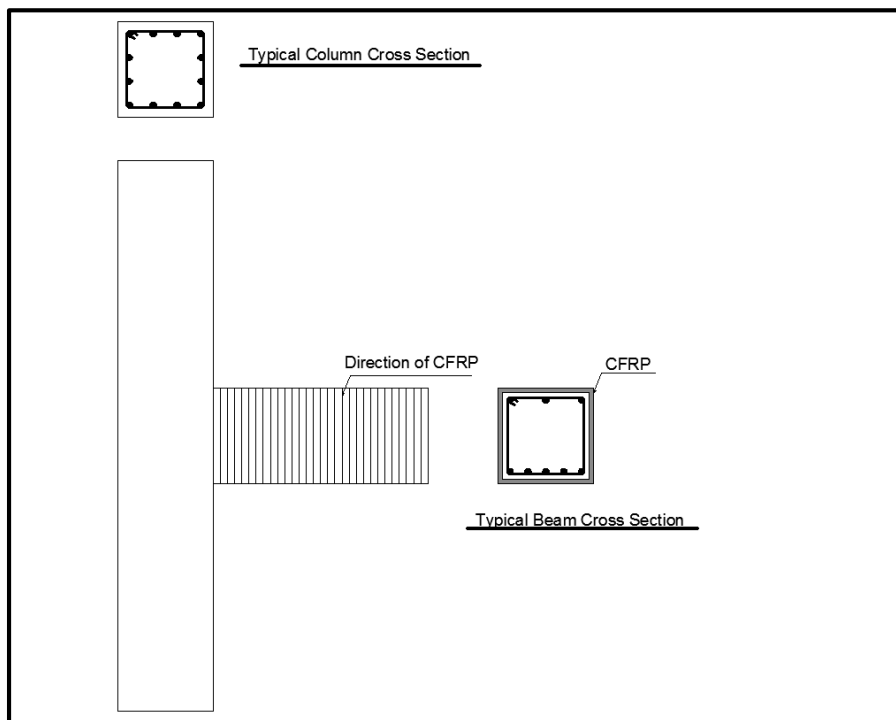


Figure A. 33: Typical wrapping arrangement of CFRP

أثر استخدام المبلمرات المدعومة بالألياف على ليونة العقد الخرسانية المسلحة المعاد تأهيلها

اعداد

يزن بسام أبو طحنات

اشراف

د. محمود دويكات

د. محمد سماعنة

قدمت هذه الأطروحة استكمالاً لمتطلبات الحصول على درجة الماجستير في هندسة الإنشاءات
بكلية الدراسات العليا في جامعة النجاح الوطنية، نابلس - فلسطين.

2018

ب

أثر استخدام المبلمرات المدعومة بالألياف على ليونة العقد الخرسانية المسلحة المعاد تأهيلها

اعداد

يزن بسام أبو طحنات

اشراف

د. محمود دويكات

د. محمد سماعنة

المخلص

إن المنشآت الخرسانية المسلحة شائعة في فلسطين. هناك نقطة ضعف في هذه المنشآت وهي منطقة التقاء الجسور مع الأعمدة (مفاصل خرسانية). وأظهر العديد من الباحثين أن هذه المفاصل تعاني من انهيار مفاجئ (هش) بسبب التأثير المشترك للقوى عليها. ولذلك فإن ليونة هذه المفاصل في المنشآت الخرسانية المسلحة يعتبر عامل مهم لمنع الإنهيار المفاجئ. تم تطوير تقنيات مختلفة من قبل العديد من الباحثين لزيادة ليونة وقوة المفاصل الخرسانية المسلحة، منها: استخدام خرسانة عالية القوة، تكثيف الكانات داخل هذه المفاصل، تغليف هذا المفصل بصفائح معدنية واستخدام المبلمرات المدعومة بالألياف.

من أحد الطرق المستخدمة لتحسين ليونة المفاصل الخرسانية هي تغليف هذه المفاصل بصفائح المبلمرات المدعومة بالألياف. ويركز هذا البحث على دراسة تأثير استخدام هذه المبلمرات على المفاصل الخرسانية المسلحة الخارجة باستخدام أحد برامج العناصر المحدودة وهو برنامج (اباكوس). حيث سيتم التحقق من صحة النموذج باستخدام بيانات تجارب عملية منشورة. ويستخدم هذا النموذج لإجراء دراسة على العوامل الرئيسية التي تؤثر على السلوك اللاخطي لهذه المفاصل. وبعد ذلك ستستخدم النتائج لتطوير معادلات بسيطة للتنبؤ بليونة المفاصل الخرسانية المسلحة الخارجية. ويمكن استخدام هذه المعادلة كخطوة مبدئية أولية للتحقق من مدى كفاءة هذه المفاصل عند التصميم الزلزالي للمباني الخرسانية المسلحة.